ROLE OF MACRO AND MICRONUTRIENTS IN THE MANAGEMENT OF GLYCOGEN STORAGE DISEASE MANIFESTATIONS – A PRECLINICAL STUDY

Thesis submitted to

KLE ACADEMY OF HIGHER EDUCATION AND RESEARCH,

BELAGAVI

(Deemed-to-be-University)

[Declared as Deemed-to-be-University u/s 3 & 12B of the UGC Act, 1956 vide Govt. of India Notification No.F.9-19/2000-U.3 (A)]
(Accredited 'A^{+}' Grade by NAAC 3rd cycle)
[Placed in Category 'A' by MoE (GoI)]

For the award of the degree of

Doctor of Philosophy

In the Faculty of Pharmacy

By

Mr. SANTOSH BASAVARAJ PATIL M.Pharm

(Registration No: KLEU/Ph.D./18-19/ DO1218016)

KLE
EMPOWERING PROFESSIONALS

Under the Guidance of

Dr. Pramod C Gadad M. PHARM, Ph.D.

Professor and Principal

Department of Pharmacology

KLE College of Pharmacy, Nipani.

2024

UNDERTAKING

I, **Santosh Basavaraj Patil,** hereby declare that the information and the data mentioned in my thesis entitled **"Role of Macro and Micronutrients in the Management of Glycogen Storage Disease Manifestations – A Preclinical Study"** belong to me and is original.

I am aware of the definition of plagiarism as detailed below:

- An act or instance of using or closely imitating the language and thoughts of another author without authorization and the representation of that author's work as one's own, as by not crediting the original author.
- A piece of writing or other work reflecting such unauthorized use or imitation.
- The deliberate or reckless representation of another's words, thoughts or ideas as one's own without attribution in connection with submission of academic work, whether graded or otherwise.

I hereby declare that the thesis prepared by me is original and does not involve plagiarism anywhere. In case at a later stage, it is found that I have indulged in plagiarism, then I am solely responsible for the same and the Institution is at liberty to take any disciplinary action against me including cancellation of the dissertation or any other penalties imposed by the University.

Place: Hubballi

Date:

Mr. Santosh Basavaraj Patil
Part time Ph.D. Research Scholar
Reg. No. DO1218016
KLE College of Pharmacy, Hubballi
KAHER, Belagavi-590010.

PLAGIARISM REPORT

KLE
EMPOWERING PROFESSIONALS

Ref. No. KAHER/AA/24-25/D-059 26th April 2024

Madam,

The soft copy of Ph.D. research thesis of **Mr. Santosh B. Patil, Faculty of Pharmacy, KAHER, Hubballi** has been submitted for anti-plagiarism check at the office of the undersigned through "Turn-it-in" package. The scan has been carried out and the scanned output reveals a match percentage of **7%** which is within the acceptable limit of 10%.

To obtain the comprehensive report of the plagiarism test, research scholar can send a mail to **diracademic@kledeemeduniversity.edu.in** along with the Registration Number, Name of the Scholar, Name of Guide/Co-guide and title of the thesis.

Dr.(Mrs.) Roopa M. Bellad
Director, Academic Affairs

DIRECTOR ACADEMIC AFFAIRS Deemed-to-be University

To,

Mr. Santosh B Patil
Part-Time Ph.D. Scholar,
2018-19 batch
KLE College of Pharmacy,
Faculty of Pharmacy,
Hubballi

Cc to :
1. The Principal, KLE College of Pharmacy, Hubballi
2. Dr. Pramod C Gadad, Professor of Pharmacology, College of Pharmacy, Nippani – Guide

KLE ACADEMY OF HIGHER EDUCATION AND RESEARCH
(Deemed-to-be-University established u/s 3 & 12B of the UGC Act, 1956)
Accredited A+ Grade by NAAC (3rd Cycle) Placed in Category A by MoE (GoI)
JNMC Campus, Nehru Nagar, Belagavi - 590 010, Karnataka, India 0831-2444444 kledeemeduniversity.edu.in

KLE ACADEMY OF HIGHER EDUCATION AND RESEARCH,

(Deemed-to-be-University)

[Declared as Deemed-to-be-University u/s 3 & 12B of the UGC Act, 1956 vide Govt. of India Notification No.F.9-19/2000-U.3 (A)]

(Accredited 'A^{+}' Grade by NAAC) (3rd Cycle)

[Placed in Category 'A by MoE (GoI)]

BELAGAVI

COPYRIGHT DECLARATION

We hereby declare that **KLE ACADEMY OF HIGHER EDUCATION AND RESEARCH, BELAGAVI, KARNATAKA,** *shall have the rights to preserve, use and disseminate this thesis in print or electronic format for academic/research purpose.*

Mr. Santosh Basavaraj Patil
Part time Ph.D. Research Scholar
Reg. No: DO1218016
KLE College of Pharmacy, Hubballi
KAHER, Belagavi-590010

Dr. Pramod C Gadad
Professor and Principal,
Department of Pharmacology
KLEs College of Pharmacy, Nipani

Place: Hubballi

Date:

Place: Nipani

Date:

KLE ACADEMY OF HIGHER EDUCATION AND RESEARCH,

(Deemed-to-be-University)

[Declared as Deemed-to-be-University u/s 3 & 12B of the UGC Act, 1956 vide Govt. of India Notification No.F.9-19/2000-U.3 (A)]

(Accredited 'A^{+}' Grade by NAAC) (3rd Cycle)

[Placed in Category 'A' by MoE (GoI)]

BELAGAVI

DECLARATION

I hereby declare that the thesis entitled **"Role of Macro and Micronutrients in the Management of Glycogen Storage Disease Manifestations – A Preclinical Study"** *is a bonafide and original research carried out by me under the guidance of* ***Dr. Pramod C Gadad,*** *Professor, Department of Pharmacology, KLE College of Pharmacy, Nipani. The thesis or any part thereof has not formed the basis for the award of any degree/fellowship or similar title to any candidate of any University.*

Place: Hubballi
Date:

Mr. Santosh Basavaraj Patil
Part time Ph.D. Research Scholar
Reg. No: DO1218016
KLE College of Pharmacy, Hubballi
KAHER, Belagavi-590010

KLE ACADEMY OF HIGHER EDUCATION AND RESEARCH,

(Deemed-to-be-University)

[Declared as Deemed-to-be-University u/s 3 & 12B of the UGC Act, 1956 vide Govt. of India Notification No.F.9-19/2000-U.3 (A)]

(Accredited 'A^{+}' Grade by NAAC) (3rd Cycle)

[Placed in Category 'A' by MoE (GoI)]

BELAGAVI

CERTIFICATE

This is to certify that the thesis entitled **"Role of Macro and Micronutrients in the Management of Glycogen Storage Disease Manifestations – A Preclinical Study"** *is a bonafide and genuine research carried out by* ***Mr. Santosh Basavaraj Patil*** *under the guidance of* ***Dr. Pramod C Gadad,*** *Professor, Department of Pharmacology, KLE College of Pharmacy, Nipani.*

Place: Hubballi
Date:

Prof. (Dr.) M S Ganachari
Dean, Faculty of Pharmacy
KAHER Belagavi

KLE ACADEMY OF HIGHER EDUCATION AND RESEARCH,

(Deemed-to-be-University)

[Declared as Deemed-to-be-University u/s 3 & 12B of the UGC Act, 1956 vide Govt. of India Notification No.F.9-19/2000-U.3 (A)]

(Accredited 'A^{+}' Grade by NAAC) (3rd Cycle)

[Placed in Category 'A' by MoE (GoI)]

BELAGAVI

KLE
EMPOWERING PROFESSIONALS

CERTIFICATE

This is to certify that the thesis entitled **"Role of Macro and Micronutrients in the Management of Glycogen Storage Disease Manifestations – A Preclinical Study"** *is a bonafide record of original research carried out by* ***Mr. Santosh Basavaraj Patil*** *for the award of the degree of* ***Doctor of Philosophy in Faculty of Pharmacy*** *under the guidance of* ***Dr. Pramod C Gadad,*** *Professor, Department of Pharmacology, KLE College of Pharmacy, Nipani.*

Place: Hubballi

Date:

Prof. (Dr). AHM Viswanatha Swamy
Principal,
KLE College of Pharmacy, Hubballi
KAHER, Belagavi.

KLE ACADEMY OF HIGHER EDUCATION AND RESEARCH,

(Deemed-to-be-University)

[Declared as Deemed-to-be-University u/s 3 & 12B of the UGC Act, 1956 vide Govt. of India Notification No.F.9-19/2000-U.3 (A)]

(Accredited 'A^{+}' Grade by NAAC) (3rd Cycle)

[Placed in Category 'A' by MoE (GoI)]

BELAGAVI

CERTIFICATE

This is to certify that the thesis entitled **"Role of Macro and Micronutrients in the Management of Glycogen Storage Disease Manifestations – A Preclinical Study"** *is a bonafide record of original research carried out by* ***Mr. Santosh Basavaraj Patil*** *the award of the degree of* ***Doctor of Philosophy in Faculty of Pharmacy*** *under my supervision and guidance.*

Place: Hubballi

Date

Dr. Pramod C Gadad
Professor and Principal,
Department of Pharmacology
KLEs College of Pharmacy, Nipani

Dedicated to my beloved parents, entire family & Almighty

ACKNOWLEDGMENT

I take this privilege and pleasure to acknowledge the contribution of multiple individuals who have been inspirational and supportive throughout for the study period and endowed me with the most precious knowledge to see success in my endeavour. This Ph.D. work bears the imprint of all those people, I am grateful to.

I would like to express my deepest sense of gratitude, thankfulness and appreciation to my esteemed and beloved research guide **Dr. Pramod C Gadad**, Professor and Principal, Department of Pharmacology, KLE College of Pharmacy, Nipani for his patience, constant inspiration, motivation, enthusiasm, immense knowledge, excellent guidance and co-operation during this study. His simplicity, caring attitude and provision of fearless work environment will be cherished in all walks of my life. I shall forever remain indebted to him for having inculcated in me a zeal for research and a quest for knowledge. I thank him for all his advice and for always guiding me in the right direction

I am highly grateful Vice- Chancellor **Dr. Nitin M. Gangane**. I express my deep gratitude to Registrar **Dr. M. S. Ganachari** for his valuable guidance, constant inspiration, encouragement and persistent help throughout my dissertation work. I express my deep gratitude to former Director of Academic Affairs **Dr. Daksha Dixit** and present director **Dr. Roopa M Bellad**. I express my special thanks to **Dr. Sunil S Jalalpure**, Principal, KLE College of Pharmacy, Belagavi for extending his help and kind co-operation.

I gratefully acknowledge **Prof. (Dr.) P.A.Patil**, Professor, USM KLE, Belagavi, **Dr. Dr Alka Kale, Dr Subhas Karki**, Dr. P.M. Ronad, Dr. G.A.Hampannavar, Dr. N.M. Jeedi, Dr. S.K. Nimbal, Dr. S.B. Nyamagoud, Shri. Harish K H, Dr. Pradeep Kumar M.R, Dr. Laxmi Pattanashetti, Dr. Revati Sagare, Dr. (Smt). A.A. Ankalikar, Dr. Abhishek B J, , Shri. R.V.Karadi, Dr. (Smt). K.S.Akki, Dr. H.N.Sholapur, Dr. (Smt). F.S.Dasanakoppa, Dr. K.P.Manjunath, Dr. S.S.Honnalli Dr. B C Koti, Dr. V G Jamakandi for their guidance and invaluable support.

My sincere thanks to Librarian Shri. V P. Patil and all the non-teaching staff for their constant guidance and invaluable help.

I owe my special thanks and gratefully acknowledge Dr. Bhrigukumar Das, Dr. Vishal Patil, Dr. Deepak Yaraguppi, Ms. Rashmi Devagudi, Ms. Najmin Muzawar, Mr. Saurav Raj, Ms. Megha Hegde, Mr. Dhanjay Tikadar, Dr. Anirudh Pai for providing invigorative and conductive environment to pursue this research work with great ease.

I express my immense gratitude and love to my greatest source of inspiration, my grandparents Shri Somanagouda I Patil and Smt. Sarojini S Patil, Shri. Vasantagouda Patil and Smt. Kamala V Patil. My parents Shri Basavaraj S Patil and Smt. Karuna B Patil and my sister Smt. Smita P Saraf for being an ever-loving family and for their endless encouragement, guidance and support through all these years.

A special word of thanks is to my dearest wife Smt. Sujata S Patil and son Shreyas S Patil who have cheerfully endured the hardships in my life and for their love, constant encouragement, patience and appreciative understanding.

Most importantly, I thank the Lord Almighty for continually blessing me, and giving me the strength and wisdom in fulfilling all my endeavours.

Mr. Santosh B Patil

Table of Contents

LIST OF ABBREVIATIONS

Sl No.	Abbreviation	Definition
1	GSD	Glycogen Storage Disease
2	SLC	Solute Carrier Proteins
3	CGA	Chlorogenic Acid
4	MD	Molecular Dynamics
5	UCCS	Uncooked Corn Starch
6	TG	Triglycerides
7	ATP	Adenosine Tri Phosphate
8	ER	Endoplasmin Reticulum
9	MRI	Magnetic Resonance Imaging
10	CRISPR	Clustered Regularly Interspaced Short Palindromic Repeats
11	SGLT	Sodium-glucose co-transporter
12	TIM	Gastro-intestinal Model
13	G6PT	Glucose-6-phosphate translocase
14	CSF	Cerebrospinal Fluid
15	TRB-3	Tribbles-related protein-3
16	GSK-3	Glycogen synthase kinase-3
17	NMR	Nuclear Magnetic Resonance
18	QGR	Quercetin 3-O-α- (2″-galloyl) rhamnoside
19	HPLC	High Performance liquid Chromatography
20	GIT	Gastro Intestinal Tract
21	CAL	Chlorogenic Acid loaded liposomes

22	IGT	Impaired Glucose Tolerance
23	FBG	Fasting Blood Glucose
24	GLUT	Glucose Transporter
25	AMP	Adenosine Mono Phosphate
26	AMPK	Adenosine Mono Phosphate Kinase
27	MALA	Metformin Associated Lactic acidosis
28	MILA	Metformin Induced lactic acidosis
29	PDB	Protein Data Bank
30	GCBE	Green coffee bean extract
31	SEM	Standard error of mean
32	ANOVA	Analysis of Variance
33	SD	Standard Deviation
34	TCA	Tricarboxylic acid cycle
35	UV-Vis	Ultraviolet-Visible
36	IR	Infrared Radiation
37	PMID	PubMed IDentifier
38	SPC	Simple Point Charge
39	NPT	Number of particles, Pressure, and Temperature
40	RMSD	Root Mean Square Deviation
41	RMSF	Root Mean Square Fluctuation
42	RG	Radius of Gyration
43	SASA	Solvent Accessible Surface Area
44	CHARMM	Chemical at Harvard Molecular Mechanics
45	SAVES	Structure Analysis and Verification Server

	PROCHECK	Program to Check the Stereochemical Qquality of Protein structures.
47	ERRAT	Errors leading to random distributions of atoms
48	MM-PBSA	Molecular mechanics Poisson–Boltzmann surface area
49	GROMACS	GROningen MAchine for Chemical Simulations
50	PCA	Principal Component Analysis
51	TSCR	Taussky-Shorr color reagent
52	LDH	Lactate Dehydrogenase
53	DGKC	Deutsche Gessel schaft fur Klinische Chemie
54	NADH	Nicotinamide Adenine Dinucleotide + Hydrogen
55	4-AAP	4-Aminoantipyrine
56	DAP	Dihydroxyacetone Phosphate
57	ESPAS	N-Ethy-N-sulfopropyl-n-methoxyaniline
58	PAS	Periodic Acid-Schiff
59	PRO	Protein Data Bank
60	LIG	Ligand
61	ASN	Asparagine
62	ASP	Aspartate
63	OD	Optical Density
64	MET	Metformin Hydrochloride
65	APO	Protein Alone
66	BE	Binding Energy
67	PMN	Polymorphonuclear Neutrophils

LIST OF TABLES

List of Figures

ABSTRACT

Background

Glycogen storage disease type 1 (GSD type 1) is an inherited metabolic disease resulted due to the impaired glucose-6-phosphatase enzyme complex, which is important in glycogen metabolism. The enzyme complex glucose-6-phosphatase (G6Pase), is encoded by G6PC1 gene, and the glucose-6 phosphate translocase or transporter subunit (G6PT), which is encoded by the SLC37A4 gene. The major manifestations of GSD type 1 are hypoglycemia, excessive glycogen accumulation, hepatomegaly, hyperuricemia, hyperlactatemia. This study investigates the induction and management of GSD I symptoms. It is known that metformin may affect the levels of lactic acid, and that chlorogenic acid (CGA), which is prevalent in green coffee and present in various kinds of fruits, inhibits the enzyme glucose-6-phosphatase complex and micronutrients which inhibits the glycogenesis process were employed for the management of hepatic glycogen accumulation, which is responsible for further other manifestations as mentioned above.

Objectives: To establish a chemically induced GSD model, which could facilitate to investigate the most common GSD type 1 manifestations and to investigate the influence of dietary regimen consisting of macronutrients and micronutrients in experimentally induced GSD manifestations.

Methodology: The study was divided into *in silico* and *in vivo* approach to assimilate the manifestations of GSD type 1 and manage the same. The *in silico* approach was employed to study the binding patterns of Glucose-6-phosphatase (G6Pase) and the SLC37A4 target using molecular docking and molecular

dynamics simulations. On the other hand the *in vivo* studies were conducted to investigate the effects of chlorogenic acid (CGA) on GSD type 1 manifestations. A dosage of 200 mg/kg of CGA was found to be effective via. pilot study to induce hypoglycemia in rats, to enhance the impact of CGA, drinking water containing CGA was continuously subjected to the animals along with Metformin 500 mg/kg. to induce other manifestations like lactic acidemia. Management of GSD type 1 manifestations was attempted through selected macro and micronutrients. In silico methods were used to select micronutrients based on drug likeness, while macronutrients were chosen based on literature review.

Results and Discussion: The molecular docking studies revealed the interaction between G6Pase and CGA ligand, and the MD simulations provided insights within the structural modifications of SLC37A4 following ligand binding. Similarly, the micronutrients were docked with the major enzymes involved in glycogenesis and were validated via MD simulations. The combination of micronutrients and cassava starch resulted in improvements in various parameters like liver weight/hepatomegaly, liver glycogen content, fasting blood glucose, and liver histology.

Conclusion: Overall, this study provides insights into the biochemical basis of GSD type 1 and potential disease management strategies. Thus, the use of chemically induced animal models and in silico approaches contributes to our understanding of the disease and its management. The inclusion of macro and micronutrients demonstrated their unique and complementary effects in different ways. Both UCCS and Cassava Starch include complex carbohydrates that are thought to undergo a sustained conversion into glucose, they both showed a

progressive retention of normoglycemia, with Cassava Starch out performing UCCS even in combination with micronutrients like, β-carotene, Vitamin-C, Vitamin-E and Riboflavin

Keywords: Glycogen Storage Disease, Chlorogenic acid, Glycogenesis, Glycogenolysis, Hypoglycemia, Glucokinase, Glycogen synthase, Protein phosphatase-1

1. INTRODUCTION

1.1 Background

The glycogenoses, also known as glycogen storage diseases (GSD), are a group of inherited metabolic diseases brought on by inadequate levels or absolute absence of the enzymes that regulate gluconeogenesis or glycogenolysis pathways.[1] Hepatic GSD is characterized by hypoglycemia, while muscular GSD is characterized by weakness and cramps in the muscles. These conditions affect between 1 in 20,000 and 43,000 live babies on average. Eighty percent of hepatic GSDs are type I, type III, and type IX, with type I being the most common.[2]

Von Gierke's disease, generally known as GSD type I, is further divided into types Ia and Ib. GSDIa is caused due to insufficient activity of G6Pase – α.[3] and scarce glucose-6-phosphate transporter activity (G6PT) results in to GSD Ib.[4] Both conditions lead to manifestations such as hypoglycemia, hepatomegaly, excessive glycogen buildup mostly in the kidney and liver, which causes hepatomegaly and nephromegaly to progress hyperuricemia, lactic acidemia, hyperlipidaemia.[5]

One in 100,000 individuals have GSD I, of which 80% suffer GSD Ia and 20% with GSD Ib.[6] Apart from the clinical signs and manifestations of GSD type Ia, type Ib is characterized by recurrent infections, neutropenia, and neutrophil dysfunction[7] due to compromised glucose transport via the polymorphonuclear leukocytes' cell membrane. It has been proposed that the transfer of microsomal glucose-6-phosphate (G6P) contributes to neutrophil antioxidant defence and that a genetic deficiency in the transporter causes apoptosis and cellular dysfunction, which serves as a possible reason for the malfunctioning of neutrophils. In older children and adults, long-term consequences can include hepatic adenomas,

hepatocellular carcinoma,[8] progressive renal failure and renal calculi, and irritable bowel disease.[9] Liver biopsy is still the most reliable diagnostic method for most GSD patients in order to determine the accumulation of glycogen in the hepatocytes. Additional diagnostic methods consist of biochemical parameter estimation, mutation analysis, and enzyme assay, which, especially in cases of GSD type Ib, can indicate neutropenia, hyperuricemia, hyperlipidaemia, hypoglycemia, and lactic acidemia.

Managing GSD symptoms is a really challenging process. The GSD patient needs to closely rely on a diet rich in carbohydrates (every three to four hours) and uncooked corn starch (UCCS), which is free of other macronutrients and simple sugars like lactose (found in dairy products), fructose (found in fruits), and sucrose (found in refined sugar). Excessive consumption of non-utilizable sugars should be avoided at all costs since this might result in the buildup of glycogen in various tissues and the natural synthesis of uric acid, triglycerides (TG), and lactate. Restricted intake of both essential micronutrients and macronutrients could result from such dietary restrictions.[10]

There is evidence that a few micronutrients, such as selenium, Riboflavin, β-carotene, Vitamin-C, Vitamin-E, thiamine, and Vitamin-D, [11–14] influence the way the glucose is metabolized and may alleviate a few GSD symptoms.

Though genetically altered cells and gene-knockout animals can serve as disease models, The literature indicates that developing and sustaining It is a difficult task to develop a disease model for GSD. These models provide significant challenges in terms of their cost, stability, survivability, and maintenance. According to a review of the literature, a few chemical derivatives, such as chlorogenic acid

(CGA), a kind of hydroxycinnamic acid, have been identified in a variety of fruits and at higher concentrations in green coffee beans [15] and have been demonstrated to inhibit the particular enzyme G6Pase complex, which can mimic the reaction or exhibit symptoms resembling GSD type I. The goal of the current study is to evaluate the impact of using macro and micronutrients to control or manage the manifestations and to ascertain how well these chemical compounds replicate the distinctive GSD manifestations. The macronutrients utilized were uncooked corn starch and cassava starch. as per the literature review and A few micronutrients were chosen for the investigation based on an *in silico* analysis like β-Carotene, Riboflavin, Vitamin C, Vitamin E. Maintaining normoglycemia during the day and night is essential in GSD It could be accomplished either by frequent consumption of meals or continuous administration of glucose via gastric tube [16] and/or feeding the uncooked raw corn starch/ flour (UCCS).[17] Nonetheless, the patient may consume frequent meals throughout the day, but at night they must rely on UCCS, which is subject to temporal constraints of its own such as inadequate dietary intake, fiber. Complex carbohydrate, stand a chance to be pursued for a superior substitute starch, such as tapioca or cassava starch, can help maintain normoglycemia longer than UCCS alone, while also preserving the nutritional value of the diet.[18] Etiology of GSD type 1 mainly depends upon the Glycogenolysis pathway, where the Glucose-6-phosphatase enzyme is either suppressed or completely absent, our hypothesis is to suppress this enzyme with CGA to induce the GSD type 1 manifestations (Figure 1).

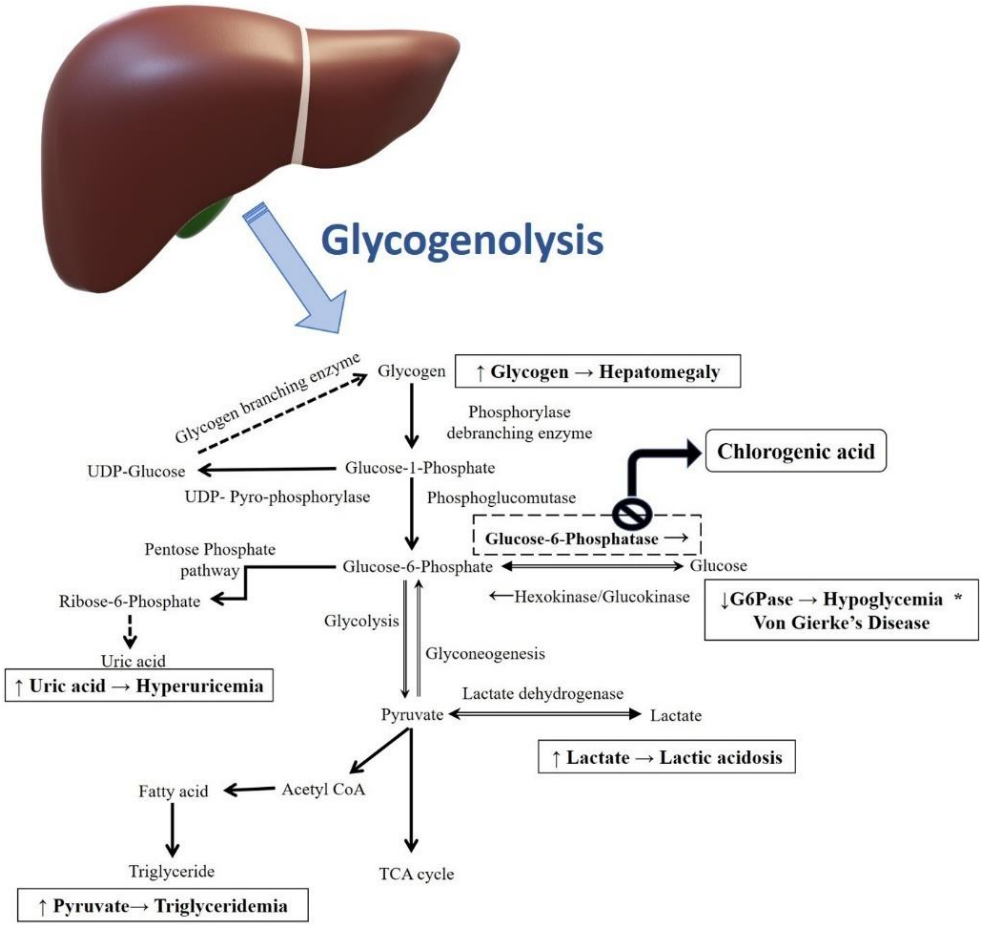

Figure 1: Glycogenolysis pathway, with emphasis on the process of enzyme inhibition and the manifestations caused due to its inhibition.

Hepatic glycogen buildup is the next significant manifestation of GSD type 1, which is attributed due to upregulated Glycogenesis and Underregulated Glycogenolysis,[19] this causes hepatic dysfunction and eventual hepatomegaly in more advanced cases, In an effort to tackle this problem, our goal was to halt the glycogenesis process by deactivating the three main enzymes involved in the glycogen production pathway: protein phosphatase 1 enzyme, glycogen synthase, and glucokinase.[20] A few specific micronutrients were used to aid in this process.

In a nutshell macronutrients are anticipated to sustain normoglycemia for as long as feasible, while micronutrients are anticipated to mitigate the build-up of glycogen in the liver, preserving the liver's normal architecture and physiology. (Figure 2).

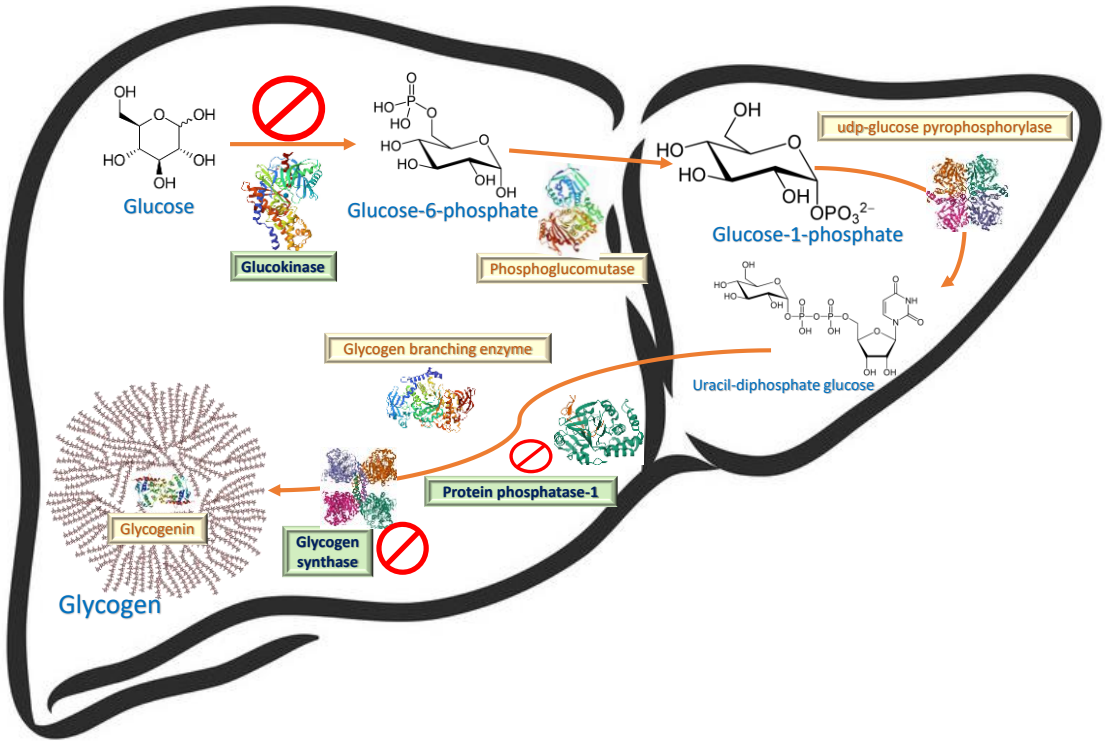

Figure 2: Glycogenesis pathway with emphasis on specific enzyme targets which can be suppressed to improve the glycogen accumulation

1.2 Justification for the study

The fundamental objective of GSD treatment should be to sustain blood glucose levels all both during the day and at night. This can be either achieved via eating more often, or by continuous glucose feeding therapy, or by consuming

uncooked corn starch (UCCS).[21] However, while the patient can have frequent meals throughout the day, they must rely on UCCS at night. and previous studies have suggested that corn starch therapy can only prevent hypoglycaemia for a median time of 4.25 h in children. As a result, the patient is required to wake-up at night for timely feed of UCCS, failing to which, may lead to episodes of hypoglycaemia, developmental delay, hepatomegaly, and poor growth.[22] Further, the UCCS is known to cause inflammatory bowel disease and gastric distress in case of GSD type Ib patients. Thus, it is required to study some alternative starches like cassava root starch or its derivatives like tapioca starch or sweet polvilho, which may prove to be better than UCCS. The main concern in the management of GSD I is consumption of non-utilizable carbohydrates in excess, which leads to glycogen storage and overproduction of uric acid, triglycerides, and lactate. In general, excessive sugar intake may increase the risk of hepatomegaly.[23] Thus, the patient has to depend meticulously on regular diet rich in carbohydrates (every 3–4 hours), devoid of simple and non-utilizable carbohydrates such as lactose (found in dairy goods), fructose (found in fruits), and sucrose (found in sugar).[24] Such dietary restrictions may result in diminished micronutrient nutrition.

Very few studies have explored about the influence of macronutrients and micronutrients on glycogen metabolic disorders. The restricted consumption of milk and fruits necessitates supplementation with a multivitamin-mineral supplement that includes calcium.[25] along with magnesium, niacin, pyridoxine, vitamin E etc. Hence, Determining the combined impact of macro and micronutrients can be aided by the current investigation with the aim of:

To prevent the manifestations associated with hepatic GSD.

For better management of existing manifestations.

To improve the prognosis of the hepatic GSD patients.

By examining the influence of macronutrients and micronutrients on GSD type 1, this study aims to provide valuable insights into the optimal dietary management of this metabolic disorder and also in process of this, understanding the role of specific nutrients in preventing and managing GSD-related complications can lead to improved patient outcomes and a better quality of life for individuals with GSD.

2. AIMS AND OBJECTIVES

To establish a suitable chemically induced GSD type 1 model, and to determine the role of macro and micronutrients in mitigating the manifestations of GSD type 1.

OBJECTIVES

Primary objective

- To induce the manifestations of hepatic GSD in Wistar rats.

Secondary objective

- To investigate the influence of dietary regimen consisting of macronutrients and micronutrients in experimentally induced GSD manifestations.

3. REVIEW OF LITERATURE

A series of systemic review, analysis based on the research question has been made focusing on the possible associated relationship between the Glycogen Storage Disease (GSD), its manifestations with nutritional deficiency, by emphasizing on the following key words as GSD, hypoglycemia, hyperuricemia, lactic acidosis, hypertriglyceridemia, hepatomegaly, uncooked corn starch, alternate starch, macronutrients and micronutrients.

3.1.1.1. Introduction to Glycogen Storage Disease

Glycogen storage diseases (GSDs) represent a heterogeneous group of hereditary metabolic disorders stemming from deficiencies in enzymes pivotal for glycogen metabolism. Glycogen, an intricately structured polysaccharide, shoulders a critical role as the primary reservoir of glucose within hepatocytes and myocytes. Its dynamic interplay with glucose regulates energy homeostasis, primarily in the liver and skeletal muscles, thereby influencing systemic glucose levels. Its role in the liver is to supply a source of glucose so that blood glucose levels remain within the normal range throughout the intervals in between meals. In the muscle, Glycogen delivers glucose for the synthesis of ATP and glycolysis, which are necessary for the energy needs of active contracting muscle cells.(17) Dysregulation in the synthesis or breakdown of glycogen, attributed to genetic aberrations affecting specific enzymes, precipitates a spectrum of clinical phenotypes.(6)

3.1.1.2. Types of GSD

Glycogen storage diseases (GSDs) are categorized according to the affected tissues and the particular enzyme deficit. Types I, III, VI, and IX are notable in this regard, each exhibiting distinct physiological disruptions and dietary treatment considerations.(26,27)

GSD type I, also referred to as Von Gierke's disease, is the most prevalent form, with type Ia corresponding to about 80% of GSD type I cases.(20) GSD type Ia is characterized by fasting hypoglycemia, growth retardation, hepatomegaly, and renal disease.(28) Whereas, GSD type Ib is distinguished from type Ia by additional complications such as neutropenia and neutrophil dysfunction, which can result in infections and inflammatory bowel disease. (9,29)

In conclusion, GSDs encompass a group of disorders with various types, each linked to specific enzyme deficiencies and clinical outcomes. Among these, GSD type I is the most prevalent, with type Ia being the most common subtype. It is characterized by a range of symptoms, including hypoglycemia, hepatomegaly, and renal complications.

3.1.1.3. Etiopathogenesis of GSD type 1

GSD type 1, is further classified into two subtypes: type 1a and type 1b. The underlying mechanisms and potential therapeutic strategies. The etiology of GSDs primarily resides in monogenic defects affecting genes encoding enzymes responsible for glycogen metabolism. The enzymes that are missing or under processed are G6Pase in case of GSD type 1a and in case of GSD type 1b the enzyme deficient is glucose-6-phosphate translocase (G6PT), these enzymes are involved in the final step of gluconeogenesis and glycogenolysis. This deficiency leads to impaired glucose

homeostasis, resulting in fasting hypoglycemia, hepatomegaly, and other manifestations like hyperuricemia, hyperlactatemia and hyper triglyceridemia. The gene that encodes The catalytic component of G6Pase, which is accountable for GSD type 1a is G6PC which is located in chromosome 17q21 and SLC37A4 gene is responsible for GSD type Ib.(30) Numerous mutations have been identified in this gene, leading to a wide spectrum of clinical manifestations and severity. Characteristically the blood glucose levels rise and endogenous glucose synthesis is inhibited during the postprandial phase. Exogenous glucose is either converted by the skeletal muscle and hepatocytes into pyruvate or stored as glycogen, and then pyruvate is transformed into acetyl coenzyme A, or acetyl-CoA, in aerobic conditions. Subsequently, acetyl-CoA initiates the citric acid cycle, producing ATP, carbon dioxide, and water, or it can be utilized to synthesize fatty acids. On the other hand, lactate, which is produced under anaerobic circumstances from pyruvate, serves as a crucial substitute fuel during hypoglycaemic episodes. (31)

These gene mutations and enzymatic deficiencies disrupt the intricate orchestration of glycogenolysis and gluconeogenesis, leading to aberrant glycogen accumulation. Such perturbations elicit a cascade of pathophysiological consequences, manifesting as distinct clinical presentations in both GSD type 1a and type 1b.

The pathogenesis of Glycogen Storage Disease (GSD) type 1a involves the dysregulation of glucose metabolism and glycogen storage. In individuals without the disease, glycogen is synthesized and stored in the liver when there is an excess of glucose available, and it is broken down to release glucose as needed. However, in GSD type 1a, the inability to convert glycogen into glucose leads to a surplus stores of glycogen in hepatocytes. This accumulation disrupts the normal architecture of the

liver and impairs its function. Additionally, the inability to carryout glycogenolysis leads to the diversion of the pathways leading to excessive synthesis of Uric acid, lactic acid and fatty acids which further exacerbate the metabolic abnormalities observed in GSD type 1a.(32)

In contrast, GSD type 1b is characterized by a deficiency of G6PT, It is in responsible for transferring glucose-6-phosphate (G6P) into the lumen of the endoplasmic reticulum (ER) from the cytoplasm. This transport step is necessary to preserve glucose homeostasis and regulating glycogen metabolism. The gene responsible for GSD type 1b is located on chromosome 11q23 and encodes the G6PT protein. Mutations in this gene result in impaired glucose transport into the ER, leading to reduced availability of G6P for glucose production and glycogen synthesis.(33) Studies have testimonies that in case of GSD type Ib, significant neutropenia is frequently observed, around 87% have reported with neutropenia. Upon further investigations. In GSD type Ib, the outcomes of bone marrow exams have been variable, ranging from normal to myeloid hyperplasia and maturation arrest. The outcome of the study confirm a wide forms of compromised neutrophil function, and neutrophils are metabolically dormant when at rest. Since neutrophils lack mitochondria, they must either mobilize extracellular glucose or intracellular glycogen in order to produce nicotinamide adenine dinucleotide phosphate and supply energy.(34)

3.1.1.4. Clinical Manifestations of Glycogen Storage Disease type 1

Clinically, the manifestations of GSDs encompass a broad spectrum of symptoms, reflecting the diverse tissue distribution and physiological roles of glycogen. Common

clinical features include hepatomegaly, hypoglycemia, lactic acidosis, hyperuricemia growth retardation, muscle weakness, and exercise intolerance. On the other hand there are few lesser common manifestations like delayed puberty, pulmonary or systemic hypertension, gout, renal insufficiency, and vitamin D deficiency.(35) The severity and onset of symptoms vary markedly among GSD subtypes, ranging from neonatal lethality to mild, late-onset presentations. (36) whereas in case of GSD type 1 b there is additional concern of neutropenia and neutrophil dysfunction along with all other manifestations of GSD type 1 a, which is the main reason for frequent infections due to compromised immune system.(37) Additionally, GSDs may precipitate life-threatening complications such as liver failure, cardiomyopathy, and neurological impairment, underscoring the multisystemic impact of disrupted glycogen metabolism.(38,39)

Diagnosis of GSDs necessitates a comprehensive approach integrating clinical evaluation, biochemical analyses, and molecular genetic testing, for screening and diagnosing glycogen storage diseases. Biochemical studies involve analysing blood samples to reveal characteristic abnormalities by measuring specific markers, such as glucose, lactate, uric acid levels, and in some cases even lipid profiles, and few lesser prominent biomarkers such as hepatic adenomas, cardiomyopathies, skeletal muscle dysfunction, growth retardation, osteopenia, neutropenia, and intestinal inflammation.(40) Further, histological findings done by tissue biopsy complement the diagnosis, Ultimately, the genetic analysis plays a pivotal role and is a more definitive method for diagnosing GSDs, as it can identify specific gene mutations associated with each type of GSD. Moreover, imaging techniques such as ultrasound and MRI can be used to assess the size and structure of organs affected by GSDs, such

as the liver and kidneys in GSD type I. These techniques not only help in confirming the diagnosis, but also in facilitating disease prognosis, and guiding familial counselling. Moreover, advancements in next-generation sequencing techniques have enhanced the precision and efficiency of genetic diagnostics, enabling timely interventions and personalized management strategies.(41,42)

3.1.1.5. Disease Management

Currently, there are no specific pharmaceutical treatments available for GSD type 1.(43) However, research is ongoing to explore potential therapeutic options. Animal models have played a crucial role in understanding GSD type 1 and developing potential treatments. For example, transgenic mouse models with a scarcity in glucose-6-phosphatase (G6Pase), the enzyme affected in GSD type 1, have been utilized to study the disease mechanisms and test therapeutic interventions. These models have provided insights into the pathophysiology of GSD type 1 and have been used to evaluate gene therapy approaches, enzyme replacement therapy, and pharmacological interventions such as gene expression modifiers. Additionally, gene editing technologies such as CRISPR-Cas9 are being investigated as potential therapeutic options for GSD type 1. However, further research is required to evaluate the stability, effectiveness and safety of these emerging therapies before they can be implemented in clinical practice. Thus, our study attempts to manage the GSD type1 manifestations using alternative starch and by using certain vitamins and micronutrients to overcome several manifestations like hypoglycemia, hepatomegaly, hyperlactatemia, and metabolic disturbances. Management of GSDs revolves around multidisciplinary care aimed at mitigating symptoms, preventing the complications, and optimizing the metabolic stability. Therapeutic modalities encompass dietary

interventions tailored to individual needs, pharmacological agents to ameliorate metabolic derangements, and supportive measures addressing specific organ involvement. In select cases, innovative approaches such as gene therapy hold promise for correcting underlying enzymatic deficiencies and attenuating disease progression.(33) In case of GSD type 1b the major manifestation is neutropenia and neutrophil dysfunction, there are few evidences that SGLT2 inhibitors can be of some help in maintaining the normal functioning of neutrophils.(44) The management of GSD type I also includes pharmacological therapy and close monitoring to prevent long standing complications like hepatic adenomas, renal disease, and hyperlipidaemia. Overall, GSD type I is a complex metabolic disorder that requires a multidisciplinary approach for optimal management, involving close collaboration between metabolic specialists, dietitians, and other healthcare professionals.(36)

3.1.1.6. Disease modifying Intervention

3.1.1.6.1. Role of Macronutrients

Patients with GSD type I require lifelong dietary management, including frequent feedings of uncooked cornstarch and continuous glucose supplementation to maintain euglycemia and prevent hypoglycaemic episodes.(18) The study by Terry *et al*., claims that in GSD patients, there is very less room for error, as the therapeutic window for dietary management is very small, due to which, under treatment may lead to hypoglycemia, whereas, over treatment can cause excessive glycogen accumulation and metabolic instability. The primary goal of the treatment for GSD should be to maintain normoglycemia, this is achievable through either, having meals more frequently, or continuous glucose therapy or including uncooked cornstarch for the nocturnal treatment. Dietary management in hepatic GSD should be designed by

restricting the diet consisting sucrose, fructose and galactose. The main concern is the unnecessary over consumption of non-utilizable carbohydrates, leading to glycogen accumulation and abnormal synthesis of lactic acid, uric acid and triglycerides in GSD I patients.(45) Managing GSD symptoms is a challenging endeavor. The GSD patient must closely rely on a diet rich in carbohydrates (every three to four hours) and uncooked corn starch (UCCS), which is devoid of other macronutrients and simple non-complex sugars like lactose (found in dairy products), fructose (found in fruits), and sucrose (found in refined sugar). Excessive consumption of non-utilizable sugars should be avoided as this can cause tissues to store glycogen and increase the body's natural synthesis of uric acid, triglycerides, and lactate. Such dietary restrictions raise the risk of inadequate intake of micronutrients.(46) Similarly, *Correia* and group of researchers compared the efficacy of a new modified experimental starch (heat-moisture processed cornstarch) with the currently used corn starch therapy in patients with type Ia and Ib GSD. The study was a crossover pilot research that was randomized, double-blinded, and had 12 participants (Each 6 with GSDIa and GSDIb) who were at least 13 years old, the experimental starch was compared to the commonly used uncooked cornstarch. The subjects were given 100 g of digestible starch at 2200, and hourly measurements of glucose and lactate were made until the subjects' plasma glucose concentration reached 60 mg/dL or until they had completed a 10-hour fast. The products were examined in a blinded, randomized sequence. The experimental starch prevented hypoglycemia better than standard treatment (i.e. ≤60 mg/dL). In addition to improving safety, this therapy may enable GSD patients to sleep through the night without waking up for treatment.[16]

There are still disagreements on the best dietary strategy for treating GSD type 1 even though there has been considerable progress in the treatment of these patients. Discussions involve around seven of the main disputes:

1) Appropriate dietary limitations 2) Dosing of carbohydrates in diet 3) Per day dosage of cornstarch 4) The utilization of waxy maize starch with prolonged release. 5) Employing continuous feeds 6) Intervention with Ketogenic diet, and 7) Supplementation with certain micronutrients, and it is established that improved diet and nutrition have changed GSDs from a fatal condition to one with a favorable prognosis. (56) Owing to the GSDs' rarity, a multicenter partnership would be beneficial for researching a bigger patient population from various cultural backgrounds. For children and adults with these uncommon illnesses, exchanging treatment plans that work will enhance their quality of life and enhance the knowledge in patients.(23,39)

Several starch fractions were characterized and analyzed by Nalin and group wherein an *in vitro* dynamic gastrointestinal model, the digestion of various starches was investigated. The following UCCS brands were used in the study: the American companies Great Value® and Argo®; Dutch Maizena Duryea® from the Netherlands; Yoki® and Brazilian Maizena Duryea® from Brazil, additionally investigated were sweet polvilho cassava starch, a Brazilian sweet starch derived from cassava, and Glycosade®, a modified starch. The Glycemic Index method was used to assess the starch fractions, and the Gastro-intestinal Model (TIM-1 system), an *in vitro* dynamic, computer-controlled gastrointestinal model that served as a replica of the stomach and small intestine, was used to determine the digestion analyses. For the UCCS and Glycosade®, the final digested quantities were from 84 to 86%, but for sweet povilho,

it was 75.5%. The amount of starch that had been digested at 180 minutes, a crucial time point for patients with GSD, was 55.5% with sweet povilho and 67.9–71.5 for UCCS and Glycosade®. A final digested amount of 78.4% was discovered in an experiment with a mixture of Brazilian Maizena Duryea® and sweet polvilho starch; the value at 180 minutes was 61.7%. Sweet polvilho starch appears to release more slowly or over a prolonged period of time.(48)

3.1.1.6.2. Role of Micronutrients

There is evidence that certain micro nutrients, such as selenium (12), β-carotene, vitamin C, riboflavin, vitamin E, vitamin D, and thiamine, (10) affect how glucose is metabolized and help with a few GSD manifestations. An investigation on the effectiveness of vitamin E on the modulation of hepatic glycogen was conducted, on neutropenia, neutrophil dysfunction and Inflammatory Bowel Disease in the total number of GSD type 1b patients in Italy by Melis *et al*. where before and throughout vitamin E medication, the effectiveness of the vitamin in modifying neutrophil count and function, hospitalization frequency for infections, and inflammatory bowel activity were assessed on a regular basis for a year. The study revealed that the glycogen levels were regulated and also improved the neutrophil function during vitamin supplementation and the patients who were on Granulocyte-colony stimulating factor (G-CSF), the dose was reduced after the end of the study. The investigators of the research came to the conclusion that vitamin E supplementation is beneficial. There are unambiguous advantages of vitamin E over G-CSF, as it can be consumed orally, and it has no severe side effects[10]. Although using the techniques they employed in their investigation, the researchers were unable to find any impact

on neutrophil function. On the other hand, the neutrophil count mean value was considerably raised by vitamin E administration. When compared to the period without vitamin supplements, the detection rate of neutrophil count values below 500/mm3, which are linked to an increased risk of infections, was much lower during the vitamin E supplementation period. [18]

Glucose-1-Phosphate represents a pivotal compound situated at the convergence of various metabolic pathways, including glycolysis, glycogenesis, glycogenolysis, and gluconeogenesis. During the process of glycogenesis, glycogenolysis is suppressed, and conversely, when glycogenolysis takes place, glycogenesis is hindered. Anomalies in glycogen metabolism, marked by irregular glycogen accumulation resulting in severe hepatomegaly and, in more severe cases, hepatic dysfunction, In an effort to resolve this problem, we tried to block the glycogenesis process by deactivating the key enzymes in the glycogen production pathway, the three main enzymes involved were: glucose kinase, glycogen synthase, and backup enzyme protein phosphatase-1, with the assistance of a few select micronutrients like β-Carotene,(12) Riboflavin, (50) Vitamin C, and Vitamin E. (11,51,52)

The literature suggests the certain micronutrients can influence the Glycogenesis and the mechanism, where the effect of Hyperhomocysteinemia (HHcystemia) on hepatic glycogen synthesis. Mice were subjected to water comprising two percent methionine, which caused them to develop hyperhomocysteinemia. The hepatic glycogen level and the rate of glycogen synthesis were significantly reduced in HHcystemia-affected mice, whereas there was a rise in the phosphorylation of glycogen synthase. In animals with HHcystemia, there was an up-regulation of TRB3

(tribbles-related protein 3) expression in the liver, which coincided with the dephosphorylation of Akt and glycogen synthase kinase-3β.(53)

Diminished glycogen synthesis in the liver during the postprandial phase and impaired insulin secretion in the pancreas are the results of glucose kinase scarcity or inactivation, which impairs glucose metabolism in the hepatocyte and pancreatic β-cells. Patients with glucokinase deficiency see a reduced net increase in hepatic glycogen content following a meal in comparison to control.(54,55)

Glycogen synthase kinase-3 (GSK3) plays a crucial role in regulating glycogen synthase and glucose metabolism, as well as energy homeostasis. It is involved in various biological and pathophysiological processes. GSK3 has major regulatory role on glycogen synthase, and on the other hand can also contribute in the development of metabolic disorders. GSK3 inhibitors show potential as therapeutic targets for treating metabolic diseases. Clinical tests of GSK3 inhibitors have been conducted, indicating their potential application in clinical settings.(56,57)

Protein Phosphatase 1 (PP-1) key enzyme regulates the delicate balance between glycogen synthesis and degradation. PP-1 manages the process by which glycogen is synthesized and stored within cells. Its importance in glycogenesis is acknowledged by its ability to dephosphorylate and activate key enzymes involved in glycogen synthesis, thereby promoting the conversion of glucose into glycogen for energy storage.

The primary target of PP-1 in glycogenesis is glycogen synthase, the enzyme responsible for catalysing the formation of α-1,4-glycosidic bonds between the glucose molecules during glycogen synthesis. Glycogen synthase exists in both

phosphorylated (inactive) and dephosphorylated (active) forms, with PP-1 playing a pivotal role in the conversion between these states. By dephosphorylating glycogen synthase, PP-1 stimulates its activity, facilitating the incorporation of glucose residues into the growing glycogen molecule.(58) In summary, it is anticipated that the macronutrients will sustain normoglycemia for as long as feasible, while the micronutrients will lessen the amount of glycogen accumulated in the liver by blocking the process of glycogenesis, thereby preserving the liver's normal architecture and physiology. (59)

3.1.2 GSD type 1 Disease models

3.1.2.1. Genetic models

Understanding the mechanisms underlying Glycogen Storage Disease Type 1 and creating treatments for it depend heavily on animal models. Genetically modified animal models, such as mice and canine model, have been used to simulate the enzyme deficiencies seen in Glycogen Storage Disease Type 1.(60) These genetically modified animal models allow researchers to study the effects of the enzyme deficiencies on glycogen metabolism and identify potential therapeutic targets. Nonetheless, research indicates that creating and developing a disease screening model for GSD is an exhausting assignment. Although genetically altered cells and animals with gene knockouts function as disease screening models, the cost, maintenance, durability, and stability of these screening models have significant challenges. Similarly to evaluate chronic liver disease, a liver specific G6pc knock-out (*k/o)* mice model (L-G6pc-/-) was developed. Unlike total G6pc *k/o* mice, L-G6pc-/- mice survived and maintained normoglycemia postnatally. However, they developed hyperlipidaemia, lactic acidosis, and uricemia initially, which improved

after 6 months. Hepatomegaly, hepatic glycogen accumulation, and hepatic steatosis were observed, with MRI revealing hepatic nodules (<1mm) at 9 months and hepatocellular adenomas (1-5mm) in 30-40% of mice at 12 months, progressing to multiple adenomas in all mice by 18 months. This model provides insights into the GSD1a-related hepatic manifestations, such as the delayed development of hepatocellular adenomas.(61)

3.1.2.2. Chemically induced GSD type 1 manifestations by inhibiting G6Pase and G6PT

According to a review of the literature, green coffee contains a high concentration of specific chemical compounds, such as chlorogenic acid (CGA), a kind of hydroxycinnamic acid, which is found in many different fruits [13] and its derivatives are known to inhibit the particular complex of enzymes called G6Pase, which can mimic the reaction or symptoms of GSD type I.

Similar to CGA, many other chemical constituents and phytoconstituents have showed promising results in inhibiting the pivotal enzyme G6Pase, by which they can imitate the manifestations of GSD type 1 disease, claims like Mumbaistatin was proposed, which is referred to as an inhibitor of the G6Pase system. Mumbaistatin was extracted from Streptomyces sp. DSM1 1641 cells by reversed-phase chromatography and anion-exchange chromatography. To aid in the discovery of its structure, the acid-labile inhibitor underwent methylation. The structure of an aromatic dispirodiketal, a molecule with a unique ring system, was clarified using single crystal X-ray structural evaluation of a triple methylated dehydrated product, C31H24O11. Comprehensive 2D-NMR analyses involving Mumbaistatin and its methylation byproducts demonstrated that Mumbaistatin has the hydroxy-di-keto-di-

carboxylic acid structure 1, $C_{28}H_{20}O_{12}$, which self-condenses with water loss to produce the dispirodiketal when acidic or activated via methyl ester production. Comprehensive 2D-NMR analyses involving Mumbaistatin and its methylation byproducts demonstrated that Mumbaistatin has the hydroxydiketodicarboxylic acid structure 1, $C_{28}H_{20}O_{12}$, which self-condenses with water loss to produce the dispirodiketal when acidic or activated via methyl ester production. Anthraquinone derivative Mumbaistatin (IC50 = 5 nM) shows strong inhibition of G6PT. The anthraquinone derivative Mumbaistatin (IC50 = 5 nM) shows strong inhibition of G6PT.(63) The goal of the current research is to ascertain how closely these chemical compounds resemble the distinctive symptoms of GSD.

One more chemical by the name Kodaistatin, was studied where, a combination of two new substances, Kodaistatin A and Kodaistatin C, were obtained from Aspergillus terreus Thom DSM1 1247 cells. A variety of 2D NMR techniques, in particular ^{13}C-^{13}C correlation assessment, were applied to clarify the structure of kodaistatin-A. Kodaistatin A and C are hydroxylated derivatives that share highly substituted polyketide units and hydroxylated aspulvinones. The G6PT subunit of the G6Pase system, which is essential for metabolic regulation, is efficiently inhibited by both Kodaistatins.(64)

Certain plant-based studies also suggested the G6Pase inhibitory property, where the study investigated the inhibitory effects of quercetin 3-O-α- (2″-galloyl) rhamnoside (QGR), a flavonoid present abundantly in the leaves of *Bauhinia megalandra*, on G6Pase in the intact microsomal cells. The results show that QGR inhibits G-6-Pase in a concentration-dependent manner. QGR also increases the Km for glucose-6-phosphate without affecting the Vmax. According to the study, QGR inhibited the

glucose-6-phosphate transporter (G6PT) in a reversible and competitive manner without influencing the phosphate/pyrophosphate transporter or the catalytic component. Furthermore, QGR inhibited the gluconeogenic capacity of liver slices, indicating its potential for reducing glucose levels in diabetic patients.(65)

3.1.2.3. Chlorogenic acid as an inducing agent

Among these shortlisted chemical agents, chlorogenic acid was most favoured chemical along with metformin, as both have more dependable when it comes to stability and availability, and also, they are well tolerated in animals CGA has many supportive evidences that it can be a successful inhibitor of both G-6-Pase and G6PT enzyme complex, it has been studied in diabetic studies, especially in *in vitro* studies. Ong K, and team conducted the study in type 2 diabetes genetic model in HepG2 hepatocytes and found that the acute administration of CGA considerably reduced blood glucose levels during fasting condition along with simultaneous suppression of G6Pase expression and the mechanism was attributed to the capacity of CGA to suppress the Glucose 6-Phosphatase activity, which is required for gluconeogenesis as well as glycogenolysis[13]. Similarly, Herling and team studied the chlorogenic acid derivatives' pharmacodynamic profiles, such as those of S-3483 and S-4048, were in line with the compound's defined mechanism of action, which involves inhibition of G6Pase activity, suppression of glucose production in the hepatocytes, and a subsequent hypoglycemia.[19] Similarly Henry C and team studied a decaffeinated green coffee extract called Svetol and concluded that the phytochemical prevented the glucose-6-phosphate hydrolysis in intact human liver microsomes and competitively inhibited G6Pase in a dose-dependent fashion. G6Pase activity in the liver is increased by two to three times during starvation and diabetes. This suggests that dietary

substances aimed at, for instance, suppressing hepatic glucose synthesis could potentially target this enzyme system for improving diabetic hyperglycaemia. [20] Adolfo Andrade-Cetto aimed to investigate the theory that reducing hepatic glucose production would occur from using an inhibitor of G6PT to target gluconeogenesis, based on the previous study by (Hemmerle et al., 1997) where it was identified that chlorogenic acid is a specific inhibitor of the G6PT component in microsomes of rat liver [20]. Similarly the liver microsomal fractions studies were conducted by Bassoli *et al.,* where, CGA and its synthetic equivalents have been shown *in vitro* studies using intact vesicles from hepatocyte endoplasmic reticulum to inhibit the G6PT of the G6Pase enzyme complex and, consequently, block G6P hydrolysis, which confirmed the inhibitory effect of CGA on G6Pase activity in a dose-reliant manner, same as its synthetic derivatives. About 40% of the reported inhibition was seen at 1 mM CGA, while only a tendency was seen at 0.25 mM. However, 0.25 mM CGA has been shown to 50% block this action in intact microsome preparations.(39,69)

Bioavailability of CGA was extensively studied by Lafay *et al*., to identify that in which form, throughout the gastrointestinal tract, CGA is absorbed through the mucosa of the gut and the absorption site, using HPLC with coulometric detection, CGA and its metabolites were measured at different time periods (1.5, 3, 4.5, and 7 h) after the meal and the cecum, small intestine, and stomach contents subsequently, plasma and urine were estimated. While the contents of the small intestine and stomach degraded CGA (by 1%), the cecum hydrolysed 15–32% of the consumed chlorogenic acid into caffeic acid. CGA and caffeic acid were detected at 1.5 hrs in the plasma as well as urine sample, indicating that the absorption of chlorogenic acid occurs in the upper gastrointestinal system. Further, in order to study the absorption

of chlorogenic acid in the stomach, CGA was placed into the ligated stomachs of overnight fasted rats. The aorta and stomach vein both contained intact chlorogenic acid after 30 minutes of infusion. These findings demonstrated that intact chlorogenic acid is rapidly absorbed in the rat GIT especially in the stomach. [22]. Similarly, Gonthier *et al.,* studied that the process of absorbing chlorogenic acid in the digestive tract and its metabolism determine its biological characteristics. Additionally, by identifying and measuring the primary metabolites produced in rats fed diets supplemented with pure chemicals, they investigated the bioavailability of chlorogenic acid and contrasted it with that of caffeic and quinic acids. Urine and plasma comprised both intact CGA and its metabolites. Urine containing intact chlorogenic acid indicated that the compound has been absorbed in its original form.(71,72)

On the other hand the challenge of the hydrophilic nature of CGA can affect its bioavailability, which was evaluated by Feng *et al.,* who evaluated the CGA's difficulty to get past the barrier of the lipophilic membrane, which can hinder its bioavailability due to rapid metabolism. These considerations limited the effective utilization and availability of CGA for prolonged duration in the gastro intestinal tract and also its clinical application is limited. Therefore, to overcome this factor, the authors attempted to investigate Chlorogenic acid-loaded liposome (CAL) and its related pharmacological effectiveness. [18]

Chlorogenic acid has also been studied for its anti-hypertensive activity along with anti-diabetic property by Bhandarkar et al., they examined the various CGA dosages and reported that the rats subjected to a high-carb, high-fat diet had a daily chlorogenic acid intake of about 100 mg/kg. Lower doses of about 30 mg/kg/day for 8 weeks or

about 50 mg/kg/day for 12 weeks did not alter body weight or insulin resistance in mice. Studies using 200 and 300 mg/kg/day of chlorogenic acid, respectively, shown positive effects with drops in blood glucose levels. Chlorogenic acid dosages ranging from 25 mg to 900 mg per day have been utilized in prior human trials. Chlorogenic acid absorption through the digestive tract was investigated and described. In the small intestine, about $1/3^{rd}$ of the chlorogenic acid was absorbed. The gut bacteria hydrolysed and thoroughly processed the portion of ingested chlorogenic acid that made it to the colon.(74). Similarly, pre-clinical and clinical studies were conducted by Zuniga *et al*., evaluated the impact of CGA treatment on insulin sensitivity, release, and glycemic management in individuals with established impaired glucose tolerance (IGT). The study was hypothesized based on cumulative evidence of *in vivo*, animal models that have indicated that chlorogenic acid has substantial antidiabetic properties by improving the regulation of glucose homeostasis. A specific type of evidence pertaining to glucose metabolism shows that db/db mice that received a 12-week dose of chlorogenic acid (80 mg/kg/day) via probe experienced a notable decrease in fasting blood glucose (FBG). Relying over these investigations, the researchers carried out a randomised, double-blind, placebo-controlled clinical investigation involving thirty patients diagnosed with impaired glucose tolerance (IGT); fifteen of the patients were randomized to receive 400 mg of oral chlorogenic acid three times a day for a duration of twelve weeks, while the remaining fifteen patients were given a placebo. Anthropometric and metabolic measures, such as FBG, glycated haemoglobin A1c, and a lipid profile, were taken both before and after the intervention. The findings demonstrated a significant reduction in FPG concentration in the individuals treated with chlorogenic acid.(75).

Apart from inhibiting G6Pase enzyme, CGA is also studied for its protective role in alcoholic liver disease by Hyunjin *et al*., based on more pertinent research demonstrating the health advantages of CGA consumption, including a decreased risk of Alzheimer's disease, diabetes type 2, and cardiovascular disorders. In addition, it possesses anti-inflammatory and antibacterial qualities and protects the liver from acetaminophen poisoning. The authors have conducted the study on mice where, the animals were subjected to multiple doses of CGA acid at fixed interval of time. The animals received CGA (10-40 mg/kg per dose) orally after every 30 min interval once the animals were exposed to alcohol (3 g/kg per dose) for 7 consecutive days antioxidant activity(76).

Green coffee beans and its extract has rich CGA content,(77) as one of the dietary supplements that promote health, green coffee can be added to food preparations or enhanced products. Its protective effects are demonstrated by the reduction of type 2 diabetes and specific cancers, such as those of the colon and liver. (78) The mode of action of CGA was studied by Jung et. al., & Ong et. al., it was proposed that the inhibition of the enzyme that transfers glucose-6-phosphate and glucose absorption may be connected to the hypoglycemic mechanism of CGA. In rat liver microsomes, CGA has been found to be a unique selective reversible inhibitor of the glucose-6-phosphate translocase. As it is essential that endogenous glucose should be produced through glycogenesis and glycogen breakdown in order to support the function of glucose-6-phosphate-transporting enzyme, which is crucial for controlling blood glucose levels *in vivo*. Consuming CGA will lessen the amount of glycogen excreted by the liver in those with type 2 diabetes. Consequently, CGA has emerged as a viable option for the management of diabetes. Additionally, it was discovered that CGA

could alter blood glucose levels and increase insulin release that is mediated by glucagon-like peptide-1 (GLP-1). According to research, CGA may elevate the gene expression of glucose transporter 4 (GLUT4), decrease the synthesis of fatty acids, inhibit gluconeogenesis, turn on AMP-activated protein kinase (AMPK), and downregulate the gene expression of glucose-6-phosphate-translocase enzyme. By activating AMPK, CGA facilitates the migration of GLUT4 to cell membranes, hence enhancing glucose absorption.(79,80)

3.1.2.4. Metformin as a candidate compound to induce GSD type 1 manifestations

Several studies have been demonstrated to prove the effect of biguanides to induce lactic acidosis, not only that biguanides have similar mechanism of suppressing the hepatic glucose synthesis as that of CGA (i.e. by activating AMP-activated protein kinase), two independent studies by Quynh et al., and Bando et al., showed that Biguanides, a class of oral hypoglycaemic agents are extensively utilized in the management of type 2 diabetes. It is well known fact that due to the high risk of phenformin-induced lactic acidosis associated with a mortality rate of 50%, the drug was banned in the US market in the year 1976. In comparison to phenformin, metformin has a 10-20 folds lesser extent of causing lactic acidosis, however, still there is possibility of hyperlactatemia. The majority of Metformin associated lactic acidosis (MALA) cases were linked to underlying conditions like acute renal dysfunction caused by loss of volume, other potentially nephrotoxic agents, and subsequent radio-contrast media use, or hepatic insufficiency. While the prevalence of MALA is low, once it has been established, the mortality rate can be extremely high, particularly in the critical care environment, so discontinuation is recommended

in patients who are about to experience renal and multi-organ failure. Metformin-induced lactic acidosis (MILA) is a less frequent condition in which metformin appears to be the only cause of lactic acidosis with no obvious pathology and is commonly synonymous with acute intoxication.(81)(82)

3.1.3. *In silico* Approach

3.1.3.1. Molecular Docking

A computational technique called "molecular docking" uses structure to determine the binding posture and affinity between ligands and targets. Molecular docking and simulation approaches have become invaluable tools in drug discovery and development.(83) They enable investigators to anticipate the interactions and binding affinities between ligands, or small molecules or ligands , and target proteins, providing insights into the potential therapeutic effects of these compounds. Predicting a compound's ability to block an enzyme is a common application of molecular docking, especially when it comes to glycogen storage diseases. With the help of Molecular Dynamic simulation technique the binding affinity and interactions of these compounds with key enzymes involved in glycogen metabolism, researchers can gain valuable insights into their potential inhibitory effects. In this study we have employed to different modules, one is disease induction by inhibiting Glycogenolysis by suppressing G6Pase and G6PT, on the other hand we are preventing the glycogen accumulation in the liver cells by inhibiting glycogen synthesis via suppressing Glycogen synthase kinase, Glucokinase, and Protein phosphatase 1, so all these can be predicted with the help of Molecular docking and dynamic simulation studies.

Inhibition of glycogenolysis

Inhibition of glucose-6-phosphatase, which plays a crucial role in glycogenolysis, molecular docking studies can help predict the inhibitory activity of compounds such as chlorogenic acid.(84) Molecular docking has been applied in predicting the enzyme inhibitory activity of certain compounds to understand their potential impact on glycogen storage disease, SLC37A4 alpha folded model is the gene protein which encodes for G6PT, which can be inhibited by forming a docking complex with CGA ligand. In the context of glycogen metabolism, this predictive approach allows researchers to simulate the binding affinity and interactions of specific compounds with key enzymes involved in the disease pathway. By elucidating the inhibitory effects of these compounds on the relevant enzymes, valuable insights can be gained into their therapeutic potential for glycogen storage disease. This application of molecular docking provides a means to screen and identify potential drug candidates that could modulate the enzyme activity associated with the disease.(85)

Inhibition of Glycogenesis

For the specific inhibition of protein phosphatase 1, the control ligand often used is okadaic acid. Okadaic acid is a natural toxin produced by certain marine dinoflagellates and is a strong inhibitor of phosphatases in proteins, including Protein Phosphatase-1 (PP-1) and Protein Phosphatase-2A (PP-2A). By inhibiting PP-1, okadaic acid disrupts the dephosphorylation of glycogen synthase, leading to its activation and increased glycogen synthesis. This inhibition ultimately results in the accumulation of glycogen in cells. Therefore, okadaic acid is frequently employed in research settings to study the regulation of glycogen metabolism and related cellular processes.(86)(87)

Substrate docking or control docking refers to the process of a substrate molecule binding to a specific site on a protein or enzyme. In the context of the provided abstracts, several papers discuss substrate docking in different systems. Substrate docking is significant because it makes it possible to anticipate the binding interactions between a substrate molecule and a target protein.(88) It helps in understanding the structural and functional properties of enzymes and their substrates, which is important in fields such as clinical and biotechnological research

It aids in comprehending the structural and functional characteristics of enzymes and their substrates, which is important in fields such as clinical and biotechnological research.(89)

3.1.3.2. Molecular Dynamics-Simulation

Drug discovery will soon routinely use computational technologies such as molecular dynamics (MD) and related techniques. Their main advantage is that they address entropic effects and structural flexibility explicitly. As increasingly sophisticated hardware architectures and algorithms are used, this makes it possible to determine the thermodynamics and kinetics of drug target identification and binding more precisely.(90) MD simulations have shown significant strengths in simulating the biological processes between receptors and ligands, particularly in allosteric binding sites. MD simulations have wide range of applications including drug discovery, prediction of macromolecule structures, model development and allostery. It has been utilised in the early phases of medication design and development, among many other applications, to define disease development pathways. The evaluation of the membrane structure and its organisation, membrane permeability, lipid–protein, lipid–drug and protein–ligand interactions, subsequently, the protein structure and

protein dynamics are only a few of the many biomolecular systems for which MD simulations are used.(91)

The molecular docking was performed by using an Alpha Fold protein model as Jumper, J et al., (2021) explained that it is possible that highly accurate protein structure predictions can be done with Alpha Fold structure model. Alpha Fold is an amalgam of physical and bioinformatics methodologies: The authors designed components that acquire information from PDB data with a minimum of handcrafted feature imposition by utilizing a physical and geometric inductive bias (for example, Alpha Fold generates hydrogen bonds well without a hydrogen bond scoring function). This leads to a network that can handle the complexity and variety of structural data while learning far more effectively from the sparse data in the PDB. Specifically, Alpha Fold can generate precise models even in the absence of the physical surroundings.(92)

4. MATERIALS AND METHODS

4.1 Chemicals and equipment's/instruments used in the study

4.2. Pilot Study: Experimental model

4.2.1. In silico Approach : GSD type 1a

4.2.1.1. Molecular Docking

4.2.1.2. Molecular Dynamics-Simulation

4.2.2. In silico Approach : GSD type1b

4.2.2.1. Protein and ligand preparation

4.2.2.2. Protein structure information

4.2.2.3. Pocket information

4.2.2.4. Molecular docking

4.2.2.5. Molecular dynamics (MD) simulation

4.2.2.6. Binding free energy calculations

4.2.2.7. Analysis of principal component

4.2.3. Animal ethical clearance

4.2.4. Experimental animal selection and housing

4.2.5. Handling of chlorogenic acid (CGA)

4.2.5.1. Preparation of extra pure Chlorogenic acid/CGA 95 %

4.2.5.2. Formulation of chlorogenic acid-loaded liposomes (CAL)

4.2.5.3. Dose preparation of GCBE consisting of 36 % CGA.

4.2.6. Experimental animal model for hypoglycemia in rats

4.3. Main Study:

4.3.1. In silico Approach to study the inhibition of Glycogenesis

4.3.2. Experimental animal model for GSD type 1 in rats

4.3.3. Dose preparation

4.3.3.1. Preparation of Macronutrients

4.3.3.2. Preparation of Micronutrients

4.3.4. Collection of blood

4.3.5. Assessment of manifestations

4.3.5.1. Blood glucose estimation

4.3.5.2. Estimation of Glucose-6-phosphatase

4.3.5.3. Estimation of liver glycogen

4.3.5.4. Estimation of lactate dehydrogenase

4.3.5.5. Estimation of uric acid

4.3.5.6. Estimation of triglycerides

4.3.5.7. Liver size, weight and histological examination of liver tissue

4.3. Data analysis

With the aid of statistics GraphPad Prism version 8, the gathered data was examined statistically. The average ± standard error of the mean, or SEM, was used to express the findings. After doing a one-way ANOVA analysis on the collected data, the multiple comparison post-hoc test by Bonferroni was used.

4.1 Chemicals and equipment's/instruments used in the study

Table 1: List of chemicals/ equipment's used in the study.

Sl.No.	Name of chemicals	Company/Manufacturer name
1.	Anaesthetic ether	Thomas Baker Chemicals Pvt Ltd., Mumbai, India.
2.	Soy lecithin	Sisco Research Laboratories Pvt. Ltd - SRL, Mumbai, India
3.	Cholesterol	SD Fine Chemicals Pvt. Ltd. Mumbai, India
4.	Dichloromethane	Erba Transasia Bio-Medicals Ltd., Baddi, H.P, India.
5.	Chlorogenic acid (CAS. No. 327-97-9)	Sigma Aldrich Chemical Company (USA).
6.	Chlorogenic acid (Green coffee bean extract 36% CGA)	SV Agrofood, Delhi, India.
7.	Trichloroacetic Acid (TCA)	Sigma Aldrich Chemical Company (USA).
8.	Ammonium Molybdate	Himedia Chemicals. Mumbai

9.	Glucose-6-Phosphate	SRL Chemicals, Mumbai
10.	BIS-TRIS Buffer	Sigma Aldrich Chemical Company (USA).
11.	1-Amino -2-Napthol -4-Sulhonic acid	SRL Chemicals, Mumbai
12.	Cassava Starch	Kudos Pvt Ltd Generic
13.	Corn flour	Brown and Polson
14.	UV/VIS spectrophotometer	Shimadzu UV-1900
15.	Semi-Autoanalyzer	Erba-Transasia
16.	Inverted microscope (CKX41).	Olympus Microsystem, Japan.
17.	Image J. freeware (Image J. 2010), I.J. (1.46r)	Developed by National Institute of Health (NIH) of Bethesda, USA.
18.	Hot air oven	Servewell Instruments Pvt. Ltd., Bangalore, India.

19.	Microtome (Rotary), RM2125 RTS	Leica Microsystems IR GmbH.
20.	Wax bath	Labline Scientific Instruments, Mumbai.
21.	Thermostat water bath	Labline Scientific Instruments, Mumbai.
22.	Tissue embedding cassette	Himedia Laboratories Pvt. Ltd., Mumbai

4.2. Pilot Study: Experimental model

4.2.1. In silico Approach: GSD type 1a

4.2.1.1. Molecular Docking with Glucose-6-phosphatase

In order to obtain a clean protein structure, water and heteroatoms were removed from the Glucose-6-phosphatase with the modelled structure. Molecular binding sites are considered in receptor cavity method docking calculations for ligand molecules bound in interactions. The study of receptor-ligand docking was conducted with AutoDock Vina with a box size of 40 x 40 x 40.

4.2.1.2. Molecular Dynamics-Simulation

The chosen protein-ligand complex was run through a molecular dynamic's simulation in Gromacs-2019. 4. To obtain the force field coordinates, The PRODRG server

provided the required ligand topology (PMID: 15272157). The vacuum minimization technique was used to prepare the system with 1500 steps with the algorithm for the steepest descent. Subsequently, a cubic periodic box of 0.5 nm was used to solve the complex structures using a simple point charge (SPC) water model. Subsequently, the salt's optimal concentration 0.15 M was maintained in the complicated systems with the addition of the appropriate amounts of Na+ and Cl-counter ions. Based on a formerly published the work, the system setup was postulated [15]. During the process of Number of particles, Pressure, and Temperature (NPT) equilibration phase, every single generated structure underwent a final production run lasting 100 ns in the NPT ensemble (PMID: 31514687). The GROMACS simulation package (PMID: 32567989) was used to carry out the trajectory investigation. It comprises Protein's RMSD, RMSF, RG, SASA, and H-Bond.

4.2.2. In silico Approach : GSD type1b

4.2.2.1. Protein and ligand preparation

The alpha folded model structure of SLC37A4 in its entirety was obtained from the webpage for the alpha fold.(94) The model structure, accession number AF-A0A1L1SUI3-F1-model_v2, the glucose-6-phosphate substrate (PubChem CID: 5958), and the chlorogenic acid (PubChem CID: 1794427) were all made available by the alpha fold website the 3D structures were obtained from PubChem and were optimized using Discovery Studio Visualizer software version 2019 utilizing the energy minimization methodology and the CHARMM (Chemical at Harvard Molecular Mechanics) force field.

4.2.2.2. Protein structure information

Distribution of amino acids and evaluation of quality: To analyse the protein's amino acid distribution and the functional sites of the protein structure that were obtained and evaluated via SAVES server. PROCHECK was used to obtain information regarding the distribution of Phi/Psi angles for amino acids. in the SLC37A4, (95) and its general quality was examined by ERRAT.(96) Following the molecular dynamic simulation, the ligand-bound complex's 0 and 100 ns frames were acquired and subjected to the PROCHECK and ERRAT servers. We analysed the overall quality and distribution of the protein's amino acids alone as well as ligand-bound state data for both CGA and G6P.

4.2.2.3. Pocket information:

The P2Rank server was employed to obtain data regarding potential residues implicated in both protein function and ligand molecule binding.(97) For the docking investigation, the location of the pocket residues with greatest probability score was taken into account for this study.

4.2.2.4. Molecular docking

The POAP pipeline was utilized to evaluate the affinities of CGA and G6P for the glucose-6-phosphate translocase using AutoDock vina.(98,99) The grid box containing residues from active sites with centre x=0.435, y=1.652, z= 2.037 was set to pocket 1 during the docking simulation; sizes x=46.89, y=39.377, and y=41.626 were set with 1Å spacing. The exhaustiveness of the docking system was adjusted to 100 ns. Discovery Studio Visualizer 2019v was used to investigate the G6P and CGA intermolecular interactions in combination with SLC37A4.(100)

4.2.2.5. Molecular dynamics (MD) simulation

Using Gromacs-2019.4, G6P-SLC37A4 and CGA-SLC37A4 complex MD simulations were carried out. Using the Amber ff99SB-ildn force field, the Amber Tools xleap module developed the complex topology. With a boundary condition of 10.0 Å in a cubic periodic box, the complex structures were solvated with the help of water simple point charge (SPCE) water model. Subsequently, the complex systems' salt content was then kept constant at 0.15 M by employing an appropriate ratio of Na+ and Cl- counter ions. The results of a previously published research served as the foundation for the system preparation. Each structure's final production run from the equilibration phase was completed utilizing an ensemble of NPT simulations run for 100 ns. Utilizing the Gromacs packages, a 100ns trajectory analysis was done. The radius of gyration (Rg), hydrogen bond (H-bond), root mean square deviation (RMSD), and root mean square fluctuation (RMSF) were taken into consideration for assessment.(99,101)

4.2.2.6. Binding free energy calculations

Throughout the simulation, An inhibitor's binding free energy (G binding) with a protein was examined using the MM-PBSA method. The g mmpbsa functionality of GROMACS was utilized to determine the binding free energy.(102) In order to achieve a precise outcome, we calculated ΔG using dt 1000 frames for the final 20 ns trajectory and the binding free energy was expressed in kcal/mol. Further, the analysis also included contributions of each individual residual energy in the development of stable complexes.(103)

4.2.2.7. Analysis of principal component

MD trajectories are analyzed by principal component analysis (PCA) to evaluate molecular motion. The translational and rotational motion of the molecule can be

stopped or eliminated by applying the "least square fit" the reference structures. After a linear translation of cartesian coordinate space, the covariance matrix is diagonalized to get a set of eigenvectors that describe the motion of the molecule. Each eigenvector's eigenvalue reveals how much energy it contributed to the motion. The trajectory is projected onto an eigenvector, and therefore one may see how the pieces perform "time-dependent motions" inside a particular vibrational mode. The temporal average of the projection shows how the vibrational components of the atoms contribute to this type of coordinated motion. Using the integrated Gromacs tool "g covar," the covariance matrix was computed and diagonalized to get the eigenvectors and eigenvalues of the trajectory". The eigenvectors were also examined and illustrated using the "g anaeig" programme. The Gromacs features g covar and g anaeig utilities were utilized to perform PCA using the least squares fit method.(104–107)

4.2.3. Animal ethical clearance

The KLE College of Pharmacy's Institutional Animal Ethics Committee (IAEC) at Vidyanagar, Hubballi, Karnataka, India, authorized the proposed animal study (Approval No. 0/KLECOPH/19), after it was evaluated by the CCSEA (Committee for Control and Supervision of Experiments on Animals). The ARRIVE principles were followed in the execution all the experimental operation.

4.2.4. Selection and housing of experimental animals

For this study the male Wistar strain albino rats weighing 150–200 grams were selected that were acquired from KLE College of Pharmacy's animal home in Hubballi, Karnataka. They were kept in polypropylene cages with a 12-hour light and dark cycle,

and their temperature was kept at 27 ± 2°C. They received regular rat food (Gold Mohur Lipton India Ltd.) and unlimited water.

4.2.5. Handling of chlorogenic acid (CGA) and Metformin

4.2.5.1. Preparation of extra pure Chlorogenic acid/CGA 95 %

The manufacturer's instructions were followed in order to get and keep the chlorogenic acid (CAS No. 327-97-9) from Sigma Aldrich/Merck, USA, between 8 and 25 o C and the metformin tablets (USV India) were maintained at room temperature, CGA and Metformin were dissolved in water for injection and were subjected to oral dose.(108,109) The other common lab chemicals were all analytical grade and purchased from different suppliers.

4.2.5.2. Formulation of chlorogenic acid-loaded liposomes [18]

For the preparation of the clear and transparent liposomes loaded with chlorogenic acid, A 15 mL solution of dichloromethane was treated with an ultrasonic treatment to dissolve 250 mg of soybean lecithin and 50 mg of cholesterol. A rotary evaporator (Buchi) was used to evaporate the product in order to remove dichloromethane. Subsequently, The product was combined with 20 mL of ethanol and 50 milligrams of dissolved chlorogenic acid and rotary evaporation was performed again at 50° C to eliminate any remaining ethanol, producing complexes that resembled like films. Water was added to the dried film to create a 5 mg/mL CAL solution. The finished mixture was allowed to stand cold, at 4 °C, awaiting additional examination.

4.2.5.3. Dose preparation of green coffee bean extract comprising of 36 % CGA.(110)

The green coffee beans are known to be one of the major sources of Chlorogenic acid, The green coffee bean powder (GCB) consisting of 36% of chlorogenic acid was procured, and stored as per the specified requirement, GCB powder was brewed and then the animals were subjected in drinking water on daily basis with a concentration of 0.1 g/ml for 49 days.(111)

4.2.6. Experimental animal model for assessing the GSD type 1 manifestations

Chlorogenic acid was selected for this study, based on its safety, availability, and effectiveness. To determine the effective dosage of CGA needed to lower the test animals' fasting blood glucose levels, a 14-day pilot study was conducted. For this experiment, the rats were housed into five different experimental groups, each consisting of six rats (n=6). All animals were allowed standard rat feed and water ad libitum, except those in the control group. The animals were subjected to daily doses of CGA at varying doses (50, 100, 200, and 400 mg/kg) for two weeks in adjuvant to their daily feed schedule (Table 2) .

Table 2: Dose Selection of Chlorogenic acid

Group **(n=6)**	**Status**	**Treatment (**for 14 days**)**
Low dose		
I	Control Group	The animals were given access to regular drinking water and diet *ad. libitum*.
II	CGA treated	Treated with chlorogenic acid, **50** mg/kg body weight orally[16]
III	CGA treated	Treated with chlorogenic acid, **100** mg/kg body weight orally
High dose		
IV	CGA treated	Treated with chlorogenic acid, **200** mg/kg body weight orally[19]
V	CGA treated	Treated with chlorogenic acid, **400** mg/kg body weight orally

An oral dose of (CGA 200 mg/kg) bodyweight was observed to be effective and showed the promising capability to induce fasting hypoglycaemia/ decreased fasting blood glucose level in albino Wistar rats. However, it was observed that CGA had a shorter biological half-life, due to which its ability to maintain hypoglycaemia was limited to 1.5 to 2.5 hours. To overcome this situation the chlorogenic acid loaded liposomes (CAL) were formulated based on the literature review for this study.14 Subsequently, for the main study, based on the literature, the green coffee been extract 11,12 comprising of 36 % (CGA 200 mg/kg) was regularly given to the animals in the treatment groups and blended into the drinking water, to sustain the CGA effect. In

order to induce further manifestations of GSD, like lactic acidosis, metformin16 was administered along with CGA in a test group of animals.

The animals were divided into three different testing groups for the main study, each with six animals, Group I, or the control group was provided with normal feed and drinking water. In Group II the animals were fed with normal feed & drinking water in addition to 95 % CGA which was administered daily by oral gavage (200 mg/kg body weight for 49 days/ 7 weeks). Group III animals received green coffee bean extract (36% CGA) admixed in drinking water (200 mg/kg body weight orally daily) in addition to metformin 500 mg/kg and 95% CGA (200 mg/ kg body weight for 49 days) along with normal feed, administered daily by oral gavage. During the measurement of blood glucose, the maintenance dose of 100 mg CGA (95%) at 45 minutes interval was administered to sustain hypoglycaemia

4.3. Main Study:

4.3.1. In silico Approach to study the inhibition of Glycogenesis

The three principal steps of molecular docking adopted were 1) ligand selection and preparation, 2) preparation of macromolecule, and 3) docking of ligand-protein.

Ligand Preparation

From the PubChem database, Using Discovery Studio 2021, the 3D structure of each ligand was extracted and converted from the .sdf to the .pdb format. The uff force field under the conjugation gradient was used as the optimal algorithm to minimize the energy. Following energy minimization, the .pdbqt format was applied to every ligand.

Macromolecule preparation

The RCSB protein databank comprised the x-ray 3D crystallographic proteins of glucokinase (PDB: 1SZ2), GSK3β (PDB:4J1R), and protein phosphatase-1 (PDB:6DNO). With the help of Discovery Studio 2021, all heteroatom were removed. Then, kollman-charged molecules were introduced. Following that, ligands were all saved in.pdb format.

Docking of ligand-protein

Using AutoDock Vina, individual ligand was docked against the following proteins: GSK3β (centre x, y, z = 34.11, 32.72, 18.41 and size x, y, z = 61.01, 54.50, 60.32), glucokinase (centre x, y, z = 10.133, -3.79, 12.89 and size x, y, z = 63.16, 53.23, 56.039), and Protein Phosphatase-1 (centre x, y, z = 15.33, 80.65, 181.65, and size x, y, z = 46.56, 46.15, 56.039). Ten distinct stances were acquired after docking. To use Discovery Studio 2021 to visualize the ligand-protein interaction, the ligand's posture with the lowest binding energy was selected.

4.3.2. Experimental animal model for GSD type 1 in rats

Chlorogenic acid (CGA) and Metformin(112)(113) (Met) were selected for this investigation based on their efficacy, availability, and safety in inducing GSD I manifestations. The study design for this experimental set-up has been split into two distinct categories in order to examine into the consequences of macro and micronutrients, respectively. For the macronutrient investigation, the animals were split up into six groups (n=6). Group I received normal food and water without restriction, Group II was given metformin 500 mg/kg and chlorogenic acid 200 mg/kg as a negative control or disease control, Group III received CGA+Met + UCCS fed, Group IV

received CGA+Met + CS fed, Group V received CGA+Met + UCCS+micronutrients, and Group VI received CGA+Met + CS+micronutrients.

4.3.3. Dose preparation

4.3.3.1. Preparation of Macronutrients and select Micronutrients

Macronutrients used

Using a pestle and mortar, the regular chow pellets were ground into a fine powder in a 1:1 ratio with maize flour.(114) and as with the crushed pellet chow, pure wated was gradually added while mixing the pellet powder and cassava flour. Since starch functions as a binding agent, no additional binding agent was needed.(115)

Macronutrients meal preparation.

- The process used to prepare a diet rich in starches.
- Normal chow pellets were mixed with the uncooked corn starch.
- Similarly, normal chow pellets were also combined with the cassava starch.

The mixture was slightly mixed with distilled water, once it had been thoroughly blended and the regular chow feed had been churned into a pestle and mortar. After pressing the material into pellets, it was left to dry for the entire night.(116)

Corn Starch and Cassava Starch

Micronutrients used

- The micronutrients were procured from reputed resources, which were subjected to the oral administration of food grade Beta carotene powder,(14) (Profoods Nutrition™), Riboflavin (Bioven Ingredients), Vitamin C (Urban Platter®) and Vitamin E (Merck-Evion) via oral gavage feed.(117)(13)

4.3.4. Collection of blood (118)

Glucometers and test strips were stored and used at an appropriately controlled temperature and humidity throughout the study duration for glucose estimation. Blood was collected by tail prick method with the help of sterile lancet and the blood glucose was measured by glucometer (Arkray glucocard) and for other blood parameters the

animals were anesthetized under mild anaesthesia. Blood was withdrawn from retro-orbital plexus puncture and centrifuged to get clear serum for biochemical estimation.

4.3.5. Assessment of manifestations

4.3.5.1. Blood glucose estimation (119)

The fasting blood glucose level for the experimental rats throughout the study period was estimated with the help of a glucometer. There are mainly two procedures for continuous measurement of blood glucose levels in rats: the punctures of the dorsal penile vein and the lateral tail vein. These methods yield enough blood volumes for the majority of experiments and enable quick sampling (just under 10 minutes). While anaesthesia is required for the dorsal penile vein puncture, the lateral tail vein puncture or commonly called as tail prick method can be executed on a conscious, restrained animals. Repeated blood draws are possible by switching between the two methods.(120) However, in this study the lateral puncture method alone was employed to measure the blood glucose levels, with the help of sterile lancet and the blood glucose was measured by glucometer (Arkray glucocard). The retro-orbital plexus puncture was used to extract blood and centrifuged to get clear serum for biochemical estimation. The glucometers and test strips were stored and used at an appropriately controlled temperature and humidity throughout the study duration.

4.3.5.2. Glucose-6-phosphatase estimation(121)(122)(123)

Glucose-6-phosphatase enzyme was estimated by the method described by Nordlie, R.C. and Arion, W.J. (1966) and Taussky, H.H. and Shorr, E. (1953) with following requirements or conditions like: Temperature of 37°C, pH = 6.5, Absorbance at 660 nm, Light path = 1 cm, Method: Spectrophotometric Stop Rate Determination.(123)(122)(121)

Reagents required:

- 100 milligrams pH 6.5, 37°C BIS-TRIS Buffer (Buffer). Using BIS-TRIS, prepare 200 millilitres of filtered water. At 37°C, adjust the pH to 6.5.

- 200 mM Glucose 6-Phosphate (Sub) and D-Glucose 6-Phosphate Sodium Salt should be prepared in 10 ml of filtered water.

- 20% of TCA, or trichloroacetic acid Prepare 10 millilitres of Trichloroacetic Acid Solution, 6.1 N, in purified water.

- Use neat Phosphorus Standard Solution, 20 µg/ml (Std)

- 5 M Solution of Sulfuric Acid Make 50 millilitres with sulfuric acid in distilled water.

- 10% Solution of Ammonium Molybdate Prepare 10 ml of ammonium molybdate tetrahydrate in Reagent 7.3.5.
- The color reagent Taussky-Shorr (TSCR) Stir 10 milliliters of Reagent 7.3.6 into 70 milliliters of filtered water. Then add 5 g of Ferrous Sulphate Heptahydrate. Stir this solution until completely dissolved and bring to a final volume of 100ml using purified water.

- Solution of glucose-6-phosphatase enzyme (Enz) Make a solution of 1.0–2.0 units/ml in cold, filtered water right before using.

Enzymatic Assay:

The following should be pipetted (in milliliters) into appropriate containers:

	Test	Blank
Buffer (7.3.1)	3.00	3.00
Substrate (7.3.2)	1.00	1.00

Stirring constantly, mix and let sit at 37°C for at least five minutes before adding:

Enzyme (7.3.8.)	0.10	-----

Swirl to mix right away, and then incubate at 37°C for exactly five minutes. Next, add:

TCA (7.3.3.)	0.90	0.90
Enzyme (7.3.8.)	-----	0.10

Close tightly and stir by flipping. Centrifuge all reaction mixtures, sample and blank, for 10 minutes at 4,000 rpm after incubating for 5 minutes at 25°C. In the color development step, use the supernatant.

Color Development:

To generate a standard curve, pipette the following amounts (milliliters) into appropriate containers:

		Test						Std
	Test	Blank	Std 1	Std 2	Std 3	Std 4	Std 5	Blank
Purified Water	----	----	1.80	1.60	1.40	1.20	1.00	2.00
Standard	----	----	0.20	0.40	0.60	0.80	1.00	----
Test	2.00	----	----	----	----	----	----	----
Blank	----	2.00	----	----	----	----	----	----

Swirl together all of the samples, blanks, and standards, then add:

TSCR	2.00	2.00	2.00	2.00	2.00	2.00	2.00	2.00

For five to six minutes, allow samples, standards, and blanks to all incubate at 25°C. After transferring each solution to the proper cuvette, note the A660nm for each. All color development reaction mixtures must be incubated for the same amount of time since the color complex will develop with time.

Calculations:

- Determine the standards' ΔA660nm using the following formula:

  (A660nm Standard - A660nm Standard Blank) = ΔA660nm

- Plot the standards' ΔA660nm against μmoles of phosphorus to find the linear regression's slope (m) and y-intercept (b). Utilize these in the test reaction mixture calculations.
- Determine each test solution's ΔA660nm using the following formula:

  (A660nm Test - A660nm Test Blank) = ΔA660nm

- Calculate the liberated μmoles of Pi using the following formula.:

$$\mu\text{moles Pi} = \frac{(\Delta A660\text{nm Test} - b)}{m}$$

Determine the following units per milligram of enzyme:

$$\text{Units/mg S} = \frac{(\mu\text{moles Pi} * 5.0 * df)}{(T * 0.1 * 2.0)}$$

Where:

5.0 = is the enzymatic reaction's final volume (measured in milliliters).

0.10 = is the amount of the enzyme solution used, measured in milliliters.

2.0 = the amount of enzyme assay required to develop color, measured in milliliters

df = represents the enzyme solution's dilution factor.

4.3.5.3. Estimation of liver glycogen(124)

The Montgomery method was used to estimate the liver glycogen content. The method involves the hydrolysis of glycogen to glucose using a specific enzyme, amyloglucosidase, followed by the quantification of glucose concentration. The glycogen was measured as soon as the autopsy was completed, according to Montgomery (1957).

Principle:

The principle is based on the phenolic sulphuric acid method for the determination of alkali soluble polysaccharides in tissue. Furfural derivatives are produced when hydroxy aldehyde, which is produced during the dehydration process of carbohydrates treated with sulfuric acid and phenol. The amount of glycogen present in the reaction causes a pink color to appear, with a corresponding intensity.

Reagents

1. Potassium hydroxide (KOH) solution = 30%

2. Phenol solution in distilled water = 80%

3. Concentrated sulphuric acid (H2SO4)

4. Glycogen standard 1.0 mg of glycogen was dissolved in 10 ml of distilled water (0.1 mg/ml).

Procedure:

- 20 mg of tissue was digested in 2 ml of 30% KOH kept in boiling water.

  The digested tissue was brought to room temperature by cooling and 4 ml of absolute alcohol was added and left for 10 minutes.

- After an interval of 10 minutes, the content was centrifuged for 30 minutes and the supernatant was discarded.
- Once again, 2.4 milliliters of absolute alcohol were added, centrifuged for ten to fifteen minutes, and the supernatant was disposed away. The tubes were kept in the desiccator for overnight.
- Then next day, 4 ml of distilled water was added to the precipitate and mixed thoroughly. Test, standard and blank solutions were prepared by mixing various ingredients as follows: -

Sl.No.	Ingredients	Test	Standard	Blank
1	Tissue solution	1 ml	---	---
2	Glycogen Standard (working)	---	0.5 ml	---
3	Distilled water	1 ml	1 ml	1 ml
4	Phenol Reagent	0.1ml		
5	Cone. H2SO4	0.5 ml	0.5 ml	0.5 ml

Calculation

The following formula was used to determine the amount of glycogen present in the tissue.

Total glycogen content (mg/gm of tissue weight) =

$$\frac{\text{O.D. of test}}{\text{O.D. of standard}} \times \frac{\text{Conc. Of Standard} \times 4 \times 1000}{\text{tissue taken} \quad 11}$$

Observation

These were kept for half an hour for cooling before taking their optical densities (O.D.) at 630 nm in Spectrophotometer apparatus (Make Shimadzu UV-1900) after setting at 100% transmission against blank.

4.3.5.4. Estimation of lactate dehydrogenase(124)

Clinical significance: The liver, kidney, heart, muscle, and other bodily tissues have high concentrations of the enzyme lactate dehydrogenase (LDH). As a result, harm to these causes serum LDH levels to rise. Increased levels are linked to malignancies, hepatitis, renal damage, myocardial infarction, anaemias, and injury or illness of the muscles and also gives an indirect assessment of lactate synthesized.

Working principle:

Optimised Kinetic method of Deutsche Gessel schaft fur Klinische Chemie (DGKC).

$$\text{Pyruvate} + \text{NADH} + \text{H}^+ \xrightleftharpoons{\text{LDH}} \text{Lactate} + \text{NAD}^+$$

LDH: Lactate dehydrogenase

The LDH activity in the sample is directly correlated with the rate at which absorbance changes at 340 nm.

Reagent composition:

Table 3: Reagent composition of LDH P kit

Phosphate buffer (pH-7.5)	50 mmol/L
Pyruvate	0.6 mmol/L
NADH	0.25mol/L

Assay procedure: The working reagent (4R1:1R2) was allowed to attain 37 ºC before the test. 20µl of the test sample was pipette out, mixed well, and aspirated.

4.3.5.5. Estimation of uric acid(125)(126)

Working principle:

Uricase converts uric acid to hydrogen peroxide and allantoin. Hydrogen peroxide oxidatively interacts in the presence of peroxidase and a phenolic chromogen to produce a crimson compound with a maximum absorbance at 505 nm. The quantity of uric acid in the sample test tube is directly correlated with the concentration of the red-coloured compound (Barham, D. et al., 1972).

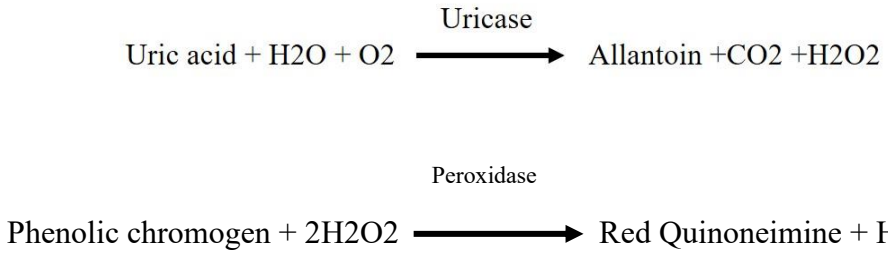

1. Uricase transforms uric acid into allantoin, which generates H2O2.

2The combination of peroxide, 4-aminoantipyrine (4-AAP), and DHBS occurs when peroxidase is involved to produce a quinoneimine color. The amount of uric acid present in the sample is proportionate to the dye's absorbance at 505 nm.

Assay Procedure

Wavelength: 505/670 nm

Cuvette: 1 cm

	Reagent blank	Standard (Calibration)	Sample
Reagent 1	1.00 ml	1.00 ml	1.00 ml
Sample	-	-	0.025 ml
Standard (Calibration)	-	0.025 ml	-
Distilled water	0.025 ml		-

Stir and let sit at 37 °C for 5 minutes. At 505/670 nm, compare the absorbance of the standard A_{st} and the sample A_{sam} against the reagent blank.

Calculation

$$\text{Uric Acid (mg/dl)} = \frac{\Delta \text{Asam}}{\Delta \text{Ast}} \times \text{Cst}$$

Cst = standard concentration (calibrator)

4.3.5.5. Estimation of triglycerides(127)(128)

Estimation of triglycerides by using method of McGowan *et al*., and Fossati *et al*.

Principle:

In this method, the presence of lipases in the kit sequentially hydrolysed serum triglycerides to yield glycerol and fatty acids. then glycerol is phosphorylated in the presence of ATP into glycerol-3-phosphate by glycerol-kinase. Further, glycerol-3-

phosphate oxidase (from kit) catalyze the oxidation of glycerol-3-phosphate to produce dihydroxyacetone phosphate (DAP) and hydrogen peroxide. Finally, ESPAS (N-Ethy-N-sulfopropyl-n-methoxyaniline) and 4-aminoantipyrine react with hydrogen peroxide in the existence of peroxidase to afford a colored complex whose color intensity is proportional to the triglycerides concentration.

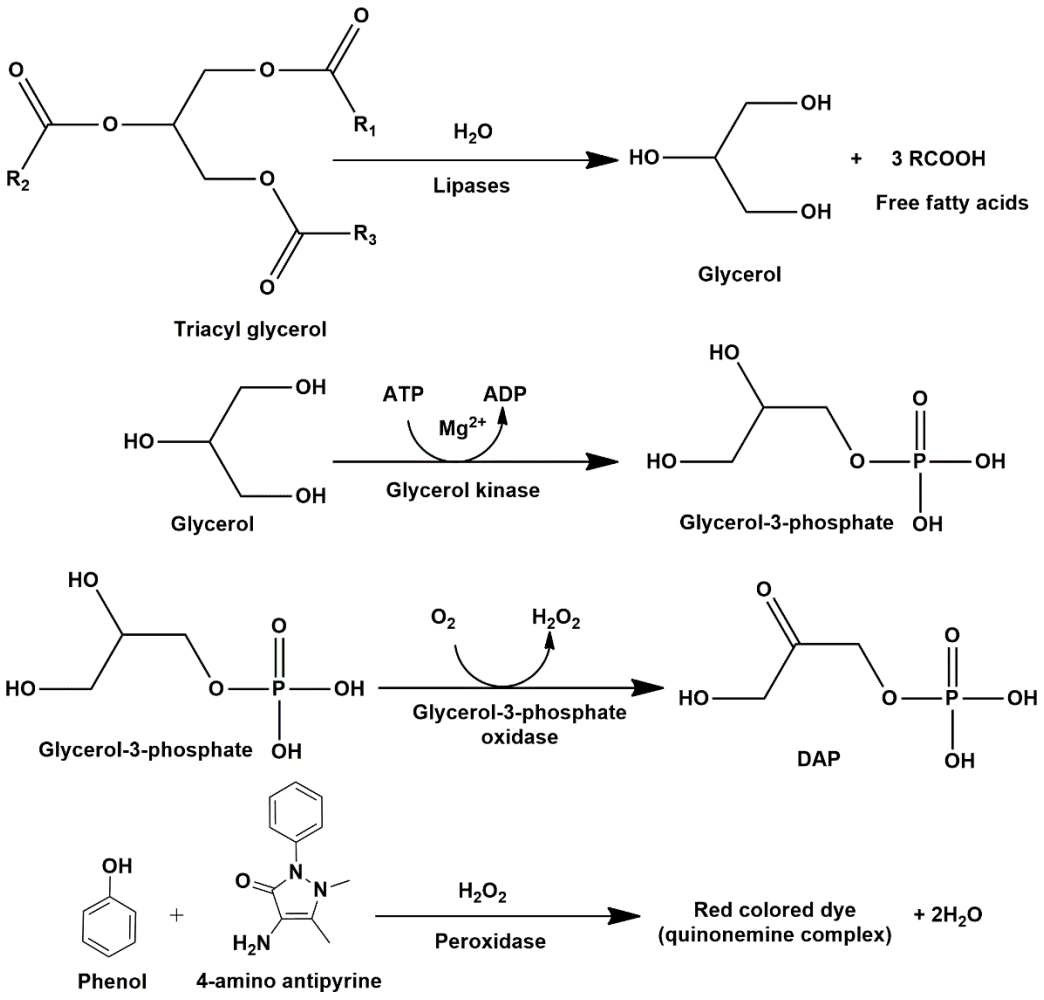

Figure 3: Reactions in triglyceride estimation.

Assay Procedure:

Table 4: Assay procedure for triglycerides estimation

Reagents to be added into labelled tubes	**Kit Contents**	**Sample**	**Standard (Cal.)**	**Reagent blank**
Reagent 1	Working reagent: 3-5 DHBS and buffer (pH 7.0) Mg2+, GPO, Glycerol kinase, glycerol-3-phosphate oxidase, lipoprotein lipase, peroxidase, 4-aminoantipyrine, and ATP.	1000 µL	1000 µL	1000 µL
Reagent 2	Triglycerides standard (200 mg/dl)	-	10 µL	-
Test Sample		10 µL	-	
Distilled water		-	-	10 µL

Mixing thoroughly, the contents were then incubated for approximately ten minutes at 37°C. The sample and standard absorbances were measured against a reagent blank. at λ_{max} 546/670 nm.

Calculation:

Calculate average absorbance of test and standard. Subtract absorbance value of standard from itself and all other values, this is corrected absorbance value. Graph the corrected absorbance as a function of final triglyceride.

$$Triglycerides\ (in\frac{mg}{dl}) = \frac{(\text{Corrected absorbance}) - (\text{y} - \text{intercept})}{\text{Slope}}$$

4.3.5.7. Liver size, weight and histological examination of liver tissue(129)

The Periodic Acid-Schiff (PAS) was used to perform histological examinations on liver tissues. All of the slides were examined for alterations in histopathological features and the results were given in the result section. Periodic acid-Schiff (PAS) was used to examine the liver tissues; all of the slides were examined for alterations in histopathological features and the results were given in the results section.

Tissue sample preparation for histology: Liver tissue specimens were tested by autopsy. To maintain the cellular architecture, the tissue was fixed in an appropriate fixative, such as formalin.

Tissue Processing: The fixed tissue was subjected to a sequence of escalating alcohol concentrations to extract water, resulting in dehydration. To enable the embedding medium to penetrate the tissue more easily and become transparent, the tissue was cleaned using a clearing agent such as xylene.

Embedding: The tissue that had been dehydrated was embedded in a solid material, such as paraffin wax, which helped to retain the architecture of the tissue and offered support for thin sectioning.

Sectioning: A microtome was used to cut thin slices of the implanted tissue, usually 4-5 micrometres thick. Usually, these portions were fixed to glass slides.

Deparaffinization: To eliminate the paraffin wax and rehydrate the tissue sections, the slides were passed through a sequence of decreasing concentrations of alcohol while immersed in xylene or a xylene replacement.

PAS Staining: The Periodic acid and Schiff's reagent was typically combined to create the Periodic acid-Schiff (PAS) staining solution.

To form aldehyde groups by oxidising the polysaccharides in the tissue, the tissue slices were incubated in a periodic acid solution.

The slides had been rinsed in distilled water to remove excess periodic acid.

The tissue sections were incubated in Schiff's solution, which prompted the aldehyde groups created in the preceding procedure to react and produce a complex with polysaccharides that imparts magenta colour to the tissue sample.

5. RESULTS

5.1. Pilot Study

5.1.1. In-silico approach to study GSD type 1a

Molecular Docking

The binding patterns of Glucose-6-phosphatase were evaluated using AutoDock vina by triplicated docking approach. The intermolecular interactions between G6Pase protein (PRO) and CGA ligand (LIG) is shown in (Tables 5 and 6) respectively. The docking images of PRO with the LIG are represented in (Figure 4A and 4B). The stability of the complex is greatly influenced by the carbon-hydrogen interaction, Vander Waal's force, and typical hydrogen bonds.

Table 5: The docking score of CGA with G6Pase

Compound Name	Affinity (T1)	Affinity (T2)	Affinity (T3)	Avg. Docking Score
LIG	-8.9	-9.0	-8.9	-8.9

Table 6: Hydrogen Bonding information

Compound	H-Donor	H-Acceptor	Distance	Type
LIG	A:ASN43:HN	B:UNK0:O	3.0318	Conventional Hydrogen Bond
	A:ASN266:HD22	B:UNK0:O	2.38869	Conventional Hydrogen Bond
	B:UNK0:H	A:ASP40:OD1	1.31199	Conventional Hydrogen Bond
	B:UNK0	A:MET123	5.24331	Pi-Alkyl

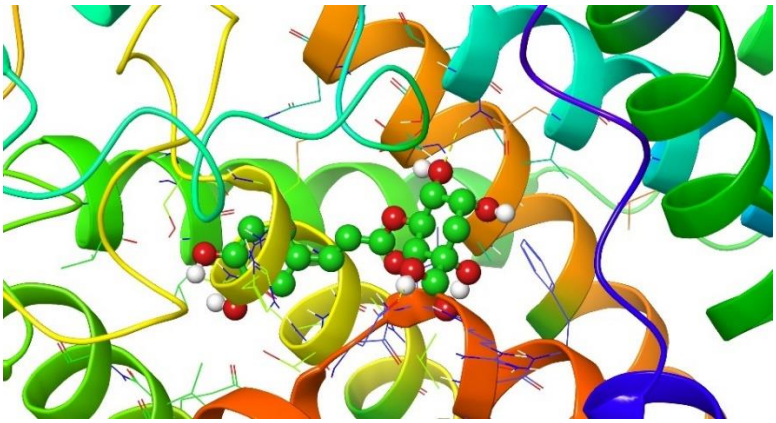

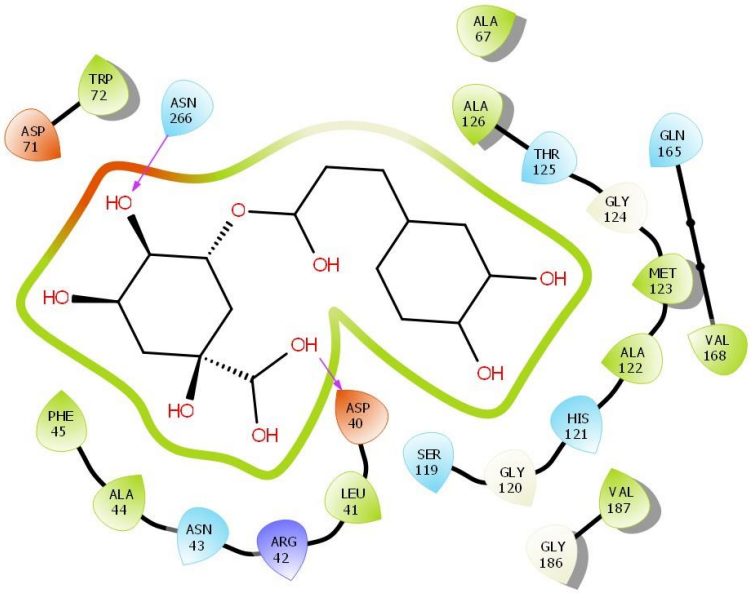

Figure 4 A; 4B: 3D image of the docking images of G6Pase (PRO) with the CGA (LIG); 2D image of the docking images of G6Pase (PRO) with the CGA (LIG)

Molecular Dynamics(MD)

To comprehend the stability of the protein-ligand complexes, an all-atom MD simulation lasting 100 nanoseconds (ns) was performed. – (1) Protein alone [PRO-APO], and (2) Protein with ligand [PRO-LIG]. Table 7 summarizes the average values for RMSD, RMSF, Rg, and SASA, this information describes the structural properties of Protein-Ligand interaction. The parameters that indicate the protein's overall structural flexibility and stability are the "Average RMSD" (root mean square deviation) and "Average RMSF" (root mean square fluctuation). Whereas a higher RMSF number indicates more flexibility, a lower RMSD value indicates a more stable protein structure. A higher radius denotes a larger protein. The "Radius of gyration" value serves as an indicator of the protein's size. The amount of protein surface area exposed to the solvent (such as water) is measured by the "Average SASA" (solvent accessible surface area) measurement. Greater SASA values signify increased protein exposure to the solvent.

Table 7: Molecular Dynamics report at 100 ns (1) Protein alone [PRO-APO], (2) Ligand-containing protein [PRO-LIG]. A tabulation of the average values for RMSD, RMSF, Rg, and SASA is as follows.

S. No.	Protein	Average RMSD (nm)	RMSF (nm)	Radius of gyration (nm)	Average SASA (nm2)
1	PRO-APO	0.22 +/- 0.03	0.4 +/- 0.07	2.36 +/- 0.03	205.07 +/- 5.20
2	PRO-LIG	0.21 +/- 0.04	0.3 +/- 0.06	2.35 +/- 0.01	203.07 +/- 4.30

Root mean square deviation:

It is a crucial factor in figuring out how the two confirmations differ from one another. The greater the RMSD value, more will be the deviation. The simulation duration of 100 ns is used to determine the RMSD values (Figure 5). The PRO-APO and PRO-LIG protein complex proteins had average RMSDs of 0.22 +/- 0.03 nm and 0.21 +/- 0.04 nm, respectively, from 0 to 100 ns. The relative stability of chemical compounds during the experiment is shown by these RMSD values. Furthermore, throughout the simulation, the complexes held their stability.

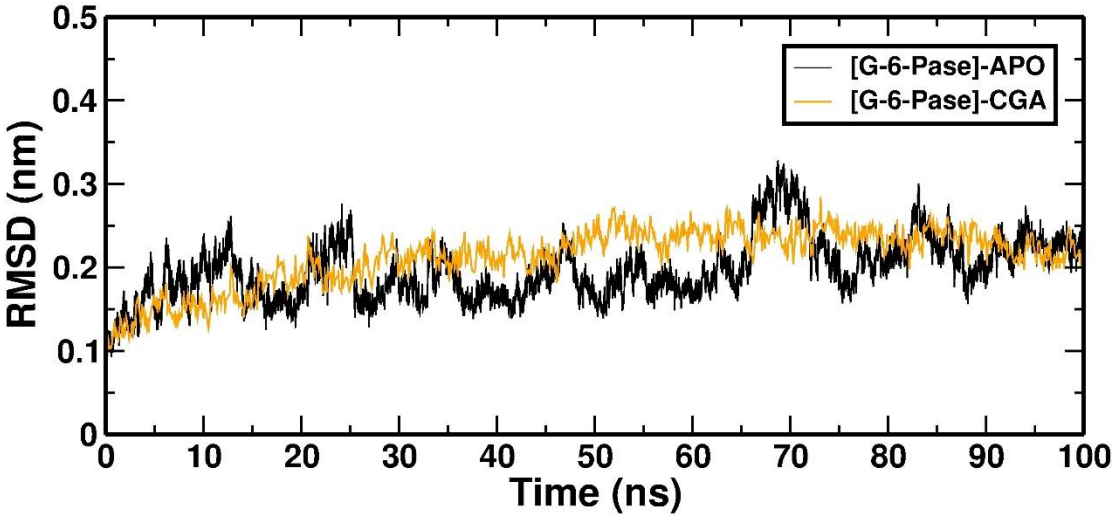

Figure 5: The backbone atoms and their Root means square deviation of

Root mean square fluctuation:

The amino acids present in the protein that produce the most vibrations are identified by RMSF analysis, causing the protein to become unstable both when the ligands are present and when they are not. To compute the RMSF values, a simulation timescale spanning from 0 to 100 ns is used. For PRO-APO and PRO-LIG protein complex proteins, the average RMSFs from 0 to 100 ns were 0.4 +/- 0.07 nm and 0.3 +/- 0.06 nm, respectively. The results for PRO-APO, PRO-LIG complexes as depicted in (Figure 6). The results implied that during the 100 ns simulation, there are no appreciable structural changes.

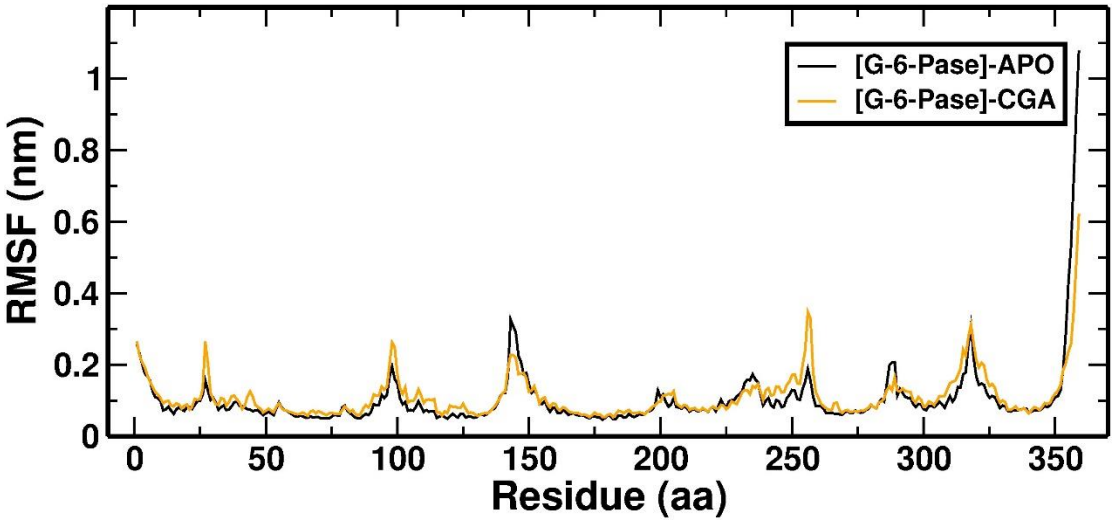

Figure 6: The c-alpha atoms and their Root means square fluctuation of

Radius of Gyration (RG):

A useful tool for representing the radius of gyration is the Root mean square distance weighted by mass of an atom from its centre of mass. The Rg plot demonstrates the competency, shape folding, as well as the overall structure at different times during the trajectory path, illustrated in Figure 7. Through every phase during the simulation process, PRO-APO, PRO-LIG complexes showed a comparable Rg value trend. An average RG value ranging from 0 to 100 nanoseconds for PRO-APO, PRO-LIG protein complex proteins were 2.36 +/- 0.03 nm and 2.35 +/- 0.01 nm respectively.

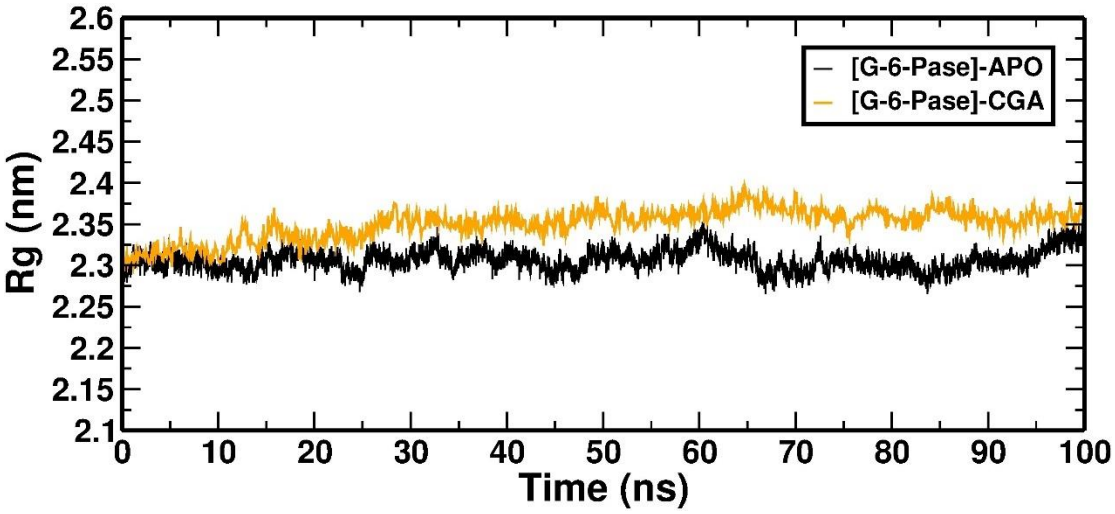

Figure 7: RG of backbone atoms

Solvent Accessible Surface Area (SASA):

The hydrophobic core's compactness was evaluated by SASA. The change in SASA of the PRO-APO, PRO-LIG protein over time is displayed in Figure 8. The average SASA value from 0 to 100 ns for PRO-APO and PRO-LIG protein complex proteins were 205.07 +/- 5.20nm and 203.07 +/- 4.30 nm respectively. This suggests that the structural level protein has not changed during the simulation.

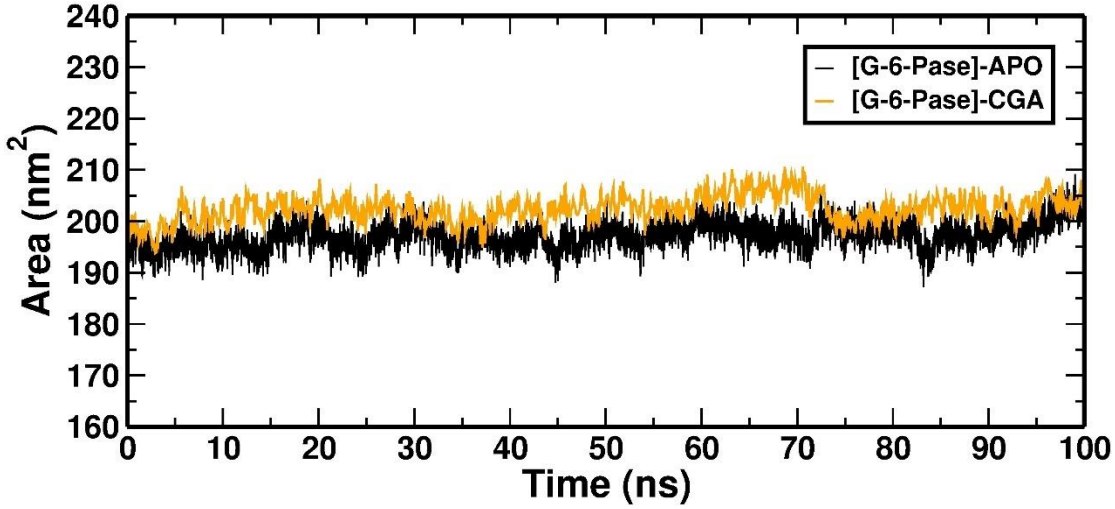

Figure 8: SASA of backbone atoms of with Protein-Substrate and Protein-Ligand

Hydrogen Bond (H bond):

Protein-ligand complex stability is achieved through the process by which hydrogen bonds form. In this study, the simulation analysis supports the hydrogen bonds established in the molecular docking analysis. The complex's H-Bond outcome with PRO-LIG. The complex's H-Bond outcome with PRO-LIG is depicted in Figure 9

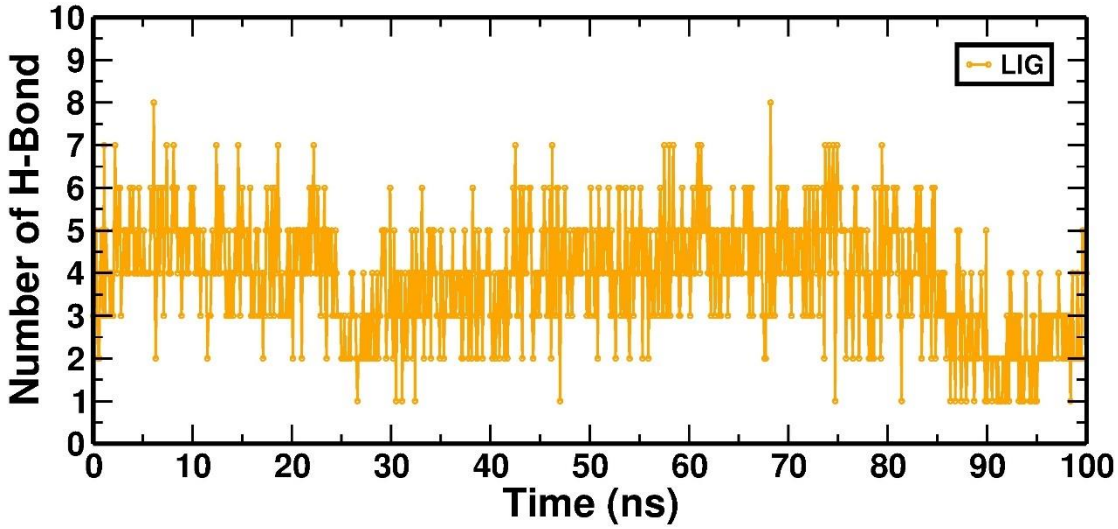

Figure 9: Hydrogen-Bond outcome of PRO-LIG

The Molecular mechanics Poisson–Boltzmann surface area (MM - PBSA):

We assessed the relative binding strength inside the energy protein to ascertain PRO-LIG's binding affinity, the data (Table 8) and (Figure 10) compares the PRO-LIG binding strength to inhibitors was calculated by applying the MM-PBSA method. During a stable simulation track, We evaluated the energy contributions to the interaction at the residue level.

Table 8: The relative binding strength of PRO-LIG computed via the MM-PBSA method

System	Van der Waal energy	Electrostatic energy	Polar solvation energy	Binding energy
PRO-LIG	-155.826 +/- 18.129 kJ/mol	-106.616 +/- 20.776 kJ/mol	290.413 +/- 34.240 kJ/mol	-30.141 +/- 14.943 kJ/mol

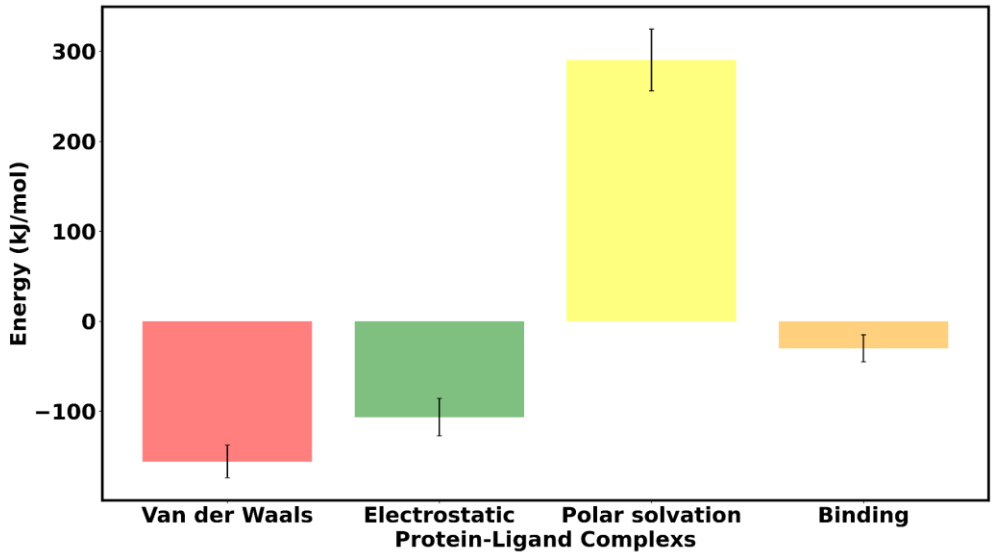

Figure 10: Determination of relative binding affinity of Protein-Ligand by MM-PBSA method.

5.1.2. Pilot Study: In-silico approach to study GSD type 1b

Protein information:

PROCHECK was used to examine the geometry of the entire structure as well as the geometry of individual residues in order to assess the stereochemical quality of the SLC37A4 protein structure (Figure 1A). The most favored and additional permitted zones contained around 96.1% and 2.8% of the residues, respectively. In the Ramachandran plot, generously allowed regions contained approximately 0.8% (3 residues), namely Lys205, Lys207, and Glu213. Nevertheless, only 0.3% (one residue) i.e., Ser413 was discovered in the disallowed region. The ERRAT plot, which illustrates the highest resolution of the structure and validates its stability, revealed that the total level of protein structural quality was 97.664% (Figure 1b). The residues in the most favored and additional allowed regions of the G6P-SLC37A4 0ns frame complex were around 91.3% and 8.2%, respectively. Ser164, one residue, was discovered in the area that was disallowed (Figure 11). In contrast, about 91.6% and 7.9% of the residues in the most favored and additional permitted regions, respectively, were located in the G6P-SLC37A4 100ns frame complex. In the generously allowed region, one residue (Thr364) was discovered, and in the disallowed region, one residue (Ser164) was discovered (Figure 12). It was discovered that all active site residues implicated in G6P binding were located in the most favored region. The overall quality of the G6P-SLC37A4 0ns and 100ns frame complex was found to be 96.250% and 95.718%, respectively (Figure 13 and Figure 14). In the disallowed region, one residue, Ser164, was discovered (Figure 15). In contrast, about 92.6% and 7.4% of the residues in the most favoured and additional permitted areas, respectively, were discovered in the CGA-SLC37A4 100ns frame complex. In the disallowed region, no traces were

discovered (Figure 16). It found that all active site residue implicated in CGA binding was located in the most preferred area. The G6P- SLC37A4 0ns and 100ns frame complex was reported to have an overall quality of 99.75% and 97.805%, respectively (Figure 17 and Figure 18).

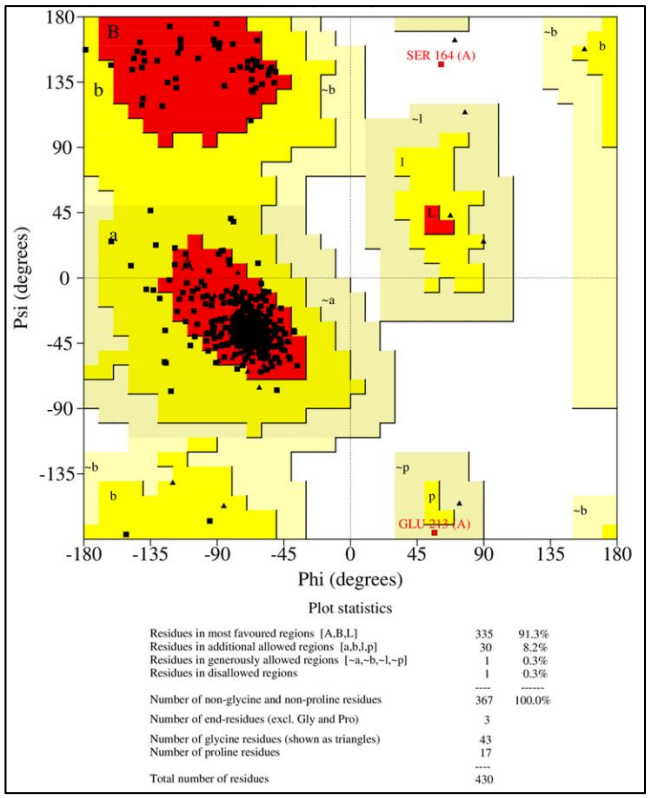

Figure 11: Ramachandran plot of 0ns G6P and SLC37A4 bound complex showed that 91.3% and 8.2% of The residues were discovered in the additional allowed and most favored regions, respectively. Ser164, one residue, was discovered in the disallowed region.

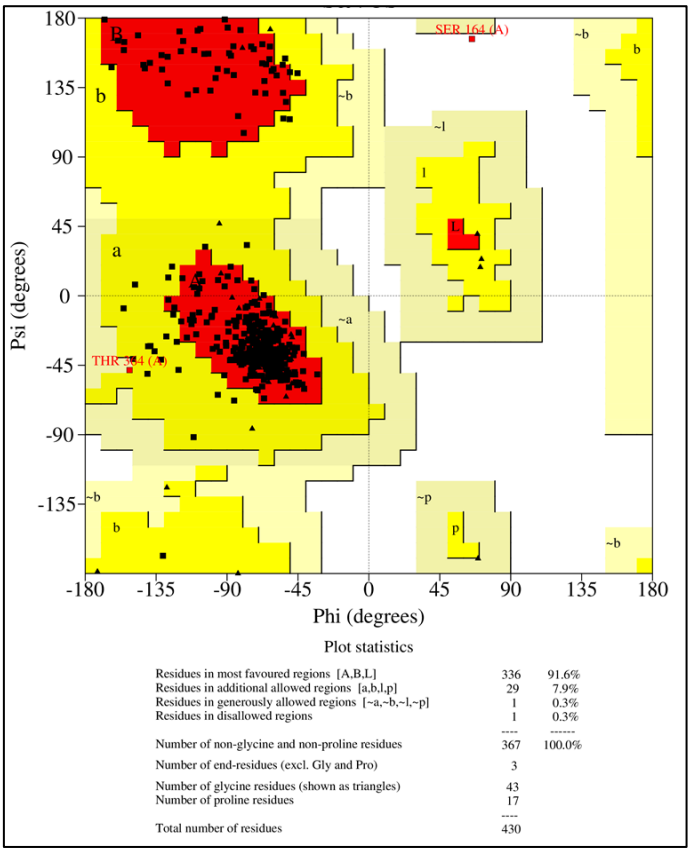

Figure 12: A Ramachandran plot of the 100 ns G6P and SLC37A4 bound complex revealed that 91.6% and 7.9%, respectively, of the residues were located in the additional allowed regions and the most favored regions. Ser164 was discovered in a disallowed region whereas Thr364 was identified in a generously allowed region.

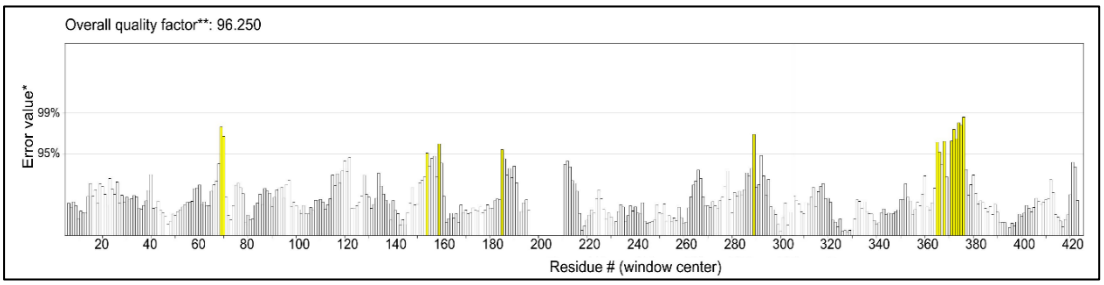

Figure 13: Error values for residues of the 0ns frame G6P are displayed in an ERRAT plot and SLC37A4 bound complex. The protein structure's overall quality was found to be 96.250%, as validated by the ERRAT values.

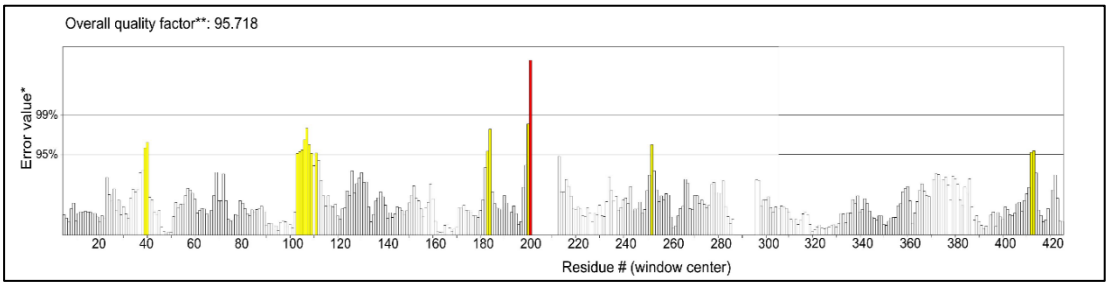

Figure 14: ERRAT plot showing error values for residues of the 100ns frame G6P and SLC37A4 bound complex. The protein structure's overall quality was determined to be 95.718% based on the ERRAT readings.

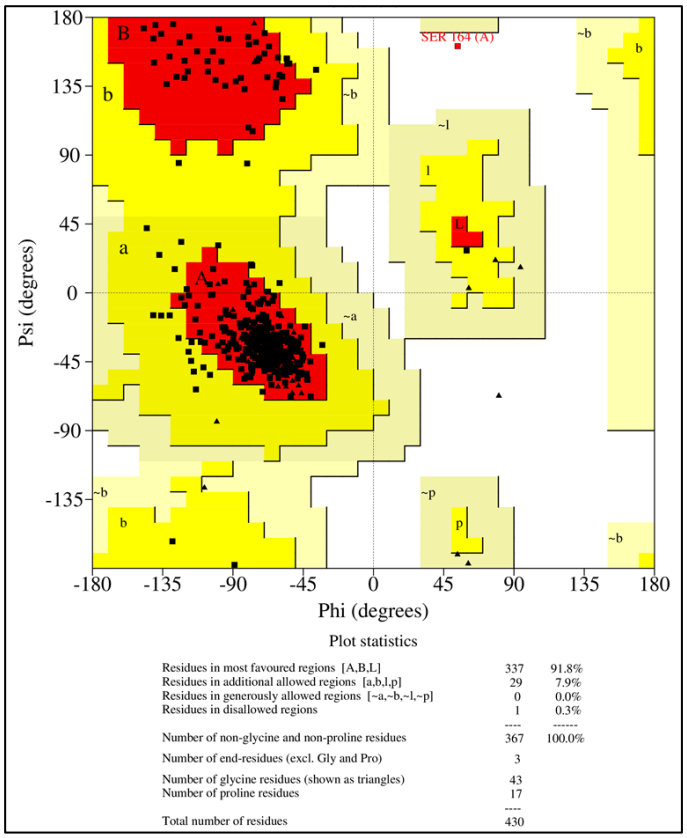

Figure 15: Ramachandran plot of 0ns CGA and SLC37A4 bound complex showed that 91.8% and 7.9% of The residues were discovered in the additional allowed and most favoured regions, respectively. Ser164, one residue, was discovered in the disallowed region.

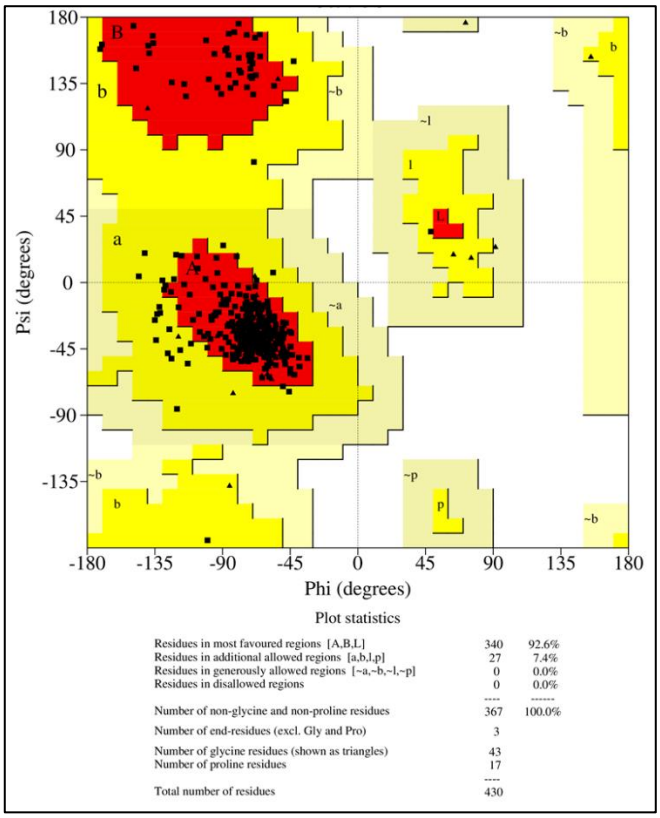

Figure 16: In the most favored and additional allowed regions, respectively, 92.6% and 7.4% of the residues were discovered, according to the Ramachandran plot of the 100 ns CGA and SLC37A4 bound complex. The disallowed region no residues were discovered.

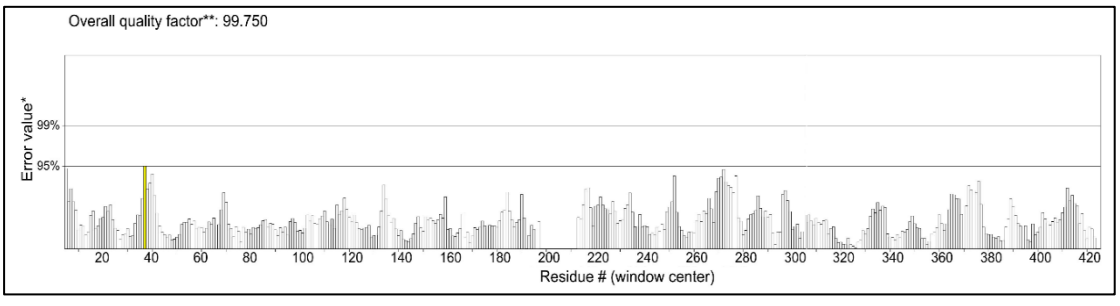

Figure 17: ERRAT plot showing error values for residues of the 0ns frame CGA and SLC37A4 bound complex. The protein structure's overall quality was determined to be 99.75% based on the ERRAT data.

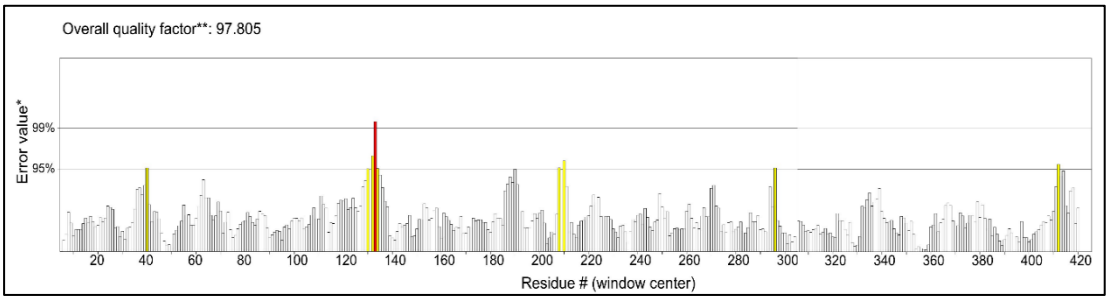

Figure 18: ERRAT plot showing error values for residues of the 100ns frame CGA and SLC37A4 bound complex. The overall quality of the protein structure was found to be 97.805%, as validated by the ERRAT values.

There are four binding pockets on the SLC37A4 protein among which the pocket 1 (Figure 19 A, B, and C) had residues number “21, 25, 28, 29, 56, 57, 60, 64, 114, 118, 139, 142, 143, 145, 146, 233, 237, 240, 241, 245, 274, 277, 278, 364, 367, 368, 391, 394, 395, 398” was found to be the main binding pocket, which gave the P2Rank web server a likelihood score of 0.879.

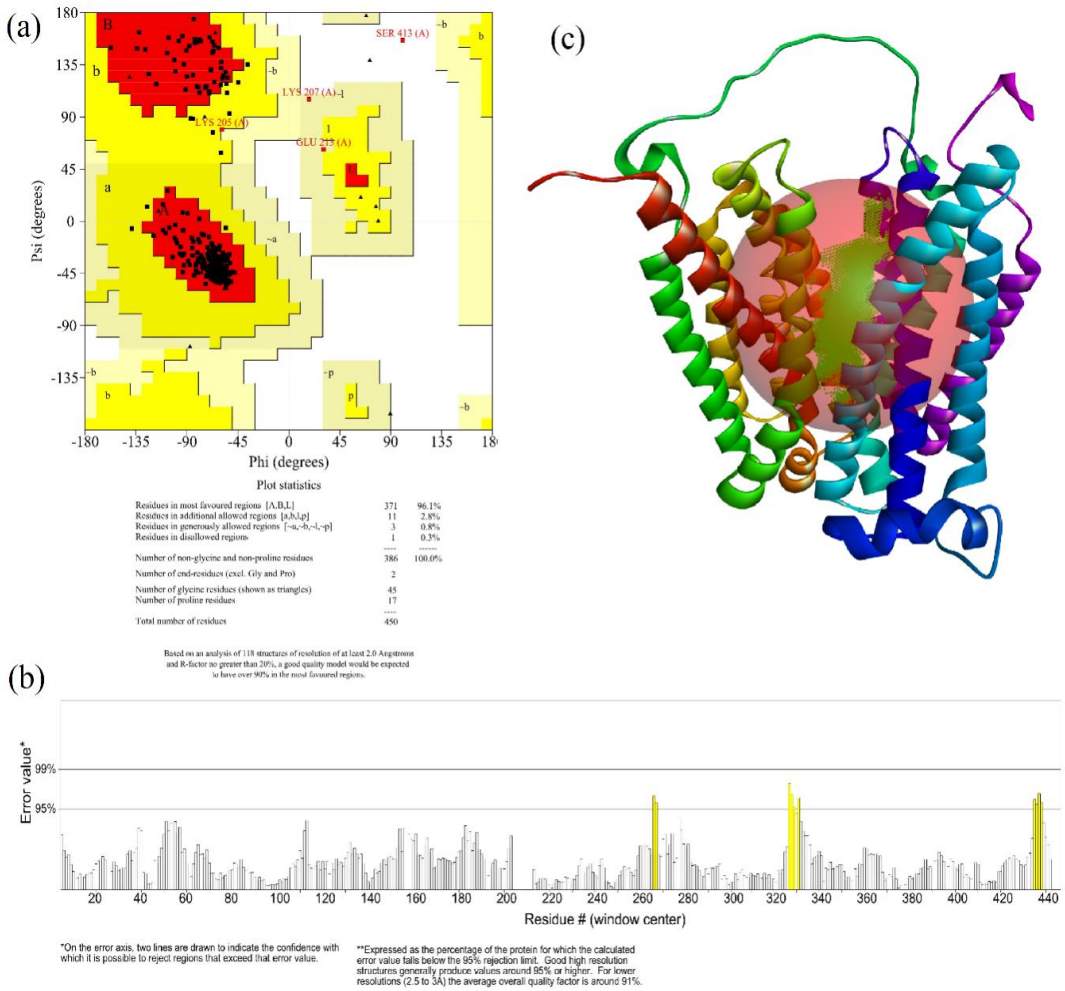

Figure 19 A, B, C: (A) Ramachandran plot, (B) ERRAT plot (C) Ligand binding pocket

Pocket Information: The P2Rank (Krivák and Hoksza, 2018) server was used to identify potential residues that could be important for both protein function and ligand binding. For the docking investigation, the pocket residues site with the highest likelihood score was taken into account (Table 9) .

Table 9: Crucial pocket residues and the probability score of SLC37A4's ligand binding pocket

Name	Probability	SAS points	SURF atoms	Pocket Residues
Pocket	0.879	163	78	Tyr25, Arg28, Lys29, Gln56, Ser57, Tyr60, Lys64, Gln114, Trp118, Ala139, Ser142, Thr143, Met145, Asn146, Tyr21, Tyr233, Phe237, Lys240, Thr241, Asp245, Leu274, Ser277, Ile278, Tyr364, Ile367, Ala368, Gly391, Ala394, Asn395, Gly398

Molecular docking

Overall two Hydrogen bonds formed through Lys29 (4.62 Å) and Ser57 (3.12 Å) and one non-H-bond generated with Asp245 (5.77 Å), G6P had the lowest BE of -6.5 kcal/mol. On the other hand, CGA formed two hydrogen bonds with Asn374 (3.55Å) and Lys29 (6.13Å), and three non-hydrogen bonds with Phe237 (6.04Å), Tyr343 (6.45Å), and Ile346 (6.83Å), resulting in the lowest BE of -8.2kcal/mol. Amongst these residues, Lys29 shared the G6P and CGA common interaction residue, while Phe237 was found to be an active site residue. G6P and CGA's respective affinities for SLC37A4 are depicted in Figures 20 and 21 (A, B, C, D).

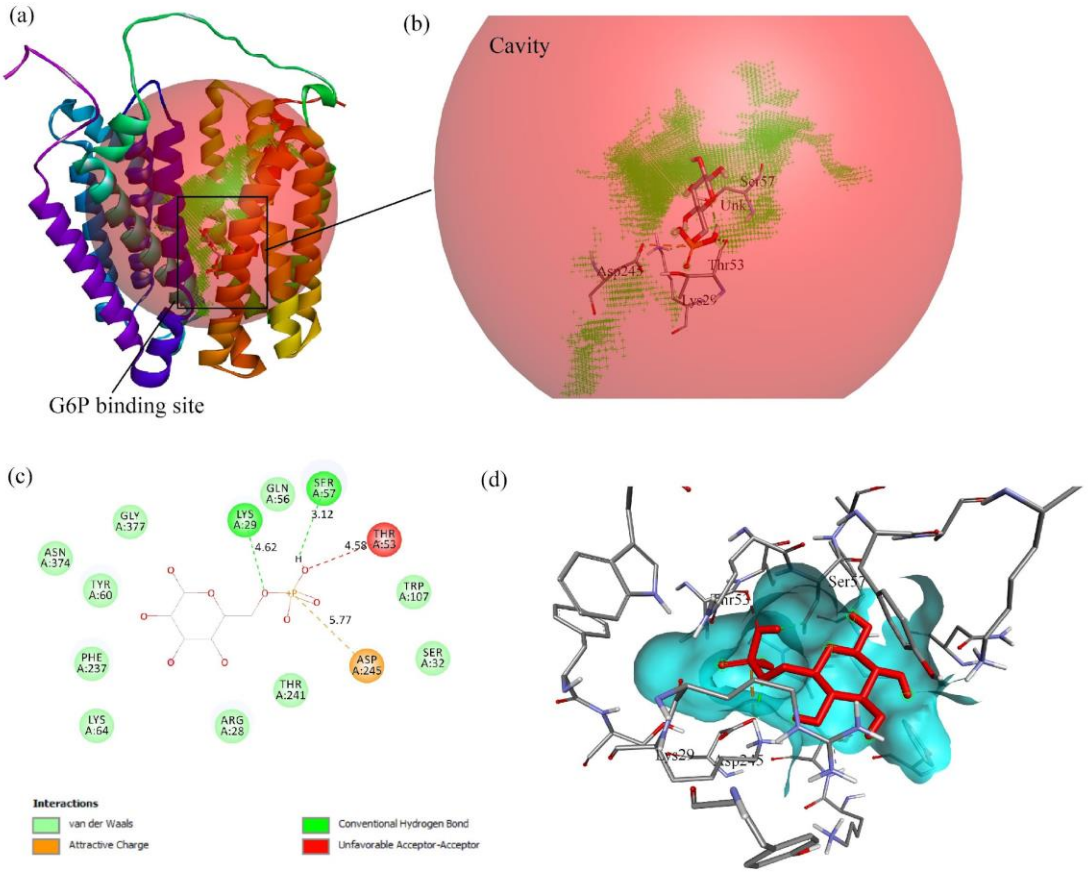

Figure 20 (A, B, C, D): The G6P intermolecular interaction with (A) SLC37A4 and (B) Ligand binding site, (C) 2D representation of the complex, (D) ligand-fit site and binding pocket

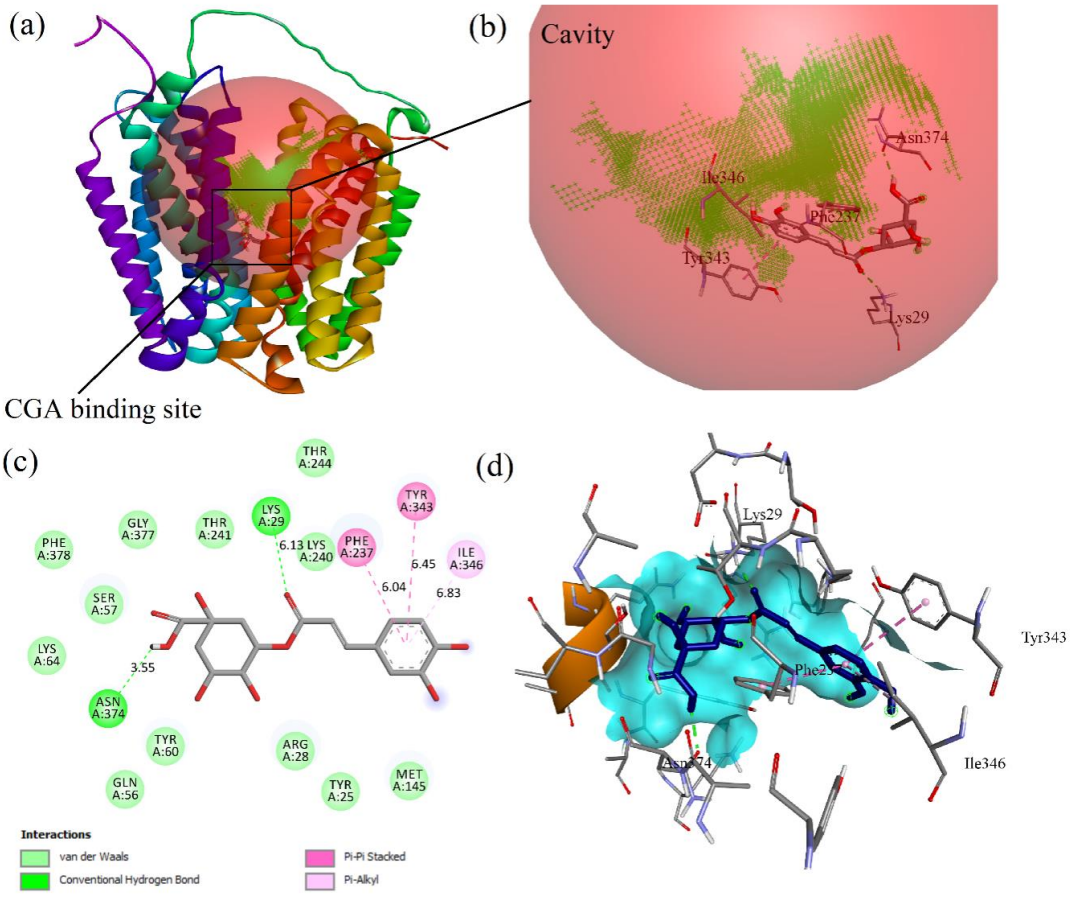

Figure 21 (A,B,C,D) : The CGA Intermolecular interaction with (A) SLC37A4 and (B) Ligand binding site, (C) 2D representation of the complex, (D) ligand-fit site and binding pocket

Molecular dynamics (MD) simulation

The G6P-SLC37A4 and CGA-SLC37A4 complexes underwent MD simulations for a 100 ns production run, with RMSD, RMSF, rGyr, H-bonds, and SASA being taken into consideration for evaluation.

RMSD:

The difference between the two confirmations can be ascertained using this parameter. An inverse relationship exists between the deviation and the RMSD value. In the G6P-SLC37A4 complex, the RMSD for both the backbone and the complex showed a small increase from around 1.5Å to approximately 3Å until 10ns. Following 10 ns, a consistent RMSD and comparable pattern were noted for the duration of the 100 ns simulation. Conversely, throughout the equilibration phase, the CGA-SLC37A4 complex's backbone and complex RMSD increased gradually from about 1.5 Å and 1.8 Å to approximately 3.0 Å and 3.5 Å, respectively, until around 40 ns. Additionally, until around 48 ns, the backbone and complex RMSDs were marginally reduced to ~2.5Å and ~3.0Å, respectively. Furthermore, it was discovered that the RMSD was steady between 48 and 100 ns, with a small variation at 85 ns. During the 100 ns production run, the complex RMSD and backbone were found to be stable and to have developed a comparable pattern. The complex RMSD and backbone for G6P and CGA in an MD simulation running for 100 ns are shown in (Figures 22 A and B), respectively.

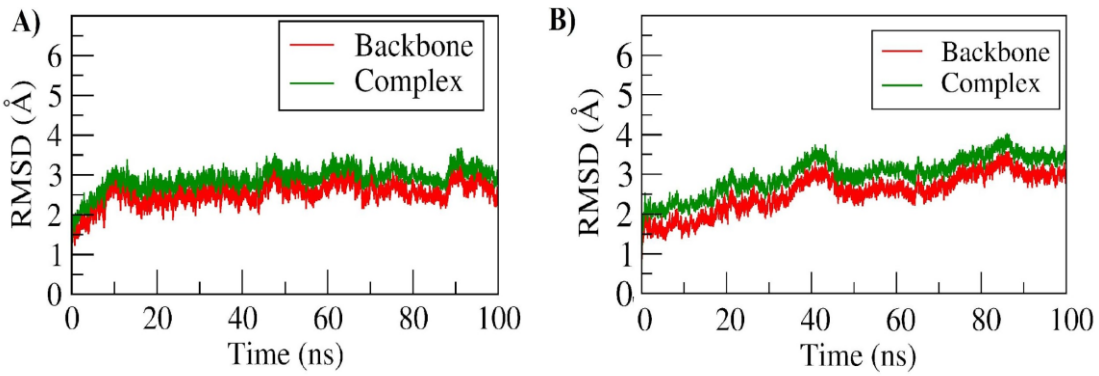

Figure 22 (A and B): RMSD of the complex's backbone atoms (A) G6P and (B) CGA-SLC37A4.

RMSF:

When a ligand molecule is present or absent, RMSF analysis helps determine which of the protein's amino acids are causing more vibrations, which leads to the instability of the protein. The longest flexible loop area in both complexes, from residue Gly195 to Leu217, displayed the greatest variability (~6 Å). Additionally, for G6P and CGA, the highest fluctuation in the C-terminal loop area from Leu414 to Glu429 was seen to be up to 4Å and 12Å, respectively. A loop linker connecting two helices (residue Gly292 to Asn298) displayed residual variation up to ~6Å and ~2Å. However, throughout the 100ns simulation in both complexes, the residues implicated in ligand binding (Lys29, Phe237, Tyr343, Ile346, and Asn374) exhibited the least amount of variation (<1.5Å). The RMSF of Cα for G6P and CGA were portrayed in the Figures 23 A and B, respectively.

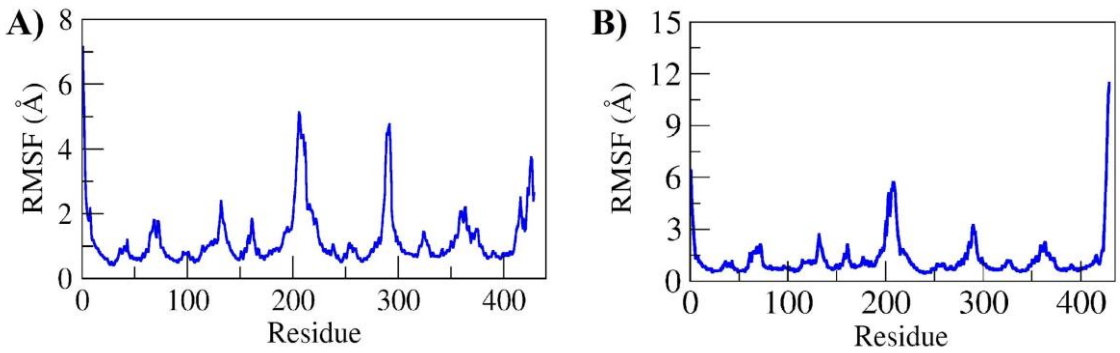

Figure 23 (A and B) : Depicts the RMSF (root mean square fluctuation) of Cα for the (A) G6P-SLC37A4 and (B) CGA-SLC37A4 complexes.

Radius of gyration (rGyr/Rg):

The protein's compactness and ligand-bound state were ascertained using the radius of gyration. Over the duration of a 100 ns simulation, the Rg values were utilized to evaluate the folding and unfolding of the protein both by itself and in conjunction with G6P and CGA. Over the course of the 100 ns production window, both proteins and complexes displayed enhanced compactness and established a comparable pattern. The complex's and protein's Rg value in the G6P-SLC37A4 complex was originally 22.5 Å, then it grew to 23 Å until 20 ns, and then it gradually fell to 22.3 Å until 65 ns. Further, up to 100ns, the Rg value raised to 22.6 Å. The equilibration period's abrupt increase in the Rg value signifies the pocket's opening, allowing the binding pocket's ligand to be buried; the pocket's closing, allowing the ligand to form a stable complex, is indicated by the Rg value's decrease following the equilibration period. Likewise, In the CGA-SLC37A4 complex, the protein and complex had a Rg value of 22.5Å. The Rg value increased to about 22.8 Å at about 46 ns and then declined to about 22.6 Å, continuing the trend throughout the entire 100 ns cycle. Following the equilibration phase, a sharp rise in the Rg value signifies the pocket's opening, allowing the binding pocket's ligand to be buried and form a stable reliable complex. Figure 24 A and B show the protein and its CGA complex Rg plots for G6P and CGA, respectively.

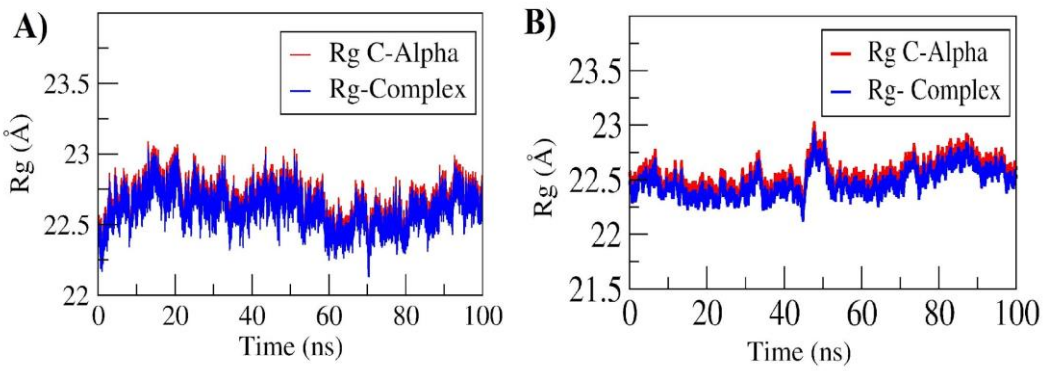

Figure 24 (A and B) : The gyration radius (Rg) of the Cα atoms in SLC37A4 complexes with A) G6P and B) CGA.

Interactions between H bonds:

Eight hydrogen bonds were formed to stabilize the G6P complex with the SLC37A4 protein of them, 3 remained constant during the course of the experiment. Similarly, eight hydrogen bonds were formed, which stabilized the CGA in combination with the SLC37A4 protein. Five of these remained stable and resilient for the course of the experiment. The G6P and CGA's H-bond interaction in combination with SLC37A4 is demonstrated in Figures 25 A and B, respectively.

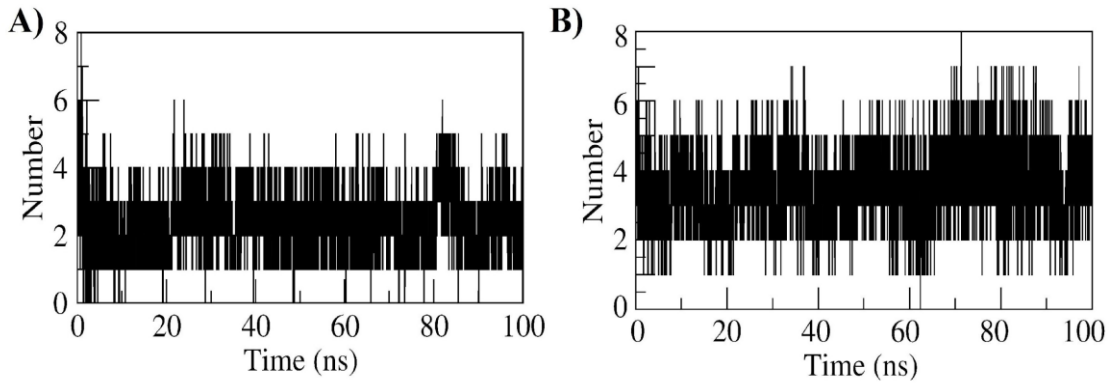

Figure 25 (A and B): During the 100ns MD simulation, hydrogen bonds were established between A) G6P and B) CGA and SLC37A4.

SASA:

The SLC37A4 protein has been displayed to consist of 12 helices arranged in a two-group structure, with residues Gly195 to Leu217 constituting the longest loop. With a surface size of 163 nm2, pocket 1 (the ligand-binding pocket) is situated amid the two group helices. Considering how flexible the binding pocket opening and loop region are, a rise in SASA was seen in both complexes after 44 ns (from about 190 nm2 to 205

nm2). However, after around 55 ns (about 197 nm2), the surface area was discovered to be constant. There were two docked complexes, with initial and final surface areas of approximately 199 and 197 nm2, respectively. The complex's average surface area was approximately 197 nm2, as shown in Figures 26 A and B for CGA and G6P, respectively.

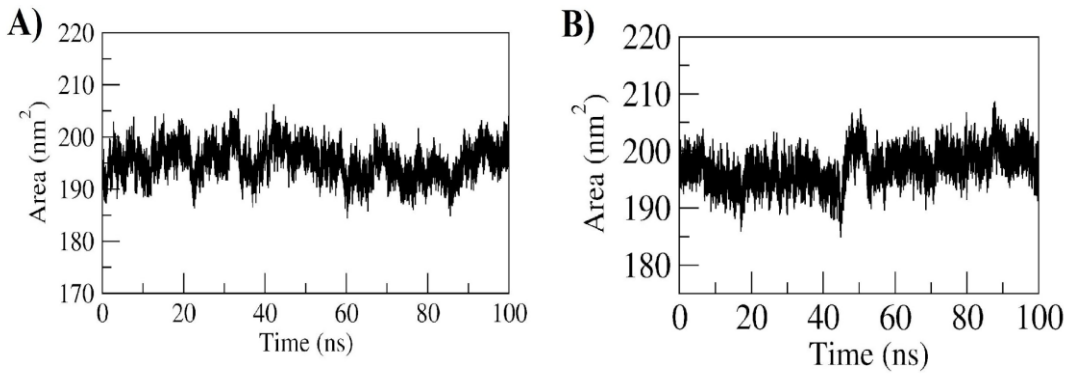

Figure 26 (A and B): SLC37A4's SASA in complex with A) G6P and B) CGA.

Calculating the binding free energy and residual decomposition energy

By employing MMPBSA, the G6P and CGA require free energy. to attach to the protein pocket was ascertained. G6P and CGA were shown to have binding free energies of -12.72±2.84 and -31.493 ± 1.486 kcal/mol, respectively, in complex with SLC37A4. The G6P-SLC37A4 complex's per-residue energy contribution showed that Arg28 and Asp245 had positive contribution energies of 6.07 and 11.18 kJ/mol, while the residues Lys29, Thr53, Gln56, Tyr60, Gln114, and Ala380 had the lowest energy contributions of -4.73, -3.57, -2.49, -6.78, -2.08, and -1.33 kJ/mol. Similarly, the CGA-SLC37A4 complex's per-residue energy contribution showed that Arg28, Lys240, Asp245,

Lys255, and Lys389 calculated the energy of the positive contribution of 3.61, 3.18, 3.07, 1.54, and 13.08kJ/mol, The residues with the lowest energy scores were Lys29, Gln56, Phe237, Glu254, and Asp325; their scores were –2.18, –2.15, –4.82, –1.87, and –10.09 kJ/mol. The per-residue contributions of G6P and CGA in combination with SLC37A4 are shown in Figures 27 A and B.

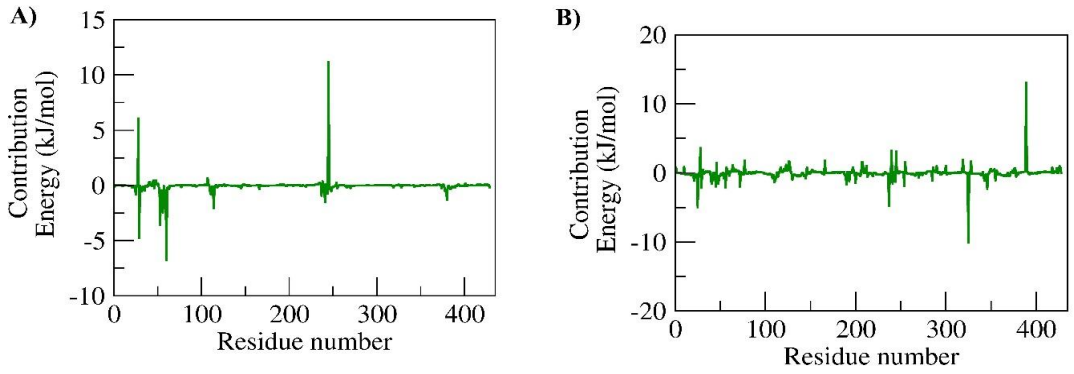

Figure 27 (A and B): The contribution energy plot highlights the role that ligand binding residues play in the creation of stable complexes.

Principle component analysis

G6P and CGA, respectively, were represented by the 2D projections for PCs 1 and the plots of the collective motion obtained by the first two principal components PCs 1 and 2. (Figures 24 A and 24 B). Compact groups in conformational spaces ranging from -5 to 5.7 are expressed by the complex of G6P with SLC37A4 (Figure 24 A). While SLC37A4 was widely clustered in the range of -5 to 7.8, and CGA with it showed little modification in the conformational space. The top two modes, PC1 and PC2, displayed a constant distribution throughout the configurational space, according to the MD trajectory of complex G6P with SLC37A4 (Figure 24 A). Furthermore, it was shown in the CGA-SLC37A4 complex that the first 50 eigenvectors captured the most

dynamics during the simulation, with the first three of them supported all the simulated complexes' collective motions in a major way. It was discovered that the CGA complex's eigenvalue was greater than that of the G6P complex (Figure 24 B).

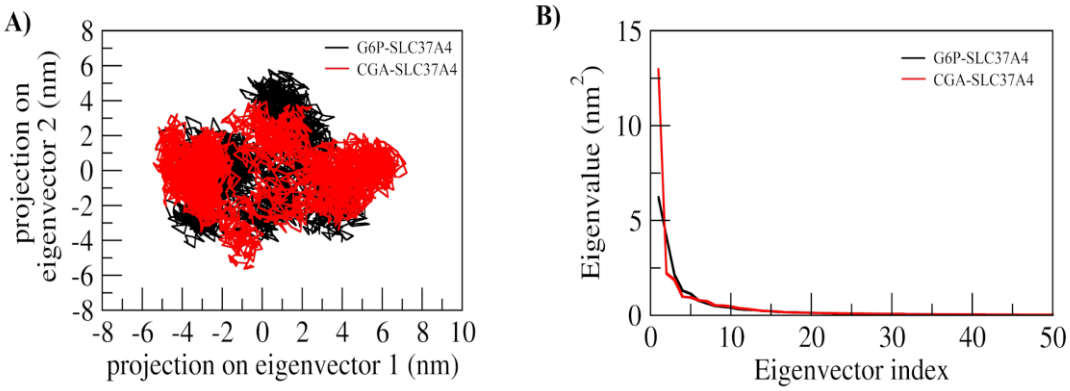

Figure 28 (A): Protein-ligand complex principal component analysis: using the first two principal components' corresponding eigenvectors as projections of the MD trajectories, we can see the G6P (black) and CGA (red) moving together using SLC37A4. (B) Using SLC37A4, the first 50 eigenvectors for G6P (black) and CGA (red) were displayed against the eigenvalue.

5.1.3. In vivo approach to establish GSD type 1 manifestations

Assessment of the fasting blood glucose level on day 14 (Pilot study):

At different intervals, the blood glucose levels were tested. (i.e., at 0.0, 60, 90, 120, and 180 mins) on day 14, to fix the dose of CGA. The fasting blood glucose levels consistently decreased at the dose of 200 mg/kg throughout the time interval (**p<0.01, up to 120 mins and **p<0.5 at 180 mins) and even 400 mg/kg dose showed good results (***p<0.001, up to 90 mins), however, the hypoglycaemia was not persistent post 90 minutes interval (Figure 29).

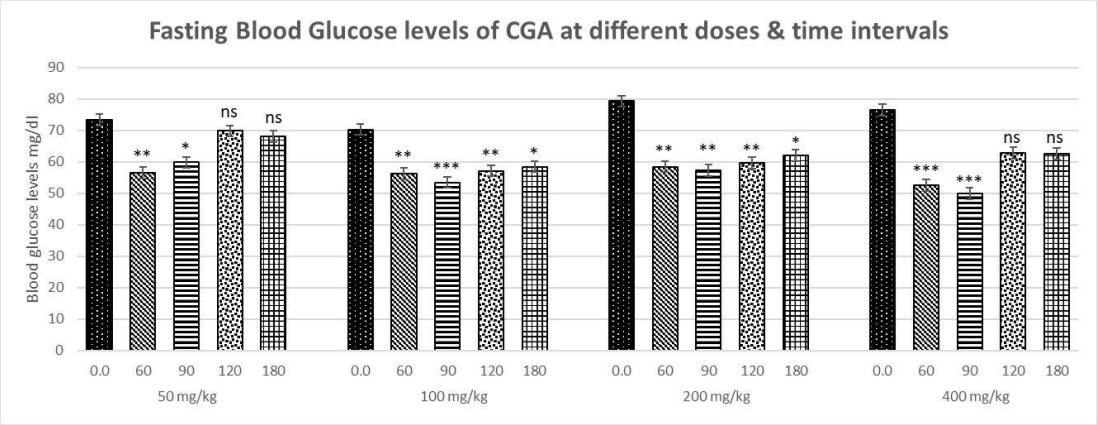

Figure 29: Pilot study to assess the fasting blood glucose levels at different time intervals, ranging from (0.0 min to 180 minutes). For each group, the findings are represented as mean ± standard error of mean (n = 6).

Assessment of the role of chlorogenic acid loaded liposome (CAL) on fasting blood glucose level to sustain hypoglycaemia:

The administration of CAL formulation did not show any success in sustaining the hypoglycaemic property of chlorogenic acid (Figure 30).

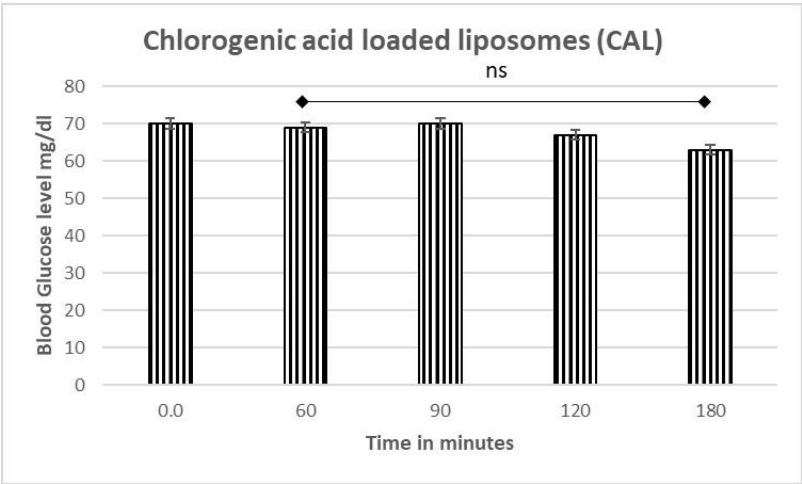

Figure 30: Impact of liposomes loaded with chlorogenic acid on blood glucose levels. The data are shown as the mean ± standard error of mean (n = 6) for each group.

Assessment of the fasting blood glucose levels at different stages of the study:

The blood glucose levels were measured on the 1st, 3rd and 7th week of the study. There was a considerable drop in blood glucose levels in Group II and III (**p<0.01) at 3 weeks interval, whereas at the 7th week interval, when compared to the animals in the control group, there was a noticeable (***p<0.001) decrease in blood glucose levels. (Figure 31).

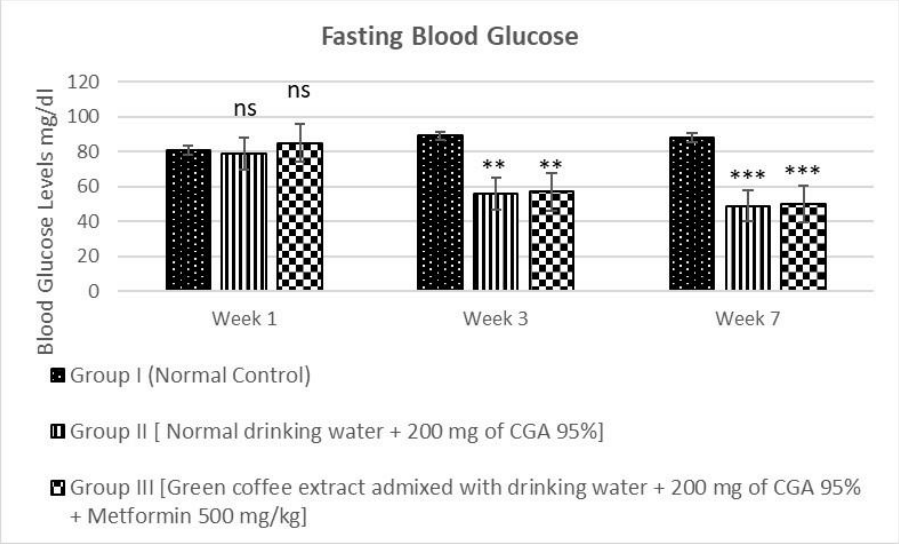

Figure 31: The fasting blood glucose was measured at fixed intervals. For each group, the findings are shown as mean ± standard error of mean (n = 6). When compared to Group I, Group II and III showed significant drops in blood glucose levels in the third week (p < 0.01) and the seventh week (***p < 0.001).**

Glucose-6-phosphatase estimation:

The glucose-6-phosphatase activity was measured as the amount of inorganic phosphate liberated. by using the standard curve approach. Group II showed no significant inhibition (p<ns), whereas, Group III showed a significant (***p<0.001)

drop in glucose-6-phosphatase activity when compared to the normal control group (Figure 32).

Table 10: Glucose-6-phosphatase estimation

Sl. No.	Groups	Mean ± SEM
1	Group I (Normal Control)	4.63 ± 0.10
2	Group II [Normal drinking water + 200 mg of CGA 95%]	4.53 ± 0.12^{ns}
3	Group III [Green coffee extract (CGA) 36% admixed with drinking water + 200 mg of CGA 95%+Metformin 500 mg/kg]	$3.12 \pm 0.03^{***}, ^{\Psi\Psi\Psi}$

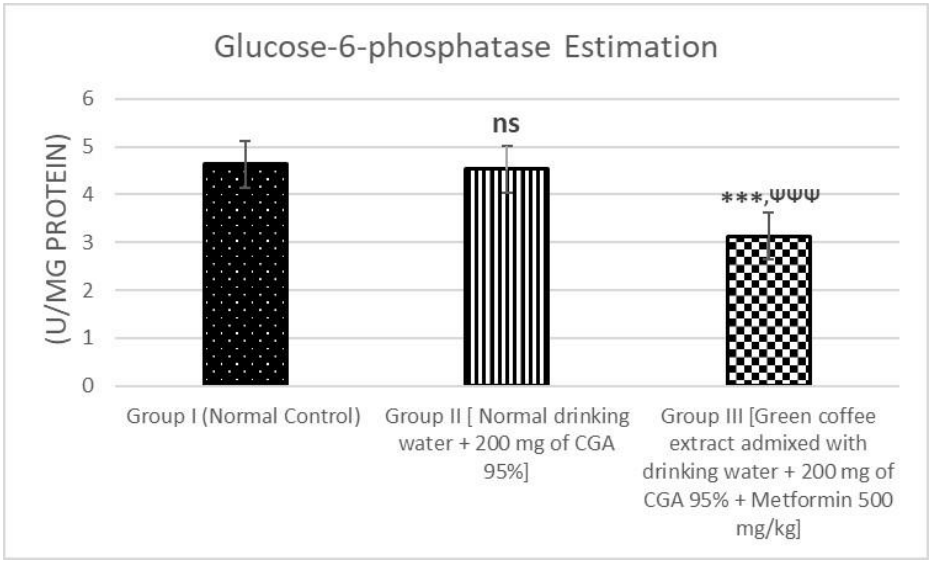

Figure 32: The glucose-6-phosphatase estimation, Group III B presented significant decrease in the blood glucose levels (*p<0.001) when compared with Control group & ($^{\Psi\Psi\Psi}$ p<0.001) when compared to Group II.**

Estimation of hepatic glycogen:

The estimated glycogen levels were analysed, in the Group II showed no significant elevation ($p<ns$), while, in comparison with the normal control, Group III showed a significant elevation in liver glycogen levels when compared to the normal control (**$p<0.01$) as well as when compared with Group II ($^{\Psi\Psi}p<0.01$) (Figure 33).

Table 11: Liver Glycogen Estimation

Sl. No.	Groups	Mean ± SEM
1	Group I (Normal Control)	33.09 ± 0.40
2	Group II [Normal drinking water + 200 mg of CGA 95%]	33.77 ± 0.32^{ns}
3	Group III [Green coffee extract (CGA) 36% admixed with drinking water + 200 mg of CGA 95%+Metformin 500 mg/kg]	$38.59 \pm 0.43^{**, \Psi\Psi}$

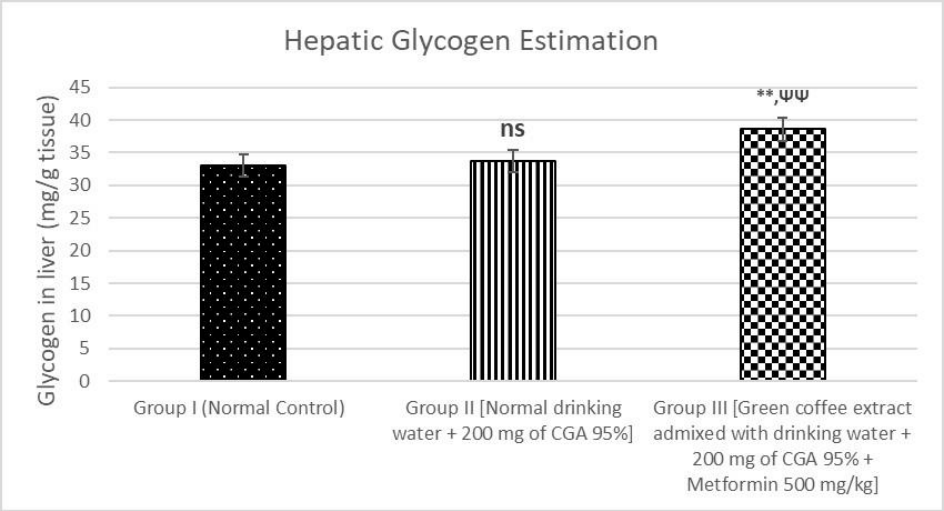

Figure 33: Hepatic glycogen content was estimated where, Group III exhibited a significant elevation in the hepatic glycogen ($p<0.01$) compared to Group I and ($^{\Psi\Psi}p<0.01$) compared to Group II.**

Measurement of serum lactate dehydrogenase:

The Lactate dehydrogenase levels increased considerably in Group II (*p<0.05), whereas in Group III there was significant increase in comparison to Group I (***p<0.001) and Group II (^{ΨΨΨ}p<0.001) (Figure 34).

Table 12: Serum Lactate dehydrogenase measurement

Sl. No.	Groups	Mean ± SEM
1	Group I (Normal Control)	182.3 ± 0.19
2	Group II [Normal drinking water + 200 mg of CGA 95%]	257 ± 0.12*
3	Group III [Green coffee extract (CGA) 36% admixed with drinking water + 200 mg of CGA 95%+Metformin 500 mg/kg]	426 ± 0.09 ***, ΨΨΨ

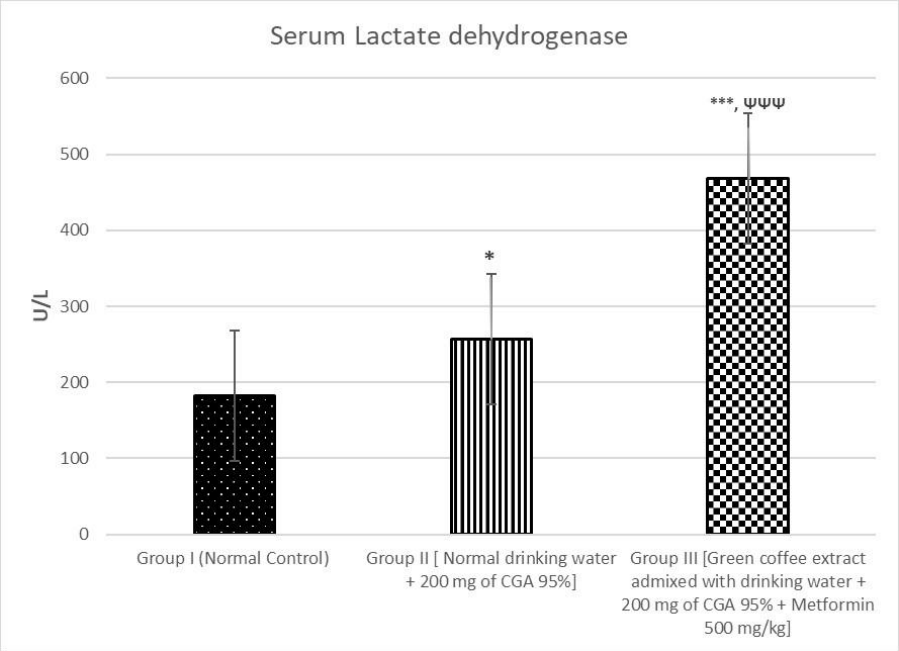

Figure 34: The serum lactate dehydrogenase evaluation where, Group II showed the significant rise in the lactate dehydrogenase (*p< 0.05), and Group III showed

(*p <0.001) high significance compared to the Group I and ($^{\Psi\Psi\Psi}p$<0.001), compared to Group II respectively.**

Measurement of Serum Uric acid :

Serum Uric acid levels did not implicate any significant differences between the experimental and control groups (^{ns}p>0.05). (Figure 35).

Table 13: Serum Uric acid measurement

Sl. No.	Groups	Mean ± SEM
1	Group I (Normal Control)	1.1 ± 0.12
2	Group II [Normal drinking water + 200 mg of CGA 95%]	1.3 ± 0.16 ^{ns}
3	Group III [Green coffee extract (CGA) 36% admixed with drinking water + 200 mg of CGA 95%+Metformin 500 mg/kg]	1.3 ± 0.08^{ns}

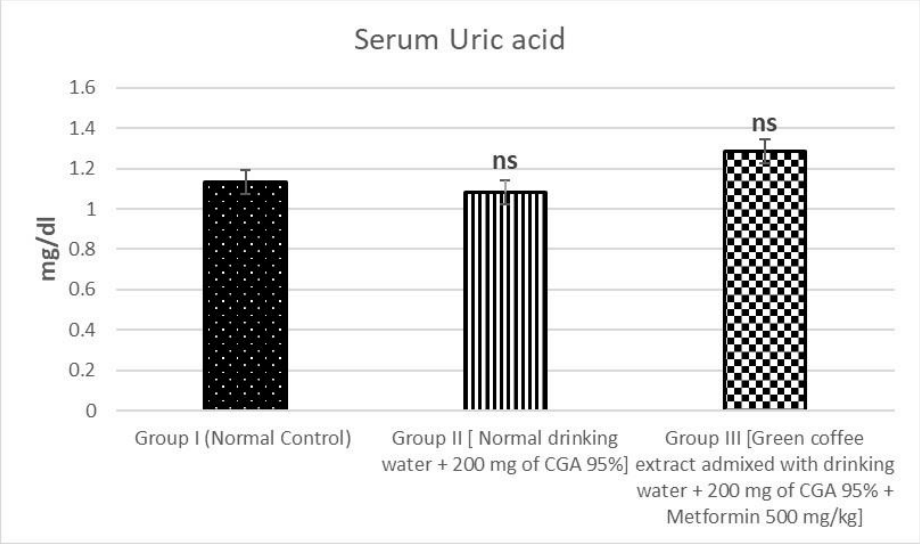

Figure 35: The serum uric acid estimation where, Group II and III were non-significant (ns, p>0.05), compared to the Group I.

Estimation of Triglyceride levels:

Serum triglyceride levels did not implicate any significant differences between the experimental and control groups ($^{ns}p>0.05$). (Figure 36).

Table 14: Estimation of serum triglycerides

Sl. No.	Groups	Mean ± SEM
1	Group I (Normal Control)	128.61 ± 0.36
2	Group II [Normal drinking water + 200 mg of CGA 95%]	135.41 ± 0.41^{ns}
3	Group III [Green coffee extract (CGA) 36% admixed with drinking water + 200 mg of CGA 95%+Metformin 500 mg/kg]	134.1 ± 0.29^{ns}

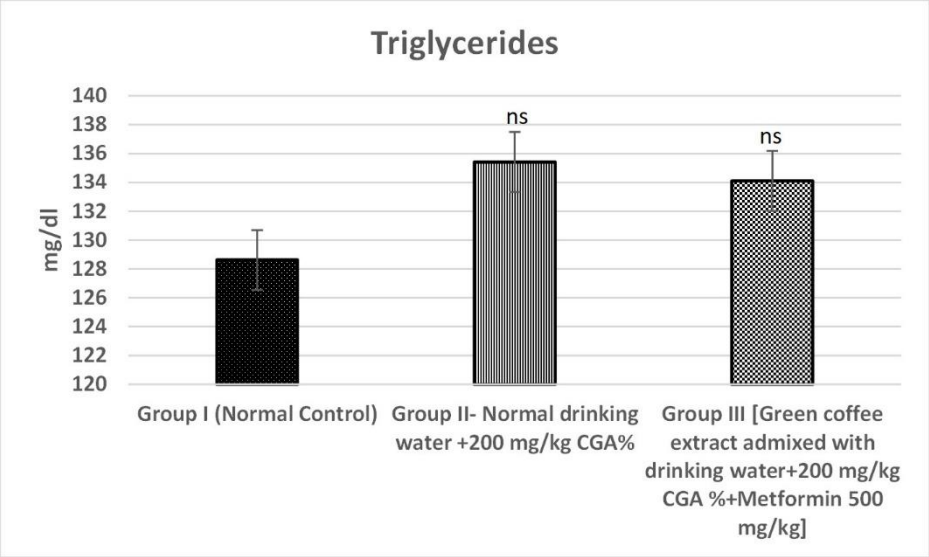

Figure 36: The serum triglyceride estimation where, Group II and III were non-significant (ns, *p*>0.05), in comparison to the Group I.

Liver weight:

The liver weight of the rats was measured after 7 weeks/49 days and it was observed that the liver weight of Group II did not increase significantly ($^{ns}p>0.05$), whereas Group III showed considerable increase in liver weight in comparison to Group I ($^{*}p<0.05$) and group II ($^{\Psi}p<0.05$) (Figure 37).

Table 15: Measurement of liver weight

Sl. No.	Groups	Mean ± SEM
1	Group I (Normal Control)	7.4 ± 0.29
2	Group II [Normal drinking water + 200 mg of CGA 95%]	7.5 ± 0.47^{ns}
3	Group III [Green coffee extract (CGA) 36% admixed with drinking water + 200 mg of CGA 95%+Metformin 500 mg/kg]	$7.9 \pm 0.34^{*,\Psi}$

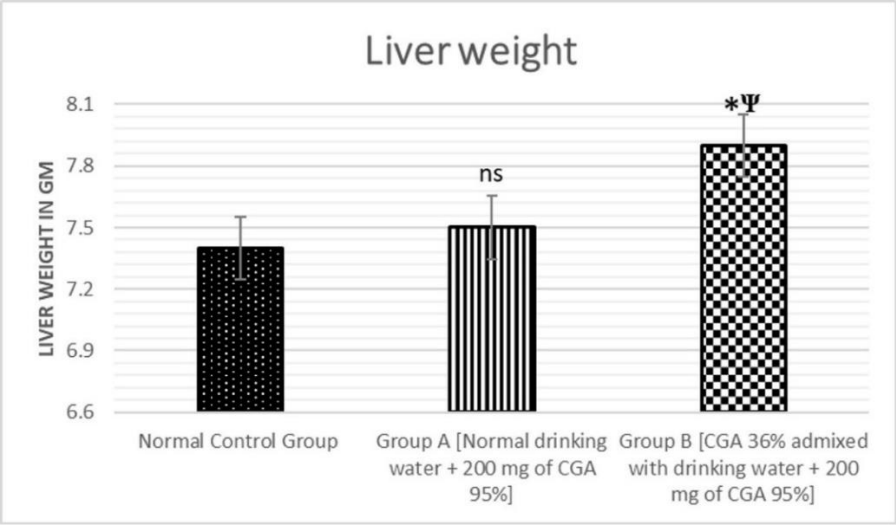

Figure 37: The liver weight of the Group III is increased ($^{*}p< 0.05$) when compared Group I and Group II ($^{\Psi}p<0.05$), whereas, Group II did not present significant changes when compared to Group I.

Histological study:

The liver tissues showed clear signs of abnormalities associated with GSD type I, in Group II, swollen hepatocytes and ballooning degeneration were observed and in Group III, Figure 34.A, B, and C.

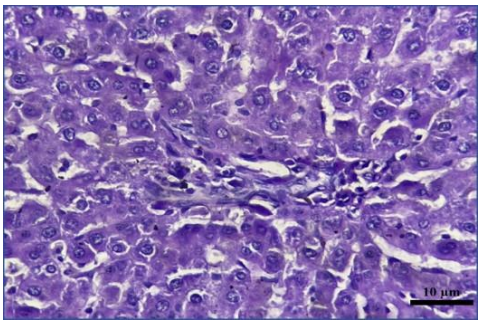

Figure 38.A: Hepatocytes are intact and there is no glycogen accumulation in the normal group, as indicated by the Periodic Acid-Schiff stain (PAS).

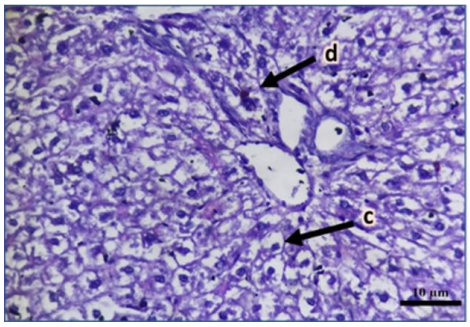

Figure 38.B: Group A; CGA (100mg/kg) treated group PAS stained, showed significant swollen hepatocytes[c] & ballooning degeneration [d]

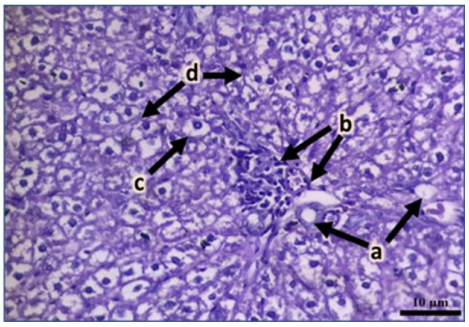

Figure 38.C: Group B; CGA (200mg/kg) treated group with PAS stain, showed notable Mosaic pattern, Glycogen nuclei [a], Glycogen [b] swollen hepatocytes [c], ballooning degeneration [d] & sinusoidal congestion [e]

5.2: Main Study

5.2.1. In silico approach

Molecular Docking

Amongst all the shortlisted bioactive micromolecules, β-carotene had the strongest binding affinity (binding energy -8.5 kcal/mol) with glucokinase. However, it did not exhibit any H-bond interaction (-6.1 kcal/mol) with the control ligand; instead, it displayed seven H-bond interactions with Ala107, Ala103, Thr102, His312, Ser153, and Trp151. With three H-bond interactions with Val135 and Pro136 and a binding energy of -8.4 kcal/mol, the control ligand exhibited the maximum binding affinity with GSK3β. When compared to the other test ligands with GSK3β, β-carotene possessed the maximum affinity for binding (binding energy: -8 kcal/mol). In a similar way riboflavin had the most binding affinity of any test ligand with protein phosphatase-1 (binding energy = -7.4 kcal/mol). Total 6 H-bond interactions with Cys278, Arg221, His248, Asp92, Arg96, and Lys98, and four H-bond interactions with Tyr69, Arg74, and Asp71 versus the control ligand (binding energy -9.9 kcal/mol). As shown in (Table 16), each ligand's binding affinity with its corresponding target. Among all the test ligands, riboflavin, β-carotene (which exhibited no H-interactions), and vitamin E interacted at a distinct position from the glucokinase control ligand-interacting molecule. On the other hand, vitamin C interacted with each amino acid that the control ligand bound to, meaning that it worked within the active site. Similar to its control ligand, riboflavin shared the Val 135 interaction residue with GSK3β, indicating that it likely has GSK3β inhibitory activity at the specified location. In similar fashion, vitamin C shared two residues of the amino acids, Arg221 and Arg96, with protein

phosphatase-1, suggesting that it may have inhibitory effects at the control ligand binding site (Tables 16 and 17) and (Table 18 and Figure 42).

Table 16: The ligands' respective binding affinities with their various targets

Ligand	Glucokinase (PDB: 1SZ2)			GSK3β (PDB: 4J1R)			Protein Phosphatase-1 (PDB: 6DNO)		
	Binding Affinity	NHBI	HBR	Binding Affinity	NHBI	HBR	Binding Affinity	NHBI	HBR
Control ligand	-6.1	7	Ala107, Ala103, Thr102, His312, Ser153, Trp151	-8.4	3	Val135, Pro136	-9.9	6	Cys278, Arg221, His248, Asp92, Arg96, Lys98
Riboflavin	-6.8	2	Asp100, Thr137	-7.3	3	Val135, Ile62, Asn64	-7.4	4	Tyr69, Arg74, Asp71
Vitamin C	-5.9	4	Thr102, Ala103, Ala107, Trp151	-5.3	4	Glu283, Met284, Thr235	-5.6	5	His125, Arg96, Tyr272, His248, Arg221
β-carotene	-8.5	-	-	-8	-	-	-7.9	-	-
Vitamin E	-5.9	1	Gly134	-7	-	-	-6.6	1	Lys98

Table 17: Selection and drug likeness of micronutrients by *in silico* approach

Sl No	Micronutrients	BE (Docking with Glycogen Synthase Kinase)	BE (Docking with Glucokinase)	BE (Docking with Protein phosphatase-1)
1	Beta Carotene	**-9.8**	**-8.9**	**-6.3**
2	Vitamin C	**-7.8**	**-6.7**	**-5.7**
3	Riboflavin	**-8.4**	**-8.1**	**-6.8**
4	Thiamine	-6.1	-3.4	--
5	Vitamin E	**-7.3**	**-8.9**	**-6.3**
6	Vitamin K	-6.1	-4.5	--

5.2.1. Strong binding affinity is shown between the chosen micronutrients and GSK3b.

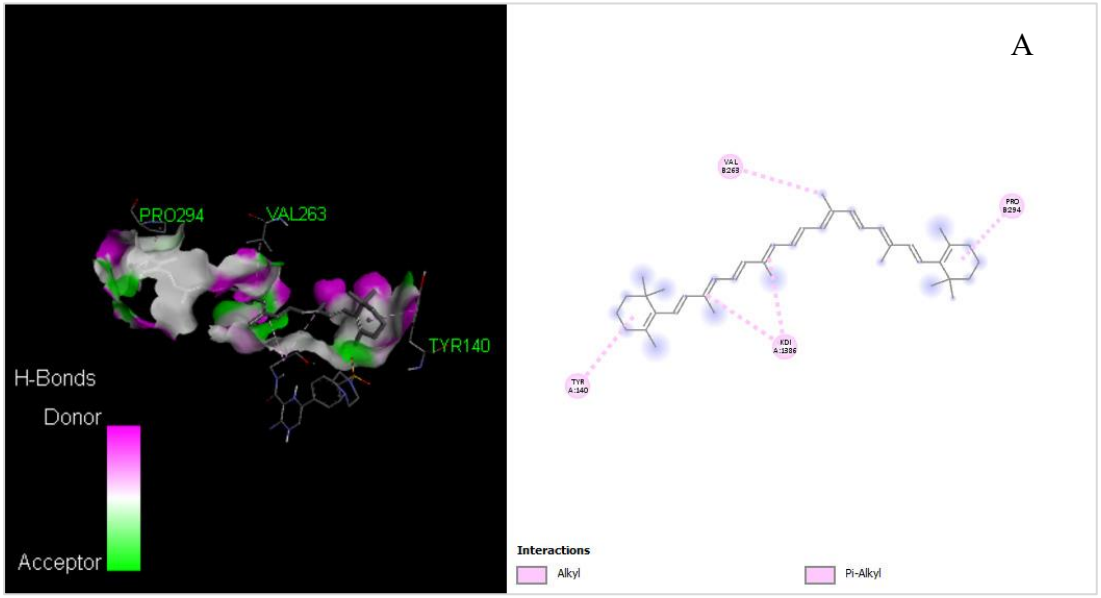

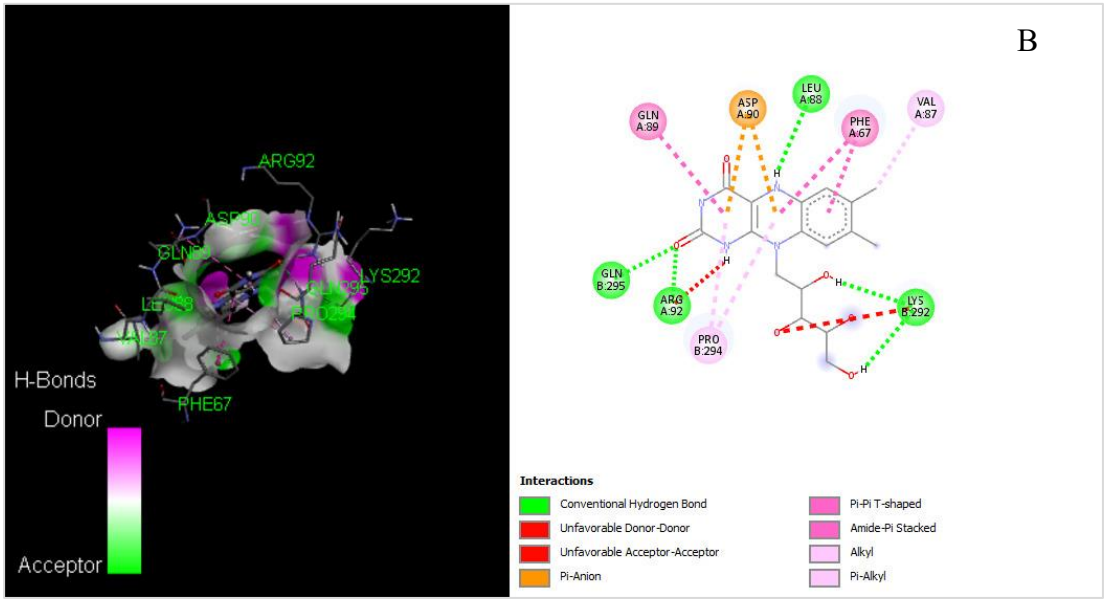

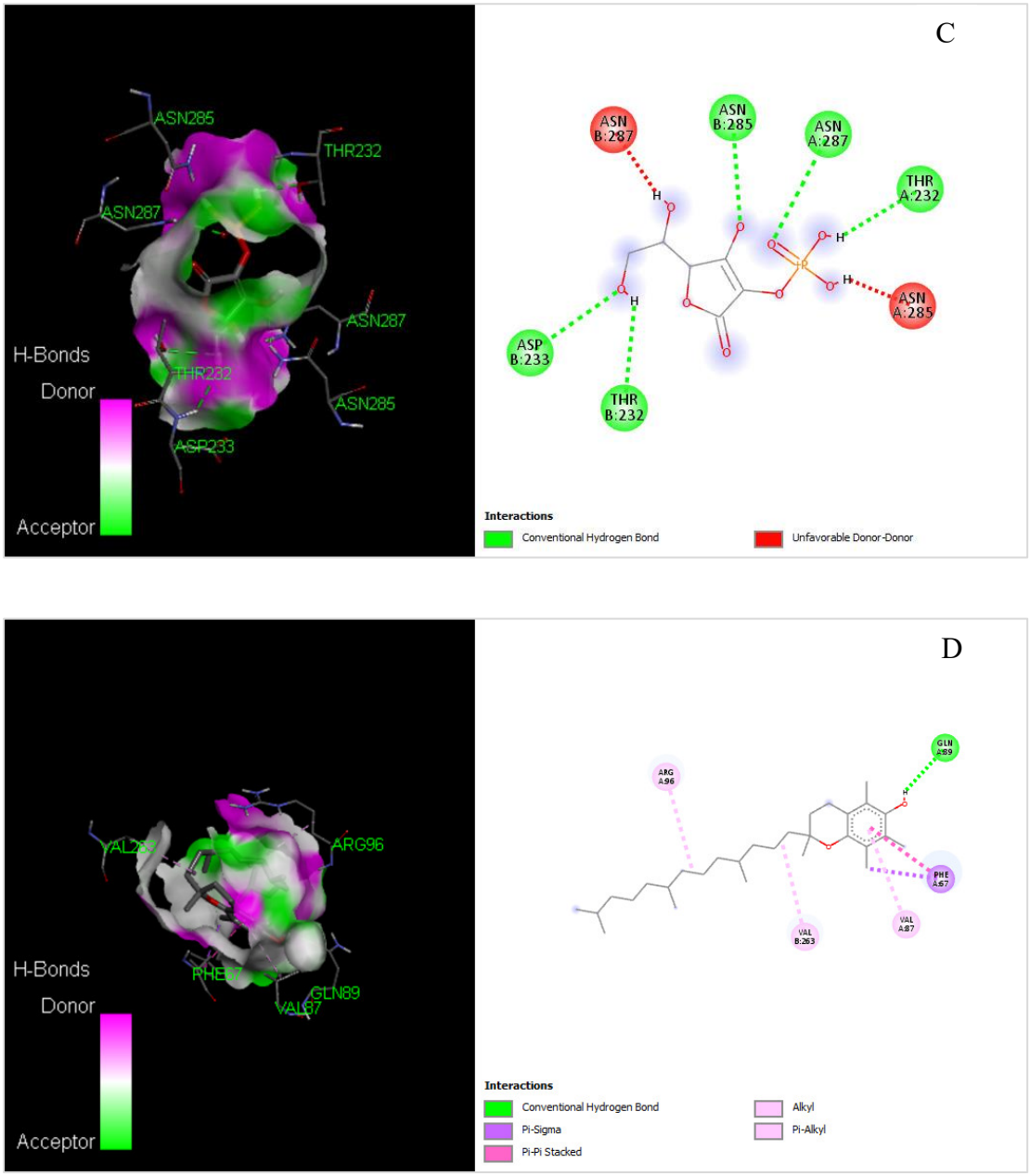

Figure 39.(A). Docking of β-carotene with GSK3b ; .(B). Docking of Riboflavin with GSK3b; (C). Docking of Vitamin C with GSK3b; (D). Docking of Vitamin E with GSK3b

5.2.2. Micronutrients with a high affinity for binding with glucokinase

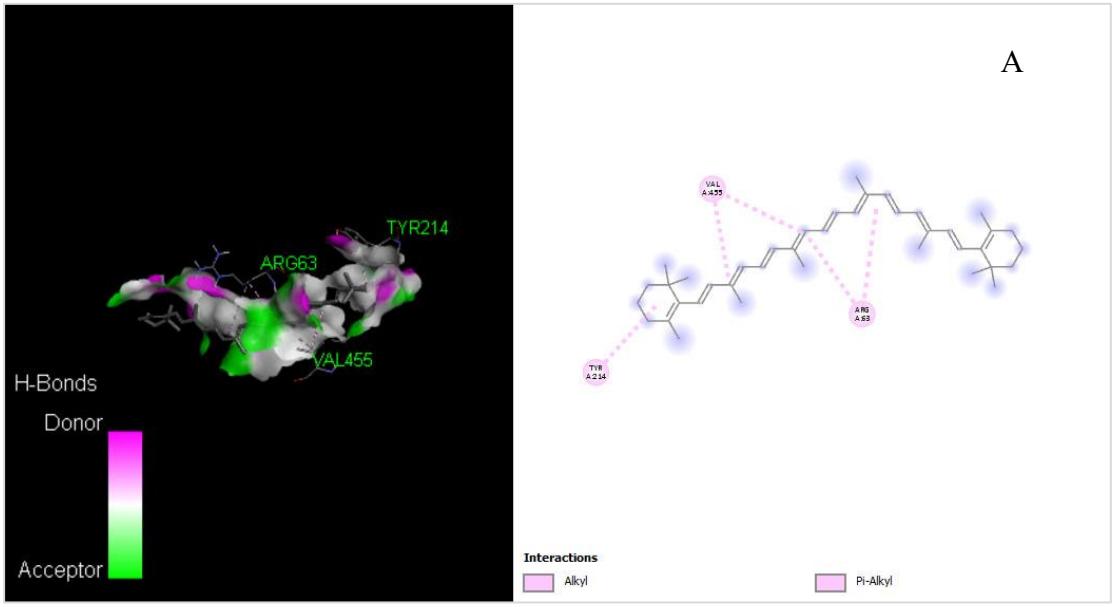

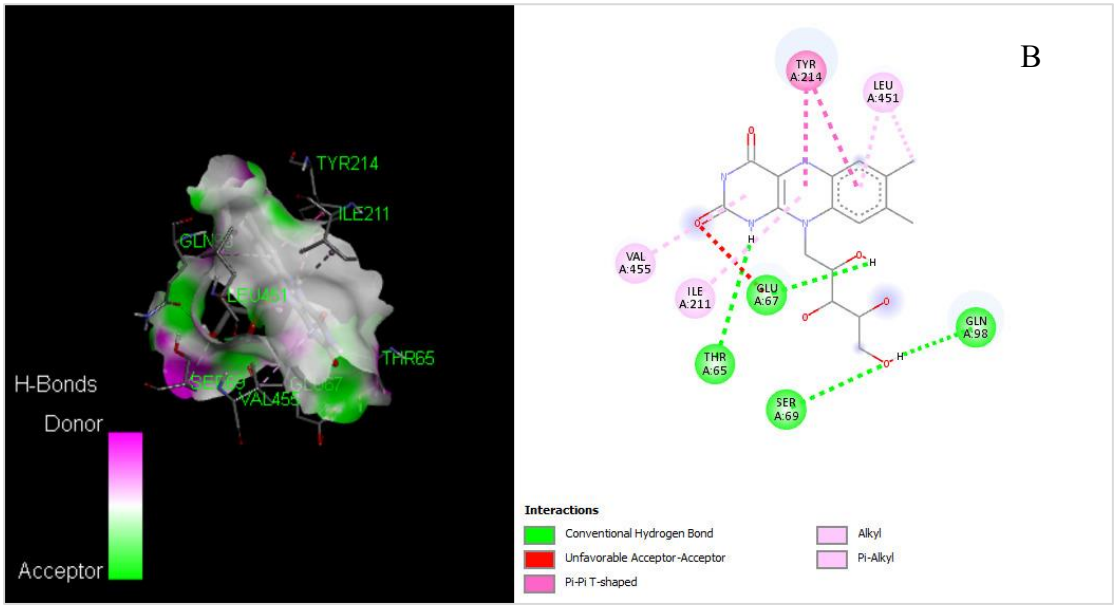

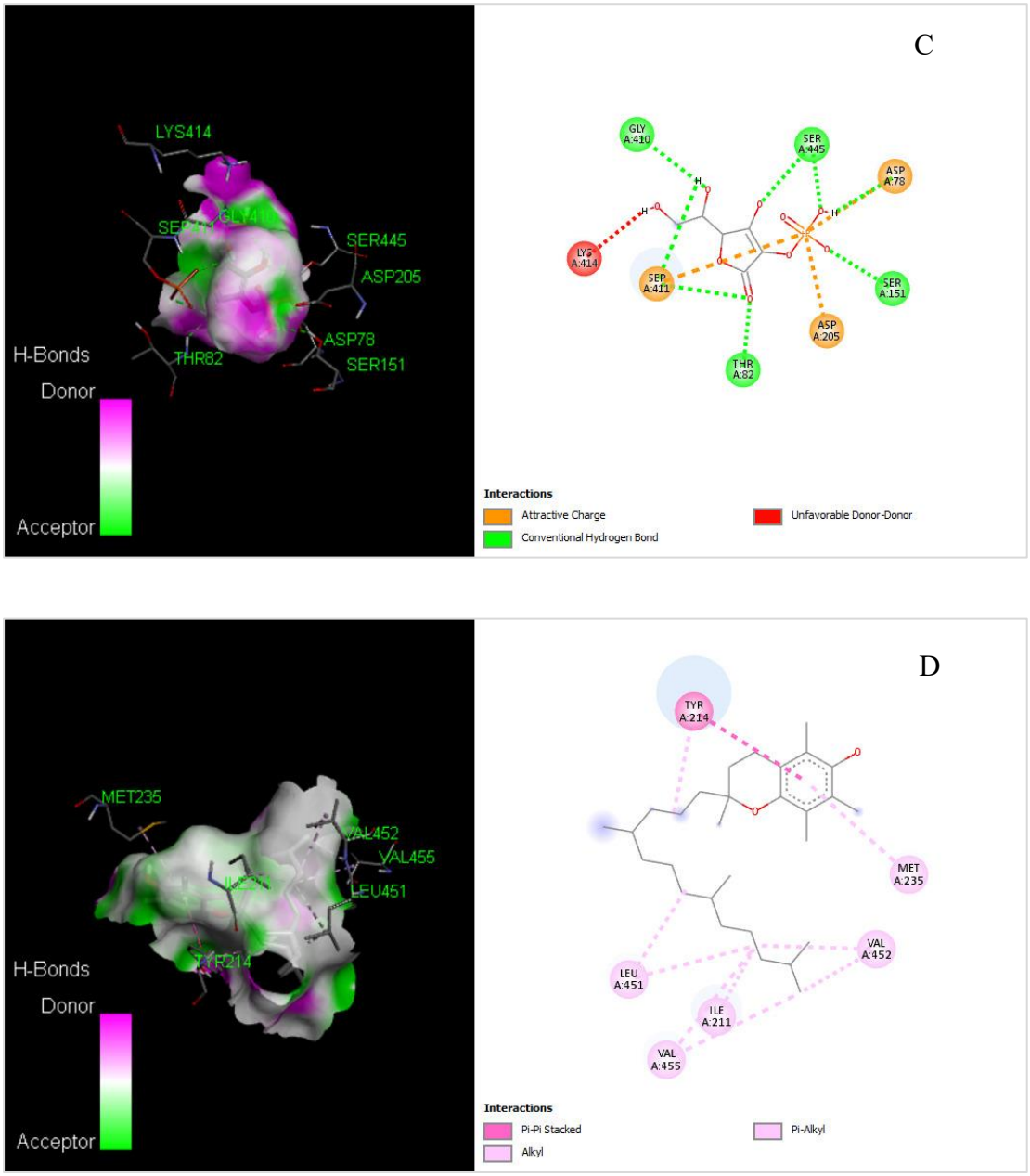

Figure 40.(A). Docking of β Carotene with Glucokinase ; (B). Docking of Riboflavin with Glucokinase ; (C). Docking of Vitamin C with Glucokinase; (D). Docking of Vitamin E with Glucokinase

5.2.3. Micronutrients possessing a high affinity for binding to protein phosphatase-1

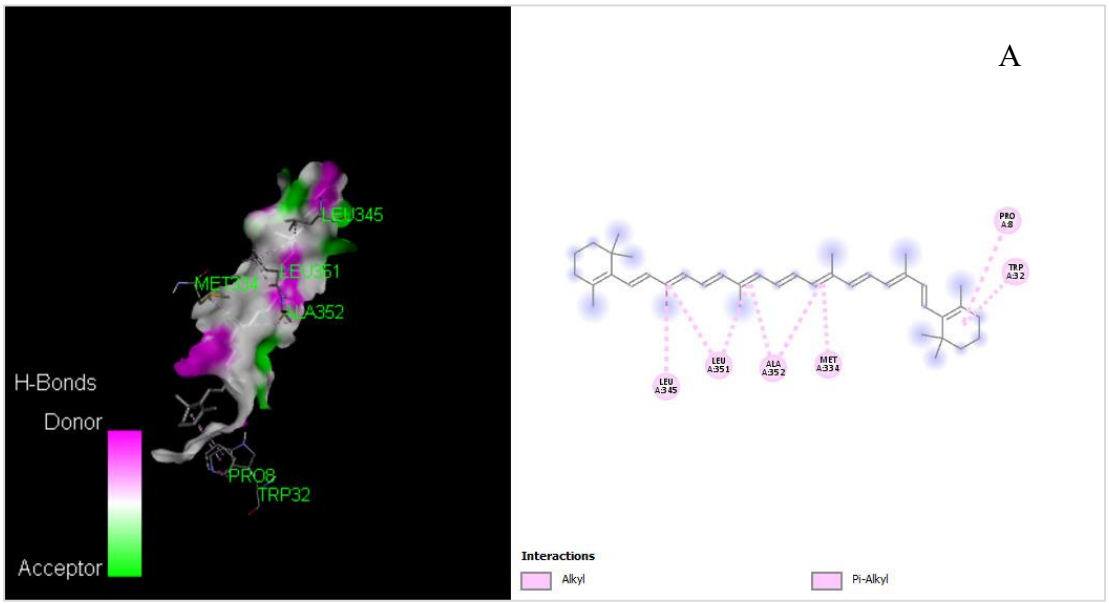

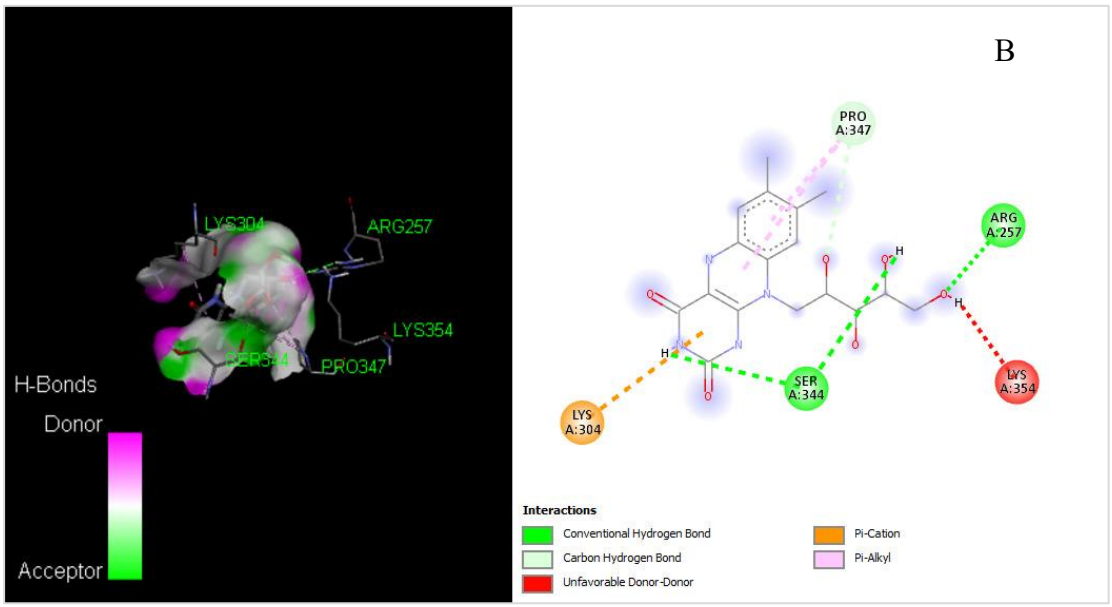

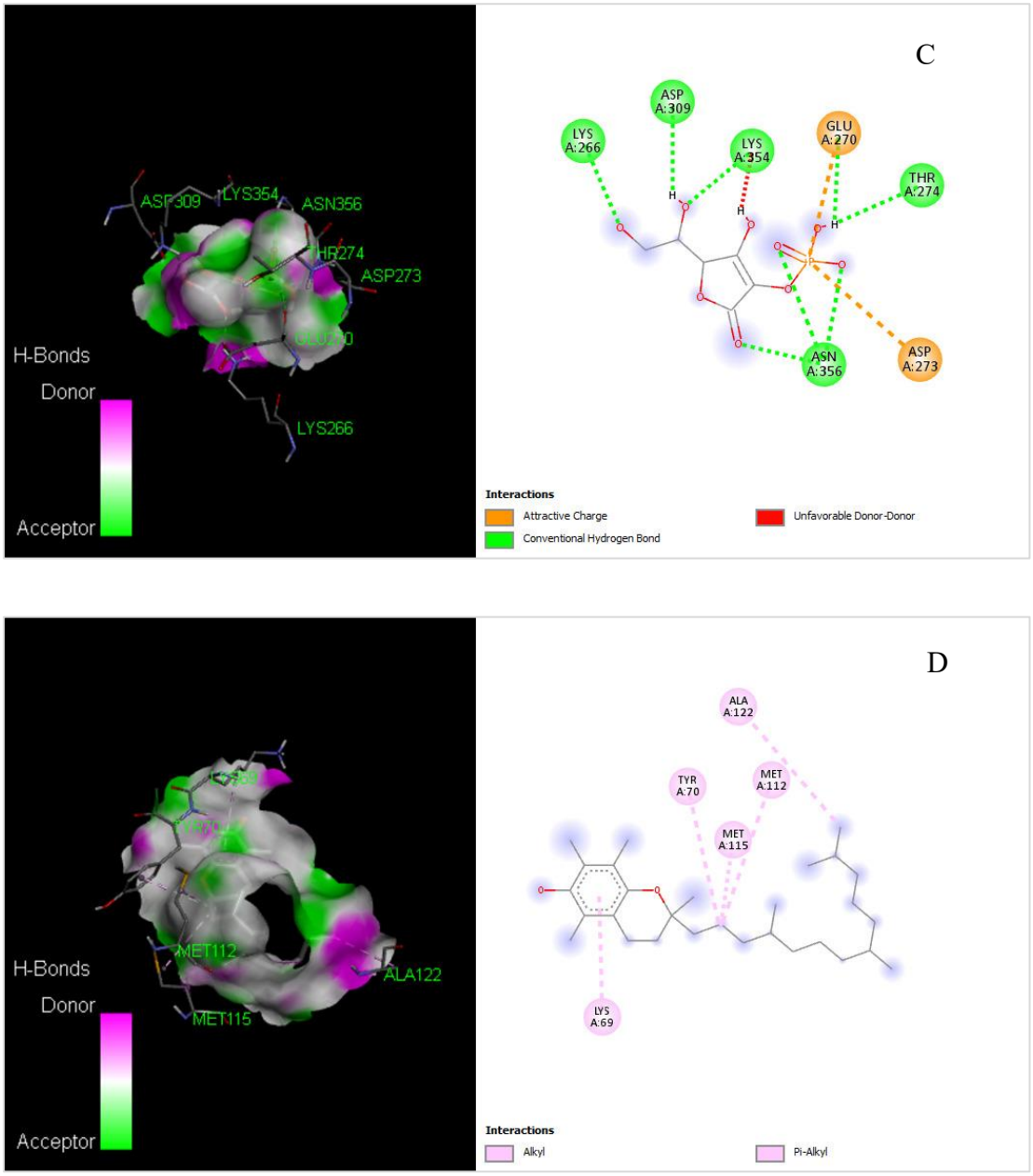

Figure 41(A). Docking of β carotene with Protein phosphatase-1;(B). Docking of Riboflavin with Protein phosphatase-1; (C). Docking of Vitamin C with Protein phosphatase-1; (D). Docking of Vitamin E with Protein phosphatase-1

5.2.3. Control ligand docking with glycogen synthase kinase 3b, Glucokinase, and Protein phosphatase-1

Table 18: Interaction of the proteins with respective control ligands

Pdb Id	Proteins	PubChem Id.	Control ligand	Receptor ligand interaction
1SZ2	Glucokinase	64689	Beta-D-glucopyranose	Glucokinase --- beta-D-glucopyranose
4J1R	Crystal Structure of GSK3b in complex with inhibitor 15R	134153953	(2r)-2-(1h-Indol-3-Ylmethyl)-1,4-Dihydropyrido[2,3-B]pyrazin-3(2h)-One	GSK3b ------- (2r)-2-(1h-Indol-3-Ylmethyl)-1,4-Dihydropyrido[2,3-B]pyrazin-3(2h)-One
6DNO	Serine/threonine-Protein phosphatase PP1-alpha catalytic subunit	446512	Okadaic acid	Serine/threonine-Protein phosphatase PP1-alpha catalytic subunit---Okadaic acid

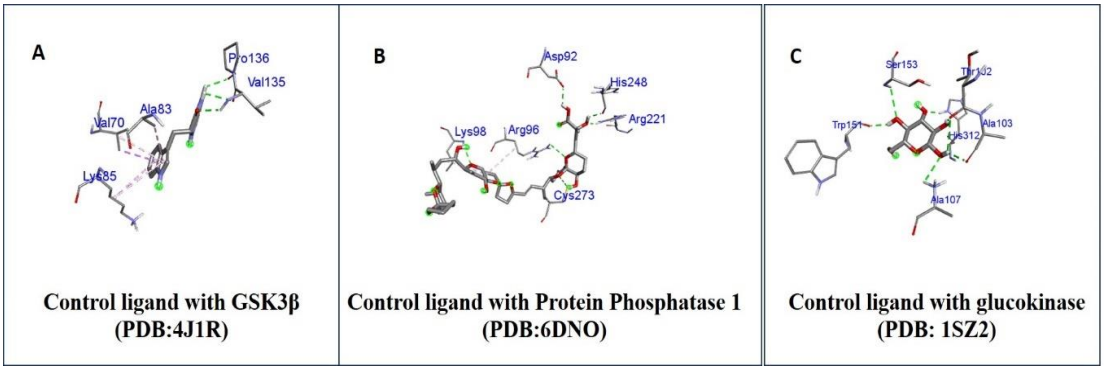

Control ligand with GSK3β (PDB:4J1R) | **Control ligand with Protein Phosphatase 1 (PDB:6DNO)** | **Control ligand with glucokinase (PDB: 1SZ2)**

Figure 42: Docked complex of proteins with their control ligand

5.2.2. In vivo study

5.2.2.1. Fasting Blood Glucose levels

The blood glucose levels of the normal group did not significantly change. On the other hand, the negative control group's blood glucose levels in figure 43 B significantly decreased (**$p<0.01$ at 30 and 60 minutes and (***$p<0.001$ at 90 and 120 minutes). The treatment group (CGA+Met+UCCS) in figure 43 C showed notable improvements in blood glucose levels (***$p<0.001$) at 30, 60, and 90 minutes, and an increase (*$p<0.05$) at 120 minutes. On the other hand, in figure 43 D, the blood glucose levels of the treatment group (CGA+Met+CS) were significantly higher than the 0.0 min measurement at 30, 60, and 120 minutes (***$p<0.001$) and at 90 minutes (**$p<0.01$). Significant persistent normoglycemia was observed in both corn and cassava starches, with cassava exhibiting the more significant normoglycemia. These results demonstrate different responses to the therapies over time with respect to blood glucose levels.

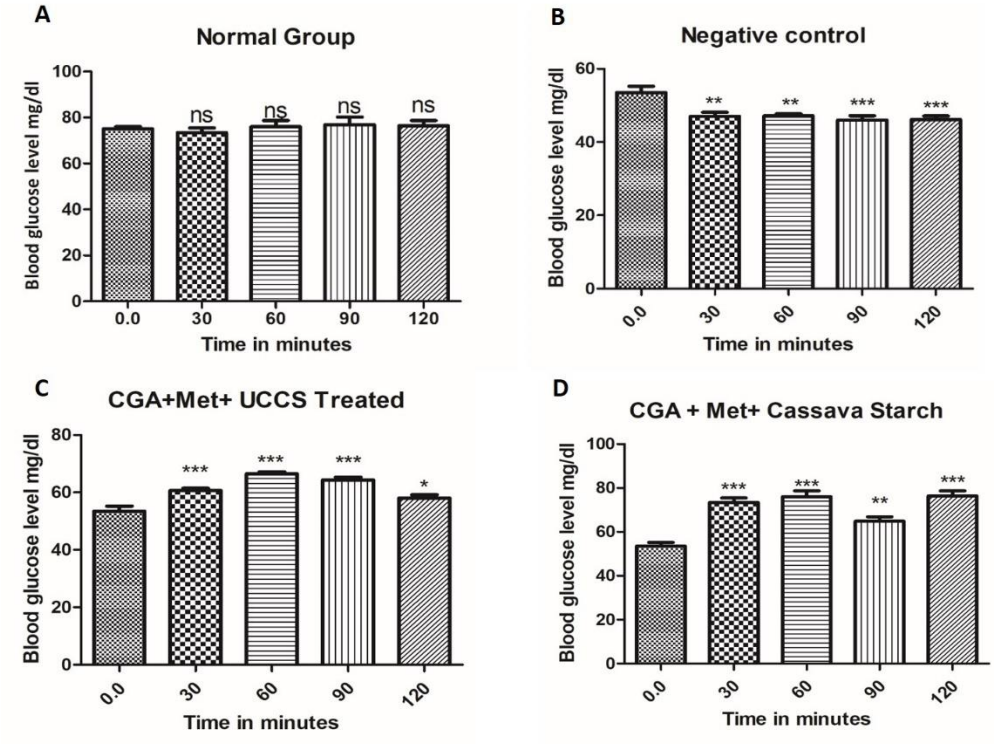

Figure 43 (A, B, C, D): Figure A showed no significant differences, but Figure B showed a considerable drop in blood glucose levels. ***p<0.001 at 90 & 120 minutes and **p<0.01 at 30 & 60 minutes) in comparison to the reading of 0.0 minutes. Figure C demonstrated a significant increase (*p<0.001) at 30, 60, and 90 minutes, whereas at 120 minutes, it was only *p<0.05. In contrast, Fig. D demonstrated a significant increase in blood glucose levels (***p<0.001) at 30, 60, and 120 minutes, as well as (**p<0.01 at 90 minutes), in comparison to a reading taken at 0.0 minutes.**

5.2.2.2. Influence of macro and micronutrients in modulating liver glycogen

Table 19: Estimation of liver glycogen

Sl. No.	Groups	Mean ± SEM
1	Control Group	33.8 ± 0.45
2	Negative Control	44.4 ± 0.50***
3	(CGA+Met)+UCCS	41.9 ± 0.48
4	(CGA+Met)+CS	40.8 ± 0.26
5	(CGA+Met)+UCCS+Micronutrients	38.8 ± 0.36 ΨΨ
6	(CGA+Met)+CS+Micronutrients	35.6 ± 0.42 ΨΨΨ,γγ,δ

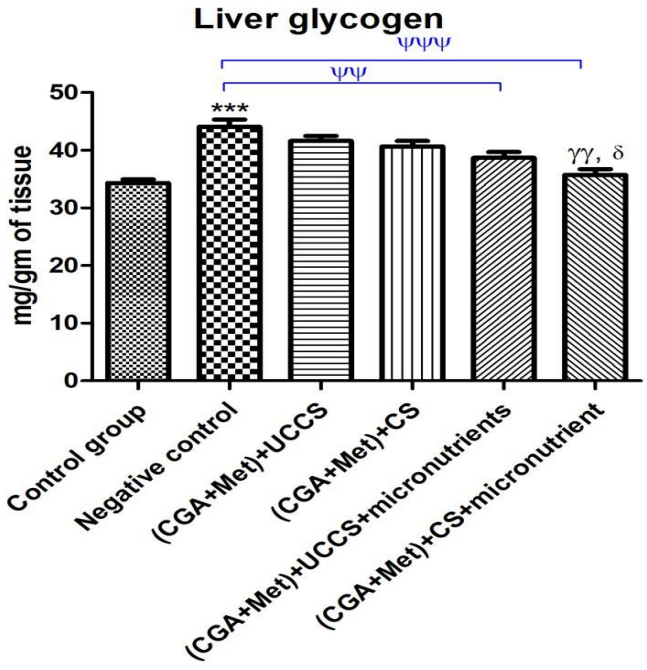

Figure 44: When compared to the Normal control, the liver glycogen content in the Negative control group revealed a significant increase (*p<0.001). In contrast, the glycogen levels in the (CGA+Met)+UCCS+micronutrients group**

and (CGA+Met) + cassava starch + micronutrients group showed a significant reduction (ΨΨ p<0.01) and p<0.001) when compared to the Negative control; in contrast, the (CGA+Met)+cassava starch+micronutrients group demonstrated (γγ p<0.01) in comparison to (CGA+Met)+UCCS, and (δ p<0.05) in comparison with (CGA+Met)+CS group.

5.2.2.3. Influence of macro and micronutrients in modulating liver weight

Table 20: Measurement of liver weight

Sl. No.	Groups	Mean ± SEM
1	Control Group	7.58 ± 0.03
2	Negative Control	8.305± 0.05***
3	(CGA+Met)+UCCS	7.91 ± 0.11
4	(CGA+Met)+CS	7.85 ± 0.10 $^{\Psi}$
5	(CGA+Met)+UCCS+Micronutrients	7.73 ± 0.11 ΨΨΨ,γγγ,δδδ
6	(CGA+Met)+CS+Micronutrients	7.62 ± 0.05 ΨΨΨ,γγγ,δδδ

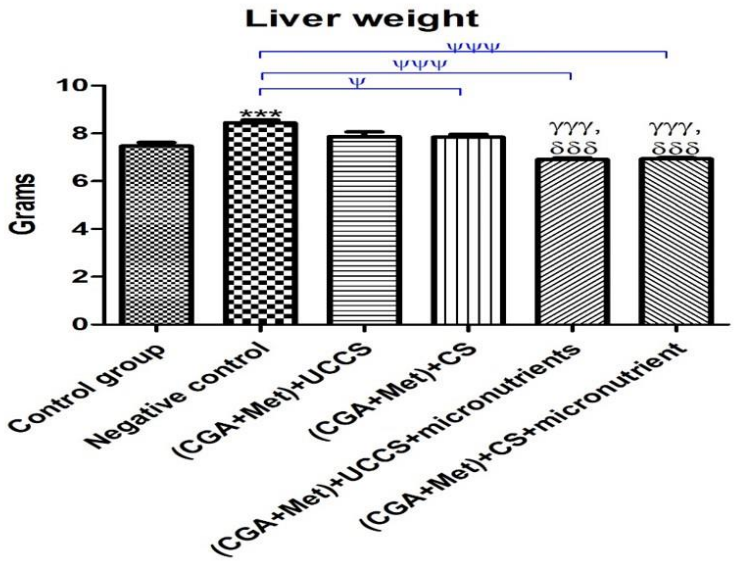

Figure 45. The negative control group's liver weight significantly increased (*p<0.001) in comparison to the control group; in contrast, the liver weight of the (CGA+Met)+cassava starch group decreased (Ψp<0.05), and both micronutrient treated groups significantly decreased (ΨΨΨ p<0.001) in comparison to the negative control group. Similarly, the liver weight of the (CGA+Met)+UCCS+micronutrients and the (CGA+Met)+cassava starch+micronutrients significantly decreased (γγγ p<0.001) when compared to the (CGA+Met)+UCCS and (δδδ p<0.001) when compared to the (CGA+Met)+cassava group.**

5.2.2.4. Histopathological analysis

Based on Periodic Acid-Schiff stain (PAS) staining, the typical histological characteristics of rat livers for each group are shown in Figure 7. In comparison to the normal group, the CGA treated group displayed substantial Glycogen, Glycogen nuclei, enlarged hepatocytes, ballooning degeneration, and sinusoidal congestion. However, the groups that received (CGA + Met) + UCCS and (CGA + Met) + Cassava Starch treatments had pronounced glycogen, enlarged hepatocytes, and ballooning degeneration. On the other hand, the groups that received UCCS + micronutrients and Cassava starch + micronutrients revealed almost undamaged hepatocytes with a normal architecture and minimal glycogen accumulation.

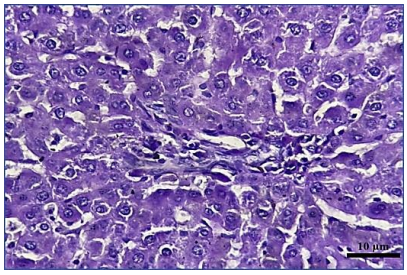

A

Figure 46 (A): Periodic Acid-Schiff stain (PAS) of the Normal Group shows typical architecture without any glycogen accumulation and with undamaged hepatocytes

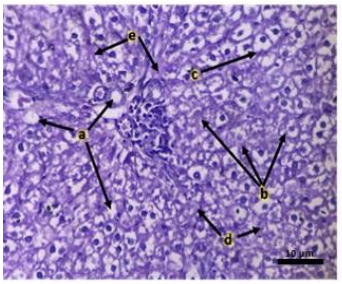

B

Figure 46 (B): CGA (200mg/kg) treated group PAS stained, showed significant Mosaic pattern, Glycogen nuclei [a], Glycogen [b]

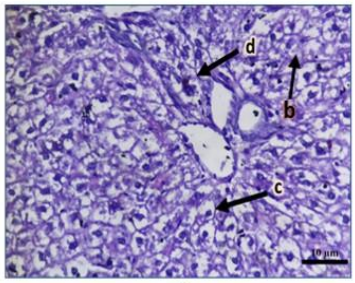

C

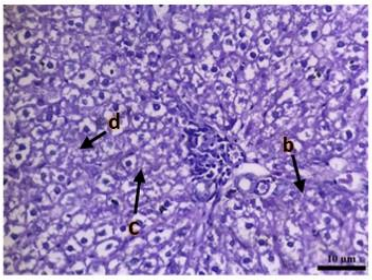

D

Figure 46 (C): (CGA+Met) + UCCS treated group and
Figure 46 (D): (CGA +Met) + Cassava Starch treated group PAS stained, showed notable Glycogen [b], swollen hepatocytes [c], & ballooning degeneration [d]

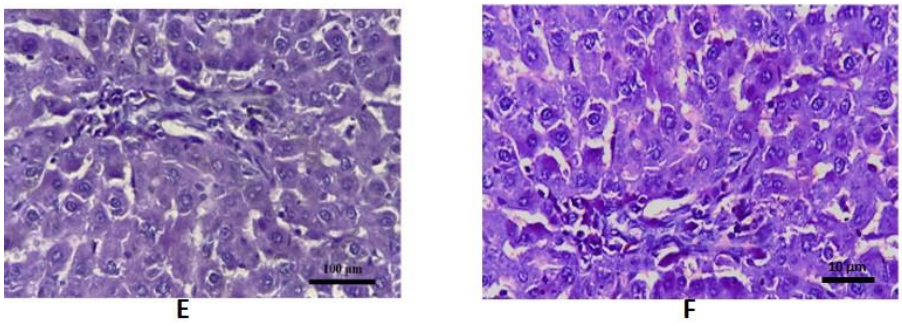

Figure 46 (E): UCCS + micronutrients treated group
and
Figure 46 (F): Cassava starch + micronutrients treated group showed near normal architecture with intact hepatocytes and no Glycogen accumulation

Statistical analysis

The statistical software named GraphPad Prism v.8.0 was utilized to evaluate all the data, which were then presented as mean SEM. The data were examined using analysis of variance (ANOVA), followed by *post-hoc* Bonferroni's multiple comparison test. where p values of < 0.05) were considered to be significant as statistical standards.

6. DISCUSSION

The absence of endogenous glucose synthesis resulting in acute hypoglycaemia after a short duration of fasting is a characteristic feature of GSD type 1.[22,23] This pathophysiology is induced due to the deficiency of enzyme complex glucose-6-phosphatase (G6Pase), involving the G6Pase catalytic subunit which is encoded by the (G6PC1) gene and the glucose-6 phosphate transporter or translocase subunit (G6PT), which is encoded by (*SLC37A4)* gene.[24] The complex macromolecules like glycogen are fundamental in keeping blood sugar levels stable within the physiologic range. The regulation of synthesis or degradation of glycogen is highly systematized and complex. Anomaly in the degradation of glycogen is referred to as glycogen storage disorders (GSDs) are rare diseases yet they make up a major category of inborn errors of metabolism or autosomal recessive illnesses and there is no specific treatment available for the disorders. GSD type 1 renders the patients vulnerable to other long-term complications, such as hyperuricemia, lactic acidemia & hepatomegaly and glycogen build up in liver, along with other chronic & serious complications like hepatocellular adenomas & renal impairment. Animal models which can be easily manipulated and maintained are essential in providing mechanistic insights that can direct eventual therapeutic strategies. To elucidate the biochemical basis of GSD type 1a and to assess the advent of gene therapy approach to rectify or improve *G6pc* deficiency have been studied on two animal models of GSD type 1a. By using *G6pc* knockout mouse, created by Dr. Janice Chou presented with low birth weight, but developed severe hypoglycaemia instantaneously & gradually exhibited a pronounced increase in the serum cholesterol and triglyceride levels.[25] Nonetheless, they did not generally

manifest lactic acidosis. Similarly, a canine (Maltese breed) model of GSD type 1a having a natural mutation in the *G6pc* gene was discovered and used to delineate the pathology of the disease.[26] The similar canine model was manipulated by crossbreeding a *G6pc* mutation carrier Maltese breed with a beagle breed.[27] These canine models presented with peculiar and specific symptoms similar to that of human disease, including lactic acidemia, however, these models proved ineffective for investigation of the long term or chronic complications observed in GSD type 1a. GSD type 1a mice models that only target deletion of *G6pc* in liver, and/or kidneys, or gut have been recently developed with a purpose of monitor the development of long term diseases or manifestations that emerge in GSD type 1a patients and to assess the potential treatment strategies.[8]

This

Development of GSD type 1 animal model

The primary goal of this work was to find out if the chemically induced GSD model can be developed, which could be more reliable and economical, and to investigate the most common GSD type 1 manifestations.

6.1. In-silico approach

6.1.1. Molecular docking and molecular dynamics to study GSD type 1a

The present study aimed to evaluate the binding patterns of Glucose-6-phosphatase (G6Pase) using AutoDock Vina through a triplicated docking approach. The intermolecular interactions between the G6Pase protein (PRO) and CGA ligand (LIG) were analyzed and it was observed that the stability of the complex is primarily influenced by carbon-hydrogen interactions, Vander Waal's forces, and typical hydrogen bonds.

To further understand the stability of ligand and protein complexes. Molecular Dynamics (MD) simulation involving all atoms lasting 100 nano seconds (ns) was accomplished. Two systems were considered: (i) Protein alone (PRO-APO) and (ii) Protein with ligand (PRO-LIG). The structural properties of the protein-ligand interaction were analyzed based on the average values of RMSD, RMSF, Rg, and SASA.

The RMSD and RMSF values provide perspectives on the overall stability and flexibility of the protein's structure. A more stable and reliable structure is indicated by a lower RMSD value, on the other hand a higher RMSF value indicates greater flexibility. In our study, the average RMSD value for the PRO-LIG complex was lower compared to the PRO-APO system, indicating that the presence of the ligand contributed to the protein structure's stability. This suggests that the binding of the ligand to the protein induces conformational changes that promote a more stable structure.

The radius of gyration, or Rg value, is a measurement of the protein's size. A larger Rg value indicates a larger protein. In our study, the Rg value for the PRO-LIG complex was found to be slightly larger compared to the PRO-APO system. This suggests that the binding of the ligand may induce a slight expansion in the size of the protein. However, this change in size is relatively minor and may not significantly affect the overall stability of the complex.

The SASA value, representing the solvent accessible surface area, gives details about the protein's surface area that has been exposed to the solvent. A higher SASA value

suggests that A greater proportion of the protein comes into contact with the solvent. In our study, the average SASA value for the PRO-LIG complex was higher than that of the PRO-APO system. This suggests that the binding of the ligand leads to a greater exposure of the protein surface to the solvent. This increased solvent accessibility may facilitate interactions with other molecules or solvent molecules, potentially influencing the overall stability of the complex.

Overall, the results of the MD simulation indicate that the presence of the ligand in the PRO-LIG complex contributes to the protein structure's stability. The binding of the ligand induces conformational changes, resulting in a more stable protein conformation. Additionally, the binding of the ligand leads to a slight expansion in the size of the protein and increased solvent accessibility. These results offer insightful information on molecular interactions between G6Pase and the CGA ligand, and contribute to our understanding of the protein-ligand complex's kinetics and stability.

It is important to note that the present study has certain limitations. The MD simulation was performed for a relatively short duration of 100 ns, and longer simulations may provide further information on the stability and dynamics between a protein and a ligand complex. Additionally, the analysis focused on specific structural properties, and further investigations may be required to explore other aspects of the protein-ligand interaction, such as specific binding sites and energetics.

6.1.2. Molecular docking and molecular dynamics to study GSD type 1b

To explore the intermolecular interactions and binding mode of chlorogenic acid (CGA) with the SLC37A4 target by assimilating the molecular docking and dynamics simulation. Interestingly, few *in-vitro* and experimental studies also support the inhibition of glucose-6-phosphate complex by CGA which corroborates our findings. CGA and its derivatives have been studied in diabetic conditions and even in normal conditions there are claims that CGA suppresses the hepatic blood glucose production by which the homeostatic regulation of blood glucose can be achieved (Hemmerle *et al.*, 1997), (Arion *et al.*, 1997). However, affinity with SLC37A4, precise binding site pockets, and inhibition of the activity of glucose-6-phosphatase complex are not been understood clearly. In this regard, rigid molecular docking was performed using AutoDock vina through the POAP pipeline to infer the possible interaction of chlorogenic acid with the SLC37A4 target. Recently, Veiga-da-Cunha et al. (2019) discovered that granulocytes from patients with defective SLC37A4 (G6PT) accumulate 1,5-anhydro-glucitol-6-phosphate (1,5-AG-6-P) can drastically limit or oppose the action of hexokinase. Accordingly, in a model of G6PT-deficient mouse neutrophils, the physiological amounts of 1,5-AG caused widespread deposition of 1,5-AG-6-P, a reduction in glucose consumption, and cell death. Phosphorylation of the 1,5-anhydro-glucitol results in the primary production of 1,5AG6P (1,5-AG). Arion et al. (1998) provide strong evidence that chlorogenic acid is a selective and reversible inhibitor of SLC37A4. It was demonstrated that G6P transporting in polymorphonuclear neutrophils (PMN) in intact cells and microsomes generated from differentiated promyelocytic HL-60 cells was inhibited by a derivative of chlorogenic acid (S3483) and a G6PT inhibitor (Leuzzi et al., 2003). Remarkably, the GSD1b PMN

phenotype, a clinical disease where there is a defective or mutant SLC37A4 protein, includes a decrease in multiple functions including as phagocytosis, chemotaxis, and calcium exchange. Similarly, alterations in a number of metabolic characteristics, including glucose phosphorylation, calcium mobilization, and hexose uptake and transport, have been suggested as likely reasons for functional abnormalities in SLC37A4 (Leuzzi et al., 2003). (Oguz et al., 2015). Therefore, the mechanism by which chlorogenic acid derivatives interact with SLC37A4 will be primarily responsible for GSD1b and persistent neutropenia. and their suppression, which will occur through altered calcium permeability, poor glucose homeostasis, apoptosis, and neutrophil chemotaxis. Chlorogenic acid presumably created three non-hydrogen bonds with Phe237, Tyr343, and Ile346 and a hydrogen bond contact with Asn374 and Lys29 based on the results of the docking study. Having been identified as residues from the active site, Lys29 and Phe237 contribute to the inhibition of SLC37A4. With Lys29 and Ser57 (3.12Å), the substrate molecule glucose-6-phosphate (G6P) created a hydrogen bond contact and with Asp245, it formed one non-hydrogen bond. This demonstrates that CGA is a strong SLC37A4 competitive inhibitor. It was discovered that the common hydrogen bond-interacting residue for both G6P and CGA is Lys29.

According to Yenamalli (2018), the use of MD simulations has become crucial in mitigating the constraints of computational modeling by determining the stability and reliability of protein-ligand interactions within a target physiological system. The findings of Du *et al.* (2016), molecular docking and dynamics provide profound insights on how ligands behave or change structurally and their impact on protein stability during binding. As a result, the findings show concordance between experimental reports and computational predictions. To deduce the structural changes

following ligand binding, a 100 ns MD production run was simulated in this study. The results demonstrate that ligand interaction stabilized the protein's RMSD, which was also suggested by the Rg values for G6P and CGA. Since it illustrates the compactness of the complex formation, during a 100 ns production run, it was discovered that the ligand became buried in the binding pocket. When compared to other residues involved in the formation of the protein-ligand complex, the longest loop area in both complexes, formed by the Gly195 to Leu217 residues, showed greater fluctuation and was extremely dynamic during MD simulation. In order to create a stable complex with SLC37A4, G6P and CGA each made eight H-bonds, of which 3 and 5 remained constant over the simulation. These computational cues offer substantial validation to support earlier assertions that chlorogenic acid is a strong competitive inhibitor of SLC37A4 and offer profound insight into the structural modifications of SLC37A4 upon ligand binding.

6.1.2.1. Protein information:

In order to assess the stereochemical quality of an SLC37A4 protein structure, PROCHECK examined the geometry of the entire structure as well as the geometry of individual residues. The most favoured and additional permitted zones contained around 96.1% and 2.8% of the residues, respectively. Lys205, Lys207, and Glu213—three residues—which account for around 0.8% of the total—were discovered in liberally permitted areas of the Ramachandran plot. However, only one residue (0.3%) i.e., Ser413 was found to be in the disallowed region. Plotting the ERRAT plot revealed that the protein structure's overall quality was 97.664%, indicating the structure's high resolution and stability. Roughly 91.3% and 8.2% of the residues in the additionally permitted areas and the most favored area, respectively, were found in the G6P-SLC37A4 0ns frame complex. Ser164, one residue, was discovered in the disallowed region. In contrast, about 91.6% and 7.9% of the residues in the most favored and additional permitted regions, respectively, were located in the G6P-SLC37A4 100ns frame complex. Two residues were found: one in the disallowed region (Ser164) and one in the generously allowed region (Thr364). It was discovered that every active site residue implicated in G6P binding was located in the most favoured region. The G6P- SLC37A4 0ns and 100ns frame complex was determined to have an overall quality of 95.718% and 96.250%, respectively. Approximately 91.8% and 7.9% of the residues in the most preferred and additional favoured regions, respectively, were found in the CGA-SLC37A4 0ns frame complex. In the disallowed region, one residue, Ser164, was discovered. On the other hand, in the CGA-SLC37A4 100ns frame complex, the most favoured and additional favoured region comprised around 92.6% and 7.4% of the residues, respectively. The disallowed region contained

no residue. It was discovered that all active site residue implicated in CGA binding were located in the most favoured region. The G6P- SLC37A4 0ns and 100ns frame complex was reported to have an overall quality of 99.75% and 97.805%, respectively.

The SLC37A4 protein is composed of four binding pockets, the primary binding pocket of which was determined to have a probability score of 0.879 in the P2Rank web server. Pocket 1 contains the residues "21, 25, 28, 29, 56, 57, 60, 64, 114, 118, 139, 142, 143, 145, 146, 233, 237, 240, 241, 245, 274, 277, 278, 367, 368, 391, 394, 395, 398."

6.1.2.2. Molecular docking

By creating two H-bonds with Lys29 (4.62 Å) and Ser57 (3.12 Å), one non-hydrogen bond with Asp245 (5.77 Å), G6P achieved the lowest BE of -6.5 kcal/mol. On the other hand, CGA formed two H-bonds with Asn374 (3.55Å) and Lys29 (6.13Å), and three non-hydrogen bonds with Phe237 (6.04Å), Tyr343 (6.45Å), and Ile346 (6.83Å), resulting in the lowest BE of -8.2kcal/mol. These residues included Lys29 and Phe237, which were found to be active site residues. Lys29 also shared the common interaction residue with CGA, indicating that CGA and G6P have an affinity for SLC37A4, respectively.

6.1.2.3. Molecular dynamics simulation studies

To evaluate the G6P-SLC37A4 and CGA-SLC37A4 complex, MD simulations were run for 100 ns during which time RMSD, RMSF, rGyr, H-bonds, and SASA were taken into account.

6.1.2.4. RMSD:

The difference between the two confirmations can be ascertained using this parameter. The deviance and the RMSD value are inversely correlated. The RMSD of the G6P-SLC37A4 complex increased somewhat for both the backbone and complex, from about 1.5 Å to about 3 Å until 10 ns. Following 10 ns, a consistent RMSD and comparable pattern were noted for the duration of the 100 ns simulation. On the other hand, The backbone and complex RMSD of the CGA-SLC37A4 combination increased gradually over the equilibration period, from about 1.5 Å and 1.8 Å to approximately 3.0 Å and 3.5 Å, respectively, until around ~40 ns. Additionally, until around 48 ns, the backbone and complex RMSDs were marginally reduced to ~2.5Å and ~3.0Å, respectively. Furthermore, it was discovered that the RMSD was steady between 48 and 100 ns, with a small variation at ~85 ns. The complex RMSD and backbone RMSD for G6P and CGA during the 100 ns MD simulation, respectively, established a similar trend and were confirmed to be stable throughout the production run.

6.1.2.5. RMSF*:*

Understanding which amino acids in a protein are more likely to produce vibrations that cause the protein to become unstable—both with and without a ligand molecule—is made easier with the help of RMSF analysis. The longest flexible loop area in both complexes, from residue Gly195 to Leu217, displayed the greatest variability (~6 Å). Additionally, for G6P and CGA, the highest fluctuation in the C-terminal loop area from Leu414 to Glu429 was seen to be up to 4Å and 12Å, respectively. A loop linker connecting two helices (residue Gly292 to Asn298) displayed residual variation up to ~6Å and ~2Å. However, throughout the 100ns simulation in both complexes, the

residues implicated in ligand binding (Lys29, Phe237, Tyr343, Ile346, and Asn374) exhibited the least amount of variation (<1.5Å).

6.1.2.6. Radius of gyration estimation (rGyr/Rg)*:*

The protein's compactness was ascertained using the radius of gyration and its ligand-bound state. The Rg values were used to analyse the assembling and disassembling of the protein both alone and in combination with G6P and CGA over a 100-ns simulation. During the 100 ns production time, both proteins and complexes displayed higher compactness and established a comparable pattern. The Rg value of the protein and complex in the G6P-SLC37A4 complex was originally 22.5 Å, then it grew to 23 Å until 20 ns, and then it gradually fell to 22.3 Å until 65 ns. Moreover, up to 100ns, the Rg value rose to 22.6 Å. The ligand can become buried in the binding pocket by the sudden increase in the Rg value during the equilibration period, and the ligand can form a stable complex by the pocket closing after the equilibration period. Likewise, the protein and complex's Rg value in the CGA-SLC37A4 complex was 22.5Å. The Rg value rose to about 22.8 Å at about 46 ns and then fell to about 22.6 Å, continuing the trend for the full 100 ns. Following the equilibration period, a sharp rise in the Rg value signifies the pocket's opening, allowing the binding pocket to bury the ligand and create a stable complex.

6.1.2.7. H-bond interactions:

Eight hydrogen bonds are formed to stabilize the complex between G6P and the SLC37A4 protein. Among them, During the entire simulation cycle, there were 3 H-bonds. The formation of 8 hydrogen bonds stabilized the CGA complex with the SLC37A4 protein. Throughout the simulation, five of them remained solid bonds.

6.1.2.8. SASA:

The longest loop in the SLC37A4 protein is produced by residues Gly195 to Leu217. The protein is observed to consist of 12 helices arranged as a two-group, with a surface size of 163 nm2, the pocket 1 (ligand-binding pocket) is situated between two clustered helices. The flexible loop region and binding pocket opening are the reasons behind the enhanced SASA reported in both complexes after ~44 ns (~190 nm2to~205 nm2). However, after around ~55 ns (about ~197 nm2), the surface area was discovered to be constant. There were two docked complexes, with initial and final surface areas of approximately ~199 and ~197 nm2, respectively. The complex occupied an average surface area of approximately ~197 nm2.

6.1.2.9. Calculating the Binding free energy and residual decomposition energy

By using MMPBSA, the free energy required for the protein pocket attachment of G6P and CGA was ascertained. In combination with SLC37A4, the binding free energies of G6P and CGA were determined to be -12.72±2.84 and -31.493 ± 1.486 kcal/mol, respectively. The G6P-SLC37A4 complex's per-residue energy contribution showed that Arg28 and Asp245 had positive contribution energies of 6.07 and 11.18 kJ/mol, while the residues Lys29, Thr53, Gln56, Tyr60, Gln114, and Ala380 had the lowest energy contributions of -4.73, -3.57, -2.49, -6.78, -2.08, and -1.33 kJ/mol. Similarly, the CGA-SLC37A4 complex's per-residue energy contribution showed that Arg28, Lys240, Asp245, Lys255, and Lys389 scored the positive contribution energy of 3.61, 3.18, 3.07, 1.54, and 13.08kJ/mol, while the residues Lys29, Gln56, Phe237, Glu254, and Asp325 scored the least energy of –2.18, -2.15, -4.82, -1.87, and -10.09kJ/mol.

6.1.2.10. Principle component analysis

The 2D projections for PC1 and PC2, along with the collective motion captured by the first two principal components (PCs), were plotted for G6P and CGA. The conformational spaces ranging from -5 to 5.7 exhibit compact clusters expressed by the complex of G6P and SLC37A4. The top two modes, PC1 and PC2, in the MD trajectory of complex G6P with SLC37A4 displayed a steady distribution throughout the configurational space, while the CGA with SLC37A4 showed no change in the conformational space and was broadly clustered in the range of -5 to 7.8. Additionally, it was noted that in the CGA-SLC37A4 complex, the first 50 eigenvectors captured the most dynamics during the simulation, with the first three of them significantly contributing to the collective motions exerted by all the simulated complexes. In comparison to the G6P complex, the CGA complex was shown to have a larger eigenvalue.

6.2. In vivo approach

Numerous *in vitro* studies have advocated that CGA and its derivatives can inhibit or attenuate the activity of glucose-6-phosphate enzyme complex (G6Pase and G6PT) resulting in altered metabolism.[11,28,29] which we substantiated with in silico studies. Based on these evidences, we carried out a pilot study, where it was evident that a dosage of 200 mg of CGA per kg of body weight was optimum to induce hypoglycaemia in rats. However, since CGA has a shorter biological half-life, its ability to maintain hypoglycaemic was limited to 1.5 to 2.5 hours.[30–32] Literature suggested the formulation of chlorogenic acid loaded liposomes (CAL) can prolong the effects of CGA.[33] Nevertheless, there was no significant difference in the outcome using the liposome formulation. In order to enhance the impact of CGA, drinking water containing 36% (200 mg/kg of CGA) was mixed with green coffee extract and given to the animals in the treatment groups on a continuous basis. Additionally, The animals received 200 mg/kg of 95% CGA orally every day via oral gavage. Glycogen levels were found to be altered in CGA treated rats which is probably due to the suppressed activity of glucose-6-phosphatase,[33] further contributing as a factor for hepatomegaly and significant increase in the liver weight. In addition to CGA, metformin was employed, as an attempt to replicate the lactic acidosis generally observed in GSD type 1 cases.

6.3. Management of GSD type 1 manifestations

In order to manage the manifestations of the GSD type 1, we conjectured to address hypoglycemia, hepatic glycogen accumulation, leading to hepatomegaly, G6Pase estimation, lactate dehydrogenase levels, serum uric acid levels with the help of selected Macro and Micronutrients. Thus, in order to maintain normoglycemia, the

macronutrients that were selected were UCCS and cassava starch; on the other hand the micronutrients that were selected were beta-carotene, riboflavin, vitamin C, and vitamin E. An *in silico* method was used to select the micronutrients based on drug likeness, while the macronutrients were chosen based on literature review. Among them, beta-carotene had the highest affinity for binding glucokinase and created seven hydrogen connections with particular amino acids, whereas the control ligand had a lower affinity for binding and did not produce any hydrogen bonds. Additionally, β-carotene showed a strong affinity for GSK3β. With regard to protein phosphatase-1 binding affinity, riboflavin had the greatest value. It also created four hydrogen bonds with particular amino acids. With protein phosphatase-1, the control ligand exhibited a greater binding and generated six hydrogen bonds. Comparing riboflavin, β-carotene, and vitamin E to their corresponding control ligands for glucokinase, they interacted at distinct regions. Every single one of the amino acids that the control ligand was targeting were interacting with vitamin C, suggesting that vitamin C may have inhibitory effect in the active site. Since riboflavin and GSK3β share an interaction residue, there may be an inhibitory action at this site. Vitamin C also shared two amino acid residues with the control ligand, suggesting that it may have some inhibitory effect on the location where the control ligand interacts with protein phosphatase-1. However, the *in vivo* findings demonstrated the significance of both macro- and micronutrients. In particular, the combination of micronutrients and cassava starch resulted in a notable improvement in parameters such as liver weight, liver glycogen content, fasting blood glucose levels, and liver histology. In an effort to address the buildup of glycogen in hepatocytes, which results in hepatomegaly and liver dysfunction, we also attempted to interrupt the glycogenesis process. Using specific micronutrients, our method

entailed deactivating important enzymes such as glycogen synthase, glucokinase, and protein phosphatase1. The *in silico* method corroborated the idea of suppressing glycogenesis and the glucose-6-phosphate enzyme complex in addition to the *in vivo* investigations.

7. SUMMARY

The goal of the current investigation was to attain the clarity on the intermolecular interactions in order to evaluate chlorogenic acid's inhibitory activity against inducing the symptoms of Glycogen Storage Disease type I (GSD type I) in rats through the inhibition of glucose-6-phosphate enzyme complex, in *in vivo* study along with chlorogenic acid (CGA) metformin was employed to elevate lactic acid levels, the *in silico* assessment was done by molecular docking and molecular dynamics simulation study, using the glucose-6-phosphate translocase encoding gene SLC37A4 and G-6PT for Glucose-6-phosphatase. With the use of the Discovery Studio software's energy minimization procedure and the CHARMM force field, The CGA 3D structure and the SLC37A4 alpha folded model were optimized. Molecular dynamics (MD) simulation was performed after glucose-6-phosphate (G6P) and CGA molecular docking and measurement of the binding free energy of the G6P-SLC37A4 and CGA-SLC37A4 complexes for 100 ns using GROMACS, principal component analysis (PCA) was performed. In comparison to the G6P-SLC37A4 complex, which had a docking score of -6.5 kcal/mol, A stronger binding relationship between CGA and SLC37A4 was shown by the CGA-SLC37A4 complex, which showed a greater docking value of -8.2 kcal/mol. Moreover, for the course of the 100 ns production run, The MD simulation revealed the least RMS fluctuation, a stable backbone, least Root Mean Square Deviation (RMSD), and stable interactions between the residues in the active site. In order to attain stability, the CGA complex with SLC37A4 established eight hydrogen bonds and showed increased compactness. The G6P-SLC37A4 and CGA-SLC37A4 complexes were discovered to have binding free energies of -12.73 and -31.493 kcal/mol, respectively. For both G6P (-4.73kJ/mol) and SLC37A4 (-

2.18kJ/mol), Lys29 established a stable interaction. This work provides structural understanding of CGA's competitive inhibition of SLC37A4. CGA exhibits promise as a possible inducer of GSD1b symptoms through its inhibition of gluconeogenesis and glycogenolysis.

Further, CGA also demonstrated good docking scores and binding patterns with G6Pase, followed by an *in vivo* pilot study to determine the effective dose. The results showed that CGA induced hypoglycemia, and when combined with metformin, resulted in manifestations similar to GSD type I. The study suggests that CGA and metformin could be an alternative animal model for GSD type I. Owing to the presence of complex carbohydrates, which are thought to release glucose gradually, both UCCS and Cassava Starch demonstrated a progressive preservation of normoglycemia. Both cassava starch alone and in combination with the micronutrients produced more beneficial outcomes than UCCS alone or in combination with the micronutrients. These two factors each demonstrated a beneficial effect in the management of GSD type 1 manifestations. Micronutrients played a critical role in preventing hepatocytes from accumulating extra glycogen, which is the primary cause of the classical symptoms of GSD, particularly hepatomegaly. Additionally, there is a lot of potential and possibilities to study the induction of GSD type 1 and other GSD types pre-clinical model, as this advocates the addition of other suitable chemicals or drugs which can be used to induce other manifestations of GSD, post which the treatment or management strategies can be planned accordingly with emphasis on role of dietary management using macro and micronutrients extensively in GSD I subjects in clinical scenario.

8. CONCLUSION

The inclusion of macro and micronutrients demonstrated their unique and complementary effects in different ways. Because both UCCS and Cassava Starch include complex carbohydrates that are thought to undergo a sustained conversion into glucose, they both showed a progressive retention of normoglycemia. However, Cassava Starch performed better both alone and in combination with micronutrients than did UCCS. To mitigate the accumulation of surplus glycogen within hepatocytes, which is considered to be one of the predominant factor contributing to the characteristic manifestations of Glycogen Storage Disease (GSD), leading into notable hepatomegaly, micronutrients played a critical role. Additionally, there is a substantial amount of possibility to investigate the protective effects of macro- and micronutrients in GSD I patients in greater detail, focusing on other symptoms such hypertriglyceridemia, hyperuricemia, and lactic acidosis.

The combination of molecular docking and MD simulation techniques advocated the valuable information regarding the binding patterns and stability of the G6Pase protein with the CGA ligand. The results suggest that the ligand induces conformational changes, leading to a more stable protein structure. Further studies are warranted to explore additional aspects of the protein-ligand interaction and to validate the findings of this study.

Limitation of the Study: The current study served as a platform to establish a relevant chemically induced GSD type 1 manifestations, where pivotal manifestations were induced. However, few GSD type 1 manifestations such as hyperuricemia, and hypertriglyceridemia were not that significantly observed.

Future perspective: In addition to this study, further the emphasis can be diverted to accomplice other manifestations of GSD type 1 by incorporating other relevant chemicals which can be effective in targeting the glycogenolysis and gluconeogenesis, and in addition to this, clinical studies to inhibit the process of glycogenesis in GSD type 1 subjects can facilitate in effective management of liver related burden and improve the prognosis.

9. BIBLIOGRAPHY

1. Chou JY, Jun HS, Mansfield BC. Type I glycogen storage diseases: disorders of the glucose-6-phosphatase/glucose-6-phosphate transporter complexes. J Inherit Metab Dis. 2015;38(3):511–9.

2. Özen H. Glycogen storage diseases : New perspectives. 2007;13(18):2541–53.

3. Labrune P, Ullrich K, Smit P, Rake J, Visser G, Leonard J. Guidelines for management of glycogen storage disease type I - European Study on Glycogen Storage Disease Type I (ESGSD I). Eur J Pediatr [Internet]. 2002;161(0):S112–9. Available from: http://link.springer.com/10.1007/s00431-002-1016-7

4. Hiraiwa H, Pan C, Lin B, Moses SW, Yang J. Inactivation of the Glucose 6-Phosphate Transporter Causes Glycogen Storage Disease Type 1b *. 1999;274(9):5532–6.

5. Kishnani PS, Austin SL, Abdenur JE, Arn P. Diagnosis and Management of Glycogen Storage Disease Type I : A Practice ACMG Standards and Guidelines Diagnosis and management of glycogen storage disease type I : a practice guideline of the American College of Medical Genetics and Genomics. 2014;(November).

6. Gümüş E, Özen H. Glycogen storage diseases: An update. World J Gastroenterol. 2023;29(25):3932–63.

7. Dieckgraefe BK, Korzenik ÆJR. Association of glycogen storage disease 1b and Crohn disease : results of a North American survey. 2002;88–92.

8. Franco LM, Krishnamurthy V, Bali D, Weinstein DA, Arn P, Clary B, et al. Hepatocellular carcinoma in glycogen storage disease type Ia: A case series. J Inherit Metab Dis. 2005;28(2):153–62.

9. Wicker C, Roda C, Perry A, Arnoux JB, Brassier A, Castelle M, et al. Infectious and digestive complications in glycogen storage disease type Ib: Study of a French cohort. Mol Genet Metab Reports [Internet]. 2020;23(April):100581. Available from: https://doi.org/10.1016/j.ymgmr.2020.100581

10. Bhattacharya K. Dietary dilemmas in the management of glycogen storage disease type I. J Inherit Metab Dis. 2011;34(3):621–9.

11. Melis D, Della Casa R, Parini R, Rigoldi M, Cacciapuoti C, Marcolongo P, et al. Vitamin E supplementation improves neutropenia and reduces the frequency of infections in patients with glycogen storage disease type 1b. Eur J Pediatr. 2009;168(9):1069–74.

12. Wong SK, Chin K, Ima-nirwana S. Vitamin C : A Review on its Role in the Management of Metabolic Syndrome. 2020;17(11).

13. Sandeep, Sahu MR, Rani L, Kharat AS, Mondal AC. Could Vitamins Have a Positive Impact on the Treatment of Parkinson's Disease? Brain Sci. 2023;13(2).

14. Althurwi HN, Abdel-Rahman RF, Soliman GA, Ogaly HA, Alkholifi FK, Abd-Elsalam RM, et al. Protective Effect of Beta-Carotene against Myeloperoxidase- Mediated Oxidative Stress and Inflammation in Rat Ischemic Brain Injury. Antioxidants. 2022;11(12):1–17.

15. Meng S, Cao J, Feng Q, Peng J, Hu Y. Roles of Chlorogenic Acid on Regulating Glucose and Lipids Metabolism : A Review. 2013;2013.

16. Heller S, Worona L, Consuelo A. Nutritional Therapy for Glycogen Storage Diseases. 2008;

17. Burda P, Hochuli M. Hepatic glycogen storage disorders: What have we learned in recent years? Vol. 18, Current Opinion in Clinical Nutrition and Metabolic Care. 2015. p. 415–21.

18. Shah KK, O'Dell SD. Effect of dietary interventions in the maintenance of normoglycaemia in glycogen storage disease type 1a: A systematic review and meta-analysis. J Hum Nutr Diet. 2013;26(4):329–39.

19. Gaboriaud-kolar N, Skaltsounis A. Glycogen phosphorylase inhibitors : a patent review. 2014;(April 2013).

20. Bali DS, El-gharbawy A, Austin S, Pendyal S, Kishnani PS. Glycogen Storage Disease Type I Summary [Internet]. Gene Reviews. 2021. 1–28 p. Available from: https://www.ncbi.nlm.nih.gov/books/NBK1312/pdf/Bookshelf_NBK1312.pdf

21. Derks TGJ, Rodriguez-Buritica DF, Ahmad A, de Boer F, Couce ML, Grünert SC, et al. Glycogen storage disease type Ia: Current management options, burden and unmet needs. Nutrients. 2021;13(11):1–17.

22. Casertano A, Rossi A, Fecarotta S, Rosanio FM, Moracas C, Di Candia F, et al. An Overview of Hypoglycemia in Children Including a Comprehensive Practical Diagnostic Flowchart for Clinical Use. Front Endocrinol (Lausanne). 2021;12(August):1–16.

23. Ross KM, Ferrecchia IA, Dahlberg KR, Dambska M, Ryan PT, Weinstein DA. Dietary Management of the Glycogen Storage Diseases: Evolution of Treatment and Ongoing Controversies. Adv Nutr. 2020;11(2):439–46.

24. Ross K. General Nutrition Guidelines for Glycogen Storage Disease Type I. Univeristy

Florida Glycogen Storage Dis Progr [Internet]. (Gsd Ix). Available from: https://ufhealth.org/sites/default/files/media/GSD/General-Nutrition-Guidelines-for-Glycogen-Storage-Disease-Type-I.pdf

25. Group F, Permitted F, Wheat S. GLYCOGEN STORAGE DISEASE TYPE 0 , III , VI & IX Limited Simple Sugars.

26. Massese M, Tagliaferri F, Dionisi-vici C, Maiorana A. Glycogen storage diseases with liver involvement : a literature review of GSD type 0 ,. Orphanet J Rare Dis [Internet]. 2022;1–12. Available from: https://doi.org/10.1186/s13023-022-02387-6

27. Ellingwood SS, Cheng A. HHS Public Access. 2019;238(3):1–18.

28. Froissart R, Piraud M, Boudjemline AM, Vianey-saban C, Petit F, Hubert-buron A, et al. Glucose-6-phosphatase deficiency. 2011;1–12.

29. Calderwood S, Kilpatrick L, Douglas SD, Freedman M, Smith-whitley K, Rolland M, et al. Recombinant human granulocyte colony-stimulating factor therapy for patients with neutropenia and / or neutrophil dysfunction secondary to glycogen storage disease type 1b. 2016;97(2):376–83.

30. Chkioua L, Amri Y, Sahli C, Rhouma F Ben, Chehida A Ben, Tebib N, et al. Identification of mutations that causes glucose-6-phosphate transporter defect in tunisian patients with glycogenosis type 1b. Diabetol Metab Syndr. 2023;15(1):1–7.

31. Roach P. Glycogen and its Metabolism. Curr Mol Med. 2005;2(2):101–20.

32. Szymańska E, Jóźwiak-Dzięcielewska DA, Gronek J, Niewczas M, Czarny W, Rokicki D, et al. Hepatic glycogen storage diseases: Pathogenesis, clinical symptoms and therapeutic management. Arch Med Sci. 2021;17(2):304–13.

33. Takao MMV, Sandy NS, Riccetto AGL, De Tommaso AMA. Long term management of glycogen storage disease type 1b: A brazilian tertiary center experience. Arq Gastroenterol. 2021;58(1):87–92.

34. Visser G, Rake JP, Fernandes J, Labrune P, Leonard J V., Moses S, et al. Neutropenia, neutrophil dysfunction, and inflammatory bowel disease in glycogen storage disease type Ib: Results of the European study on glycogen storage disease type I. J Pediatr. 2000;137(2):187–91.

35. • EMW• AL• PA, Sirrs JG• DLM• S. Molecular characterization of hepatocellular adenomas developed in patients with glycogen storage disease type I [Internet]. Vol. 36, JIMD Reports. European Association for the Study of the Liver; 2016. 78–84 p. Available from: http://dx.doi.org/10.1016/j.jhep.2012.09.030

36. Kishnani PS, Austin SL, Abdenur JE, Arn P, Bali DS, Boney A, et al. Diagnosis and management of glycogen storage disease type I: A practice guideline of the American College of Medical Genetics and Genomics. Genet Med [Internet]. 2014;16(11):1–29. Available from: https://doi.org/10.1038/gim.2014.128

37. Grünert SC, Derks TGJ, Adrian K, Al-Thihli K, Ballhausen D, Bidiuk J, et al. Efficacy and safety of empagliflozin in glycogen storage disease type Ib: Data from an international questionnaire. Genet Med. 2022;24(8):1781–8.

38. Garbade SF, Ederer V, Burgard P, Wendel U, Spiekerkoetter U, Haas D, et al. Impact of glycogen storage disease type I on adult daily life: a survey. Orphanet J Rare Dis [Internet]. 2021;16(1):1–10. Available from: https://doi.org/10.1186/s13023-021-02006-w

39. Varga V, Murányi Z, Kurucz A, Marcolongo P, Benedetti A, Bánhegyi G, et al. Species-

specific glucose-6-phosphatase activity in the small intestine—studies in three different mammalian models. Int J Mol Sci. 2019;20(20):1–15.

40. Molares-vila A, Corbalán-rivas A, Carnero-gregorio M, González-cespón JL, Rodríguez-cerdeira C. Biomarkers in glycogen storage diseases: An update. Int J Mol Sci. 2021;22(9):1–31.

41. Karthi S, Manimaran P, Varalakshmi P, Ganesh R, Kapoor S, Goyal M, et al. Mutational spectrum and identification of five novel mutations in G6PC1 gene from a cohort of Glycogen Storage Disease Type 1a. Gene. 2019 Jun 5;700:7–16.

42. Tamhankar PM, Boggula V, Girisha KM, Phadke SR. Profile of patients with von Gierke disease from India. Indian Pediatr. 2012;49(3):228–30.

43. Rake J, Visser G, Labrune P, Leonard J, Ullrich K, Smit P. Glycogen storage disease type I: diagnosis, management, clinical course and outcome. Results of the European Study on Glycogen Storage Disease Type I (ESGSD I). Eur J Pediatr. 2002;161(0):S20–34.

44. Wortmann SB, van Hove JLK, Derks TGJ, Chevalier N, Knight V, Koller A, et al. Treating neutropenia and neutrophil dysfunction in glycogen storage disease type Ib with an SGLT2 inhibitor. Blood. 2020;136(9):1033–43.

45. Derks TGJ, Nemeth A, Adrian K, Arnell H, Roskjær AB, Beijer E, et al. Hepatic Glycogen Storage Diseases: Toward One Global Collaborative Network. J Inborn Errors Metab Screen. 2017;5:1–4.

46. Kishnani PS, Austin SL, Abdenur JE, Arn P, Bali DS, Boney A, et al. Diagnosis and management of glycogen storage disease type I: A practice guideline of the American

College of Medical Genetics and Genomics. Genet Med. 2014;16(11):1–29.

47. Correia CE, Bhattacharya K, Lee PJ, Shuster JJ, Douglas W, Shankar MN, et al. NIH Public Access. 2013;88(5):1272–6.

48. Nalin T, Venema K, Weinstein DA, de Souza CFM, Perry IDS, van Wandelen MTR, et al. In vitro digestion of starches in a dynamic gastrointestinal model: an innovative study to optimize dietary management of patients with hepatic glycogen storage diseases. J Inherit Metab Dis. 2015;38(3):529–36.

49. Philip L P, Keith H, J C, Colleen L M, Yuezhou Y, Donald T. Partial Pyridoxine Responsiveness in PNPO Deficiency. JIMD Rep. 2012;4:113–6.

50. Schnorr CE, da Silva Morrone M, Simões-Pires A, da Silva Bittencourt L, Zeidán-Chuliá F, Moreira JCF. Supplementation of adult rats with moderate amounts of β-carotene modulates the redox status in plasma without exerting pro-oxidant effects in the brain: A safer alternative to food fortification with vitamin A? Nutrients. 2014;6(12):5572–82.

51. Patino SC, Mohiuddin SS. Biochemistry, Glycogenesis [Internet]. StatPearls. StatPearls Publishing; 2020 [cited 2024 Feb 18]. Available from: https://www.ncbi.nlm.nih.gov/books/NBK549820/

52. María M. Adeva-Andany ∗, Manuel González-Lucán CD-G, Carlos Fernández-Fernández EA-R. Glycogen metabolism in human. Ferrol Spain; 2016. p. 85–100.

53. Liu WJ, Ma LQ, Liu WH, Zhou W, Zhang KQ, Zou CG. Inhibition of hepatic glycogen synthesis by hyperhomocysteinemia mediated by TRB3. Am J Pathol. 2011;178(4):1489–99.

54. Raimondo A, Rees MG, Gloyn AL. Glucokinase regulatory protein: Complexity at the crossroads of triglyceride and glucose metabolism. Curr Opin Lipidol. 2015;26(2):88–95.

55. Sternisha SM, Miller BG. Molecular and cellular regulation of human glucokinase. Arch Biochem Biophys. 2019;663:199–213.

56. Wang L, Li J, Di L jun. Glycogen synthesis and beyond, a comprehensive review of GSK3 as a key regulator of metabolic pathways and a therapeutic target for treating metabolic diseases. Med Res Rev. 2022;42(2):946–82.

57. Marr L, Biswas D, Daly LA, Browning C, Vial SCM, Maskell DP, et al. Mechanism of glycogen synthase inactivation and interaction with glycogenin. Nat Commun. 2022;13(1):1–14.

58. Semrau MS, Giachin G, Covaceuszach S, Cassetta A, Demitri N, Storici P, et al. Molecular architecture of the glycogen- committed PP1/PTG holoenzyme. Nat Commun. 2022;13(1).

59. Pursell N, Gierut J, Zhou W, Dills M, Diwanji R, Gjorgjieva M, et al. Inhibition of Glycogen Synthase II with RNAi Prevents Liver Injury in Mouse Models of Glycogen Storage Diseases. Mol Ther. 2018;26(7):1771–82.

60. Chandler RJ. From Puppies to adults: In vivo editing of hepatocytes in a canine model of glycogen storage disease type Ia. Mol Ther Methods Clin Dev [Internet]. 2023;29(June):347–9. Available from: https://doi.org/10.1016/j.omtm.2023.04.006

61. Mutel E, Abdul-Wahed A, Ramamonjisoa N, Stefanutti A, Houberdon I, Cavassila S, et al. Targeted deletion of liver glucose-6 phosphatase mimics glycogen storage disease

type 1a including development of multiple adenomas. J Hepatol. 2011;54(3):529–37.

62. Ong KW, Hsu A, Tan BKH. Anti-diabetic and anti-lipidemic effects of chlorogenic acid are mediated by ampk activation. Biochem Pharmacol. 2013;85(9):1341–51.

63. Vertesy L, Kurz M, Paulus EF, Schummer D, Hammann P, Pharma A, et al. The Chemical Structure of Mumbaistatin , a Novel Glucose-6-phosphate Translocase Inhibitor Produced by Streptomyces sp . DSM11641 used . Preparative HPLCwas performed using Pharmacia Sepharose Fast Flow column (Pharmacia , Uppsala , Sweden ,. 2001;54(4).

64. Laszlo Vertesy1"'* , Hans-Jorg Burger1", Jayvanti Kenja1"1", Martin Knauf1" HK, Erich F. Paulus1", Nirogi V S. Ramakrishna1"1" KHSS, Hammann1 EKSV and P. Kodaistatins, novel inhibitors of glucose-6-phosphate translocase T1 from Aspergillus terreus Thom DSM 11247. Isolation and structural elucidation. J Antibiot (Tokyo). 2000;53(7):677–86.

65. Al ET, Gonzalez-mujica F, Motta N, Estrada O, Perdomo E, Méndez J, et al. Inhibition of Hepatic Neoglucogenesis and Glucose-6-Phosphatase by Quercetin 3- O - α - (2 ″ - galloyl) rhamnoside Isolated From Bauhinia megalandra Leaves. 2005;627(September 2003):624–7.

66. Herling AW, Schwab D, Burger HJ, Maas J, Hammerl R, Schmidt D, et al. Prolonged blood glucose reduction in mrp-2 deficient rats (GY/TR-) by the glucose-6-phosphate translocase inhibitor S 3025. Biochim Biophys Acta - Gen Subj. 2002;1569(1–3):105–10.

67. Itrac CAHE, Barra ALI, Oller MARCR, Itrac XA V. Contribution of Chlorogenic Acids to the Inhibition of Human Hepatic Glucose-6-phosphatase Activity in Vitro by Svetol

, a Standardized Decaffeinated Green Coffee Extract. 2010;4141–4.

68. Andrade-cetto A, Cárdenas R. Gluconeogenesis inhibition and phytochemical composition of two Cecropia species. J Ethnopharmacol [Internet]. 2010;130(1):93–7. Available from: http://dx.doi.org/10.1016/j.jep.2010.04.016

69. Bassoli BK, Cassolla P, Borba-Murad GR, Constantin J, Salgueiro-Pagadigorria CL, Bazotte RB, et al. Chlorogenic acid reduces the plasma glucose peak in the oral glucose tolerance test: Effects on hepatic glucose release and glycaemia. Cell Biochem Funct. 2008;

70. Lafay S, Gil-izquierdo A, Manach C, Morand C, Besson C, Scalbert A. Nutrient Physiology , Metabolism , and Nutrient-Nutrient Interactions Chlorogenic Acid Is Absorbed in Its Intact Form in the Stomach of Rats 1. 2018;(November 2005):1192–7.

71. Gonthier MP, Verny MA, Besson C, Rémésy C, Scalbert A. Chlorogenic acid bioavailability largely depends on its metabolism by the gut microflora in rats. J Nutr. 2003;133(6):1853–9.

72. Santana-Gálvez J, Cisneros-Zevallos L, Jacobo-Velázquez DA. Chlorogenic Acid: Recent advances on its dual role as a food additive and a nutraceutical against metabolic syndrome. Molecules. 2017;22(3):7–9.

73. Feng Y, Sun C, Yuan Y, Zhu Y, Wan J, Firempong CK, et al. Enhanced oral bioavailability and in vivo antioxidant activity of chlorogenic acid via liposomal formulation. Int J Pharm [Internet]. 2016;501(1–2):342–9. Available from: http://dx.doi.org/10.1016/j.ijpharm.2016.01.081

74. Bhandarkar NS, Brown L, Panchal SK. Chlorogenic acid attenuates high-carbohydrate,

high-fat diet–induced cardiovascular, liver, and metabolic changes in rats. Nutr Res [Internet]. 2019;62:78–88. Available from: https://doi.org/10.1016/j.nutres.2018.11.002

75. Zuñiga LY, Aceves-De La Mora MCA De, González-Ortiz M, Ramos-Núñez JL, Martínez-Abundis E. Effect of Chlorogenic Acid Administration on Glycemic Control, Insulin Secretion, and Insulin Sensitivity in Patients with Impaired Glucose Tolerance. J Med Food. 2018;21(5):469–73.

76. Kim H, Pan JH, Kim SH, Lee JH, Park JW. Chlorogenic acid ameliorates alcohol-induced liver injuries through scavenging reactive oxygen species. Biochimie [Internet]. 2018;150:131–8. Available from: https://doi.org/10.1016/j.biochi.2018.05.008

77. Atlabachew M, Abebe A, Alemneh Wubieneh T, Tefera Habtemariam Y. Rapid and simultaneous determination of trigonelline, caffeine, and chlorogenic acid in green coffee bean extract. Food Sci Nutr. 2021;9(9):5028–35.

78. Budryn G, Zaczyńska D, Żyżelewicz D, Grzelczyk J, Zduńczyk Z, Juśkiewicz J. Influence of the Form of Administration of Chlorogenic Acids on Oxidative Stress Induced by High fat Diet in Rats. Plant Foods Hum Nutr. 2017;72(2):184–91.

79. Un JJ, Lee MK, Yong BP, Jeon SM, Choi MS. Antihyperglycemic and antioxidant properties of caffeic acid in db/db mice. J Pharmacol Exp Ther. 2006;318(2):476–83.

80. Ong KW, Hsu A, Tan BKH. Chlorogenic acid stimulates glucose transport in skeletal muscle via AMPK activation: A contributor to the beneficial effects of coffee on diabetes. PLoS One. 2012;7(3).

81. Moe OW, Pham AQT, Xu LHR. Drug-Induced Metabolic Acidosis. F1000Research.

2015;4(0).

82. Bando K, Ochiai S, Kunimatsu T, Deguchi J, Kimura J, Funabashi H, et al. Comparison of potential risks of lactic acidosis induction by biguanides in rats. Regul Toxicol Pharmacol [Internet]. 2010;58(1):155–60. Available from: http://dx.doi.org/10.1016/j.yrtph.2010.05.005

83. Muhammed MT, Aki-Yalcin E. Molecular Docking: Principles, Advances, and Its Applications in Drug Discovery. Lett Drug Des Discov. 2022;21(3):480–95.

84. Saqallah FG, Hamed WM, Talib WH, Dianita R, Wahab HA. Antimicrobial activity and molecular docking screening of bioactive components of Antirrhinum majus (snapdragon) aerial parts. Heliyon [Internet]. 2022;8(8):e10391. Available from: https://doi.org/10.1016/j.heliyon.2022.e10391

85. Agu PC, Afiukwa CA, Orji OU, Ezeh EM, Ofoke IH, Ogbu CO, et al. Molecular docking as a tool for the discovery of molecular targets of nutraceuticals in diseases management. Sci Rep [Internet]. 2023;13(1):1–18. Available from: https://doi.org/10.1038/s41598-023-40160-2

86. Cruz PG, Daranas AH, Fernández JJ, Norte M. 19-Epi-Okadaic Acid, a Novel Protein Phosphatase Inhibitor With Enhanced Selectivity. Org Lett. 2007;9(16):3045–8.

87. Dounay A, Forsyth C. Okadaic Acid: The Archetypal Serine / Threonine Protein Phosphatase Inhibitor. Curr Med Chem. 2012;9(22):1939–80.

88. Peña-varas C, Kanstrup C, Vergara-jaque A, Gonz M, Crocoll C, Mirza O, et al. Structural Insights into the Substrate Transport Mechanisms in GTR Transporters through Ensemble Docking. 2022;

89. Svedruži ŽM. The Binding of Different Substrate Molecules at the Docking Site and the Active Site of γ -Secretase Can Trigger Toxic Events in Sporadic and Familial Alzheimer ' s Disease. 2023;

90. De Vivo M, Masetti M, Bottegoni G, Cavalli A. Role of Molecular Dynamics and Related Methods in Drug Discovery. J Med Chem. 2016;59(9):4035–61.

91. Yang M. Molecular dynamics simulations: Chemical advances and applications. J Phys Conf Ser. 2023;2608(1):4–6.

92. Jumper J, Evans R, Pritzel A, Green T, Figurnov M, Ronneberger O, et al. Highly accurate protein structure prediction with AlphaFold. Nature [Internet]. 2021;596(7873):583–9. Available from: http://dx.doi.org/10.1038/s41586-021-03819-2

93. S.P S, C.R G, Satish C. Transition Metal Complexes of Ligand containing Aminophenol moiety: Synthesis, Characterization and Antimicrobial Studies of Schiff Base Ligand and its Mixed Ligand Metal Complexes. Iarjset. 2022;9(2):423–33.

94. Jumper J, Evans R, Pritzel A, Green T, Figurnov M, Ronneberger O, et al. Highly accurate protein structure prediction with AlphaFold. Nature. 2021;596(7873):583–9.

95. Laskowski RA, MacArthur MW, Moss DS, Thornton JM. PROCHECK: a program to check the stereochemical quality of protein structures. J Appl Crystallogr. 1993;26(2):283–91.

96. Colovos C, Yeates TO. Verification of protein structures: Patterns of nonbonded atomic interactions. Protein Sci. 1993;2(9):1511–9.

97. Krivák R, Hoksza D. P2Rank: machine learning based tool for rapid and accurate

prediction of ligand binding sites from protein structure. J Cheminform [Internet]. 2018;10(1):1–12. Available from: https://doi.org/10.1186/s13321-018-0285-8

98. Samdani A, Vetrivel U. POAP: A GNU parallel based multithreaded pipeline of open babel and AutoDock suite for boosted high throughput virtual screening. Comput Biol Chem [Internet]. 2018;74:39–48. Available from: https://doi.org/10.1016/j.compbiolchem.2018.02.012

99. Dwivedi PSR, Patil VS, Khanal P, Bhandare V V., Gurav S, Harish DR, et al. System biology-based investigation of Silymarin to trace hepatoprotective effect. Comput Biol Med. 2022 Mar 1;142:105223.

100. Khanal P, Patil VS, Bhandare V V., Dwivedi PSR, Shastry CS, Patil BM, et al. Computational investigation of benzalacetophenone derivatives against SARS-CoV-2 as potential multi-target bioactive compounds. Comput Biol Med [Internet]. 2022 Jul 1 [cited 2023 Feb 15];146:105668. Available from: /pmc/articles/PMC9135652/

101. Van Der Spoel D, Lindahl E, Hess B, Groenhof G, Mark AE, Berendsen HJC. GROMACS: Fast, flexible, and free. J Comput Chem. 2005;26(16):1701–18.

102. Kumari R, Kumar R, Lynn A. G-mmpbsa -A GROMACS tool for high-throughput MM-PBSA calculations. J Chem Inf Model. 2014;54(7):1951–62.

103. DasNandy A, Patil VS, Hegde H V., Harish DR, Roy S. Elucidating type 2 diabetes mellitus risk factor by promoting lipid metabolism with gymnemagenin: An in vitro and in silico approach. Front Pharmacol. 2022;13(December):1–18.

104. Amadei A, Linssen ABM, Berendsen HJC. Essential dynamics of proteins Opportunities Connect with Wiley. Proteins Struct Funct Genet. 1993;17(4):412–25.

105. Aalten DMFV, Findlay JBC, Amadei A, Berendsen HJC. Essential dynamics of the cellular retinol-binding protein evidence for ligand-induced conformational changes. Protein Eng Des Sel. 1995;8(11):1129–35.

106. Bhandare VV, Ramaswamy A. The proteinopathy of D169G and K263E mutants at the RNA Recognition Motif (RRM) domain of tar DNA-binding protein (tdp43) causing neurological disorders: A computational study. J Biomol Struct Dyn [Internet]. 2018;36(4):1075–93. Available from: http://dx.doi.org/10.1080/07391102.2017.1310670

107. Khanal P, Patil VS, Bhandare V V., Patil PP, Patil BM, Dwivedi PSR, et al. Systems and in vitro pharmacology profiling of diosgenin against breast cancer. Front Pharmacol. 2023;13(January):1–25.

108. Mitrea DR, Malkey R, Florian TL, Filip A, Clichici S, Bidian C, et al. DAILY ORAL ADMINISTRATION OF CHLOROGENIC ACID PREVENTS THE EXPERIMENTAL CARRAGEENAN-INDUCED OXIDATIVE STRESS. 2020;(9):55–65.

109. Yasmin T, Rahman M, Khan F, Kabir F, Nahar K. Metformin treatment reverses high fat diet- induced non-alcoholic fatty liver diseases and dyslipidemia by stimulating multiple antioxidant and anti-inflammatory pathways. Biochem Biophys Reports [Internet]. 2021;28:101168. Available from: https://doi.org/10.1016/j.bbrep.2021.101168

110. Rizk S, Taha H, Abdel AE, Hatem M. Neuroprotective effect of green and roasted coffee bean extracts on cerebral ischemia-induced injury in rats. Metab Brain Dis [Internet]. 2021;(0123456789). Available from: https://doi.org/10.1007/s11011-021-00769-6

111. Abdel-mohsen DM, Akabawy AMA, El-khadragy MF, Moneim AEA, Amin HK. Green Coffee Bean Extract Potentially Ameliorates Liver Injury due to HFD / STZ-Induced Diabetes in Rats. 2023;2023.

112. Moonira T, Chachra SS, Ford XBE, Marin XS, Alshawi A, Adam-primus NS, et al. Metformin lowers glucose 6-phosphate in hepatocytes by activation of glycolysis downstream of glucose phosphorylation. 2020;295:3330–46.

113. Dyatlova N, Tobarran N V., Kannan L, North R, Wills BK. Metformin-Associated Lactic Acidosis (MALA). 2023 Apr 17 [cited 2024 Feb 26]; Available from: https://www.ncbi.nlm.nih.gov/books/NBK580485/

114. Ferreira RS, Morelini LDS, Azeredo EMC De, Azevedo L. The impact of laboratory chow for rats in the experiments : Chemical and biological evaluation of nine grain-based diet options. 2018;

115. Abdallah DB, Charoo NA, Elgorashi AS. Comparative binding and disintegrating property of Echinochloa colona starch (difra starch) against maize, sorghum, and cassava starch. Pharm Biol. 2014;52(8):935–43.

116. Boaventura F, Kuritza LN, Kaelle GCB, Bastos TS, Oliveira SG, Félix AP. Evaluation of postprandial glycemic response in rats (Wistar) fed with different starch sources. J Anim Physiol Anim Nutr (Berl) [Internet]. 2023 May 1 [cited 2024 Feb 26];107(S1):11–7. Available from: https://onlinelibrary.wiley.com/doi/full/10.1111/jpn.13806

117. Chandran D, Jayaraman S, Sankaran K, Veeraraghavan VP, R G. Antioxidant Vitamins Attenuate Glyphosate-Induced Development of Type-2 Diabetes Through the Activation of Glycogen Synthase Kinase-3 β and Forkhead Box Protein O-1 in the Liver of Adult Male Rats. Cureus. 2023;15(12):1–9.

118. Tahergorabi Z, Rahmani H, Williams J, Moodi M. The effect of methadone on blood glucose, lipids and glucose-modulating hormones in methadone-dependent Wistar rats. Toxicol Res [Internet]. 2020;36(3):221–6. Available from: https://doi.org/10.1007/s43188-019-00019-z

119. Berlim GL, Oliveira ACP, Portinho CP, Morello E, Linhares CB, Collares MVM. Glucose level evaluation in monopedicled rectus abdominis myocutaneous flap after venous occlusion: experimental study in rats. Rev Col Bras Cir. 2018;45(1):1–6.

120. Brown C. Blood collection from the tail of a rat. Lab Anim (NY). 2006;35(8):24–5.

121. Nordlie, R.C. and Arion W. Glucose-6-phosphatase. Fresenius' Zeitschrift für Anal Chemie. 1965;214(1):76.

122. Taussky, H.H. and Shorr E. Enzymatic Activity of Glucose-6-Phosphatase [EC 3.1.3.9] [Internet]. [cited 2024 Feb 25]. Available from: https://www.sigmaaldrich.com/IN/en/technical-documents/protocol/protein-biology/enzyme-activity-assays/enzymatic-assay-of-glucose-6-phosphatase

123. Foster RCN and JDAJL. Regulation of Glucose Metabolism. Underst Diabetes. 2013;113–52.

124. Bauer AW, Kirby W, Sherris J, Turck M. Technical Section Technical Section. Am J Clin Pathol. 1966;36(3):493–6.

125. Barham D, Trinder P. An Improved Colour Reagent for the Determination of Blood Glucose by the Oxidase System Pdf. Analyst. 1972;97(1151):142.

126. Green P. Serum uric acid. Manit Med Rev. 1966;46(10):651–3.

127. McGowan MW, Artiss JD, Strandbergh DR, Zak B. A peroxidase-coupled method for

the colorimetric determination of serum triglycerides. Clin Chem. 1983;29(3):538–42.

128. Fossati P, Prencipe L. Serum triglycerides determined colorimetrically with an enzyme that produces hydrogen peroxide. Clin Chem. 1982;28(10):2077–80.

129. Zakout YMA, Abdellah MA, Abdallah MA, Batran SA. Optimization of PAS stain and similar Schiff's based methods for glycogen demonstration in liver tissue. Histochem Cell Biol. 2023;1–18.

130. Chou JY, Jun HS, Mansfield BC. Glycogen storage disease type I and G6Pase-β deficiency: Etiology and therapy. Nat Rev Endocrinol [Internet]. 2010;6(12):676–88. Available from: http://dx.doi.org/10.1038/nrendo.2010.189

131. Froissart R, Piraud M, Boudjemline AM, Vianey-Saban C, Petit F, Hubert-Buron A, et al. Glucose-6-phosphatase deficiency. Orphanet J Rare Dis. 2011;6(1):1–12.

132. Soty M, Chilloux J, Casteras S, Grichine A, Mithieux G, Gautier-Stein A. New insights into the organisation and intracellular localisation of the two subunits of glucose-6-phosphatase. Biochimie [Internet]. 2012;94(3):695–703. Available from: http://dx.doi.org/10.1016/j.biochi.2011.09.022

133. Lei KJ, Chen H, Pan CJ, Ward JM, Mosinger B, Lee EJ, et al. Glucose-6-phosphatase dependent substrate transport in the glycogen storage disease type-1a mouse. Nat Genet. 1996;13(2):203–9.

134. Kishnani PS, Bao Y, Wu JY, Brix AE, Lin JL, Chen YT. Isolation and nucleotide sequence of canine glucose-6-phosphatase mRNA: Identification of mutation in puppies with glycogen storage disease type Ia. Biochem Mol Med. 1997;61(2):168–77.

135. Kishnani PS, Faulkner E, VanCamp S, Jackson M, Brown T, Boney A, et al. Canine

model and genomic structural organization of glycogen storage disease type Ia (GSD Ia). Vet Pathol. 2001;38(1):83–91.

136. Rajas F, Clar J, Gautier-Stein A, Mithieux G. Lessons from new mouse models of glycogen storage disease type 1a in relation to the time course and organ specificity of the disease. J Inherit Metab Dis. 2015;38(3):521–7.

137. Budryn G, Zaczy D, Ż D. Influence of the Form of Administration of Chlorogenic Acids on Oxidative Stress Induced by High fat Diet in Rats. 2017;184–91.

138. Hiraiwa H, Pan CJ, Lin B, Moses SW, Chou JY. Inactivation of the glucose 6-phosphate transporter causes glycogen storage disease type 1b. J Biol Chem. 1999;274(9):5532–6.

ANNEXURE I

Institutional Animal Ethical Committee Approval Certificate

Form B per rule 8(a)* **Proposal No: 01/KLECOPH/19**

Annexure – I

CERTIFICATE

This is to certify that the project title " Role of Macro and Micronutrients in the management of Glycogen Storage Disease Manifestations – A Preclinical Study" **Proposal No. : 01/KLECOPH/19** has been approved by the IAEC.

Name of Chairman/Member Secretary IAEC : Dr.V.G. Jamakandi.

Name of CPCSEA Nominee : Dr. Vinod Kumar C.S.

Signature with date:

Chairman/Member Secretary of IAEC: **CPCSEA Nominee:** 11/05/2019

Institute Animal Ethics Committee (IAEC)
K. L. E. Society's
COLLEGE OF PHARMACY
Vidyanagar, HUBLI-580 031.

Application for approval of IAEC and CPCSEA (KLEHBL/2019)
Page 8/8

ANNEXURE II

Publications

Sl No.	Journal	Index	Impact Factor	Status
01	3 Biotech	Scopus, Pubmed, SCI, UGC	3.1	Published
02	International Journal of Pharmaceutical Investigation	Web of Science, UGC	0.5	Published
03	Indian Journal of Pharmaceutical Education and Research	Scopus, Web of Science, UGC	0.8	Accepted

Publication 1

3 Biotech (2023) 13:250
https://doi.org/10.1007/s13205-023-03661-5

ORIGINAL ARTICLE

Elucidation of intermolecular interactions between chlorogenic acid and glucose-6-phosphate translocase: A step towards chemically induced glycogen storage disease type 1b model

Santosh B. Patil[1] · Pramod C. Gadad[1]

Received: 2 November 2022 / Accepted: 5 June 2023 / Published online: 26 June 2023

Abstract
Glucose-6-phosphate translocase enzyme, encoded by SLC37A4 gene, is a crucial enzyme involved in transporting glucose-6-phosphate into the endoplasmic reticulum. Inhibition of this enzyme can cause Von-Gierke's/glycogen storage disease sub-type 1b. The current study dealt to elucidate the intermolecular interactions to assess the inhibitory activity of Chlorogenic acid (CGA) against SLC37A4 was assessed by molecular docking and dynamic simulation. The alpha folded model of SLC37A4 and CGA 3D structure were optimized using CHARMM force field, using energy minimization protocol in the Discovery Studio software. Glucose-6-phosphate (G6P) and CGA molecular docking, Molecular dynamics (MD) simulation, analysis of binding free energy of G6P-SLC37A4 and CGA-SLC37A4 complexes was performed for 100 ns using GROMACS, followed by principal component analysis (PCA). The docking score of the CGA-SLC37A4 complex exhibited a higher docking score (– 8.2 kcal/mol) when compared to the G6P-SLC37A4 complex (– 6.5 kcal/mol), suggesting a stronger binding interaction between CGA and SLC37A4. Further, the MD simulation demonstrated a stable backbone and complex Root Mean Square Deviation (RMSD), the least RMS fluctuation, and stable active site residue interactions throughout the 100 ns production run. The CGA complex with SLC37A4 exhibits higher compactness and formed 8 hydrogen bonds to achieve stability. The binding free energy of the G6P-SLC37A4 and CGA-SLC37A4 complex was found to be – 12.73 and – 31.493 kcal/mol. Lys29 formed stable contact for both G6P (– 4.73 kJ/mol) and SLC37A4 (– 2.18 kJ/mol). This study imparts structural insights into the competitive inhibition of SLC37A4 by CGA. CGA shows potential as a candidate to induce manifestations of GSD1b by inhibiting glycogenolysis, and gluconeogenesis.

Keywords Glycogen storage disease type 1 · Glucose-6-phosphate exchanger · Chlorogenic acid · Molecular docking · Molecular dynamics · SLC37A4

Introduction

A group of genetic metabolic disorders known as the glycogen storage diseases (GSD) or glycogenoses is caused due to deficiency of the enzymes required to regulate glycogenolysis or gluconeogenesis (Chou et al. 2015). Hepatic GSD manifestations primarily include hypoglycemia, whereas muscular GSD manifests itself mostly through weakness and muscle spasms. These disorders affect about 1 in every 20,000–43,000 live births, and 80% of hepatic GSDs are Types I, III, and IX, of which GSD I is most prevalent (Özen 2007). The GSD I, also known as Von Gierke's disease, is further categorized into type Ia and Ib. Reduced of complete inactivity of Glucose-6-phosphatase-α (G6Pase-α) causes GSDIa (Rake et al. 2002) and deficient activity of glucose-6-phosphate transporter (G6PT) or mutations in SLC37A4 gene, responsible for the production of G6PT causes GSDIb (Hiraiwa et al. 1999), (Bennett and Burchell 2013). SLC37A4, is responsible for transporting glucose-6-phosphate (G6P) from the cytoplasm into to the endoplasmic reticulum (ER) lumen. G6PT hydrolyses intraluminal G6P to Pi and glucose in a combination with either glucose-6-phosphatase (G6Pase) or G6Pase. Fasting blood glucose levels are regulated by G6PT/G6Pase complex activity, whereas G6PT/G6Pase is necessary for neutrophil

✉ Pramod C. Gadad
gadadpramod@gmail.com

[1] Department of Pharmacology, KLE College of Pharmacy (A constituent unit of KLE Academy of Higher Education and Research, Belagavi, Karnataka, India), Hubballi, Karnataka, India

activities (Cappello et al. 2018). The incidence of GSD I is 1 in 100,000, 80% of the patients represent GSDIa and 20% by GSD Ib (Rake et al. 2002). Both disorders result in burdens such as hypoglycaemia, hypertriglyceridemia, hyperuricemia, lactic acidosis, and increased accumulation of glycogen primarily in the liver and kidneys lead to progressive hepatomegaly and nephromegaly (Parikh and Ahlawat 2021).

Along with the clinical manifestations and abnormalities reported in type Ia, neutropenia, persistent infections, and neutrophil dysfunction are specifically observed in type Ib (Calderwood et al. 2001) due to the impairment of glucose transportation across the cell membrane of the polymorphonuclear leukocytes. Long-term problems such as hepatic adenomas, inflammatory bowel disease, renal calculi, and progressive renal dysfunction, and hepatocellular cancer are all possible. (Franco et al. 2005) can develop in older children and adults (Dieckgraefe and Korzenik 2002).

The literature suggests that designing and establishing a disease model for GSD is an uphill task, though the gene knockout animals and genetically mutated cells serve as disease models. The stability, survivability, maintenance, and cost of these models are a big challenge. Based on the previous reports, The activity of G6PT transport is particularly and substantially hindered by a certain chemical derivatives like Chlorogenic acid (CGA), (Arion et al. 1997 and 1998); (Hemmerle et al. 1997) serving as a reversible inhibitor. Also, few chlorogenic acid derivatives, viz S3483 (Khan et al. 1998); (Leuzzi et al. 2003), and S4048 (Herling et al. 1999), are known to inhibit G6PT in diabetic subjects (Ong et al. 2013), this helped us to ideate that CGA can simulate the response or manifestations similar to GSD I.

Thus, this study is an attempt to comprehend the possible interactions and affinity of CGA towards SLC37A4 via chemoinformatics approaches viz., molecular docking and dynamics, and Molecular Mechanics Poisson−Boltzmann surface area (MMPBSA) calculations, which is further compared with the substrate docking, that CGA can be a suitable candidate to induce GSD I manifestations by inhibiting enzyme activity of G6PT.

Materials and methods

Protein and ligand preparation

The full-length SLC37A4 alpha folded model was downloaded from the alpha fold website (Jumper et al. 2021). The model structure having accession number AF-A0A1L-1SUI3-F1-model_v2, organism: *Mus musculus*, was retrieved from the alpha fold website, and the Glucose-6-phosphate (PubChem CID: 5958) and CGA (PubChem CID: 1,794,427) 3D structure was from PubChem and optimized them using CHARMM (Chemical at Harvard Molecular Mechanics) force field using energy minimization protocol in the Discovery Studio Visualizer software version 2019.

Protein structure information

Amino acid distribution and quality assessment

To check the functional sites of the protein, the amino acid distribution of the obtained protein structure was assessed by the SAVES server. PROCHECK (Laskowski et al. 1993) was executed to acquire the data on the distribution of the amino acid Phi/Psi angles in the SLC37A4 and its overall quality was checked by ERRAT (Colovos and Yeates 1993). After molecular dynamic simulation, 0 ns and 100 ns frames for ligand bound complex were obtained and subjected to PROCHECK and ERRAT server. The data of protein alone and ligand bound form for both G6P and CGA were compared for amino acid distribution and overall quality.

Pocket information

P2Rank (Krivák and Hoksza 2018) server was utilized to find information of possible residues involved in the function of the protein and involved in the binding of ligand molecules. The pocket residues site possessing a higher probability score was considered for the docking study.

Molecular docking

The affinity of G6P and CGA towards the glucose-6-phosphate translocase was assessed by AutoDock vina and executed through the POAP pipeline (Samdani and Vetrivel 2018; Patil et al. 2022). During docking simulation, the grid box set to pocket 1 covering active site residues with center x = 0.435, y = 1.652, z = 2.037; sizes x = 46.89, y = 39.377, y = 41.626 were set with 1 Å spacing. The docking system exhaustiveness was set to 100. The intermolecular interactions between G6P and CGA in complex with SLC37A4 were examined through Discovery Studio Visualizer 2019v (Patil et al. 2020).

Molecular dynamics (MD) simulation

MD simulation for G6P-SLC37A4 and CGA-SLC37A4 complex were performed using Gromacs-2019.4 (Dwivedi et al. 2022) (Van Der Spoel et al. 2005). The complex topology was prepared by using the Amber ff99SB-ildn force field. A water simple point charge (SPCE) water model was used to solvate the complex structures in a cubic periodic box boundary condition of 10.0 Å. Subsequently the salt concentration of the complex systems was maintained at 0.15 M using a suitable number of Na^+ and Cl^- counter

ions. Using an ensemble of NPT simulations for 100 ns, the final production run of each structure from the equilibration phase was carried out. An analysis of 100 ns trajectory was conducted using the packages in Gromacs. The root mean square deviation (RMSD), root mean square fluctuation (RMSF), the radius of gyration (rGyr/Rg), and hydrogen bond (H-bond) contacts were considered for evaluation.

Binding free energy calculations

To analyse the binding free energy (ΔG binding) of an inhibitor with the protein across simulation time, the MM-PBSA technique was used and the binding free energy was estimated using the g mmpbsa function in GROMACS. (Kumari et al. 2014). In order to obtain an accurate result, we computed ΔG for the last 20 ns of the trajectory with dt 1000 frames and expressed the binding free energy in kcal/mol. Additionally, individual residue energy contributions in stable complex formation were also analysed (DasNandy et al. 2022).

Analysis of principal component

Principal component analysis (PCA) was employed to investigate the molecular motion using MD trajectories. The "least square fit" to the reference structure was used to eliminate the molecule's translational and rotational motion. The covariance matrix obtained by a linear transformation of Cartesian coordinate space is diagonalized to provide a set of eigenvectors that exemplify the motion of the molecule. Where, the eigenvalue associated with each eigenvector indicates its energy contribution to the motion and also, projecting the trajectory onto an eigenvector illustrates the "time-dependent motions" that the parts do in a specific vibrational mode. The temporal average of the projection indicates the contribution of the atomic vibrational components to this type of coordinated motion. The eigenvectors and eigenvalues of the trajectory were generated by computing and diagonalizing the covariance matrix using the built-in gromacs utility "g covar.". The "g anaeig" tool was also used to examine and illustrate the eigenvectors (Andrea Amadei et al. 1993); (Aalten et al. 1995); (Amadei et al. 1996); (Bhandare and Ramaswamy 2018); (Khanal et al. 2022); (Khanal et al. 2023). Over all, for analysing PCA, the least squares fit, g covar, a built-in feature of Gromacs, and g anaeig tools were employed.

Results and discussion

The current study intended to explore the intermolecular interactions and binding mode of chlorogenic acid (CGA) with the SLC37A4 target by assimilating the molecular docking and dynamics simulation. Previously, Interestingly, few in-vitro and experimental studies also support the inhibition of glucose-6-phosphate complex by CGA which corroborates our findings. CGA and its derivatives have been studied in diabetic conditions and even in normal conditions there are claims that CGA suppresses the hepatic blood glucose production by which the homeostatic regulation of blood glucose can be achieved (Hemmerle et al. 1997), (Arion et al. 1997). However, affinity with SLC37A4, precise binding site pockets, and inhibition of the activity of glucose-6-phosphatase complex are not been understood clearly. In this regard, rigid molecular docking was performed using AutoDock vina through the POAP pipeline to infer the possible interaction of chlorogenic acid with the SLC37A4 target. Recently, Veiga-da-Cunha et al. (2019) discovered that granulocytes from patients with defective SLC37A4 (G6PT) accumulate 1,5-anhydroglucitol-6-phosphate (1,5AG6P) that severely restrict/antagonize hexokinase function. The 1,5-anhydroglucitol is phosphorylated to produce the 1,5AG6P primarily (1,5AG),and hence the physiologic concentrations of 1,5AG produce extensive deposition of 1,5AG6P, a reduction in glucose utilization, and cell death in a model of G6PT-deficient mice neutrophils (Veiga-da-Cunha et al. 2019). Chlorogenic acid is well demonstrated as a specific, reversible inhibitor of SLC37A4 (Arion et al. 1998). A chlorogenic acid derivative (S3483), and G6PT inhibitor, were shown to impede G6P transport in differentiated promyelocytic HL-60 cells and microsomes derived from polymorphonuclear neutrophils (PMN) in intact cells (Leuzzi et al. 2003). Interestingly, the PMN phenotype in GSD1b, a clinical illness in which the SLC37A4 protein is faulty or mutated, involves a reduction in numerous activities including chemotaxis, respiratory bursts, phagocytosis, and calcium signaling. Similarly, changes in numerous metabolic parameters – hexose uptake and transport, calcium mobilization, glucose phosphorylation, and have been proposed as probable causes for SLC37A4 functional abnormalities (Leuzzi et al. 2003), (Oguz et al. 2015). Hence, the interaction of chlorogenic acid and its derivatives with SLC37A4 and its inhibition will be a major contribution in causing GSD1b and chronic neutropenia via decreased glucose homeostasis, altered calcium permeability, apoptosis, and neutrophil chemotaxis. From the docking study, it is inferred that chlorogenic acid formed a hydrogen bond interaction with Asn374 and Lys29 and formed three non-hydrogen bonds with Phe237, Tyr343, and Ile346. The Lys29 and Phe237 were identified as active site residues and hence support the inhibition of SLC37A4. The substrate molecule Glucose-6-Phosphate (G6P) formed a hydrogen bond interaction with Lys29 and Ser57 (3.12Å) and formed one non-hydrogen bond with Asp245. This confirms that the CGA is a

potent competitive inhibitor to SLC37A4. Lys29 residue was found to be the common hydrogen bond interactive residue for both G6P and CGA.

The MD simulation has become a very essential approach in reducing the limitation of computational prediction via inferring the stability of protein and ligand interactions in a desired physiological system (Yennamalli 2018). The molecular docking followed by dynamics gives deep insights into the behavior or structural changes information of ligands as well as its influence on protein stability upon binding (Du et al. 2016). Hence, the obtained data indicate concordance between computational prediction and experimental reports. In this study, a 100 ns MD production run was simulated to infer the structural changes upon ligand binding. The findings demonstrated that the RMSD of the protein was stabilized upon ligand interaction which was also inferred by the R*g* value for both G6P and CGA. As it represents the compactness of complex formation in which ligand was found to get buried in the binding pocket during a 100 ns production run. In both the complexes, among the total residues, the longest loop region formed by Gly195 to Leu217 residues exhibited more fluctuation and was highly dynamic during MD simulation compared to other residues participating in the protein-ligand complex formation. Both G6P and CGA formed 8 H-bonds with SLC37A4 to form a stable complex in which 3 and 5 were consistent throughout the simulation, respectively. These computational hints provide deep insight into the structural changes of SLC37A4 upon ligand binding and offer essential evidence to corroborate the previous claims on chlorogenic acid as a potent competitive inhibitor of SLC37A4.

Protein information

The residue-by-residue geometry and overall structure geometry were studied by PROCHECK to check the stereochemical quality of a SLC37A4 protein structure (Fig. 1a). About 96.1% and 2.8% of the residues were found in the most favoured and additional allowed regions, respectively. Around 0.8% (3 residues) viz., Lys205, Lys207, and Glu213 were found in generously allowed regions in the Ramachandran plot. However, only 0.3% (one residue) i.e., Ser413 was found in the disallowed region. The overall quality of the protein structure was found to be 97.664%, by plotting the ERRAT plot which confirms the stability and represents the high resolution of the structure (Fig. 1b). In G6P- SLC37A4 0 ns frame complex, about 91.3%, and 8.2% residues were in the most favoured and additional allowed regions, respectively. One residue, Ser164 was found in the disallowed region (Figure S1). Whereas, in G6P- SLC37A4 100 ns frame complex, about 91.6% and 7.9% of the residues were found in the most favoured and additional allowed regions, respectively. One residue Thr364 was found in the generously allowed region and one residue, Ser164 was found in the disallowed region (Figure S2). All the active site residues involved in G6P binding were found to be in the most favoured region. The overall quality of the G6P-SLC37A4 0 ns and 100 ns frame complex was found to be 96.250% and 95.718%, respectively (Figures S3 and S4). In CGA- SLC37A4 0 ns frame complex, about 91.8%, and 7.9% residues were in the most favoured and additional allowed regions, respectively. One residue, Ser164 was found in the disallowed region (Figure S5). Whereas, in CGA- SLC37A4 100 ns frame complex, about 92.6% and 7.4% of the residues were found in the most favoured and additional allowed regions, respectively. No residues were found in the disallowed region (Figure S6). All the active site residues involved in CGA binding were found to be in the most favoured region. The overall quality of the G6P-SLC37A4 0 ns and 100 ns frame complex was found to be 99.75% and 97.805%, respectively (Figure S7 and Figure S8).

The SLC37A4 protein comprises of 4 binding pockets in which pocket 1 (Fig. 1c) has residues number "21, 25, 28, 29, 56, 57, 60, 64, 114, 118, 139, 142, 143, 145, 146, 233, 237, 240, 241, 245, 274, 277, 278, 364, 367, 368, 391, 394, 395, 398" was found to be the major binding pocket that scored the probability score of 0.879 in P2Rank web server (Table 1).

Molecular docking

G6P scored the lowest BE of – 6.5 kcal/mol via forming two H-bonds with Lys29 (4.62 Å) and Ser57 (3.12 Å) and formed one non-hydrogen bond with Asp245 (5.77 Å). Whereas, CGA scored the lowest BE of – 8.2 kcal/mol via forming two H-bonds with Asn374 (3.55 Å) and Lys29 (6.13 Å) and forming three non-hydrogen bonds with Phe237 (6.04 Å), Tyr343 (6.45 Å), and Ile346 (6.83 Å). Among these residues, Lys29 and Phe237 were identified as active site residues and Lys29 shared the common interacting residue for both G6P and CGA Figs. 2 and 3a–d shows the affinity of G6P and CGA with SLC37A4, respectively.

Molecular dynamics (MD) simulation

MD simulations were performed for G6P-SLC37A4 and CGA-SLC37A4 complex for 100 ns production run and RMSD, RMSF, rGyr, H-bonds, and SASA were considered for evaluation.

RMSD

This parameter can be used to determine whether the two confirmations differ from each other. The RMSD value is inversely proportional to the deviation. In the G6P-SLC37A4

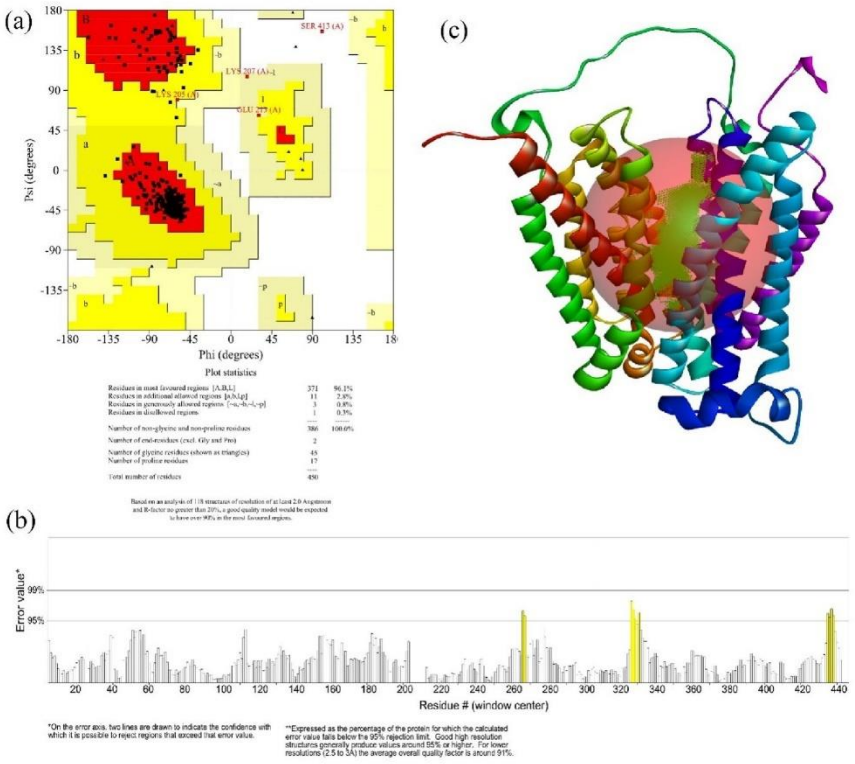

Fig. 1 **a** Ramachandran plot of SLC37A4 structure (AF-A0A1L-1SUI3-F1-model_v2) showed that 96.1% and 2.8% of the residues were found in most favoured and additional allowed regions, respectively. Around 0.8% (3 residues) viz., Lys205, Lys207, and Glu213. However, only 0.3% (one residue) i.e., Ser413 was found in disallowed region. **b** ERRAT plot showing error values for residues of the protein, the ERRAT values confirmed that overall quality of the protein structure was found to be 97.664%, **c** Ligand binding pocket of SLC37A4 showed that protein consists of 4 binding pockets in which pocket 1 was found to be the major binding pocket that scored the probability score of 0.879

Table 1 The table explains major ligand binding pocket of SLC37A4 with its probability score and pocket residues

Name	Probability	Sas points	Surf atoms	Pocket residues
Pocket	0.879	163	78	Tyr25, Arg28, Lys29, Gln56, Ser57, Tyr60, Lys64, Gln114, Trp118, Ala139, Ser142, Thr143, Met145, Asn146, Tyr21, Tyr233, Phe237, Lys240, Thr241, Asp245, Leu274, Ser277, Ile278, Tyr364, Ile367, Ala368, Gly391, Ala394, Asn395, Gly398

complex, a slight increase in the RMSD was observed from ~ 1.5 Å to ~ 3 Å till 10 ns for both backbone and complex. After 10 ns, a stable RMSD and a similar trend were observed throughout the 100 ns simulation. Whereas, in the CGA-SLC37A4 complex, during the equilibration period, the backbone and complex RMSD were gradually increased from ~ 1.5 Å and ~ 1.8 Å to ~ 3.0 Å and ~ 3.5 Å, respectively till ~ 40 ns. Further, both backbone and complex RMSD were slightly decreased to ~ 2.5Åand ~ 3.0 Å, respectively till ~ 48 ns. Further, from ~ 48 ns to ~ 100 ns the RMSD was found to be stable with slight fluctuation at ~ 85 ns. The backbone and complex RMSD was confirmed to be stable, and formed a similar trend throughout the 100 ns production run. (Fig. 4a and b) represents the backbone and complex

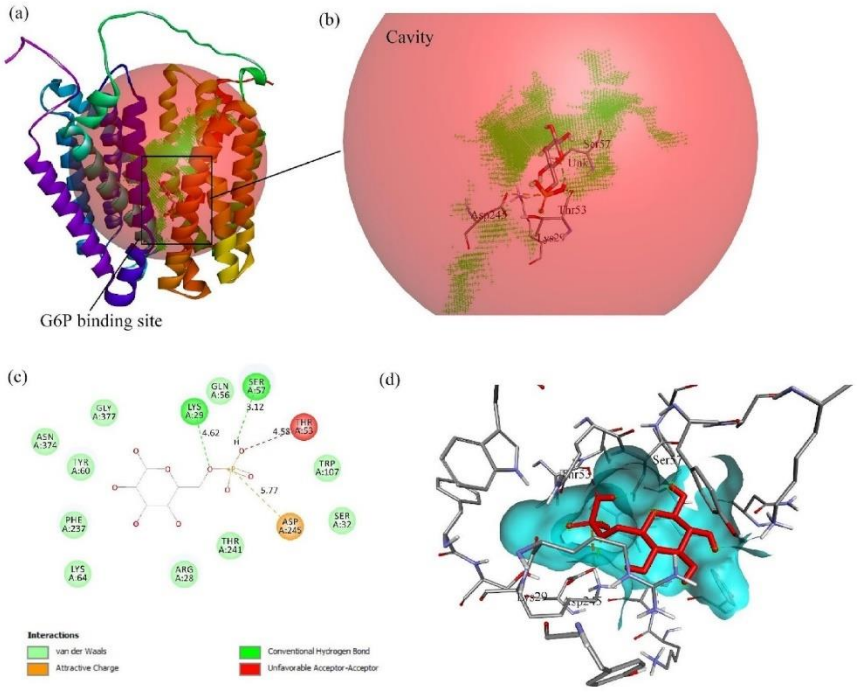

Fig. 2 Demonstrates the Intermolecular interaction of G6P-SLC37A4 complex. **a** Demonstrates the G6P binding site within the SLC37A4 protein pocket. **b** Shows the magnified picture of **(a)** Affinity of G6P at ligand binding site, where CGA scored the lowest BE of – 6.5 kcal/mol via forming two H-bonds with Lys29 (4.62 Å) and Ser57 (3.12 Å) and formed one non-hydrogen bond with Asp245 (5.77 Å). **c** 2D picture characterizes the complex of G6P with SLC37A4 and its van der Waals, hydrogen bond, *Pi- Pi* and *Pi*-alkyl interaction. **d** Represents the ligand-fit site at SLC37A4 pocket 1

RMSD for G6P and CGA throughout 100 ns MD simulation, respectively.

RMSF

RMSF analysis aids in order to understand which amino acids of the proteins are making more vibrations, that results in the destabilization of the protein, both in presence or in absence of the ligand molecule. In both the complexes, the longest flexible loop region i.e., residue Gly195 to Leu217 showed the maximum fluctuation (~6 Å). Further, the C-terminal loop region from Leu414 to Glu429 showed a maximum fluctuation up to 4 Å and 12 Å, respectively for G6P and CGA. A loop linker (residue Gly292 to Asn298) joining two helices showed a residual fluctuation up to ~6 Å and ~2 Å. However, residues involved in ligand binding (Lys29, Phe237, Tyr343, Ile346, and Asn374) showed the least fluctuation (< 1.5 Å) throughout 100 ns simulation in both complexes. The RMSF of Cα for G6P and CGA were depicted in Fig. 5a and b, respectively.

Radius of gyration (rGyr/Rg)

Compactness of the protein and ligand-bound form was determined by the radius of gyration. Folding and unfolding of the protein alone and in complex with G6P and CGA was analysed by the Rg values throughout 100 ns simulation. Both protein and complexes showed higher compactness throughout the 100 ns production period and formed a similar trend. In G6P- SLC37A4 complex, initially, the Rg value of protein and complex was 22.5 Å and gradually increased to 23 Å till 20 ns and again gradually decreased to 22.3 Å till 65 ns. Further, the Rg value increased to 22.6 Å till 100 ns. The sudden increase in the Rg value during the equilibration period indicates the opening of the pocket, which allows the ligand to get buried in the binding pocket, and the decrease

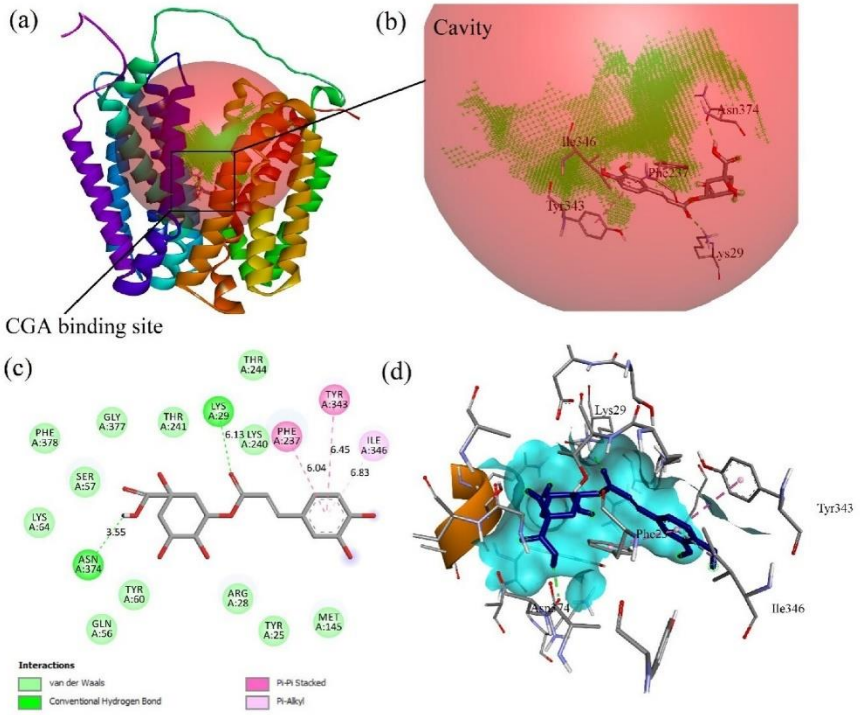

Fig. 3 Demonstrates the Intermolecular interaction of CGA-SLC37A4 complex. **a** Demonstrates the CGA binding site within the SLC37A4 protein pocket. **b** Shows the magnified picture of **(a)** Affinity of CGA at ligand binding site, where CGA scored the lowest BE of − 8.2 kcal/mol via forming two H-bonds with Asn374 (3.55 Å) and Lys29 (6.13 Å), and forming three non-hydrogen bonds with Phe237 (6.04 Å), Tyr343 (6.45 Å), and Ile346 (6.83 Å). **c** 2D picture characterizes the complex of CGA with SLC37A4 and its van der Waals, hydrogen bond, *Pi- Pi* and *Pi*-alkyl interaction. **d** Represents the ligand-fit site at SLC37A4 pocket 1

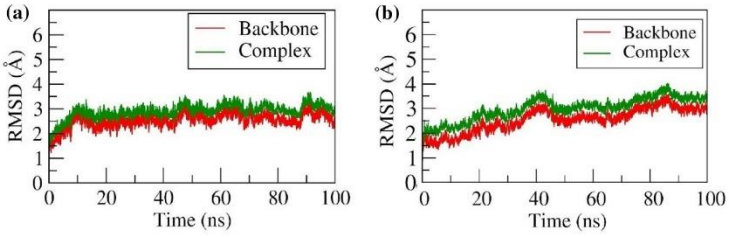

Fig. 4 RMSD of backbone atoms and complex of **a** G6P and **b** CGA with SLC37A4

in the Rg value after the equilibration period indicates the closing of the pocket, which allows ligand to form a stable complex (Movie 1). Similarly, in the CGA-SLC37A4 complex, the Rg value of protein and complex was 22.5 Å. After ~ 46 ns, the Rg value increased to ~ 22.8 Å and further decreased to ~ 22.6 Å and maintained the trend throughout the 100 ns run. The sudden increase in the Rg value after the equilibration period indicates the opening of the pocket, which allows the ligand to get buried in the binding pocket to form a stable complex (Movie 2). The Rg plots of protein and in complex with CGA were shown in Fig. 6a and b for G6P and CGA, respectively.

H-bond interactions

G6P in complex with SLC37A4 protein stabilized by forming 8 hydrogen bonds. Among them, 3 were consistent throughout the simulation. CGA in complex with SLC37A4 protein stabilized by the formation of 8 hydrogen bonds. Among them, 5 bonds were strong throughout the simulation. The H-bond contact of the G6P and CGA in complex with SLC37A4 was shown in Figs. 7a and b, respectively.

SASA

It is observed that the SLC37A4 protein comprises of 12 helices separated as a two-group with the longest loop formed by residues Gly195 to Leu217. The ligand-binding pocket (pocket 1) is present in between two group helices with a surface area of 163 nm^2. In both complexes, the increased SASA after 44 ns (~ 190 nm^2 to ~ 205nm^2) was observed which is because of the flexible nature of the loop region and opening of the binding pocket. However, the surface area was found to be steady after ~ 55 ns (~ 197nm^2). The initial and final surface area occupied by both docked complexes was ~ 199 nm^2 and ~ 197 nm^2. The average surface area occupied by the complex was ~ 197 nm^2 (refer to Fig. 8a for G6P and Fig. 8b for CGA).

Binding free energy calculations and residual decomposition energy

The free energy required for the G6P and CGA to bind to the protein pocket was determined by MMPBSA. The binding free energy of G6P and CGA in complex with SLC37A4 was found to be – 12.72 ± 2.84 and – 31.493 ± 1.486 kcal/mol, respectively. The per residue energy contribution of the G6P-SLC37A4 complex revealed that the residues Lys29, Thr53, Gln56, Tyr60, Gln114, and Ala380 scored the least contribution energy of – 4.73, – 3.57, – 2.49, – 6.78, – 2.08, and – 1.33 kJ/mol, whereas, Arg28 and Asp245 scored the positive contribution energy of 6.07 and 11.18 kJ/mol. Similarly, the per residue energy contribution of the CGA- SLC37A4

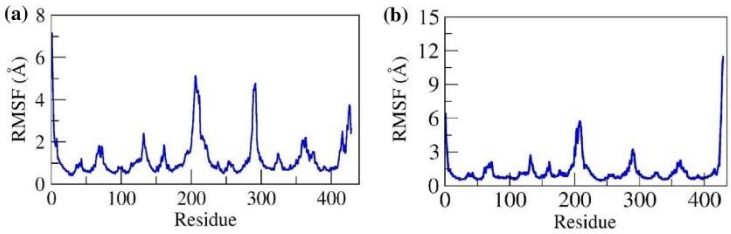

Fig. 5 Represents Root mean square fluctuation (RMSF) of Cα for **a** G6P-SLC37A4 and **b** CGA-SLC37A4 complexes

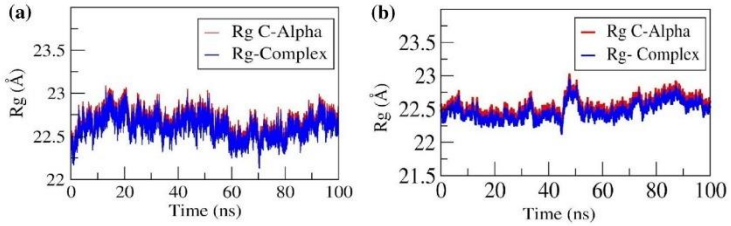

Fig. 6 Radius of gyration (Rg) of Cα atoms of SLC37A4 in complex with **a** G6P and **b** CGA

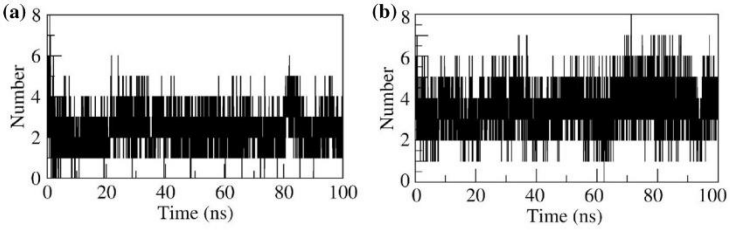

Fig. 7 H-bonds formed between **a** G6P and **b** CGA with SLC37A4 throughout 100 ns MD simulation

complex revealed that the residues Lys29, Gln56, Phe237, Glu254, and Asp325 scored the least contribution energy of – 2.18, – 2.15, – 4.82, – 1.87, and – 10.09 kJ/mol, whereas, Arg28, Lys240, Asp245, Lys255, and Lys389 scored the positive contribution energy of 3.61, 3.18, 3.07, 1.54, and 13.08 kJ/mol. Figure 9a and b represents the per residue contribution for G6P and CGA in complex with SLC37A4.

Principle component analysis

The collective motion sampled by the first two principal components (PCs) and 2D projections for PC1 and PC2 were plotted for G6P and CGA (Fig. 10a and b, respectively). The complex of G6P with SLC37A4 expresses the compact clusters in the conformational spaces those range from – 5 to 5.7 (Fig. 10a). In the MD trajectory of complex G6P with SLC37A4, PC1, and PC2 (top two modes) showed a constant distribution across the configurational space, in which CGA with SLC37A4 revealed little variation in the conformational space and was widely grouped in the range of – 5 to 7.8 (Fig. 10a). Further, it was observed that in CGA-SLC37A4 complex, during the simulation the maximum dynamics have been captured by the first 50 eigenvectors, of which the first three contributed substantially to the collective motions exerted by all the simulated complexes. The eigenvalue for the CGA complex was found to be higher compared to the G6P complex (Fig. 10b).

Conclusion

The present study utilized chemoinformatics approaches viz., molecular docking, dynamics, and MM-PBSA calculation to decode the intermolecular interactions and binding affinity of Glucose 6 phosphate and chlorogenic acid against SLC37A4. The results reveal that chlorogenic acid forms

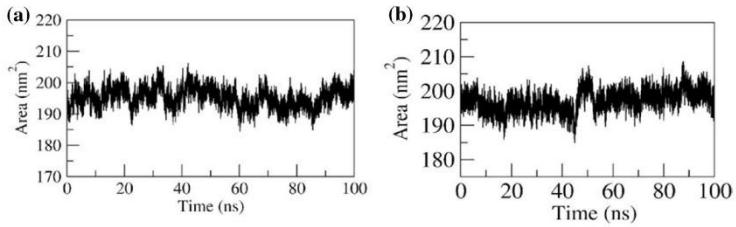

Fig. 8 Solvent Accessible Surface Area (SASA) of SLC37A4 in complex with **a** G6P and **b** CGA

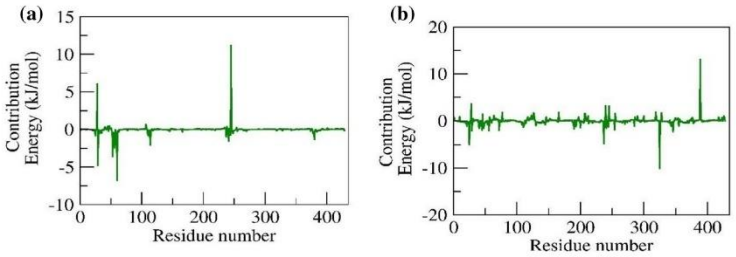

Fig. 9 Contribution energy plot demonstrate the significance of the ligand binding residues in stable complex formation **a** G6P and **b** CGA in complex with SLC37A4

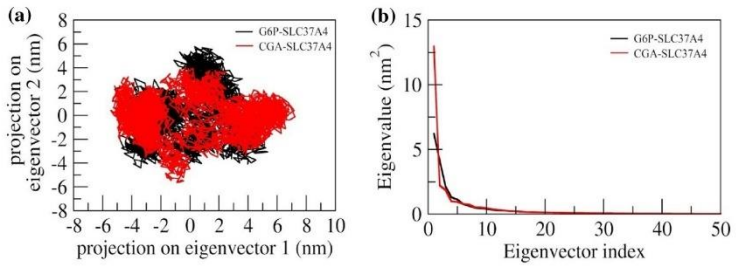

Fig. 10 **a** Principal component analysis of protein–ligand complexes: the collective motion of G6P (black) and CGA (red) with SLC37A4 using projections of MD trajectories on two eigenvectors corresponding to the first two principal components. **b** The first 50 eigenvectors were plotted versus the eigenvalue for G6P (black) and CGA (red) with SLC37A4

a stable complex via interacting with active site residues Lys29 and Phe237 of SLC37A4 and exhibits its inhibitory activity. The SLC37A4 gene is responsible for synthesizing G6PT enzyme, Glucose-6-phosphate must be transported into the lumen of the endoplasmic reticulum by the G6PT enzyme, where it is hydrolysed into glucose and inorganic phosphate. Inhibition of G6PT would evidently lead to Von-Gierke's/glycogen storage disease sub-type 1b, characterized by decrease in fasting blood glucose levels. A suitable G6PT inhibitor, would however be useful to researchers to manifest the disease model in research pertaining to Glycogen storage disease I. This study therefore aims to decipher the intermolecular interaction between Chlorogenic acid (an anticipated G6PT inhibitor) and G6PT enzyme by molecular docking and dynamic simulation studies. The current study is solely based on the computational approaches to assess the inhibitory interaction of CGA with the SLC37A4 gene. Thus, this study unwinds the scope for further experimental studies and validation of the GSD I model in experimental animals.

Supplementary Information The online version contains supplementary material available at https://doi.org/10.1007/s13205-023-03661-5.

Acknowledgements Authors would like to express the help provided by the Principal of the Institution in carrying out the present work.

Funding No funding was received from any funding institute for this study.

Data availability The data supporting the findings of this study are available within the article and supplementary files.

Declarations

Conflict of interest The authors declare that they have no competing interests.

Ethical approval Not applicable.

Consent to participate Not applicable.

Consent for publication All authors approved the manuscript for publication.

References

Amadei A, Linssen ABM, Berendsen HJ (1993) Essential dynamics of proteins. Proteins 17(4):412–425. https://doi.org/10.1002/prot.340170408

Amadei A, Linssen AB, De GBL, Van Aalten DM, Berendsen HJ (1996) An efficient method for sampling the essential subspace of proteins. J Biomol Struct Dyn 13(4):615–625. https://doi.org/10.1080/07391102.1996.10508874

Arion WJ et al (1997) Chlorogenic acid and hydroxynitrobenzaldehyde: new inhibitors of hepatic glucose 6-phosphatase. Arch Biochem Biophys 339(2):315–322

Arion WJ et al (1998) Chlorogenic acid analogue S 3483: a potent competitive inhibitor of the hepatic and renal glucose-6-phosphatase systems. Arch Biochem Biophys. https://doi.org/10.1006/abbi.1997.0563

Bennett K, Burchell A (2013) Von Gierke disease. Brenner's encyclopedia of genetics, 2nd edn. Elsevier, NY, pp 304–307. https://doi.org/10.1016/B978-0-12-374984-0.01631-4

Bhandare VV, Ramaswamy A (2018) The proteinopathy of D169G and K263E mutants at the RNA recognition motif (rrm) domain of tar DNA-binding protein (tdp43) causing neurological disorders: a computational study. J Biomol Struct Dyn 36(4):1075–1093. https://doi.org/10.1080/07391102.2017.1310670

Calderwood S et al (2001) Recombinant human granulocyte colony-stimulating factor therapy for patients with neutropenia and/or neutrophil dysfunction secondary to glycogen storage disease type 1b. Blood 97(2):376–382. https://doi.org/10.1182/blood.V97.2.376

Chou JY, Jun HS, Mansfield BC (2015) Type I glycogen storage diseases: disorders of the glucose-6-phosphatase/glucose-6-phosphate transporter complexes. J Inherit Metab Dis 38(3):511–519. https://doi.org/10.1007/s10545-014-9772-x

Colovos C, Yeates TO (1993) Verification of protein structures: patterns of nonbonded atomic interactions. Protein Sci 2(9):1511–1519. https://doi.org/10.1002/pro.5560020916

DasNandy A, Patil VS, Hegde HV, Harish DR, Roy S (2022) Elucidating type 2 diabetes mellitus risk factor by promoting lipid metabolism with gymnemagenin: an in vitro and in silico approach. Front Pharmacol. https://doi.org/10.3389/fphar.2022.1074342

Dieckgraefe BK, Korzenik ÆJR (2002) Association of glycogen storage disease 1b and Crohn disease: results of a North American survey. Eur J Pediatr 161:S88–S92. https://doi.org/10.1007/s00431-002-1011-z

Du X et al (2016) Insights into protein–ligand interactions: mechanisms, models, and methods. Int J Mol Sci 17(2):1–34. https://doi.org/10.3390/ijms17020144

Dwivedi PSR et al (2022) System biology-based investigation of Silymarin to trace hepatoprotective effect. Comput Biol Med 142:105223. https://doi.org/10.1016/j.compbiomed.2022.105223

Franco LM et al (2005) Hepatocellular carcinoma in glycogen storage disease type Ia: a case series. J Inherit Metab Dis 28(2):153–162. https://doi.org/10.1007/s10545-005-7500-2

Hemmerle H et al (1997) Chlorogenic acid and synthetic chlorogenic acid derivatives: novel inhibitors of hepatic glucose-6-phosphate translocase. J Med Chem 40(2):137–45

Hiraiwa H et al (1999) Inactivation of the glucose 6-phosphate transporter causes glycogen storage disease type 1b. J Biol Chem 274(9):5532–5536. https://doi.org/10.1074/jbc.274.9.5532

Jumper J et al (2021) Highly accurate protein structure prediction with AlphaFold. Nature 596(7873):583–589. https://doi.org/10.1038/s41586-021-03819-2

Khanal P, Patil VS, Bhandare VV, Dwivedi PS, Shastry CS, Patil BM et al (2022) Computational investigation of benzalacetophenone derivatives against SARS-CoV-2 as potential multi-target bioactive compounds. Comput Biol Med. https://doi.org/10.1016/j.compbiomed.2022.105668

Khanal P, Patil VS, Bhandare VV, Patil PP, Patil BM, Dwivedi PS, Bhattacharya K, Harish DR, Roy S (2023) Systems and in vitro pharmacology profiling of diosgenin against breast cancer. Front Pharmacol 13:1052849. https://doi.org/10.3389/fphar.2022.1052849

Krivák R, Hoksza D (2018) P2Rank: machine learning based tool for rapid and accurate prediction of ligand binding sites from protein structure. J Cheminformatics 10(1):1–12. https://doi.org/10.1186/s13321-018-0285-8

Kumari R, Kumar R, Lynn A (2014) G-mmpbsa -A GROMACS tool for high-throughput MM-PBSA calculations. J Chem Inf Model 54(7):1951–1962. https://doi.org/10.1021/ci500020m

Laskowski RA et al (1993) PROCHECK: a program to check the stereochemical quality of protein structures. J Appl Crystallogr 26(2):283–291. https://doi.org/10.1107/s0021889892009944

Leuzzi R et al (2003) Inhibition of microsomal glucose-6-phosphate transport in human neutrophils results in apoptosis: a potential explanation for neutrophil dysfunction in glycogen storage disease type 1b. Blood 101(6):2381–2387. https://doi.org/10.1182/blood-2002-08-2576

Oguz MM et al (2015) Glycogen storage disease type 1B: An early onset severe phenotype associated with a novel mutation (IVS4) in the glucose 6-phosphate translocase (SLC37A4) gene in a Turkish patient. Genetic Couns 25(4):389–394

Ong KW, Hsu A, Tan BKH (2013) Anti-diabetic and anti-lipidemic effects of chlorogenic acid are mediated by ampk activation. Biochem Pharmacol 85(9):1341–1351. https://doi.org/10.1016/j.bcp.2013.02.008

Özen H (2007) 'Glycogen storage diseases: new perspectives. World J Gastroenterol 13(18):2541–2553

Parikh NS, Ahlawat R (2021) Glycogen storage disease type I, StatPearls. Available at: https://www.ncbi.nlm.nih.gov/books/NBK534196/. Accessed 9 Oct 2022

Patil VS, Deshpande SH, Harish DR, Patil AS, Virge R, Nandy S, Roy S (2020) Gene set enrichment analysis, network pharmacology and in silico docking approach to understand the molecular mechanism of traditional medicines for the treatment of diabetes mellitus. J Proteins Proteom 11:297–310

Patil VS, Harish DR, Vetrivel U, Deshpande SH, Khanal P, Hegde HV et al (2022) Pharmacoinformatics analysis reveals flavonoids and diterpenoids from *Andrographis paniculata* and *Thespesia populnea* to target hepatocellular carcinoma induced by hepatitis B virus. Appl Sci 12(21):10691

Rake J et al (2002) Glycogen storage disease type I: diagnosis, management, clinical course and outcome. Results of the European study on glycogen storage disease type I (ESGSD I). Eur J Pediatr 161:S20–S34. https://doi.org/10.1007/s00431-002-0999-4

Samdani A, Vetrivel U (2018) POAP: a GNU parallel based multithreaded pipeline of open babel and AutoDock suite for boosted high throughput virtual screening. Comput Biol Chem 74:39–48. https://doi.org/10.1016/j.compbiolchem.2018.02.012

Van Aalten DMF, Findlay JBC, Amadei A, Berendsen HJC (1995) Essential dynamics of the cellular retinol-binding protein evidence for ligand-induced conformational changes. Protein Eng 8(11):1129–1135. https://doi.org/10.1093/protein/8.11.1129

Van Der Spoel D et al (2005) GROMACS: fast, flexible, and free. J Comput Chem 26(16):1701–1718. https://doi.org/10.1002/jcc.20291

Veiga-da-Cunha M et al (2019) Failure to eliminate a phosphorylated glucose analog leads to neutropenia in patients with G6PT and G6PC3 deficiency. Proc Natl Acad Sci USA 116(4):1241–1250. https://doi.org/10.1073/pnas.1816143116

Yennamalli RM (2018) Protein design. Encycl Bioinform Comput Biol: ABC Bioinform 1–3(1):644–651. https://doi.org/10.1016/B978-0-12-809633-8.20151-9

Publication II

Int. J. Pharm. Investigation, 2024; 14(1):141-150.
https://www.jpionline.org

Original Article

Novel Approaches in Glycogen Storage Disease Type I Management: Harnessing the Potential of Micronutrients and Macro Molecules

Santosh B Patil, Pramod C Gadad*

Department of Pharmacology, KLE College of Pharmacy, Hubballi (A Constituent Unit of KLE Academy of Higher Education and Research, Belagavi), Karnataka, INDIA.

ABSTRACT

Background: Genetic metabolic illnesses called Glycogen Storage Disease type I (GSD I) are caused due to abnormalities in the glucose-6-phosphatase enzyme complex involved in the metabolism of glycogen. **Objectives:** The current study explores the induction and management of GSD I manifestations. **Materials and Methods:** Chlorogenic Acid (CGA), a hydroxycinnamic acid found in various fruits and abundant in green coffee, can inhibit the enzyme glucose-6-phosphatase complex and metformin can alter the lactic acid levels. **Results:** The *in silico* and *in vivo* approach unveiled, that β-carotene showed the highest binding affinity with glucokinase, forming 7 hydrogen bonds. Riboflavin exhibited the highest binding affinity with protein phosphatase 1, forming 4 hydrogen bonds. Vitamin C interacted at the active site of the control ligand. Vitamin E also displayed significant binding affinity with glucokinase. Overall, these bioactive micro molecules show promising interactions with their respective target proteins. *In vivo* results revealed the significant impact of Macronutrients and Micronutrients, particularly when combining Cassava starch with the micronutrients. This combination showed notable improvements in various parameters, including liver glycogen levels, liver weight, fasting blood glucose levels, and liver histology. The findings suggest the potential of this synergistic approach in enhancing liver function and glucose regulation. To conclude this work, it was evident that the combination of Macro and Micronutrients revealed distinct advantages. UCCS and Cassava starch effectively maintained normoglycemia due to their sustained glucose release from complex carbohydrates. Remarkably, Cassava starch, both alone and combined with micronutrients, outperformed UCCS in promoting better outcomes. This highlights the potential for comprehensive research on Cassava starch's effects in GSD subjects, exploring its impact on other manifestations such as lactic acidosis, hypertriglyceridemia, and hyperuricemia. **Conclusion:** These findings offer promising avenues for further investigation and potential therapeutic applications.

Keywords: Glycogen Storage Disease type I, Chlorogenic acid, Glycogenesis, Hypoglycemia, glucokinase, Protein phosphatase-1.

Correspondence:
Dr. Pramod C Gadad
Department of Pharmacology, KLE College of Pharmacy, Hubballi-580 031 KLE College of Pharmacy, Hubballi (A Constituent Unit of KLE Academy of Higher Education and Research, Belagavi), Karnataka, INDIA.
Email: gadadpramod@gmail.com

Received: 06-08-2023;
Revised: 23-08-2023;
Accepted: 10-10-2023.

INTRODUCTION

The Glycogen Storage Diseases (GSD) or glycogenoses are a group of inherited metabolic diseases caused due to deficiency of the enzymes required to regulate glycogenolysis or gluconeogenesis.[1,2] Hypoglycemia is the prominent manifestation of hepatic GSD, whereas weakness and muscle cramps are the predominant features of muscle GSD. The overall incidence of these diseases is approximately 1 in 20,000 to 43,000 live births. Types I, III, and IX represent 80% of hepatic GSDs, of which GSD type I is most prevalent.[3]

The GSD type I, also known as Von Gierke's disease, is further categorized into type Ia and Ib. Deficient activity of Glucose-6-phosphatase - α (G6Pase-α) causes GSDIa and deficient activity of Glucose-6-Phosphate Transporter (G6PT) causes GSD Ib.[2] Both disorders results in hypoglycemia, hyperlipidemia, hyperuricemia, lactic acidosis, and excessive accumulation of glycogen primarily in the liver and kidney leading to progressive hepatomegaly and nephromegaly.[4]

The incidence of GSD I is 1 in 100000, 80% of the patients represent GSD Ia and 20% by GSD Ib.[5] In addition to the clinical symptoms and findings seen in GSD type Ia, recurrent infections, neutropenia, and neutrophil dysfunction are observed in type Ib[6]

DOI: 10.5530/ijpi.14.1.18

due to impaired glucose transport across the cell membrane of the polymorphonuclear leukocytes. It has been suggested that microsomal Glucose-6-Phosphate (G6P) transportation has a role in the antioxidant protection of neutrophils and that the genetic defect of the transporter leads to the impairment of cellular functions and apoptosis, which may be a potential explanation for neutrophil dysfunction. Long term complications like renal calculi and progressive renal disease, inflammatory bowel disease, hepatic adenomas, and hepatocellular carcinoma[7] can develop in older children and adults.[8] In most GSD patient's liver biopsy remains the gold standard diagnostic tool to determine the glycogen accumulation in hepatocytes, and other diagnostic measures include enzyme assay, mutation analysis, estimating the biochemical parameters, which reveal hypoglycemia, hyperlipidemia, hyperuricemia, lactic acidosis, and neutropenia specifically in case of GSD type Ib.[9]

The management of manifestation of GSD is a daunting task. The GSD patient needs to meticulously depend on frequent carbohydrate enriched diet (every 3-4 hr) and uncooked corn starch (UCCS),[9] devoid of simple sugars like sucrose (refined sugar), fructose (fruits) and lactose (dairy products) and other macronutrients. Special care should be taken to avoid excessive consumption of non-utilizable sugars, which may lead to accumulation of glycogen in tissues and endogenous production of lactate, triglycerides, and uric acid. Due to such diet constraints there is possibility of diminished macronutrient and micronutrient nourishment.[9]

There is evidences that certain micronutrients like Beta Carotene, Riboflavin, Vitamin C, Vitamin E,[10] thiamine, Vitamin D,[11] selenium,[12] etc. influence the glucose metabolism and improve a few GSD manifestations.

The literature suggests that the designing and establishing of disease model for GSD is an uphill task, though the gene knockout animals and genetically mutated cells serve as disease models. The stability, survivability, maintenance, and the cost of these models is a big challenge. As per literature review, certain chemical derivatives like Chlorogenic Acid (CGA), a type of hydroxycinnamic acids, occurs in many types of fruits and in high concentration in green coffee[12] and its derivatives are known to inhibit the particular enzyme glucose-6-phosphatase complex, along with Metformin (Met), which can simulate the manifestations similar to GSD type I. The present work is an attempt to determine how best these chemical derivatives mimic the characteristic manifestations of GSD and to assess the role of macro and micronutrients in the management of the manifestations. Based on literature review Uncooked corn starch and Cassava Starch (CS) were used as macronutrients and based on *in silico* trial few micronutrients were selected for the study (*viz.* Beta Carotene,[13] Riboflavin, Vitamin C, Vitamin E).[10] In GSD, it is necessary to maintain normoglycemia throughout the day and night, which can be achieved by either frequent meals, continuous glucose therapy and/or uncooked corn starch (UCCS).[12] However, frequent meals can be fed during day, but during night the patient needs to rely on UCCS,[14] which has its own time bound limitations, like lack of nutrition, fiber, complex carbohydrate, which arises the chance to pursue better alternative starch, like Cassava starch/tapioca starch to help maintain the nutritional value of the diet and at the same time sustain the normoglycemia better than UCCS.[13] The next major manifestation of GSD type 1 is glycogen accumulation in hepatocytes which leads to progressive hepatomegaly and hepatic dysfunction in advanced conditions,[14] to overcome this issue we attempted to inhibit the process of Glycogenesis, by inactivation of major enzymes involved in the glycogen synthesis pathway, *viz,* Glycogen synthase,[15] Glucokinase and standby enzyme called Protein phosphatase-1 enzyme,[16] with the help of few selected micronutrients. So, to sum up, the macronutrients are expected to maintain the normoglycemia for the maximum period possible and on the other hand the micronutrients are expected to reduce the glycogen accumulation in the liver, thus maintaining the normal architecture and physiology of the liver.

MATERIALS AND METHODS

In silico study

Molecular Docking

The molecular docking was performed under the three main steps i.e., ligand preparation, macromolecule preparation and ligand-protein docking.

Ligand Preparation

The 3D structure of each ligand was retrieved from PubChem database in .sdf format and converted into .pdb format using Discovery Studio 2021. The energy minimized using uff force field under conjugation gradient as an optimum algorithm. After energy minimization each ligand was converted into .pdbqt format.

Macromolecule preparation

The x-ray 3D crystallographic protein of Protein Phosphatase-1 (PDB:6DNO), GSK3β (PDB:4J1R), glucokinase (PDB: 1SZ2) were retrieved from RCSB protein databank. All the hetero atoms were removed using Discovery Studio 2021. Molecules were then added with kollman charges. Later, all the ligands were saved in .pdb format.

Ligand-protein docking

Each ligand was docked against Protein Phosphatase-1 (center x, y, z=15.33, 80.65, 181.65, and size x, y, z=46.56, 46.15, 56.039), GSK3β (center x, y, z=34.11, 32.72, 18.41 and size x, y, z=61.01, 54.50, 60.32), and glucokinase (center x, y, z=10.133, -3.79, 12.89 and size x, y, z=63.16, 53.23, 57.57) using AutoDock Vina. After docking 10 different poses were obtained. The ligand's

due to impaired glucose transport across the cell membrane of the polymorphonuclear leukocytes. It has been suggested that microsomal Glucose-6-Phosphate (G6P) transportation has a role in the antioxidant protection of neutrophils and that the genetic defect of the transporter leads to the impairment of cellular functions and apoptosis, which may be a potential explanation for neutrophil dysfunction. Long term complications like renal calculi and progressive renal disease, inflammatory bowel disease, hepatic adenomas, and hepatocellular carcinoma[7] can develop in older children and adults.[8] In most GSD patient's liver biopsy remains the gold standard diagnostic tool to determine the glycogen accumulation in hepatocytes, and other diagnostic measures include enzyme assay, mutation analysis, estimating the biochemical parameters, which reveal hypoglycemia, hyperlipidemia, hyperuricemia, lactic acidosis, and neutropenia specifically in case of GSD type Ib.[9]

The management of manifestation of GSD is a daunting task. The GSD patient needs to meticulously depend on frequent carbohydrate enriched diet (every 3-4 hr) and uncooked corn starch (UCCS),[9] devoid of simple sugars like sucrose (refined sugar), fructose (fruits) and lactose (dairy products) and other macronutrients. Special care should be taken to avoid excessive consumption of non-utilizable sugars, which may lead to accumulation of glycogen in tissues and endogenous production of lactate, triglycerides, and uric acid. Due to such diet constraints there is possibility of diminished macronutrient and micronutrient nourishment.[9]

There is evidences that certain micronutrients like Beta Carotene, Riboflavin, Vitamin C, Vitamin E,[10] thiamine, Vitamin D,[11] selenium,[12] etc. influence the glucose metabolism and improve a few GSD manifestations.

The literature suggests that the designing and establishing of disease model for GSD is an uphill task, though the gene knockout animals and genetically mutated cells serve as disease models. The stability, survivability, maintenance, and the cost of these models is a big challenge. As per literature review, certain chemical derivatives like Chlorogenic Acid (CGA), a type of hydroxycinnamic acids, occurs in many types of fruits and in high concentration in green coffee[12] and its derivatives are known to inhibit the particular enzyme glucose-6-phosphatase complex, along with Metformin (Met), which can simulate the manifestations similar to GSD type I. The present work is an attempt to determine how best these chemical derivatives mimic the characteristic manifestations of GSD and to assess the role of macro and micronutrients in the management of the manifestations. Based on literature review Uncooked corn starch and Cassava Starch (CS) were used as macronutrients and based on *in silico* trial few micronutrients were selected for the study (*viz.* Beta Carotene,[13] Riboflavin, Vitamin C, Vitamin E).[10] In GSD, it is necessary to maintain normoglycemia throughout the day and night, which can be achieved by either frequent meals, continuous glucose therapy and/or uncooked corn starch (UCCS).[12] However, frequent meals can be fed during day, but during night the patient needs to rely on UCCS,[14] which has its own time bound limitations, like lack of nutrition, fiber, complex carbohydrate, which arises the chance to pursue better alternative starch, like Cassava starch/tapioca starch to help maintain the nutritional value of the diet and at the same time sustain the normoglycemia better than UCCS.[13] The next major manifestation of GSD type 1 is glycogen accumulation in hepatocytes which leads to progressive hepatomegaly and hepatic dysfunction in advanced conditions,[14] to overcome this issue we attempted to inhibit the process of Glycogenesis, by inactivation of major enzymes involved in the glycogen synthesis pathway, *viz,* Glycogen synthase,[15] Glucokinase and standby enzyme called Protein phosphatase-1 enzyme,[16] with the help of few selected micronutrients. So, to sum up, the macronutrients are expected to maintain the normoglycemia for the maximum period possible and on the other hand the micronutrients are expected to reduce the glycogen accumulation in the liver, thus maintaining the normal architecture and physiology of the liver.

MATERIALS AND METHODS

In silico study

Molecular Docking

The molecular docking was performed under the three main steps i.e., ligand preparation, macromolecule preparation and ligand-protein docking.

Ligand Preparation

The 3D structure of each ligand was retrieved from PubChem database in .sdf format and converted into .pdb format using Discovery Studio 2021. The energy minimized using uff force field under conjugation gradient as an optimum algorithm. After energy minimization each ligand was converted into .pdbqt format.

Macromolecule preparation

The x-ray 3D crystallographic protein of Protein Phosphatase-1 (PDB:6DNO), GSK3β (PDB:4J1R), glucokinase (PDB: 1SZ2) were retrieved from RCSB protein databank. All the hetero atoms were removed using Discovery Studio 2021. Molecules were then added with kollman charges. Later, all the ligands were saved in .pdb format.

Ligand-protein docking

Each ligand was docked against Protein Phosphatase-1 (center x, y, z=15.33, 80.65, 181.65, and size x, y, z=46.56, 46.15, 56.039), GSK3β (center x, y, z=34.11, 32.72, 18.41 and size x, y, z=61.01, 54.50, 60.32), and glucokinase (center x, y, z=10.133, -3.79, 12.89 and size x, y, z=63.16, 53.23, 57.57) using AutoDock Vina. After docking 10 different poses were obtained. The ligand's

Cassava Starch admixed with normal Chow pellets.

The normal chow feed was churned into the pestle and mortar and equal quantity of starch (UCCS and Casava Starch Individually) (i.e. 10 gms of each per animal) was admixed and small quantity of distilled water was added to mix well, now the mixture was pressed into pellets and dried overnight.

Management of the manifestations using Micronutrient

Oral administration of Beta carotene (6 mg/kg/day), Riboflavin (10 mg/kg/day), Vitamin C (100 mg/ kg/day) and Vitamin E (60 mg/kg/day).

Data analysis

The collected data was subjected to statistical analysis using statistical GraphPad Prism version 7. The results were expressed as the mean ± SEM (Standard Error of the Mean). The results obtained were analysed using one-way ANOVA followed by Bonferroni's multiple comparison *post-hoc* test.

RESULTS

In silico study

Molecular Docking

Among all the bioactive micro molecules, β-carotene showed the highest binding affinity with glucokinase (Figure 2A) (binding energy -8.5 kcal/mol) and however, it had no H- bond interaction vs control ligand (-6.1 kcal/mol); showed 7 H-bond interactions with Ala107, Ala103, Thr102, His312, Ser153, Trp151. However, the control ligand had the highest binding affinity with GSK3β (binding energy -8.4 kcal/mol, 3 H-bond interactions with Val135 and Pro136) (Figure 1A, 2A, and 3A). Among the test ligands, β-carotene showed the maximum binding affinity compared to rest of test ligands with GSK3β (binding energy -8 kcal/mol) (Table 1). Likewise, among all the test ligands, riboflavin showed the highest binding affinity with protein phosphatise 1 (Figure 3B) (binding energy -7.4 kcal/mol 4 H-bond interactions with Tyr69, Arg74, Asp71 vs control ligand (Figure 4) (binding energy -9.9 kcal/mol, 6 H-bind interactions with Cys278, Arg221, His248, Asp92, Arg96, Lys98. The binding affinity of each ligand with a respective target is presented in (Table 1). Among all the test ligands, these compounds i.e., Riboflavin (Figure 2B), β-carotene (had no H-interactions) and vitamin E (Figure 2D) interacted on different site compared to the control ligand for glucokinase (Figure 1D). However, vitamin C had the interaction with all the amino acids that control ligand has meaning it acts within active site where control ligand binds (Figure 1C, 2C, and 3C). Likewise, riboflavin had the common Val 135 interacting residue with GSK3β (Figure 1B) compared to its control ligand, meaning its probable GSK3β inhibitory activity within the given site. Similarly, Vitamin C had the common 2 amino acid residues i.e., Arg221 and Arg96 to interact with protein phosphatase 1 (Figure 3 C) reflecting its probable inhibitory activity within the site of control ligand's interaction (Figure 4).

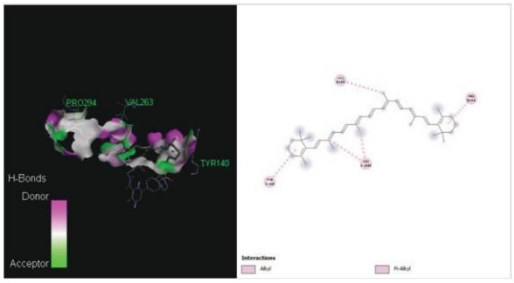

Figure 1 (A): Beta carotene docked with glycogen synthase kinase 3b.

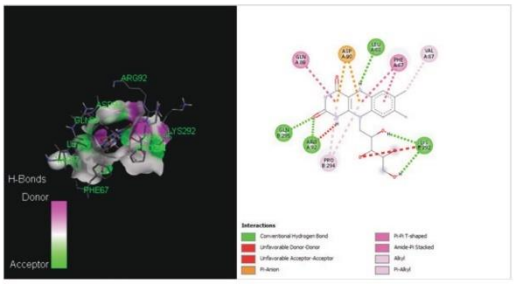

Figure 1 (B): Riboflavin docked with glycogen synthase kinase 3b.

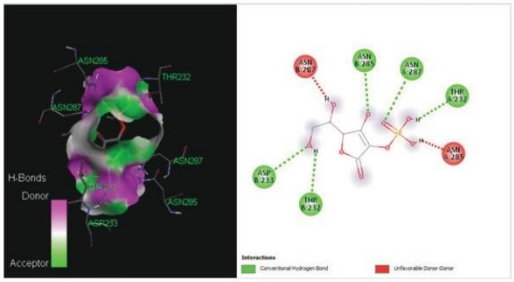

Figure 1 (C): Vitamin C docked with glycogen synthase kinase 3b.

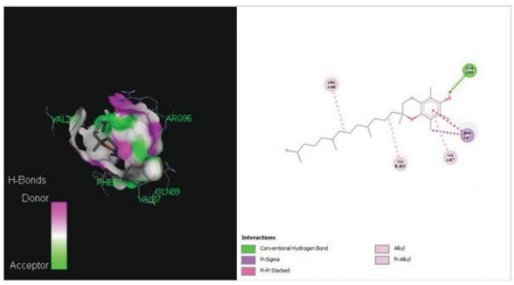

Figure 1 (D): Vitamin E docked with glycogen synthase kinase 3b.

Selected Micronutrients having Good Binding Affinity with Glycogen Synthase Kinase 3b (GSK3b)

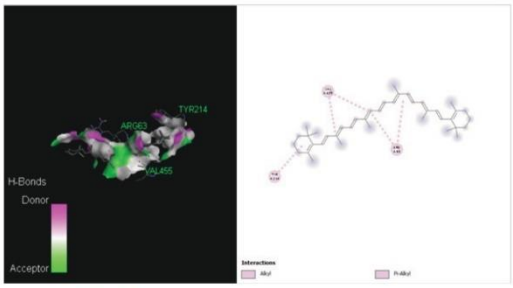

Figure 2 (A): Beta Carotene docked with Glucokinase.

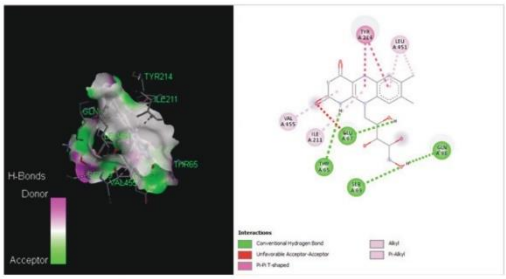

Figure 2 (B): Riboflavin docked with Glucokinase.

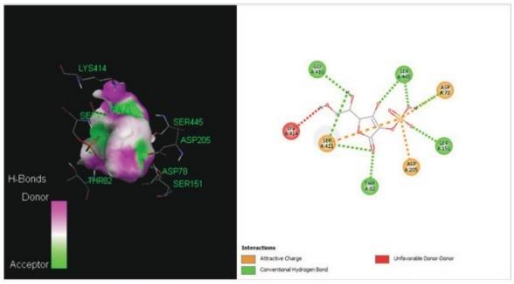

Figure 2 (C): Vitamin C docked with Glucokinase.

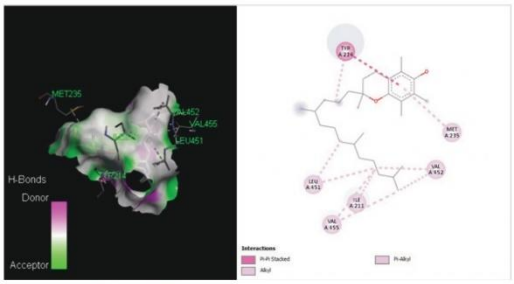

Figure 2 (D): Vitamin E docked with Glucokinase.

Micronutrients having good binding affinity with Glucokinase

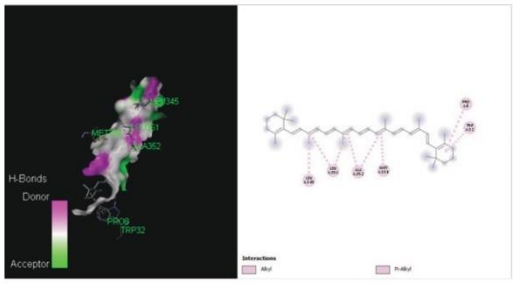

Figure 3 (A): Beta carotene docked with Protein Phosphatase-1.

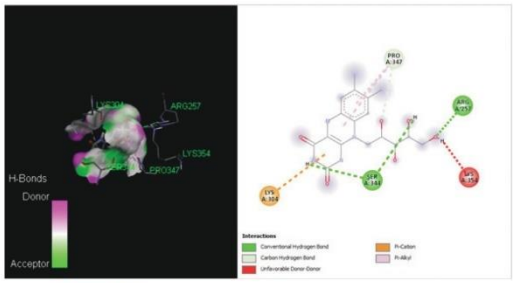

Figure 3 (B): Riboflavin docked with Protein Phosphatase-1.

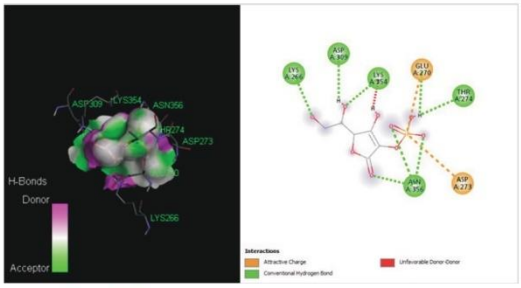

Figure 3 (C): Vitamin C docked with Protein Phosphatase-1.

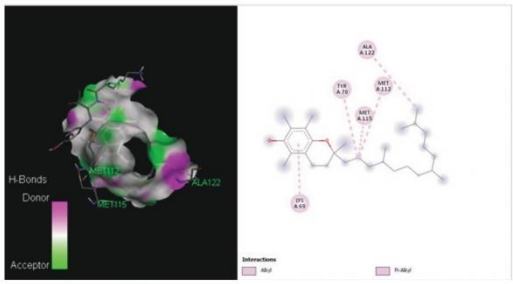

Figure 3 (D): Vitamin E docked with Protein Phosphatase-1.

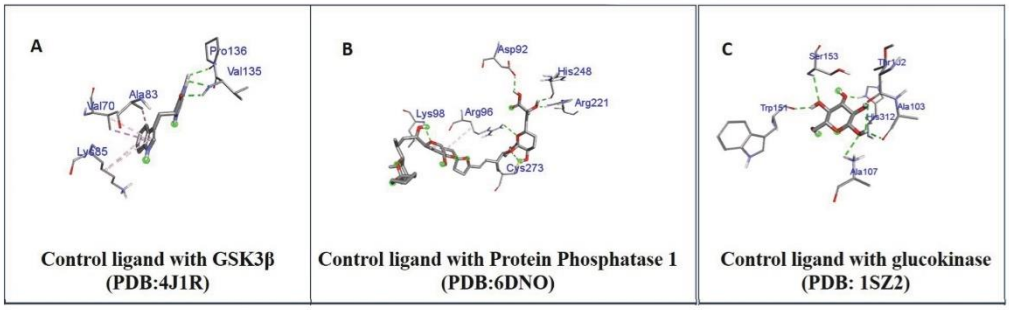

Figure 4 (A, B and C): Showing the interactions of the control ligands with GSK3β, Protein Phosphatase 1, and Glucokinase

Micronutrients having good binding affinity with Protein Phosphatase-1

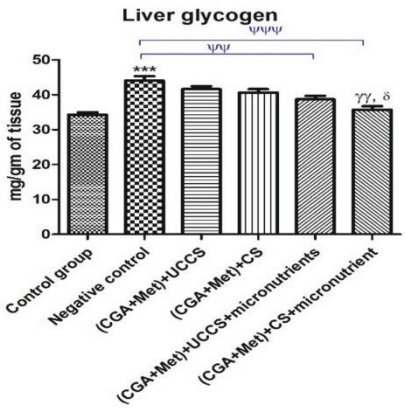

Figure 5: Values are expressed as mean±standard error of the mean (n=6). Negative control group showed significant increase in the liver glycogen content (***p<0.001), (CGA+Met)+UCCS+micronutrients showed the significant reduction in glycogen ($^{\Psi\psi}p$<0.01) and (CGA+Met)+cassava starch+micronutrients ($^{\Psi\Psi\psi}p$<0.001) when compared to Negative control, whereas, (CGA+Met)+cassava starch+micronutrients group showed ($^{\gamma}p<0.01$) when compared to (CGA+Met)+UCCS and ($^{\delta}p<0.05$) when compared to (CGA+Met)+CS.

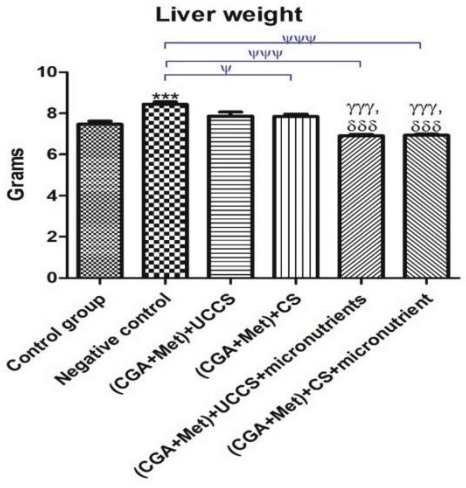

Figure 6: Results are expressed as mean±standard error of the mean (n=6), there was notable increase in the liver size of Negative control when compared to Control group (***p<0.001), (CGA+Met)+cassava starch group showed significant decrease ($^{\Psi}p<0.05$) when compared with negative control and both micronutrient treated groups showed significant decrease in the liver weight when compared to Negative Control ($^{\Psi\Psi\psi}p$<0.001) similarly (CGA+Met)+UCCS+micronutrients and (CGA+Met)+cassava starch+micronutrients, decreased the liver weight significantly ($^{\gamma\gamma\gamma}p$<0.001) when compared to (CGA+Met)+UCCS and ($^{\delta\delta\delta}p$<0.001) when compared to (CGA+Met)+cassava group.

In vivo study

Liver glycogen estimation

Liver Glycogen Estimation

The negative control group exhibited a substantial increase in liver glycogen content (***p<0.001). However, the (CGA+Met)+UCCS+micronutrients group showed significant reduction in liver glycoen ($\Psi\Psi p$<0.01), and the (CGA+Met)+cassava starch+micronutrients group displayed even higher significance ($\Psi\Psi\Psi p$<0.001) when compared to the negative control. Furthermore, the (CGA+Met)+cassava starch+micronutrients group exhibited statistical significant reduction in liver glycogen ($\gamma\gamma p$<0.01) when compared to (CGA+Met)+UCCS, and (δp<0.05) when compared to (CGA+Met)+CS (Figure 5).

Liver weight

The liver weight varied across groups. The negative control group had significantly increased liver weight (***p<0.001) compared

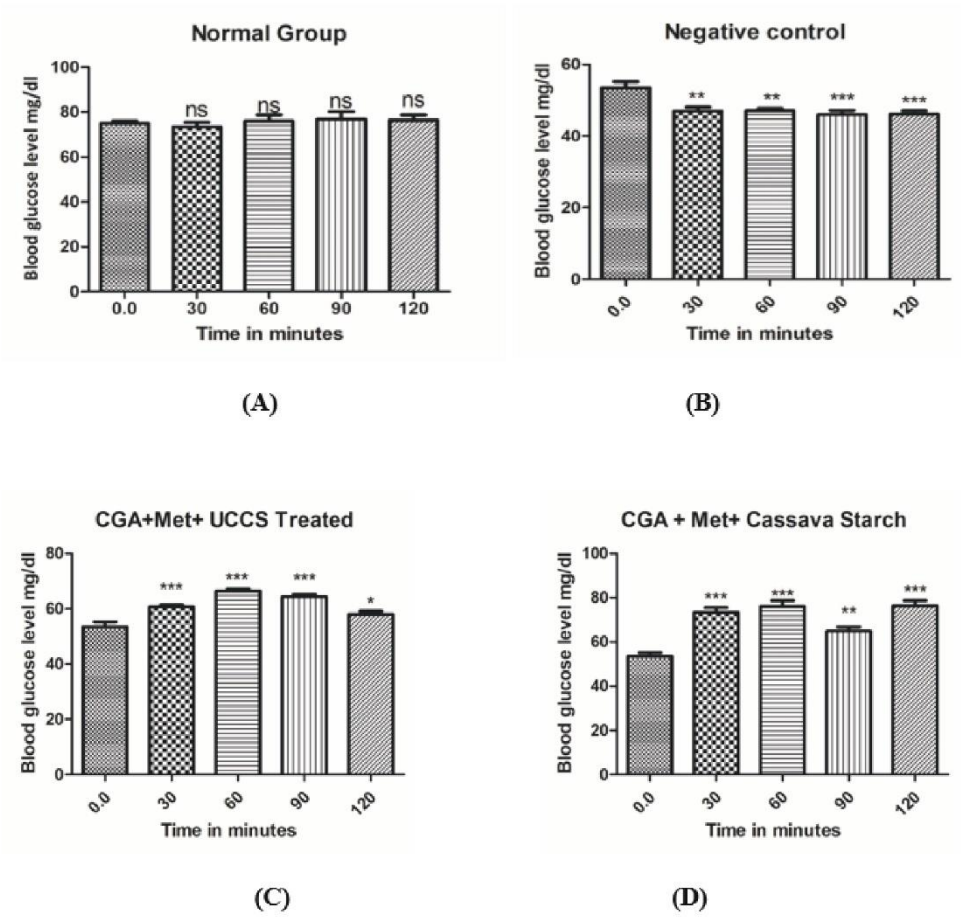

Figure 7: The statistical significance was analysed by one-way ANOVA followed by Bonferroni's multiple comparison *post-hoc* test, (A) showed no significant changes, whereas (B) showed significant decrease in blood glucose level (**p<0.01 at 30 and 60 min) and (***p<0.001 at 90 and 120 min). (C) showed significant elevation (***p<0.001) at 30, 60, 90 min, whereas (*p<0.05) at 120 min, On the other hand, (D) showed significant elevation in blood glucose levels (***p<0.001) at 30, 60 and 120 min and (**p<0.01 at 90 min) when compared to 0.0 min reading.

to the control group, while the (CGA+Met)+cassava starch group decreased liver weight (Ψp<0.05) compared to the negative control. Both micronutrient-treated groups significantly reduced liver weight (ΨΨΨp<0.001) compared to the negative control.

Additionally, combining (CGA+Met)+UCCS+micronutrients and (CGA+Met)+cassava starch+micronutrients led to a significant decrease in liver weight (γγγp<0.001) compared to (CGA+Met)+UCCS and (δδδp<0.001) compared to (CGA+Met)+cassava starch (Figure 6). These findings illustrate the treatment effects on liver weight in our study.

Fasting Blood Glucose levels

The normal group exhibited no significant changes in blood glucose levels. Conversely, the negative control group in Figure B displayed a substantial decrease in blood glucose levels (**p<0.01 at 30 & 60 minutes) and (***p<0.001 at 90 & 120 minutes). In Figure C, the treatment group (CGA+Met+UCCS) demonstrated significant elevations in blood glucose levels (***p<0.001) at 30, 60, and 90 minutes, with a (*p<0.05) increase at 120 minutes. In contrast, in Figure D, the treatment group (CGA+Met+CS) showed remarkable elevations in blood glucose levels (***p<0.001) at 30, 60 & 120 minutes and (**p<0.01 at 90 minutes) when compared to the 0.0 min reading.

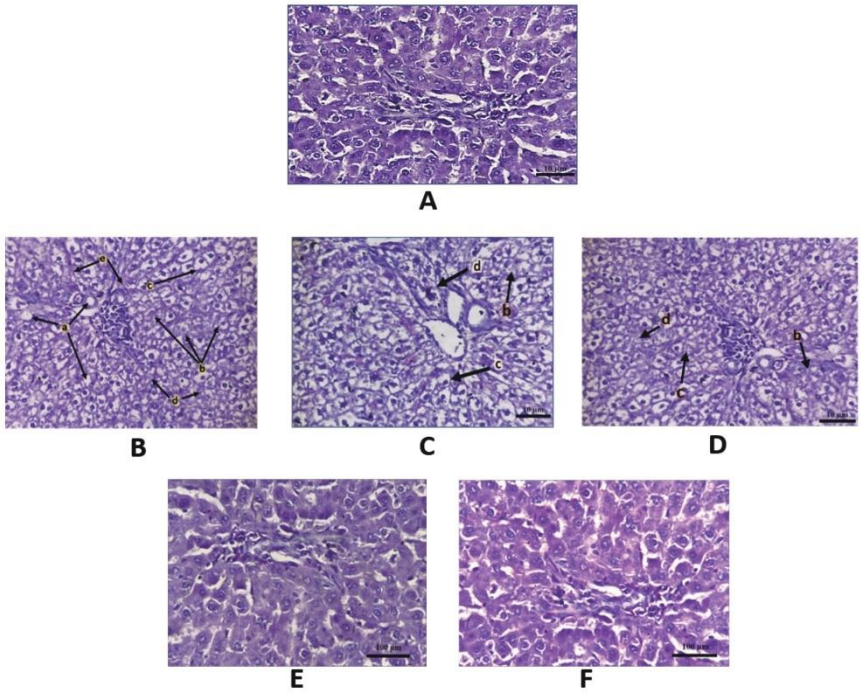

Figure 8: (A) Normal Group Periodic Acid-Schiff stain (PAS) showing normal architecture with intact hepatocytes and no Glycogen accumulation. (B) CGA (200mg/kg) treated group PAS stained, showed significant Mosaic pattern, Glycogen nuclei [a], Glycogen [b] swollen hepatocytes [c], ballooning degeneration [d] and sinusoidal congestion [e]. (C) (CGA+Met)+UCCS treated group. (D) (CGA +Met)+Cassava Starch treated group PAS stained, showed notable Glycogen [b], swollen hepatocytes [c], and ballooning degeneration [d]. (E) UCCS+micronutrients treated group. (F): Cassava starch+micronutrient treated group showed near normal architecture with intact hepatocytes and no Glycogen accumulation.

Table 1: Binding affinity of each ligand with their respective targets.

Ligand	Glucokinase (PDB: 1SZ2)			GSK3β (PDB: 4J1R)			Protein Phosphatase-1 (PDB: 6DNO)		
	Binding Affinity	NHBI	HBR	Binding Affinity	NHBI	HBR	Binding Affinity	NHBI	HBR
Control ligand	-6.1	7	Ala107, Ala103, Thr102, His312, Ser153, Trp151	-8.4	3	Val135, Pro136	-9.9	6	Cys278, Arg221, His248, Asp92, Arg96, Lys98
Riboflavin	-6.8	2	Asp100, Thr137	-7.3	3	Val135, Ile62, Asn64	-7.4	4	Tyr69, Arg74, Asp71
Vitamin C	-5.9	4	Thr102, Ala103, Ala107, Trp151	-5.3	4	Glu283, Met284, Thr235	-5.6	5	His125, Arg96, Tyr272, His248, Arg221
β-carotene	-8.5	-	-	-8	-	-	-7.9	-	-
Vitamin E	-5.9	1	Gly134	-7	-	-	-6.6	1	Lys98

Histopathological analysis

The typical histopathological features of rat livers for all the groups by Periodic Acid-Schiff stain (PAS) staining are represented in Figure 7. The CGA treated group showed significant Mosaic pattern, Glycogen nuclei, Glycogen, swollen hepatocytes, ballooning degeneration & sinusoidal congestion when compared to normal group. On the other hand (CGA+Met) + UCCS treated group and (CGA +Met) + Cassava Starch treated group showed notable Glycogen, swollen hepatocytes, & ballooning degeneration. Whereas, the UCCS + micronutrients and Cassava starch + micronutrients treated group showed near normal architecture with intact hepatocytes and no Glycogen accumulation (Figure 8).

Statistical analysis

All the data were analysed using the statistical program GraphPad Prism version 6.0 and expressed as mean SEM. Where, Analysis of Variance (ANOVA) was used to examine the data, followed by Bonferroni's multiple comparison *post-hoc* test, where p values of <0.05) were set to be considered as statistically significant.

DISCUSSION

The aim of the study was to explore the predominant manifestation of GSD type I i.e., hypoglycemia, A phytochemical called CGA was considered optimum at 200 mg/ kg/ *po*. Which showed some promising capability to induce fasting hypoglycemia in albino wistar rats. Several *in vitro* studies have claimed that CGA can inhibit glucose-6-phosphate enzyme complex (glucose-6-phosphatase and glucose-6-phosphate translocase).[18] Thus, in this study the green coffee extract,[19] consisting of 36 % CGA was admixed in the drinking water and was fed continuously to the animals in the treatment groups, with an expectation of maintain the CGA effect, along with that the animals received a daily dose of 200 mg of 95% CGA via oral gavage. Glycogen levels are slightly elevated in CGA treated rats which can be due to the specific inhibition of glucose-6-phosphatase and it is also one of the contributing factors for hepatomegaly. Throughout the experiment the animals were subjected to overnight fasting and 1 hr before the experiment, all the groups except Normal group were subjected to 95% CGA at 200 mg/kg via oral gavage as a loading dose, followed by a 100 mg/kg dose of 95% CGA after every 45 min interval to maintain the bioavailability of the CGA. In addition to 95% CGA animals were subjected to 36% CGA, continuously in drinking water throughout the study. The UCCS and Cassava starch were used as Macronutrients whereas Beta-Carotene, Riboflavin, Vitamin- C and Vitamin-E were selected as Micronutrients based on drug likeness using *in silico* approach, where, β-carotene exhibited the highest binding affinity with glucokinase and formed 7 hydrogen bonds with specific amino acids, while the control ligand showed lower binding affinity with no hydrogen bonds. β-carotene also displayed significant binding affinity with GSK3β. Riboflavin demonstrated the highest binding affinity with protein phosphatase-1 and formed 4 hydrogen bonds with specific amino acids. The control ligand showed stronger binding with protein phosphatase-1 and formed 6 hydrogen bonds. Riboflavin, β-carotene, and Vitamin E interacted at different sites compared to their respective control ligands for glucokinase. Vitamin C interacted with all the amino acids targeted by the control ligand, indicating potential inhibitory activity in the active site. Riboflavin shared a common interacting residue with GSK3β, suggesting a probable inhibitory activity at that site. Similarly, Vitamin C had two common amino acid residues with the control ligand, reflecting its potential inhibitory activity at the site of control ligand's interaction with protein phosphatase-1. On the other hand, *in vivo* results demonstrated the influence of Macronutrients and Micronutrients, especially Cassava starch in combination with the micronutrients showed significant improvement in the parameters such as liver glycogen, liver weight, fasting blood glucose levels and liver histology, and to address the glycogen accumulation in hepatocytes, leading to hepatomegaly and hepatic dysfunction, we attempted to inhibit the process of glycogenesis. Our approach involved inactivating key enzymes, including glycogen synthase, glucokinase, and protein phosphatase-1, using selected micronutrients.

CONCLUSION

Inclusion of Macro and Micronutrients demonstrated their beneficial effect in their own ways, UCCS and Cassava Starch showed gradual maintenance of normoglycemia, due to the presence of complex carbohydrates, which is believed to convert into glucose in sustained manner. Among these two, Cassava starch alone as well as in combination with the micronutrients showed better results when compared to UCCS alone and in combination with micronutrients. The micronutrients were pivotal in preventing excess glycogen accumulation in hepatocytes which is the major cause for the classical GSD manifestations especially hepatomegaly. Further there is considerable scope to study the beneficial role of macro and micronutrients extensively in GSD I subjects, targeting other manifestations such as lactic acidosis, hypertriglyceridemia, and hyperuricemia.

ACKNOWLEDGEMENT

We gratefully acknowledge the Principal, KLE College of Pharmacy, Hubballi, Karnataka for providing research facilities.

CONFLICTS OF INTEREST

The authors declare that they have no conflict of interest.

AUTHOR CONTRIBUTIONS

Santosh B Patil: Conceptualization, Methodology, Investigation, Visualization and Project administration; **Pramod C Gadad:** Supervision, Validation and Data curation.

ABBREVIATIONS

GSD: Glycogen Storage Disease; **CGA:** Chlorogenic acid; **UCCS:** Uncooked corn starch; **CS:** Cassava Starch; **Met:** Metformin; **PAS:** Periodic Acid-Schiff stain.

ORCID

ORCID: 0000-0001-5691-546X

REFERENCES

1. Özen H. Glycogen storage diseases: new perspectives. World J Gastroenterol. 2007;13(18):2541-53. doi: 10.3748/wjg.v13.i18.2541, PMID 17552001.
2. Chou JY, Jun HS, Mansfield BC. Type I glycogen storage diseases: disorders of the glucose-6-phosphatase/glucose-6-phosphate transporter complexes. J Inherit Metab Dis. 2015;38(3):511-9. doi: 10.1007/s10545-014-9772-x, PMID 25288127.
3. Hiraiwa H, Pan CJ, Lin B, Moses SW, Chou JY. Inactivation of the glucose 6-phosphate transporter causes glycogen storage disease type 1b. J Biol Chem. 1999;274(9):5532-6. doi: 10.1074/jbc.274.9.5532, PMID 10026167.
4. Chou JY, Jun HS, Mansfield BC. Type I glycogen storage diseases: disorders of the glucose-6-phosphatase/glucose-6-phosphate transporter complexes. J Inherit Metab Dis. 2015;38(3):511-9. doi: 10.1007/s10545-014-9772-x, PMID 25288127.
5. Labrune P, Ullrich K, Smit P, Rake J, Visser G, Leonard J. Guidelines for management of glycogen storage disease type I - European study on glycogen storage disease Type I (ESGSD I). Eur J Pediatr. 2002; 161(0):S112-9. doi: 10.1007/s00431-002-1016-7.
6. Calderwood S, Kilpatrick L, Douglas SD, Freedman M, Smith-whitley K, Rolland M, *et al.* Recombinant human granulocyte colony-stimulating factor therapy for patients with neutropenia and/or neutrophil dysfunction secondary to glycogen storage disease type 1b. 2016;97(2):376-83.
7. Franco LM, Krishnamurthy V, Bali D, Weinstein DA, Arn P, Clary B, *et al.* Hepatocellular carcinoma in glycogen storage disease type Ia: A case series. J Inherit Metab Dis. 2005;28(2):153-62. doi: 10.1007/s10545-005-7500-2, PMID 15877204.
8. Dieckgraefe BK, Korzenik ÆJR. Association of glycogen storage disease 1b and Crohn disease: results of a North American survey. 2002;161:S88-92.
9. Kishnani PS, Austin SL, Abdenur JE, Arn P, Bali DS, Boney A, *et al.* Diagnosis and management of glycogen storage disease type I: A practice guideline of the American College of Medical Genetics and Genomics. Genet Med. 2014;16(11):e1. doi: 10.1038/gim.2014.128, PMID 25356975.
10. Derks TGJ, Rodriguez-Buritica DF, Ahmad A, de Boer F, Couce ML, Grünert SC, *et al.* Glycogen storage disease type Ia: current management options, burden and unmet needs. Nutrients. 2021;13(11):1-17. doi: 10.3390/nu13113828, PMID 34836082.
11. Bhattacharya K. Dietary dilemmas in the management of glycogen storage disease type I. J Inherit Metab Dis. 2011;34(3):621-9. doi: 10.1007/s10545-011-9322-8, PMID 21491105.
12. Melis D, Della Casa R, Parini R, Rigoldi M, Cacciapuoti C, Marcolongo P, *et al.* Vitamin E supplementation improves neutropenia and reduces the frequency of infections in patients with glycogen storage disease type 1b. Eur J Pediatr. 2009;168(9):1069-74. doi: 10.1007/s00431-008-0889-5, PMID 19066956.
13. Kalkan Ucar S, Coker M, Sözmen E, Goksen Simsek D, Darcan S. An association among iron, copper, zinc, and selenium, and antioxidative status in dyslipidemic pediatric patients with glycogen storage disease types IA and III. J Trace Elem Med Biol. 2010;24(1):42-5. doi: 10.1016/j.jtemb.2009.10.004, PMID 20122579.
14. Ong KW, Hsu A, Tan BKH. Anti-diabetic and anti-lipidemic effects of chlorogenic acid are mediated by AMPK activation. Biochem Pharmacol. 2013;85(9):1341-51. doi: 10.1016/j.bcp.2013.02.008, PMID 23416115.
15. Schnorr CE, Morrone M, Simões-Pires A, Bittencourt L, Zeidán-Chuliá F, Moreira JCF. Supplementation of adult rats with moderate amounts of β-carotene modulates the redox status in plasma without exerting pro-oxidant effects in the brain: A safer alternative to food fortification with vitamin A? Nutrients. 2014;6(12):5572-82. doi: 10.3390/nu6125572, PMID 25470379.
16. Chen YT, Cornblath M, Sidbury JB. Cornstarch therapy in Type I glycogen-storage disease. N Engl J Med. 1984;310(3):171-5. doi: 10.1056/NEJM198401193100306, PMID 6581385.
17. Bhattacharya K, Mundy H, Lilburn MF, Champion MP, Morley DW, Maillot F. A pilot longitudinal study of the use of waxy maize heat modified starch in the treatment of adults with glycogen storage disease type I: A randomized double-blind cross-over study. Orphanet J Rare Dis. 2015;10(1):18. doi: 10.1186/s13023-015-0229-6, PMID 25758258.
18. Pursell N, Gierut J, Zhou W, Dills M, Diwanji R, Gjorgjieva M, *et al.* Inhibition of glycogen synthase II with RNAi prevents liver injury in mouse models of glycogen storage diseases. Mol Ther. 2018;26(7):1771-82. doi: 10.1016/j.ymthe.2018.04.023, PMID 29784585.
19. Marr L, Biswas D, Daly LA, Browning C, Vial SCM, Maskell DP, *et al.* Mechanism of glycogen synthase inactivation and interaction with glycogenin. Nat Commun. 2022;13(1):3372. doi: 10.1038/s41467-022-31109-6, PMID 35690592.

Cite this article: Patil SB, Gadad PC. Novel Approaches in Glycogen Storage Disease Type I Management: Harnessing the Potential of Micronutrients and Macro Molecules. Int. J. Pharm. Investigation. 2024;14(1):141-50.

Publication III (Accepted)

Ind. J. Pharm. Edu. Res., 2024; 58(2):1-10.
https://www.ijper.org

Original Article

Chlorogenic Acid, a Potential Glucose-6-Phosphatase Inhibitor: An Approach to Develop a Pre-Clinical Glycogen Storage Disease Type I Model

Santosh B Patil, Pramod C Gadad*

Department of Pharmacology, KLE College of Pharmacy, Hubballi, A Constituent Unit of KLE Academy of Higher Education and Research, Belagavi, Karnataka, INDIA.

ABSTRACT

Introduction: Gluconeogenesis and glycogenolysis are highly regulated metabolic processes that are critical in maintaining blood glucose levels within the physiological range. Any aberration in the regulation of these processes can lead to an inadequate repository or accumulation of excess glycogen in hepatocytes. Glycogen Storage Disease type I (GSD type I), also known as Von Gierke's disease, is categorized under inborn errors of metabolism caused due to either inactivity or complete absence of the Glucose-6-phosphatase enzyme (G6Pase). **Objectives:** This study's focus is to suppress G6Pase, hepatic glucose synthesis, and induce the symptoms of GSD type I in experimental rats. **Materials and Methods:** The *in silico* approach using Chlorogenic Acid (CGA) and G6Pase exhibited a good docking score (-8.9), and promising binding patterns, molecular dynamic simulation studies (at 100 nanoseconds) also confirmed the stability of the docked complex. Based on this *in silico* speculation, the *in vivo* study was designed, where, in the pilot study varying doses (50, 100, 200, 400 mg/kg) and CGA-liposome formulation were scrutinized, **Results:** It was corroborated that the CGA can cause hypoglycemia, hence CGA (200 mg/kg) was chosen for the study, to further augment the other major GSD type I manifestations, metformin (500 mg/kg) was included in the study for 49 days, manifestations like hypoglycemia, suppressed G6Pase activity, elevated hepatic glycogen and lactate dehydrogenase were evident. **Conclusion:** The observations suggest that chlorogenic acid has the potential to induce GSD type I manifestations along with metformin, which can be an alternative animal model to match the genetically modified disease models.

Keywords: Chlorogenic acid, Metformin, Fasting blood glucose, Glucose-6-phosphatase, Glycogen storage disease type I, Glycogenolysis.

Correspondence:
Dr. Pramod C Gadad
Department of Pharmacology, KLE College of Pharmacy, Hubballi – 580031, A Constituent Unit of KLE Academy of Higher Education and Research, Belagavi, Karnataka, INDIA.
Email: gadadpramod@gmail.com
ORCiD : 0000-0001-5691-546X

Received: x-x-x;
Revised: x-x-x;
Accepted: x-x-x.

INTRODUCTION

Glycogen Storage Diseases (GSD's) or glycogenoses are a category of inborn errors of metabolism that result due to a deficiency of certain enzymes required to regulate glycogenolysis or gluconeogenesis.[1] The predominant storage sites for glycogen are the liver and muscles. Hence, glycogen breakdown and/or utilization can affect the liver, muscles, or both. Hepatic GSD is characterized by hypoglycaemia, whereas GSDs with muscular involvement are marked by muscle weakness and spasms. These disorders affect about 1 in every 20,000 to 43,000 live births approximately in the United States every year. Moreover, GSD (types I, III, and IX) account for 80% of hepatic GSD's, with type I being the most predominant.[2,3]

DOI: ["DOI"].11.2.1

GSD type I is caused due to diminished activity or complete absence of glucose-6-phosphatase (G6Pase) and has an incidence of 1 in 1,00,000. It is further classified into subgroups based on the anomaly in the G6Pase system. Around 80% of the clinical GSD type I cases are categorized as GSD type Ia (Von Gierke's disease) which is caused due to diminished activity or absence of glucose-6-phosphatase-α enzyme (G6Pase-α) and 20 % are GSD type Ib caused due to the deficient activity of Glucose-6-Phosphate Translocase/transporter (G6PT).[4] Patients with GSD type -I encounter life-threatening symptoms if they are left untreated. Despite having intensive dietary therapeutic strategies, they suffer serious untoward effects, like renal failure and liver tumours, as age progresses. Both GSD type Ia and Ib share same manifestations like hypoglycaemia, hyperlipidaemia, hyperuricemia, lactic acidosis, and extensive glycogen accumulation primarily in the liver followed by kidneys, leading to hepatomegaly and nephromegaly (Figure 1).[2,5] Due to hindered glucose mobilization across the cell membrane and within the cell of the polymorphonuclear leukocytes, GSD type Ib patients are

also presented with symptoms like frequent infections, decrease in neutrophil count, and neutrophil dysfunction in addition to the other clinical features of impaired glycogen metabolism.[6]

The clinical presentation of GSD type I hints at the initial diagnosis, a series of biochemical abnormalities in liver biopsy tissue, as well as molecular genetic tests and/or enzymology, which can confirm the diagnosis.[7] Until today, there is no cure for this disorder, and the management of its manifestation is a daunting task. The most common management strategy for this multisystem disorder is dietary therapy. Despite adherence to dietary therapy, GSD type Ia patients suffer from acute and chronic complications.[1] The complex nature of the disorder warrants the need for animal models to provide mechanistic insights that undoubtedly will direct eventual therapies. However, designing and establishing a disease model for GSD-type I is an uphill task. The gene knockout animals and genetically mutated cells serve as perfect disease models, however, the issues of stability, survivability, maintenance, and the cost of these models are a big challenge.[8] Therefore, new animal models which are easier to induce, manage and maintain are required to be explored and contribute to the improvement of the treatment strategies from both pharmacological and nutritional perspectives. Developing a chemically induced animal model could help in overcoming some of the hurdles faced while designing a transgenic model like avoiding the developmental abnormalities caused by the genetic defect (in turn affecting survival). As per the literature review, certain synthetic and phytochemical compounds such as Mumbaistatin,[9] Kodaistatin,[10] for this study, Chlorogenic Acid (CGA) was considered, CGA belongs to a class of hydroxycinnamic acid derivative, which is present in a variety of fruits and abundantly present in green coffee beans[11,12] and its derivatives[13] known to efficiently inhibit the particular enzyme glucose-6-phosphatase complex in the liver and can lead to decrease the fasting blood glucose levels, which can simulate the major manifestation similar of GSD type I, on the other hand, metformin is known to induce lactic acidosis[14] which is also one of the dominant manifestations of GSD type I. The present work is an attempt to determine how best these chemicals mimic the characteristic manifestations of GSD type I.

MATERIALS AND METHODS

In silico study

Molecular Docking

In order to obtain a clean protein structure, water and heteroatoms were removed from the Glucose-6-phosphatase with the modelled structure. Molecular binding sites are considered in

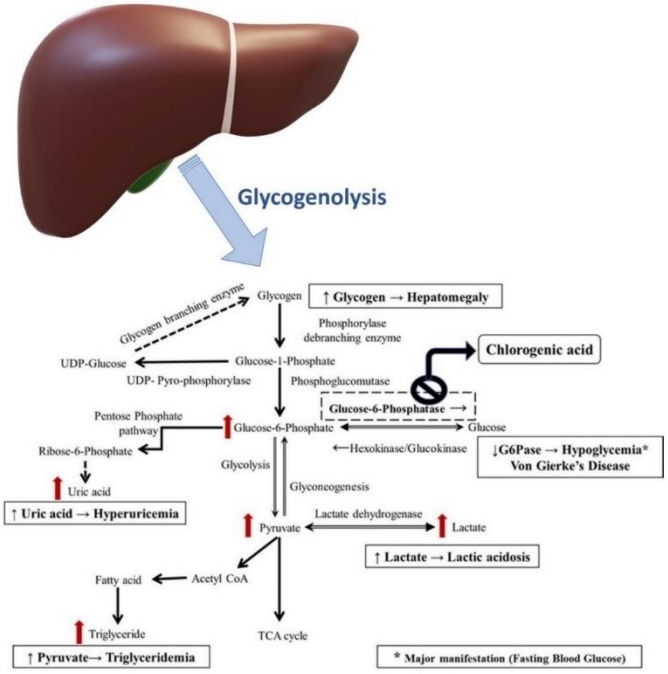

Figure 1: Graphical abstract emphasising the pathway explaining the manifestations of GSD type I upon Glucose-6-Phosphatase inhibition.

receptor cavity method docking calculations for ligand molecules bound in interactions. The study of receptor-ligand docking was conducted with AutoDock Vina with a box size of 40 x 40 x 40.

Molecular Dynamics-Simulation

The chosen protein-ligand complex was run through a molecular dynamic's simulation in Gromacs-2019. 4. To obtain the force field coordinates, the specified ligand topology was obtained from the PRODRG server (PMID: 15272157). The vacuum minimization technique was used to prepare the system with 1500 steps with the steepest descent algorithm. Subsequently, in a cubic periodic box of 0.5 nm, the complex structures were solvated using a Simple Point Charge (SPC) water model. Subsequently the complex systems were maintained with the optimum concentration of salt at 0.15 M by adding suitable numbers of Na^+ and Cl^- counter ions. Based on a previously published paper, the system preparation was postulated.[15] Each resultant structure from the Number of particles, Pressure, and Temperature (NPT) equilibration phase was subjected to a final production run in the NPT ensemble for 100 ns simulation time (PMID: 31514687). The GROMACS simulation suite of Protein RMSD, RMSF, RG, SASA, and H-Bond was used to perform the trajectory analysis (PMID: 32567989).

Chemicals and Drugs

The chlorogenic acid (Sigma Aldrich, USA) was procured and maintained at 8 to 25°C as per the manufacturer's instructions and metformin tablets (USV India) were maintained at room temperature. All other common laboratory chemicals were of analytical grade and procured from various manufacturers.

Experimental animals and ethical consideration

The investigation was carried out on male albino Wistar rats (n=24), weighing between 150-200 g. Animals were equally distributed into four different groups, housed in polypropylene cages, and the temperature of 27°C±2°C was maintained, with 12 hr, light and dark cycle for acclimatization for about a week. Standard/ routine rat feed (Gold Mohur Lipton India Pvt. Ltd.), and potable water (*ad libitum)* was fed to the animals throughout the study. The proposed animal study was reviewed by the Committee for Control and Supervision of Experiments on Animals (CCSEA) in India and was approved (Approval No. 0/KLECOPH/19) by the Institutional Animal Ethics Committee (IAEC) and ARRIVE guidelines were followed for all the experimental methods.

Induction of GSD type I manifestations

Chlorogenic acid was chosen for this study, considering its safety, availability, and effectiveness. A pilot study was carried out for 14 days to establish the efficient dose of CGA required decreasing the fasting blood glucose level in the test animals. For this experimental setup, the rats were housed into five different groups, each group consisting of six rats. All animals were allowed standard rat feed and water *ad libitum*, except those in the control group. The animals were subjected to daily doses of CGA at varying doses (50, 100, 200, and 400 mg/kg) for two weeks in adjuvant to their daily feed schedule.

An oral dose of (CGA 200 mg/kg) bodyweight was observed to be effective and showed the promising capability to induce fasting hypoglycaemia/decreased fasting blood glucose level in albino Wistar rats. However, it was observed that CGA had a shorter biological half-life, due to which its ability to maintain hypoglycaemia was limited to 1.5 to 2.5 hr. To overcome this situation the Chlorogenic Acid Loaded liposomes (CAL) were formulated based on the literature review for this study.[14] However, the formulation did not achieve the desired result. Subsequently, for the main study, based on the literature, the green coffee extract[11,12] consisting of 36% (CGA 200 mg/kg) was admixed in the drinking water and was fed routinely to the animals in the treatment groups, to sustain the CGA effect. In order to induce further manifestations of GSD, like lactic acidosis, metformin[16] was administered along with CGA in a test group of animals.

The animals were divided into three different testing groups for the main study, each with six animals, Group I, or the control group was provided with normal feed and drinking water. In Group II the animals were fed with normal feed and drinking water in addition to 95% CGA which was administered daily by oral gavage (200 mg/kg body weight for 49 days/7 weeks). Group III animals received green coffee bean extract (36% CGA) admixed in drinking water (200 mg/kg body weight orally daily) in addition to metformin 500 mg/kg and 95% CGA (200 mg/kg body weight for 49 days) along with normal feed, administered daily by oral gavage. During the measurement of blood glucose, the maintenance dose of 100 mg CGA (95%) at 45 min interval was administered to sustain hypoglycaemia (Figure 2, C).

Collection of blood and tissue samples

Blood collection was performed by tail prick method with the help of a sterile lancet and the blood glucose was measured by glucometer (Arkray glucocard). Glucometer and test strips were stored and used at an appropriately controlled temperature and humidity throughout the study duration. Subsequently, for the estimation of other blood parameters the animals were anaesthetised with ketamine and xylazine before retro-orbital blood withdrawal, and for euthanasia high dose of ketamine and xylazine was subjected as per the guidelines, post which the liver tissues were isolated. Blood was blotted from the liver tissues and rinsed using a cold physiological saline solution (consisting of 0.9%, w/v NaCl). For staining processes, the tissues were weighed and preserved in 10% v/v neutral buffered formalin.

Biochemical assessments

Assessment of hypoglycemia

The fasting blood glucose level for the experimental rats throughout the study period was estimated with the help of a glucometer.

Glucose-6-phosphatase estimation

The glucose-6-phosphatase enzyme was estimated by the method described by[17,18] with the following experimental conditions: Temperature of 37°C, pH=6.5, Absorbance at 660nm, with Lightpath=1 cm, Method adopted: Spectrophotometric Stop Rate Determination.

Liver glycogen

The liver glycogen was estimated as described by Montgomery, (1957) immediately after the autopsy.[19]

Serum Lactate dehydrogenase

Lactate dehydrogenase levels were estimated using commercial kits procured from Erba Transasia BioMedicals Ltd., India following the instructions provided along with the kit. A semi-automated clinical chemistry auto analyser (Erba Transasia BioMedicals Ltd., India, Model Chem7) was used to record the measurements.

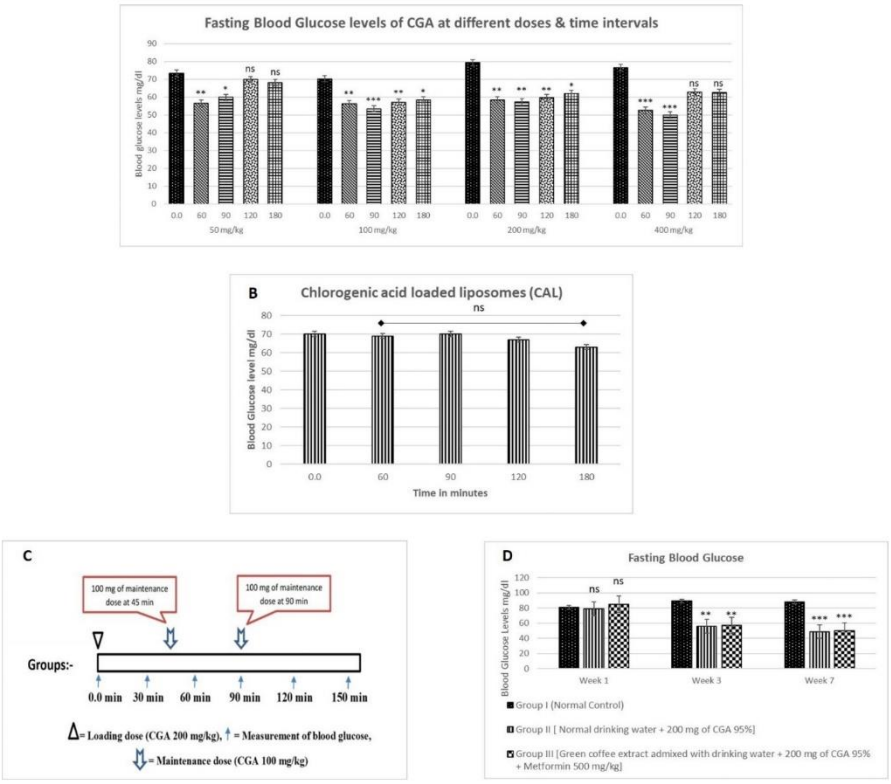

Figure 2: Fasting blood glucose levels, (A) Pilot study to assess the fasting blood glucose levels at different time intervals, ranging from (0.0 min to 180 min), (B) Effect of Chlorogenic acid loaded liposomes on blood glucose levels. The values obtained are expressed as mean±standard error of mean (n=6) in each group, there was no significant decrease in the blood glucose levels (p>0.05), (C) Representative depiction of the experimental set-up, where maintenance dose of CGA 100 mg was administered at every 45 min interval to sustain the enzyme inhibition, during the biochemical estimations, (D) The fasting blood glucose was measured at fixed intervals. The values obtained are expressed as mean±standard error of mean (n=6) in each group, the statistical significance was analysed by one-way ANOVA followed by Bonferroni's post-hoc test during the 1st week there was no significant decrease in the blood glucose, whereas in 3rd week, Group II and III showed significant decrease in the blood glucose levels (**p<0.01) and in 7th week (***p<0.001) when compared to Group I.

Serum Uric acid

Serum Uric acid levels were measured as per Trivedi and Kabasakalian method.[20,21]

Biometric assessment

Liver weight

The liver of the individual animals was surgically isolated, and its weight was measured on the last day of the study.

Statistical analysis

All the data were analysed using the statistical program GraphPad Prism version 6.0 and expressed as mean SEM. Where, Analysis of Variance (ANOVA) was used to examine the data, followed by Bonferroni's multiple comparison *post hoc* test, where p values of <0.05) were set to be considered as statistically significant.

RESULTS

In silico study

Molecular Docking

The binding patterns of Glucose-6-phosphatase were evaluated using AutoDock vina by triplicated docking approach. The intermolecular interactions between G6Pase protein (PRO) and CGA ligand (LIG) is shown in Tables 1 and 2 respectively. The docking images of PRO with the LIG are represented in Figure

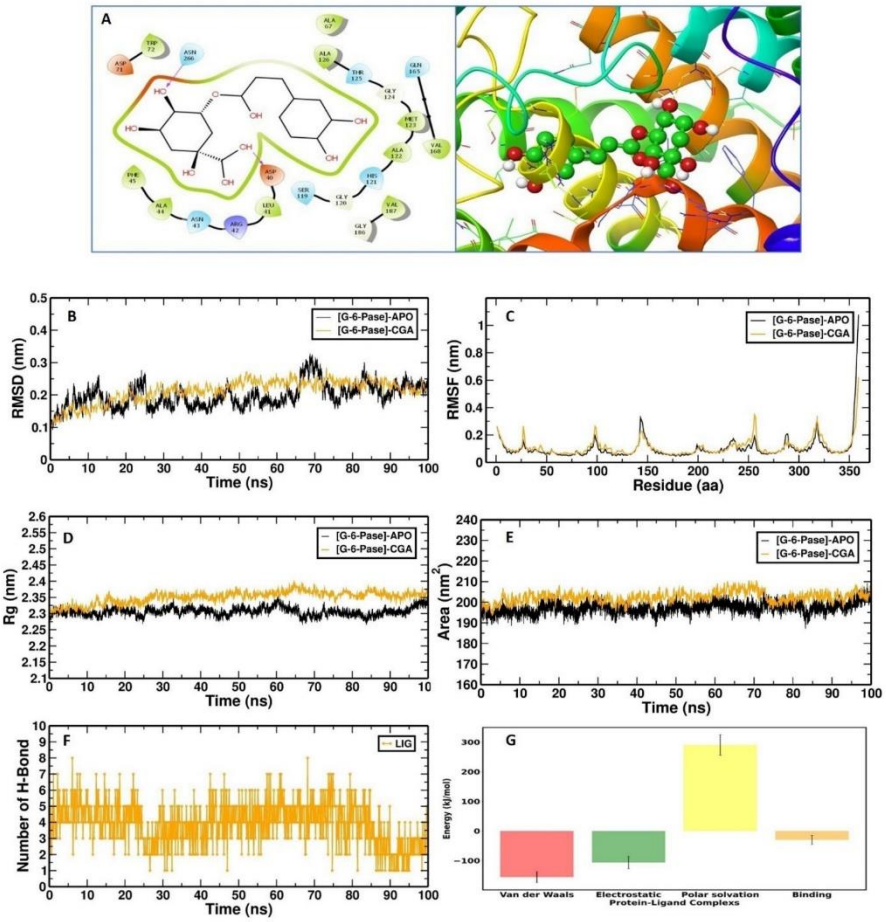

Figure 3: Molecular docking and Molecular dynamics simulation, (A) 2D and 3D interaction of Protein and ligand, (B) Root means square deviation of backbone atoms, (C) Root means square fluctuation of c-alpha atoms, (D) RG of backbone atoms, (E) SASA of backbone atoms of with Protein-Substrate and Protein-Ligand, (F) H-Bond, and (G) Determination of relative binding affinity of Protein-Ligand by MM-PBSA method.

3, A. The stability of the complex is greatly influenced by the carbon-hydrogen interaction, Vander Waal's force, and typical hydrogen bonds.

Molecular Dynamics

To comprehend the stability of the protein-ligand complexes, an all atom MD simulation lasting 100 nanoseconds (ns) was performed. (i) Protein alone [PRO-APO], and (ii) Protein with ligand [PRO-LIG]. The average value of RMSD, RMSF, Rg and SASA has been tabulated in Table 3, this information describes the structural properties of Protein-Ligand interaction. The "Average RMSD" (root mean square deviation) and "Average RMSF" (root mean square fluctuation) values are measures of the overall conformational stability and flexibility of the protein. A lower RMSD value indicates that the protein has a more stable structure, while a higher RMSF value indicates that the protein is more flexible. The "Radius of gyration" value is a measure of the size of the protein, with a larger radius indicating a larger protein. The "Average SASA" (Solvent Accessible Surface Area) value is a measure of the amount of surface area of the protein that is exposed to the solvent (such as water). A larger SASA value indicates that more of the protein is exposed to the solvent.

Root mean square deviation

It is a crucial factor in figuring out how the two confirmations differ from one another. The greater the RMSD value, the more will be the deviation. The RMSD values are calculated against the simulation timescale of 100 ns (Figure , B). The average RMSDs from 0 to 100 ns for PRO-APO, PRO-LIG protein complex proteins were 0.22+/-0.03 nm, 0.21+/-0.04 nm respectively. The relative stability of chemical complexes during the simulation is represented by these RMSD values. The complexes were also stable throughout the simulation.

Root mean square fluctuation

The amino acids in the protein that produce the most vibrations are identified by RMSF analysis, causing the protein to become unstable in both the presence and absence of the ligands. The RMSF values are calculated against the simulation timescale of 0 to 100 ns. The average RMSFs from 0 to 100 ns for PRO-APO, PRO-LIG, protein complex proteins were 0.4+/-0.07 nm and 0.3+/-0.06 nm respectively. The results for PRO-APO, PRO-LIG complexes as depicted in Figure , C. The result suggested that there are no significant structural changes during the 100 ns simulation.

Radius of Gyration (RG)

The radius of gyration can be well described as the mass-weighted root mean square distance of atoms from their centre of mass. The Rg plot shows the competency, shape folding, and overall structure at varying times during the trajectory, illustrated in Figure , D. Throughout the simulation, PRO-APO, PRO-LIG complexes exhibited a similar pattern of Rg value. The average RG value from 0 to 100 ns for PRO-APO, PRO-LIG protein complex proteins were 2.36+/-0.03 nm and 2.35+/-0.01 nm respectively.

Solvent Accessible Surface Area (SASA)

The hydrophobic core's compactness was evaluated by SASA. The change in SASA of the PRO-APO, PRO-LIG protein with time is shown in Figure , E. The average SASA value from 0 to

Table 1: The docking score of CGA with G6Pase.

Compound Name	Affinity (T1)	Affinity (T2)	Affinity (T3)	Average Docking Score
LIG	-8.9	-9.0	-8.9	-8.9

Table 2: Hydrogen Bonding information.

Compound	H-Donor	H-Acceptor	Distance	Type
LIG	A: ASN43:HN	B: UNK0:O	3.0318	Conventional Hydrogen Bond
	A: ASN266:HD22	B: UNK0:O	2.38869	Conventional Hydrogen Bond
	B: UNK0:H	A: ASP40:OD1	1.31199	Conventional Hydrogen Bond
	B: UNK0	A: MET123	5.24331	Pi-Alkyl

Table 3: Molecular Dynamics report at 100 ns.

Sl. No.	Protein	Average RMSD (nm)	RMSF (nm)	Radius of gyration (nm)	Average SASA (nm2)
1	PRO-APO	0.22+/-0.03	0.4+/-0.07	2.36+/-0.03	205.07+/-5.20
2	PRO-LIG	0.21+/-0.04	0.3+/-0.06	2.35+/-0.01	203.07+/-4.30

Table 4: The relative binding strength of PRO-LIG computed via the MM-PBSA method.

System	van der Waal energy	Electrostatic energy	Polar solvation energy	Binding energy
PRO-LIG	-155.826+/-18.129 kJ/ mol	-106.616+/- 20.776 kJ/ mol	290.413+/- 34.240 kJ/ mol	-30.141+/- 14.943 kJ/ mol

100 ns for PRO-APO and PRO-LIG protein complex proteins were 205.07+/-5.20 nm and 203.07+/-4.30 nm respectively. This indicates that there is no change in structural level protein throughout the simulation.

Hydrogen Bond (H Bond)

Hydrogen bonds are formed to stabilise protein-ligand complexes. In our study, the simulation analysis supports the hydrogen bonds established in the molecular docking analysis. The complex's H-Bond outcome with PRO-LIG. The complex's H-Bond outcome with PRO-LIG is depicted in Figure , F.

Molecular Mechanics Poisson–Boltzmann Surface Area (MM - PBSA)

In order to determine the binding affinity of PRO-LIG, we examined the relative binding strength within the protein of summery energy. Table 4 and Figure , G compares the binding strength of PRO-LIG concerning inhibitors computed via the MM-PBSA method. Across a stable simulation trajectory, we calculated residue level contributions to the interaction energy.

Assessment of the effect of chlorogenic acid on fasting blood glucose level

Assessment of the fasting blood glucose level on day 14 (Pilot study)

The blood glucose levels were measured at different time intervals (i.e., at 0.0, 60, 90, 120, and 180 min) on day 14, to fix the dose of CGA. The fasting blood glucose levels consistently decreased at the dose of 200 mg/kg throughout the time interval (**p<0.01, up to 120 mins and **p<0.5 at 180 min) and even 400 mg/kg dose showed good results (***p<0.001, up to 90 min), however, the hypoglycaemia was not persistent post 90 min interval (Figure , A).

Assessment of the role of Chlorogenic Acid loaded Liposome (CAL) on fasting blood glucose level to sustain hypoglycaemia

The administration of CAL formulation did not show any success in sustaining the hypoglycaemic property of chlorogenic acid (Figure , B).

Assessment of the fasting blood glucose levels at different stages of the study

The blood glucose levels were measured on the 1st, 3rd and 7th week of the study. There was a considerable drop in blood glucose levels in Group II and III (**p<0.01) at 3 weeks interval, whereas at the 7th week interval, significant decrease in the blood glucose levels was evident (***p<0.001) when compared with control group animals (Figure , D).

Glucose-6-phosphatase estimation

The glucose-6-phosphatase activity was measured as the amount of inorganic phosphate liberated. by using the standard curve approach. Group II showed no significant inhibition (p<ns), whereas, Group III showed a significant (***p<0.001) drop in glucose-6-phosphatase activity when compared to the normal control group (Figure 4, A).

Estimation of hepatic glycogen

The estimated glycogen level was analysed by one-way ANOVA followed by Bonferoni's *post hoc* test. Group II showed no significant elevation (p<*ns*), whereas, in comparison with the normal control, Group III showed a significant elevation in liver glycogen levels when compared to the normal control group (**p<0.01) as well as when compared with Group II ($^{\Psi\Psi}p$<0.01) (Figure , B).

Measurement of serum lactate dehydrogenase

The Lactate dehydrogenase levels increased considerably in Group II (*p<0.05), whereas in Group III there was significant increase when compared to Group I (***p<0.001) and Group II ($^{\Psi\Psi\Psi}p$<0.001) (Figure , C).

Measurement of Serum Uric acid

Serum Uric acid levels did not implicate any substantial difference between the control and experimental groups (^{ns}p>0.05) (Figure , D).

Liver weight

The liver weight of the rats was measured after 7 weeks/49 days and it was observed that the liver weight of Group II did not increase significantly (^{ns}p>0.05), whereas Group III showed considerable increase in liver weight when compared to Group I (*p<0.05) and group II ($^{\Psi}p$<0.05) (Figure , E).

Histological study

The liver tissues showed clear signs of abnormalities associated with GSD type I, in Group II, swollen hepatocytes and ballooning degeneration were observed and in Group III, significant mosaic pattern, glycogen nuclei, glycogen, swollen hepatocytes, ballooning degeneration and sinusoidal congestion were evident (Figure 5, A, B, and C).

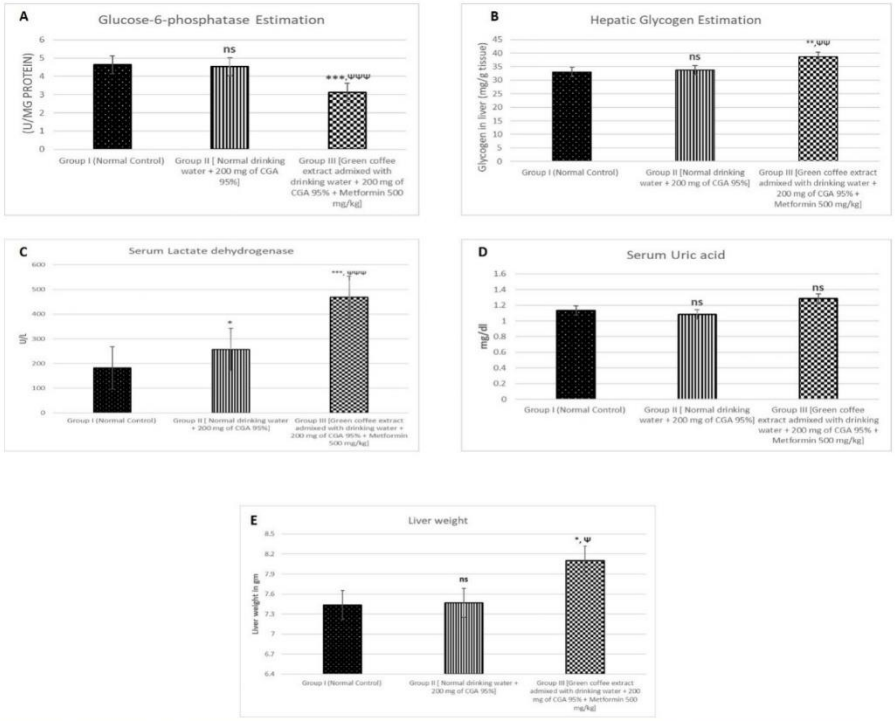

Figure 4: GSD Manifestations (A) The glucose-6-phosphatase estimation, where Group III presented significant decrease in the blood glucose levels (***p<0.001) when compared with Control group and ($^{\Psi\Psi}p$<0.001) when compared to Group II. (B) Hepatic glycogen content estimation, where all the values obtained are expressed as mean±standard error of mean (n=6), Group III showed a significant elevation in the hepatic glycogen (**p<0.01) when compared to Group I and ($^{\Psi\Psi}p$<0.01) when compared to Group II. where all the values obtained are expressed as mean±standard error of mean (n=6). (C) The lactate dehydrogenase levels significantly increased in Group II (*p<0.05), and in Group III (***p <0.001) high significance was observed when compared to the Group I respectively and ($^{\Psi\Psi\Psi}p$<0.001), when compared to Group II respectively. (D) The serum uric acid was non-significant (ns, p>0.05), when compared to the both, Group I and Group II. (E) The liver weight of the Group III is increased (*p< 0.05) when compared Group I and Group II ($^{\Psi}p$<0.05), whereas Group II did not present significant changes when compared to Group I.

All the results obtained are expressed as mean±standard error of mean (n=6). The statistical significance was analysed by one-way ANOVA and Bonferroni's post-hoc test where *p<0.5, **<0.05 and ***p<0.01.

DISCUSSION

The absence of endogenous glucose synthesis resulting in acute hypoglycaemia after a short duration of fasting is a characteristic feature of GSD type I. This pathophysiology is induced due to the deficiency of enzyme complex glucose-6-phosphatase (G6Pase), involving the G6Pase catalytic subunit which is encoded by the (G6PC1) gene and the glucose-6 phosphate transporter or translocase subunit (G6PT), which is encoded by (*SLC37A4*) gene. The complex macromolecules like glycogen are fundamental in the maintenance of glucose levels within the physiologic range. The regulation of synthesis or degradation of glycogen is highly systematized and complex. Anomaly in the degradation of glycogen is referred to as Glycogen Storage Disorders (GSDs) are rare diseases yet they make up a major category of inborn errors of metabolism or autosomal recessive illnesses and there is no specific treatment available for the disorders. GSD type I renders the patients vulnerable to other long-term complications, such as hyperuricemia, lactic acidemia and hepatomegaly and glycogen build up in liver, along with other chronic and serious complications like hepatocellular adenomas and renal impairment. Animal models which can be easily manipulated and maintained are essential in providing mechanistic insights that can direct eventual therapeutic strategies. To elucidate the biochemical basis of GSD type Ia and to assess the advent of gene therapy approach to rectify or improve *G6pc* deficiency have been studied on two animal models of GSD type Ia. By using *G6pc* knockout mouse, created by Dr. Janice Chou presented with low birth weight, but

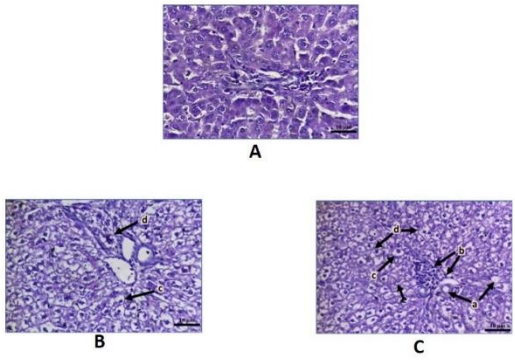

Figure 5: A: Periodic Acid-Schiff stain (PAS) of Group I showed normal architecture with intact hepatocytes and no Glycogen accumulation. B: Group II; CGA (100mg/kg) treated group PAS stained, showed significant swollen hepatocytes[c] and ballooning degeneration [d]. C: Group III; CGA (200mg/kg) treated group PAS stained, showed significant Mosaic pattern, Glycogen nuclei [a], Glycogen [b] swollen hepatocytes[c], ballooning degeneration [d] and sinusoidal congestion [e].

developed severe hypoglycaemia instantaneously and gradually exhibited a pronounced increase in the serum cholesterol and triglyceride levels. Nonetheless, they did not generally manifest lactic acidosis. Similarly, a canine (Maltese breed) model of GSD type Ia having a natural mutation in the *G6pc* gene was discovered and used to delineate the pathology of the disease. The similar canine model was manipulated by crossbreeding a *G6pc* mutation carrier Maltese breed with a beagle breed. These canine models presented with peculiar and specific symptoms similar to that of human disease, including lactic acidemia, however, these models proved ineffective for investigation of the long term or chronic complications observed in GSD type Ia. GSD type Ia mice models that only target deletion of *G6pc* in liver, and/or kidneys, or gut have been recently developed with a purpose of monitor the development of long term diseases or manifestations that emerge in GSD type Ia patients and to assess the potential treatment strategies.

The primary goal of this work was to find out if the chemically induced GSD model can be developed, which could be more reliable and economical. Several *in vitro* studies have claimed that CGA and its derivatives can inhibit or attenuate the activity of glucose-6-phosphate enzyme complex (G6Pase and G6PT) resulting in altered metabolism. which we substantiated with *in silico* studies. Based on this evidence, we carried out a pilot study, where it was evident that a dosage of 200 mg of CGA per kg of body weight was optimum to induce hypoglycaemia in rats. However, since CGA has a shorter biological half-life, its ability to maintain hypoglycaemic was limited to 1.5 to 2.5 hr. Literature suggested the formulation of Chlorogenic Acid loaded Liposomes (CAL) can prolong the effects of CGA. However, there was no significant difference in the outcome using the liposome formulation. Hence, to augment the effect of CGA, green coffee extract consisting of 36% (CGA 200 mg/kg) was admixed with drinking water to be fed continuously to the animals in the treatment groups along with the daily dose of 200 mg/kg of 95% CGA via oral gavage. Glycogen levels were found to be altered in CGA treated rats which is probably due to the suppressed activity of glucose-6-phosphatase, further contributing as a factor for hepatomegaly and significant increase in the liver weight. In addition to CGA, metformin was employed, as an attempt to replicate the lactic acidosis generally observed in GSD type I cases. Thus, it indicates that along with CGA, administering other drugs or chemicals can be used to induce and augment the manifestation of GSD type I like symptoms in the rats.

CONCLUSION

The article discusses a pre-clinical study aimed at inducing the symptoms of Glycogen Storage Disease Type I (GSD type I) in rats through the inhibition of the glucose-6-phosphatase enzyme using Chlorogenic Acid (CGA) and metformin. The *in silico* study, demonstrated that CGA had good docking scores and binding patterns with G6Pase, followed by an *in vivo* pilot study to determine the effective dose. This study concludes that CGA was evidently responsible to induce major manifestations of GSD type I, and when it was combined with metformin, further there was significant augmentation of the manifestations. Thus, this model can serve as an alternative to genetically engineered animal models, that can promote research on GSD like diseases. However, there is future scope to explore other combinations of chemicals/drugs which can contribute to induce other GSD type I manifestations such as, hyperlipidaemia, neutropenia, hepatic fibrosis etc. in experimental animals.

ACKNOWLEDGEMENT

We gratefully acknowledge the Principal, KLE College of Pharmacy, Hubballi, Karnataka for providing research facilities.

FUNDING

This research did not receive any specific grant from funding agencies in the public, commercial, or not-for-profit sectors.

CONFLICT OF INTEREST

The authors declare that there is no conflict of interest.

CONSENT FOR PUBLICATION

All authors approved the manuscript for publication.

AUTHOR CONTRIBUTIONS

Santosh B Patil: Conceptualization, Methodology, Investigation, Visualization and Project administration; Pramod C Gadad: Supervision, Validation and Data curation.

ABBREVIATIONS

GSD: Glycogen Storage Disease; **CGA:** Chlorogenic acid; **CAL:** Chlorogenic acid Loaded Liposomes; **PRO-LIG:** Protein and Ligand; **PRO-APO:** Protein Alone; **RMSD:** Root mean square deviation; **RMSF:** Root mean square fluctuation; **RG:** Radius of gyration; **SASA:** Solvent accessible surface area; **MM-PBSA:** Molecular mechanics Poisson-Boltzmann surface area; **G6Pase:** Glucose-6-phosphatase; **G6PT:** Glucose-6 phosphate transporter.

REFERENCES

1. Chou JY, Jun HS, Mansfield BC. Type I glycogen storage diseases: disorders of the glucose-6-phosphatase/glucose-6-phosphate transporter complexes. J Inherit Metab Dis. 2015; 38(3): 511-9. doi: 10.1007/s10545-014-9772-x, PMID 25288127.
2. Heller S, Worona L, Consuelo A. Nutritional therapy for glycogen storage diseases. J Pediatr Gastroenterol Nutr. 2008; 47;Suppl 1:S15-21. doi: 10.1097/MPG.0b013e3181818ea5, PMID 18667910.
3. Özen H. Glycogen storage diseases: new perspectives. World J Gastroenterol. 2007; 13(18): 2541-53. doi: 10.3748/wjg.v13.i18.2541, PMID 17552001.
4. Cappello AR, Curcio R, Lappano R, Maggiolini M, Dolce V. The physiopathological role of the exchangers belonging to the SLC37 family. Front Chem. 2018; 1-17. doi: 10.3389/fchem.2018.00122, PMID 29719821.
5. Bhattacharya K. Dietary dilemmas in the management of glycogen storage disease type I. J Inherit Metab Dis. 2011; 34(3): 621-9. doi: 10.1007/s10545-011-9322-8, PMID 21491105.
6. Calderwood S, Kilpatrick L, Douglas SD, Freedman M, Smith-whitley K, Rolland M, *et al.* Recombinant human granulocyte colony-stimulating factor therapy for patients with neutropenia and/or neutrophil dysfunction secondary to glycogen storage disease type 1b. 2016; 97(2): 376-83.
7. Kishnani PS, Austin SL, Abdenur JE, Arn P, Bali DS, Boney A, *et al.* Diagnosis and management of glycogen storage disease type I: A practice guideline of the American College of Medical Genetics and Genomics. Genet Med. 2014; 16(11): e1. doi: 10.1038/gim.2014.128, PMID 25356975.
8. Rajas F, Clar J, Gautier-Stein A, Mithieux G. Lessons from new mouse models of glycogen storage disease type 1a in relation to the time course and organ specificity of the disease. J Inherit Metab Dis. 2015; 38(3): 521-7. doi: 10.1007/s10545-014-9761-0, PMID 25164786.
9. Vértesy L, Kurz M, Paulus EF, Schummer D, Hammann P, Pharma A, *et al.* The chemical structure of Mumbaistatin, a novel glucose-6-phosphate translocase inhibitor produced by *Streptomyces* sp. DSM 11641. DSM11641 used. Preparative HPLCwas performed using Pharmacia Sepharose Fast Flow column (Pharmacia, Uppsala, Sweden,. J Antibiot (Tokyo). 2001; 54(4): 354-63. doi: 10.7164/antibiotics.54.354, PMID 11426660.
10. Sakemi S, Hirai H, Ichiba T, Inagaki T, Kato Y, Kojima N, *et al.* Thielavins as glucose-6-phosphatase (G6Pase) inhibitors: producing strain, fermentation, isolation, structural elucidation and biological activities. J Antibiot (Tokyo). 2002; 55(11): 941-51. doi: 10.7164/antibiotics.55.941, PMID 12546415.
11. Itrac CAHE, Barra ALI, Oller M, Itrac XAV. Contribution of chlorogenic acids to the inhibition of human hepatic glucose-6-phosphatase activity *in vitro* by Svetol, a standardized decaffeinated green coffee extract; 2010. p. 4141-4.
12. Ong KW, Hsu A, Tan BKH. Anti-diabetic and anti-lipidemic effects of chlorogenic acid are mediated by AMPK activation. Biochem Pharmacol. 2013; 85(9): 1341-51. doi: 10.1016/j.bcp.2013.02.008, PMID 23416115.
13. Hemmerle H, Burger H, Below P, Schubert G, Rippel R, Schindler PW, *et al.* of Hepatic glucose-6-phosphate translocase. 1997; 40(2): 4-12.
14. Lalau JD. Lactic acidosis induced by metformin: incidence, management and prevention. Drug Saf. 2010; 33(9): 727-40. doi: 10.2165/11536790-000000000-00000, PMID 20701406.
15. Satish C. Transition Metal Complexes of Ligand containing aminophenol moiety: synthesis, Characterization and antimicrobial Studies of Schiff base Ligand and its Mixed Ligand Metal Complexes. larjset. SP S, C.R G. 2022; 9(2): 423-33.
16. Wang DS, Kusuhara H, Kato Y, Jonker JW, Schinkel AH, Sugiyama Y. Involvement of organic cation Transporter 1 in the lactic acidosis caused by metformin. Mol Pharmacol. 2003; 63(4): 844-8. doi: 10.1124/mol.63.4.844, PMID 12644585.
17. Taussky HH, Shorr E, Kurzmann G. A microcolorimetric method for the determination of inorganic phosphorus. J Biol Chem. 1953; 202(2): 675-85. doi: 10.1016/S0021-9258(18)66180-0, PMID 13061491.
18. Arion WJ, Wallin BK, Carlson PW, Lange AJ. The specificity of glucose liver microsomes *. J Biol Chem. 1972; 247(8): 2558-65. doi: 10.1016/S0021-9258(19)45462-8, PMID 4336378.
19. Montgomery R. Determination of Glycogenl. 1956; 336.
20. Trivedi RC, Rebar L, Berta E, Stong L. New enzymatic method for serum uric acid at 500 nm. Clin Chem. 1978; 24(11): 1908-11. doi: 10.1093/clinchem/24.11.1908, PMID 709818.
21. Kabasakalian P, Kalliney S, Westcott A. Determination of uric acid in serum, with use of uricase and a tribromophenol aminoantipyrine chromogen. Clin Chem. 1973; 19(5): 522-4. doi: 10.1093/clinchem/19.5.522, PMID 4703662.

Cite this article: Patil SB, Gadad PC. Chlorogenic Acid, a Potential Glucose-6-Phosphatase Inhibitor: An Approach to Develop a Pre-Clinical Glycogen Storage Disease Type I Model. Indian J of Pharmaceutical Education and Research. 2024;58(2):1-10.

ANNEXURE III

Certificates of Poster Presentations

9th International Congress of
SOCIETY FOR ETHNOPHARMACOLOGY, INDIA
SFEC 2022
22nd to 24th April 2022
(Globalizing Local Knowledge and Localizing Global Technologies)
Theme : Redefining Ethnopharmacology for the Global Health and Wellbeing

Certificate of Participation

This is to certify that Prof./Dr./Mr./Ms. Santhosh B Patil
has Presented a PAPER in ORAL/POSTER SESSION in the 9th International Congress of the Society for Ethnopharmacology, India (SFEC-2022) held at JSS College of Pharmacy, JSS Academy of Higher Education & Research, Mysuru, Karnataka, India from 22nd to 24th, April 2022.
Title of presentation: Chemically induced glycogen storage disease type I manifestation in Wistar rats

Dr. T.M. Pramod Kumar
Organizing Chairman, SFEC - 2022

Dr. K. Mruthunjaya
Organizing Secretary, SFEC - 2022

Mr. Birendra K. Sarkar
President - SFE - India

IBRO Supported Meeting and Workshop on **"Recent Progress in Brain Research and Drug Delivery"**

INTERNATIONAL BRAIN IBRO RESEARCH ORGANIZATION

Organized by

ISF College of Pharmacy, Moga, Punjab

(An Autonomous College) NAAC Accredited "A" Grade College

Sponsored by

International Brain Research Organization (IBRO)

13th-15th May, 2022

Certificate of Poster Presentation

This is to certify that Prof./Dr./ Mr./Ms. **Santosh B Patil**

Presented a Poster in

IBRO Supported Meeting and Workshop on May 14, 2022 (Online Mode).

Organizing Secretary	Organizing Secretary	Convener	Patron	Patron
Dr. Charan Singh	Prof. (Dr.) R. K. Narang	Prof. (Dr.) G. D. Gupta	Parveen Garg	Dr. Y. K. Gupta
Associate Professor	Vice-Principal	Director-cum-Principal	Chairman	Chairman, RAC
ISFCP, Moga	ISFCP, Moga	ISFCP, Moga	ISFCP, Moga	ISFCP, Moga

ISFCP/22/IBRO/216

NPTEL Course completion certificate

This certificate is computer generated and can be verified by scanning the QR code given below. This will display the certificate from the NPTEL repository, https://nptel.ac.in/noc/

Roll No: NPTEL20HS20S41380068

To
SANTOSH PATIL
SOMSAROJ BANGALOW, RAMNAGAR 3RD CROSS,
NEAR ADARSH SCHOOL
DHARWAD
KARNATAKA - 580001
PH. NO :9880572632

Score	Type of Certificate
>=90	Elite+Gold
75-89	Elite+Silver
>=70	Elite
50-69	Successfully Completed
<50	No Certificate

No. of credits recommended by NPTEL:2
An additional 1 credit may be awarded if the University deems it fit, based on the actual student effort involved.

NPTEL Online Certification

(Funded by the Ministry of HRD, Govt. of India)

This certificate is awarded to

SANTOSH PATIL

for successfully completing the course

Health Research Fundamentals
(ICMR-NIE e-Certificate course: NIeCer 101)

with a consolidated score of **77** %

Online Assignments	25/25	Proctored Exam	52.28/75

Total number of candidates certified in this course: **803**

Dr. Manoj Murhekar
Scientist 'G' & Director
ICMR-National Institute of Epidemiology, Chennai

Prof. Balram Bhargava
Secretary to Govt. of India, Dept. of Health Research &
Director-General, Indian Council of Medical Research

Prof. Andrew Thangaraj
NPTEL Coordinator
IIT Madras

icmr INDIAN COUNCIL OF MEDICAL RESEARCH | NIE NATIONAL INSTITUTE OF EPIDEMIOLOGY

Jan-Mar 2020
(8 week course)

FREE ONLINE EDUCATION swayam शिक्षित भारत, उन्नत भारत

Roll No: NPTEL20HS20S41380068 To validate and check scores: https://nptel.ac.in/noc